Substrate Binding: Interactions in Ascorbate Peroxidase

Thesis submitted for the degree of Doctor of Philosophy at the University of Leicester

by

Katherine Helen Sharp, MChem Chemistry

Department of Chemistry
Faculty of Science
University of Leicester

December 2004

ProQuest LLC
789 East Eisenhower Parkway
P.O. Box 1346
Ann Arbor, MI 48106-1346

Acknowledgements

I would like to thank my supervisor Dr. E. L. Raven for her guidance, support and help throughout the three years and Prof. P. M. Cullis for helpful discussions on the progress of the project. Thanks also to Dr. P. C. E. Moody (University of Leicester, Biochemistry Department) for his expertise when crystallising rsAPX, and Dr. D. Leys (University of Leicester, Biochemistry Department) for collecting the diffraction data. I would also like to thank Dr T. Fleming and Prof. N. Turner (University of Edinburgh, Chemistry Department) for their guidance with the directed evolution of rsAPX. I am also grateful to Dr. C. Metcalfe, Mr K. Singh, Dr. N. Patel, Dr. I. Macdonald, Dr. D. Wood, Miss N. Papadopoulou, Dr. M. Mewies and Miss S. Badyal for their assistance and encouragement. For financial support I am indebted to the Institute of Applied Catalysis, the EPSRC, and the University of Leicester. Finally, I would like to thank my parents, Clare and Jon for their help and support.

Substrate Binding: Interactions in Ascorbate Peroxidase

Katherine Helen Sharp

Abstract

X-ray crystallography, kinetics, spectroscopy and directed evolution have been used to define substrate binding in recombinant soybean cystolic ascorbate peroxidase (rsAPX), which catalyses the hydrogen peroxide-dependant oxidation of ascorbate in plants.

The rsAPX crystal structure has been solved to 1.8 Å (Chapter 2) and provides a useful comparison for the substrate bound structures. Nitric oxide and cyanide bound rsAPX crystal structures have also been solved to 2.0 Å and are used to model the binding of hydrogen peroxide in APX (Chapter 2).

Ascorbate binding interactions are defined by the rsAPX/ascorbate crystal structure, which has been solved to 1.4 Å (Chapter 3). This structure provides new rationalization of the unusual functional features of the related cytochrome *c* peroxidase enzyme, and a mechanism for electron transfer from the substrate to the heme has been proposed (Chapter 3).

The crystal structure of the rsAPX/salicylhydroxamic acid (SHA) complex has been solved to 1.46 Å (Chapter 4). Spectroscopic and kinetic techniques were used to show that guaiacol and SHA bind at the same site in APX. These data define the aromatic binding site in rsAPX and, along with the other crystal structures, have been used to propose a mechanism for proton transfer (Chapter 4).

A screen for enhanced aromatic oxidation has been developed, using guaiacol (colourless), which is oxidised to tetraguaiacol (red) by rsAPX (Chapter 5). The colour change and the fact it can be carried out on whole cells, allows many mutants to be assessed very efficiently. As a result it will be ideal for screening libraries of rsAPX mutants created by directed evolution.

Contents

		Page
Acknowledgements		**i**
Abstract		**ii**
Table of Contents		**iii**
Abbreviations		**xi**
Chapter 1	**Introduction**	**1**
1.1	Heme	2
1.2	Heme Proteins	2
1.2.1	Electron Transfer Heme Proteins	3
1.2.2	Oxygen Storage and Transport Proteins	3
1.2.3	Reduction-Oxidation Proteins	5
1.3	Heme Peroxidases	6
1.4	Plant Peroxidase	7
1.4.1	Classification	7
	1.4.1.1 Class I	8
	1.4.1.2 Class II	8
	1.4.1.3 Class III	8
1.4.2	The Catalytic Cycle	9
1.4.3	Model Peroxidases	10
	1.4.3.1 Evidence for the Structure of Compound I and II	11
	1.4.3.2 Expression	12
1.4.4	Bacterial Catalase-Peroxidases	13
1.5	Ascorbate Peroxidase	14
1.5.1	Catalysis	15
1.5.2	The X-Ray Crystal Structure of rpAPX	15
1.5.3	Compounds I and II	16
1.5.4	APX Sequences	17

1.5.5 Active Site Residues 18
1.5.6 Substrate Binding 19
1.5.7 Conclusions 19
1.6 Protein X-Ray Crystallography 19
1.6.1 X-Rays and X-Ray Diffraction 20
1.6.1.1 Scattering of X-Rays 21
1.6.1.2 Crystals 21
1.6.1.3 X-Ray Generators 23
1.6.1.4 Bragg's Law 24
1.6.2 Symmetry of Protein Crystals 25
1.6.3 Fourier Transforms 26
1.6.4 Molecular Replacement 26
1.6.5 Rebuilding 27
1.6.6 Refinement 27
1.6.7 Validation of the Model 28
1.6.7.1 Resolution 28
1.6.7.2 R-factor 29
1.7 Aims 29
1.8 References 30

Chapter 2 The X-Ray Crystal Structures of rsAPX and the rsAPX/NO and rsAPX/CN Complexes 39

2.1 Introduction 40

2.1.1 Crystal Structures of Peroxidases 40

2.1.2 Hydrogen Peroxide Binding and Compound I Formation 41

2.1.3 Aims 43

2.2 Results 44

2.2.1 Isolation and Purification of rsAPX 44

2.2.2 Crystallisation 45

2.2.2.1 Initial Experiments 45

2.2.2.2 Screens with Homogeneous Protein 46

2.2.3 Crystal Preparation and Data Collection 47

2.2.3.1 Crystal Preparation 47

2.2.3.2 Confirmation of the Binding 48

2.2.3.3 Data Collection 48

2.2.3.4 Data Interpretation 49

2.2.3.5 Refinement 49

2.2.4 Structures 50

2.2.4.1 Overall Structure 50

2.2.4.2 rsAPX Active Site Structure 52

2.2.4.3 Ion Binding Site 52

2.2.4.4 Binding of Ligands 54

2.3 Discussion 55

2.3.1 The rsAPX Structure 55

2.3.1.1 Comparison with rpAPX 55

2.3.2 The rsAPX/CN and rsAPX/NO Structures 55

2.3.2.1 Comparison of the rsAPX/NO and *Cc*P/O_2 Complexes 56

2.3.2.2 Comparison of the rsAPX/NO and HRP/CN Complexes 57

2.4 Conclusions 59

2.5 References 60

Chapter 3 The X-Ray Crystal Structure of the rsAPX/Ascorbate Complex 66

3.1 Introduction 67

3.2 Results 70

3.2.1 Preparation of Crystals and Data Collection 70

3.2.1.1 Crystal Soak 70

3.2.1.2 The Binding of Ascorbate 70

3.2.1.3 Data Collection 70

3.2.1.4 Data Interpretation 71

3.2.1.5 Data Refinement and Rebuilding 71

3.2.2 The X-Ray Crystal Structure 71

3.2.2.1 Overall Structure 71

3.2.2.2 Ion Binding Site 72

3.2.2.3 Ascorbate Binding 73

3.3 Discussion 75

3.3.1 The Role of Individual Residues in Ascorbate Binding 75

3.3.2 Ion Binding Site 75

3.3.2.1 Comparison with *Cc*P 77

3.3.3 Comparisons with Other Peroxidases 78

3.3.3.1 Comparison with *Cc*P 78

3.3.3.2 Comparison with MnP 82

3.4 Conclusions 84

3.5 References 85

Chapter 4 X-Ray Crystal Structure of the rsAPX/SHA Complex 88

4.1 Introduction 89

4.1.1 Aims 90

4.2 Results 91

4.2.1 UV-Visible Absorption Spectra 91

4.2.1.1 Steady State Kinetics 91

4.2.1.2 Is SHA a Substrate? 92

4.2.1.3 Equilibrium Binding Constants 93

4.2.2 Data Collection and Preparation of the Crystals 94

4.2.2.1 Crystal Soaks 94

4.2.2.2 Co-Crystallisation 95

4.2.2.3 Data Collection 96

4.2.2.4 Data Interpretation 96

4.2.2.5 Refinement and Rebuilding 96

4.2.3 The rsAPX/SHA Complex 97

4.2.3.1 Overall Structure 97

4.2.3.2 Cation Site 98

4.2.3.3 SHA Binding 98

4.3 Discussion 100

4.3.1 Steady State Kinetics and Dissociation Constants 100

4.3.2 Comparison with Other Peroxidases 100

4.3.2.1 Comparisons with HRP (class III) and ARP (class II) 101

4.3.2.2 Comparison with Myeloperoxidase 105

4.3.2.3 Comparison with C*c*P (class I) 105

4.3.3 Comparison with the rsAPX/Ascorbate Structure 106

4.3.4 Mechanism of Proton Transfer 106

4.4 Conclusions 109

4.5 References 110

Chapter 5 Towards Enhanced Aromatic Oxidation in rsAPX 112

5.1 Introduction 113

5.1.1 Background 113

5.1.2 Population Genetics 114

5.1.3 Evolution in the Laboratory 116

5.1.4 Direct Evolution of Enzymes 116

5.1.4.1 The Screen 118

5.1.4.2 The Mutagenesis Step 118

5.1.4.3 DNA Shuffling 120

5.1.5 Directed Evolution of Heme Enzymes 121

5.1.5.1 Peroxidases 121

5.1.6 Aims 122

5.2 Results and Discussion 123

5.2.1 Screen for Directed Evolution 123

5.2.1.1 DAB Screen 123

5.2.1.2 Guaiacol Screen 124

5.2.2 DNA Library Preparation 125

5.2.2.1 Random Mutagenesis by DNA Repair Pathway Deficient *E. coli* 125

5.2.2.2 Random Mutagenesis by PCR 127

5.2.2.3 Saturated Point Mutagenesis 128

5.3 Conclusions 130

5.4 References 131

Chapter 6 Experimental 136

6.1 General Experimental 137

6.1.1 Materials and Stock Solutions 137

6.1.2 UV-Visible Spectroscopy 137

6.1.3 Protein Expression 137

6.1.4 Protein Isolation and Purification 138

6.1.4.1 Cell Lysis 138

6.1.4.2 Nickel Resin Column 138

6.1.4.3 Reconstitution 139

6.1.4.4 FFQ Column 140

6.1.5 Polyacrylamide Gel Electrophoresis (SDS-PAGE) 140

6.2 X-Ray Crystal Structures of rsAPX 142

6.2.1 FPLC and Purity of rsAPX 142

6.2.2 Crystallisation 142

6.2.3 Crystal Soaks 145

6.2.5 The Binding of Cyanide (in mother liquor) 146

6.2.6 Data Collection and Interpretation 146

6.3 rsAPX/Ascorbate Complex 147

6.3.1 Crystal Soak 147

6.3.2 Confirmation of Ascorbate Binding 147

6.4 rsAPX/SHA Complex 148

6.4.1 Crystal Soak 148

6.4.2 Co-Crystallisation 148

6.4.3 Steady State Kinetics 148

6.4.4 Equilibrium Dissociation Constants 149

6.5 Directed Evolution 151

6.5.1 DNA Preparation 151

6.5.2 Sequencing of DNA 151

6.5.3 Guaiacol Screen 151

6.5.4 Transformation of the rsAPX Vector into Top 10 Cells 152

6.5.5 Random Library Generation using XL1-Red Competent Cells 152

6.5.6 Transformation of a DNA Library to a Protein Library 153

6.5.7 Random Mutagenesis by PCR 154
6.5.7.1 Primer Design 154
6.5.7.2 Mutagenesis 155
6.5.8 Saturated Point Mutagenesis 156
6.5.8.1 Primer Design 156
6.5.8.2 Mutagenesis 157
6.5.9 Agarose Gel Electrophoresis 158
6.6 References 159

Appendix I

Publications V

Abbreviations

Amino Acids are abbreviated according to the three-letter codes recommended by the I. U. P. A.C. Joint Commission on Biochemical Nomenclature (1985).

Enzymes

APX	ascorbate peroxidase
rpAPX	recombinant cytsolic pea ascorbate peroxidase
rsAPX	recombinant cytsolic soybean ascorbate peroxidase
ARP	*arthromyces ramosus* peroxidase
C*c*P	cytochrome *c* peroxidase
CP	catalase-peroxidase
DNase	deoxyribonuclease
HP I	hydroperoxidase I
HP II	hydroperoxidase II
HRP	horseradish peroxidase
MnP	manganese peroxidase
MAO	monoamine oxygenase
RNase	ribonuclease

Chemicals

ABTS	2,2'-azino,di(3-ethyl-benzothiazoline-6-sulfonic acid)
Amp	Ampicillin
BHA	benzhydroxamic acid
C	cytosine
DAB	3,3'-diaminobenzalidine
DNTB	5,5'-dithiobis(2-nitrobenzoic acid)
dNTPs	deoxynucleotide triphosphates
EDTA	ethylenediaminetetraacetic acid
FA	ferulic acid
G	guanine
Hepes	N-2-hydroxyethylpiperazine-N'-2-ethanesufonic acid

IPTG	isopropyl-β-D thiogalactopyanoside
Kan	kanamycin
NTA	nitrilotriacetic acid
PEG 4000	poly (ethylene glycol) of average molecular weight 4000
SDS	sodium dodecyl sulfate
SHA	salicylhydroxamic acid
T	thymine
Tris	trizma base (tri[hydroxymethyl]aminomethene)
X-gal	5-bromo-4-chloro-3-indolyl β-D-galoside

Techniques

ENDOR	electron nuclear double resonance
EPR	electron paramagnetic resonance
EXAFS	extended X-ray absorption fine structure
FPLC	fast protein liquid chromatography
LB	Luria-Bertani broth
NMR	nuclear magnetic resonance
PAGE	polyacrylamide gel electophoresis
PCR	polymerase chain reaction
Rz	Reinheitzahl
StEP	staggered extension process
UV	ultra violet
Vis	visible

Units/Symbols

A	absorption
ε	absorption coefficient
Å	Ångström (1 Å = 10^{-10} m)
K_a	association constant
θ	Bragg angle
°C	degrees Celsius

°	degrees
K_d	dissociation constant
d	distance between lattice planes
$\overline{Y}$	fractional saturation
g	grams
μ	ionic strength
kDa	kilo Daltons
l	litres
m	metres
min	minutes
M	molar
rpm	revolutions per minute
s	seconds
V	volts
λ	wavelength
w/v	weight per volume
n	whole number

Miscellaneous

DNA	deoxyribonucleic acid
E. coli	*Escherichia coli*
ESRF	European Synchrotron Research Facility
FFQ	fast flow Q Sepharose
I. U. P. A.C.	International Union of Pure and Applied Chemistry
MDL	Molecular Dimensions Ltd
PDB	Protein Data Bank
PNCL	Protein and Nucleic Acid Chemistry Laboratory
r.m.s.	root mean squared
RNA	ribonucleic acid

Chapter 1

Introduction

1.1 Heme

Metal ions are used extensively in biological systems and it is well known that the reactivity of a metal ion, or of a metal complex, can be greatly altered by incorporation into a protein structure. A metal complex that is used for various functions in a wide variety of proteins is the iron complex of protoporphyrin IX (Figure 1.1A). Protoporphyrin IX consists of four pyrrole rings joined by methene bridges in a conjugated system. Technically, ferriprotoporphyrin IX (iron III) is hemin and ferroprotoporphyrin IX (iron II) is heme; however since the heme iron used in proteins can have many oxidation states, any form of iron-containing protoporphyrin IX is usually denoted heme and the oxidation state is given. The overall charge of ferriprotoporphyrin IX is +1.

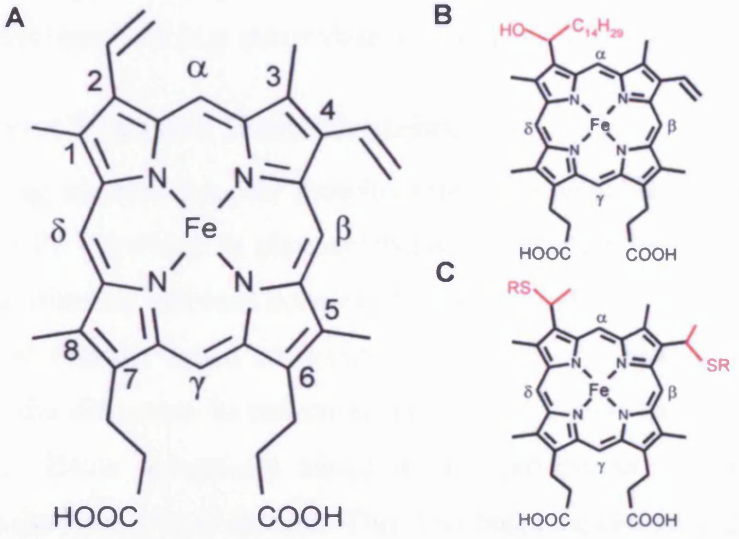

Figure 1.1: Three types of heme. The methene bridges are designated α, β, γ and δ. **(A)** Iron complex of protoporphyrin IX (heme) with the nomenclature used in this thesis. **(B)** Modified heme found in cytochromes of class *a*. **(C)** Modified heme found in cytochrome *c*s. The side chain R is an aliphatic group. The modifications to the side groups are highlighted in red for B and C.

1.2 Heme Proteins

A wide variety of proteins incorporate the heme complex into their overall structure and yet their biological functions are very diverse. There are several variables that are known to influence the function of a heme enzyme, including altering the side groups on the heme, *i.e.* by a covalent link to the protein (myeloperoxidase) or by changing the exact structure of the prosthetic heme group (Figure 1.1B and C). Another way is by changing the identity of the axial ligands that occupy the 5th and 6th coordination positions of the iron (Figure 1.2). The ligands at these positions can

affect the spin state of the iron: strong field ligands lead to low spin heme and weak field ligands have high spin heme. In addition, the solvent accessibility, the polarity of the heme environment, and the coordination number of the iron also affect the function of the enzyme.

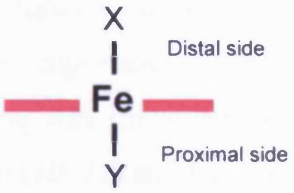

Figure 1.2: Heme. X and Y represent the 5th and 6th ligand respectively. The pink lines represent the heme group.

Heme enzymes can be grouped into three categories: electron transfer (*e.g.* cytochrome *c*), oxygen transport and storage (*e.g.* haemoglobin), and reduction-oxidation (redox) catalysis (*e.g.* peroxidases). These are discussed below.

1.2.1 Electron Transfer Heme Proteins

Heme-containing electron transfer proteins undergo reversible oxidation/reduction and are especially important in photosynthesis and respiration. Electron transport depends on the distance involved between the protein and substrate, and whether the electrons travel through space or bonds. The rate of electron transfer is also influenced by the difference in reduction potentials between the electron acceptors and donators. Heme groups are suited to this process as the electron can be delocalised in the porphyrin π–system. This distributes the charge and minimises the amount of local reorganisation in the heme. Heme reduction potentials can be altered to between –400 and +400 mV by binding to a particular protein, thus making it possible to speed up electron transfer. The protein affects this by alterations in ligation of the heme (*1-3*), orientation of the heme (*4*), the identity of the 5th and 6th ligands and their hydrogen bonding (*5-7*), and the orientation of the heme vinyl groups (*8*) (Figure 1.1).

1.2.2 Oxygen Storage and Transport Proteins

The primary class of heme proteins used to regulate oxygen in biological systems is the globin group. Globins are found in animals, insects, fungi, bacteria and plants, and they too can provide an insight into how protein structure affects the chemistry of the heme molecule. The globins bind oxygen at the distal side of the iron (Figure

1.2) using the residue equivalent to His64 in sperm whale myoglobin (Figure 1.3). Conserved histidine and valine residues close to the active site control the way small molecules bind to the iron.

Substitution of this distal histidine in sperm whale, human and pig myoglobins by site-directed mutagenesis has enhanced the understanding of the oxygen binding process and has emphasised the importance of this residue (*9, 10*). This distal histidine has been substituted by Ala (in sperm whale (*10, 11*) and human (*9*) myoglobin), Gly (in sperm whale (*10, 12*) and human (*9*) myoglobin), Gln (in sperm whale myoglobin (*10, 12*)), Ile (in sperm whale (*9*) and human (*9*) myoglobin), Met (in sperm whale myoglobin (*12*)), Phe (in sperm whale myoglobin (*11, 12*)), Tyr (in sperm whale myoglobin (*13*)), Trp (in sperm whale myoglobin (*9*)), Arg (in sperm whale myoglobin (*12*)), Asp (in sperm whale myoglobin (*12*)), Val (in sperm whale (*10, 11*), pig (*14*) and human (*9*) myoglobin), Leu (in sperm whale (*10, 11*) and human (*9*) myoglobin) and Thr (in sperm whale myoglobin (*10, 11*)). All site directed mutagenesis at this site decreases the affinity for oxygen but the decrease depends on the ability of the residue to act as a proton donor to the oxygen and therefore stabilise the polar iron oxygen complex.

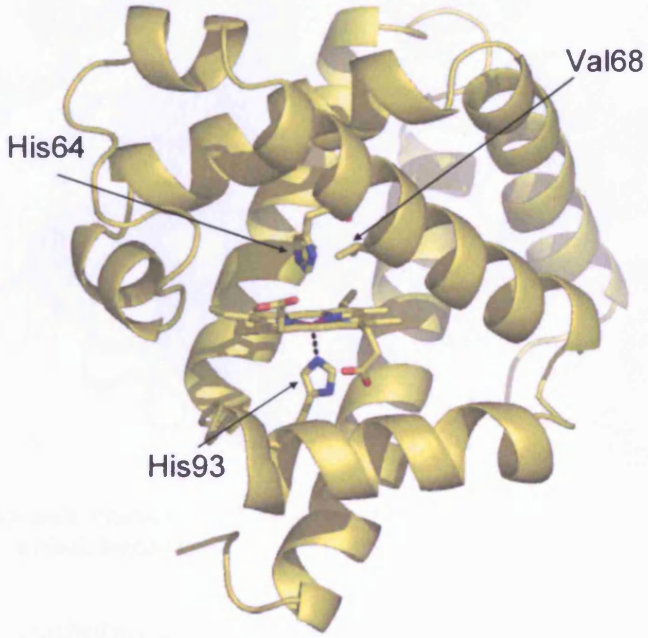

Figure 1.3: Overall structure of sperm whale myoglobin (*15*). The iron-nitrogen coordination bond is represented by a black dashed line.

1.2.3 Reduction-Oxidation Proteins

Redox heme proteins are used to reduce and oxidise a variety of substrates. In particular, monooxygenases oxidise a substrate by incorporating an atom from molecular oxygen (Equation 1.1 , S = substrate) (*16, 17*).

$$SH + O_2 + 2e^- + 2H^+ \xrightarrow{\text{monooxygenase}} SOH + H_2O \qquad \ldots(1.1)$$

A common type of monooxygenase is the cytochrome P450 family of enzymes, which are found in most life forms. These enzymes are five coordinate with the fifth ligand being a cysteine residue. In comparisons with myoglobin, it was found that the thiolate ligand gives the heme in P450 a lower affinity for anionic ligands due to its electron releasing character (*1, 18*) (Figure 1.4).

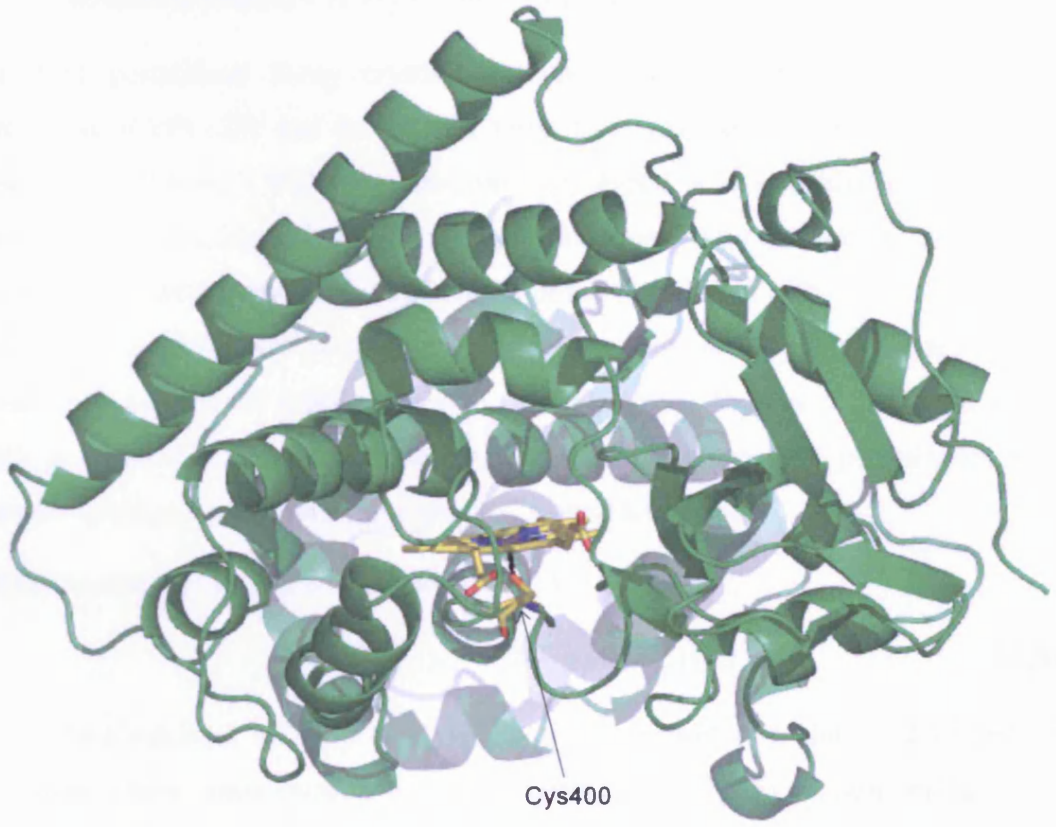

Figure 1.4: Overall structure of cytochrome P450 (*19*). The iron-thiolate coordination bond is represented by a black dashed line.

For the redox enzymes, access to the iron by a substrate is very important and so, for example, P450 enzymes have a weak 6th ligand while peroxidases are predominately 5-coordinate. Heme peroxidases are another major group of redox heme enzymes. They catalyse the reduction of hydrogen peroxide and are found in most biological

systems. The next two sections of the Introduction will concentrate on this family of enzymes.

1.3 Heme Peroxidases

Peroxidases are used for a variety of purposes in biology. For example, lignin degradation (lignin and manganese peroxidases) (*20, 21*), hydrogen peroxide removal in eye disease (*22*) or in plants (ascorbate peroxidase (*23, 24*)), antibacterial (myeloperoxidase (*25*) and lactoperoxidase (*26*)) and hormone synthesis (thyroid peroxidase (*27*)). All heme peroxidases reduce hydrogen peroxide and oxidise a substrate; the substrate can be from a wide variety of inorganic and organic compounds (Equation 1.2).

$$2\,\text{substrate (reduced)} + H_2O_2 \xrightarrow{\text{peroxidase}} 2\,\text{substrate (oxidised)} + 2\,H_2O \quad \ldots(\mathbf{1.2})$$

The first peroxidase X-ray crystal structure to be solved was cytochrome *c* peroxidase (C*c*P) (*28*) and for several years this was the only peroxidase crystal structure available. Welinder therefore developed a classification system for peroxidases and catalases based on structure and function so that the 3D structure of an enzyme could be approximated from its primary sequence (*29*). This system was based on the yeast CcP structure (*30*) and was validated by partial data on the horseradish peroxidase (HRP) structure (*31, 32*) which became available in 1991-1993, and later by other peroxidase structures. From this system, peroxidases were grouped into three superfamilies: catalases, animal and plant.

Catalases catalyse the reaction in Equation 1.3.

$$2\,H_2O_2 \xrightarrow{\text{catalase}} O_2 + 2\,H_2O \quad \ldots(\mathbf{1.3})$$

Some heme catalases will also catalyse the peroxidase reaction and similarly certain peroxidases have some catalase activity. Heme catalases also contain similar heme prosthetic groups to peroxidases, and because of this and the crossover in activities they are classified as part of the peroxidase group. However, studies of the two known crystal structures (*33, 34*) and primary sequence analysis show that they form a separate superfamily within the group.

The animal peroxidase superfamily includes myeloperoxidase, lactoperoxidase, thyroid peroxidase and eonisophil peroxidase (*35*). They contain similar helices to

the plant peroxidases in the region binding the heme (*36*), but the crystal structures of myeloperoxidase (*37*) and prostaglandin H synthase (*36*), as well as sequence correlations (*38*), indicate that animal and plant peroxidases are separate superfamilies.

1.4 Plant Peroxidases

1.4.1 Classification

Fungal, bacteria and plant peroxidases form the plant peroxidase superfamily (*39*). They catalyse the oxidation of a wide variety of substrates, from small inorganic ions (e.g. manganese peroxidase) to large proteins (e.g. cytochrome *c* peroxidase).

Each member of the plant peroxidase superfamily contains 10 α-helices connected by amino acid chains of various lengths (Figure 1.5).

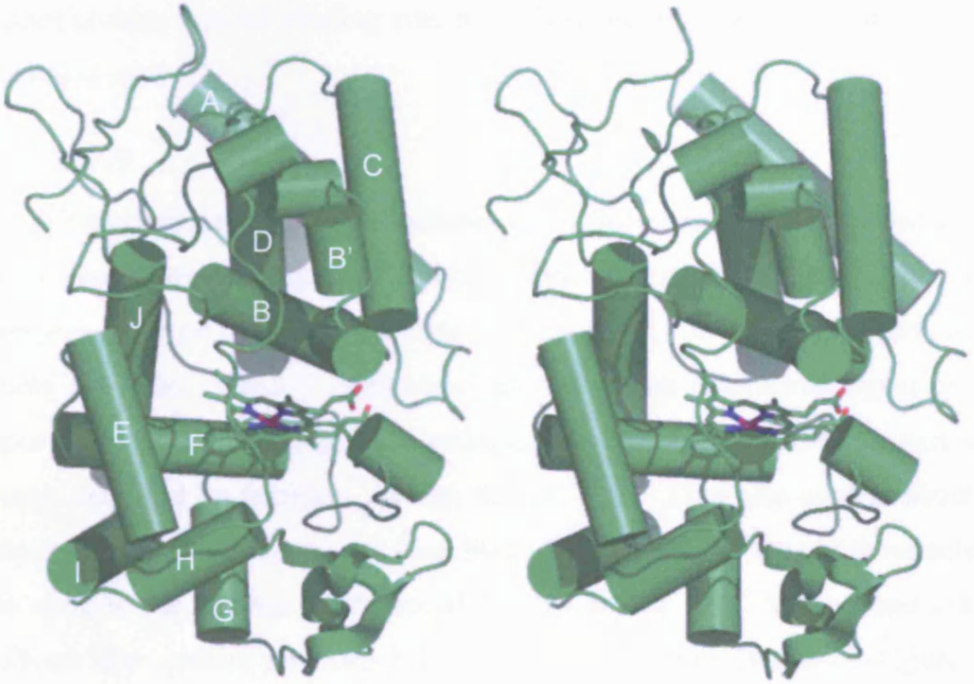

Figure 1.5: Stereo representation of *Cc*P with the 10 α-helices labelled A to J (*40*). B' is only found in class I and class II peroxidases.

The heme is located between helices B and F in the plant peroxidase and there are nine invariant residues in the plant peroxidase family. In *Cc*P, these conserved residues are:- Arg48 and His52 in helix B, Asn82 on the distal side of the heme, Val169 and His175 in helix F, Asp235 on the proximal side of the heme, Asp106 in

helix D, Gly129 and Arg130. His175 is the fifth ligand of the heme iron, and is hydrogen bonded to Asp235.

The plant peroxidase superfamily can be subdivided into three classes (*29*):

I. Intercellular peroxidase of prokaryotic origin
II. Secretory fungal peroxidase
III. Secretory plant peroxidase

1.4.1.1 Class I

Examples of Class I peroxidases for which crystal structures are available are yeast C*c*P (*28*), bacterial catalase-peroxidase (*41-44*) and (both chloroplastic (*45, 46*) and cytosolic (*47*)) APX. Class I peroxidases have no carbohydrate, no cysteine bridges, no calcium ions and no signal peptide for secretion. Bacterial catalase-peroxidases are approximately double the molecular weight of C*c*P due to gene duplication (*41*). APX does contain a metal binding site, but it is thought to contain a potassium and not a calcium ion (*47*).

1.4.1.2 Class II

Lignin (*48*) and manganese (*49*) peroxidases from *Phanerochaete chrysosporium* and ink cap mushroom peroxidase from *Coprinus cinereus* (alternative name *Arthromyces ramosus*) (*50*) are examples of this class, for which there are crystal structures available. Class II peroxidases all contain an N-terminal signal peptide sequence for secretion through the endoplasmic reticulum (a tubular part of a eukaryotic cell used for transport through the cell (*51*)). They also contain about 5% carbohydrate, two calcium ions and four disulfide bridges (*29*). One of these calcium sites is close to the location of the metal binding site in APX. Class I and class II peroxidases also contain an extra helix B' between helices B and C (Figure 2.1) which is not present in class III.

1.4.1.3 Class III

In 1810, horseradish peroxidase (HRP) was the first peroxidase to be discovered (*39*). Crystal structures have subsequently been published for horseradish (*52*), peanut (*53*) and barley (*54*) peroxidases from class III. These peroxidases contain two calcium ions, four sulfide bridges, a terminal signal peptide for secretion, and

extra helices used to modify access to the heme edge (*29*) (Figure 1.6, helices D', F' and F").

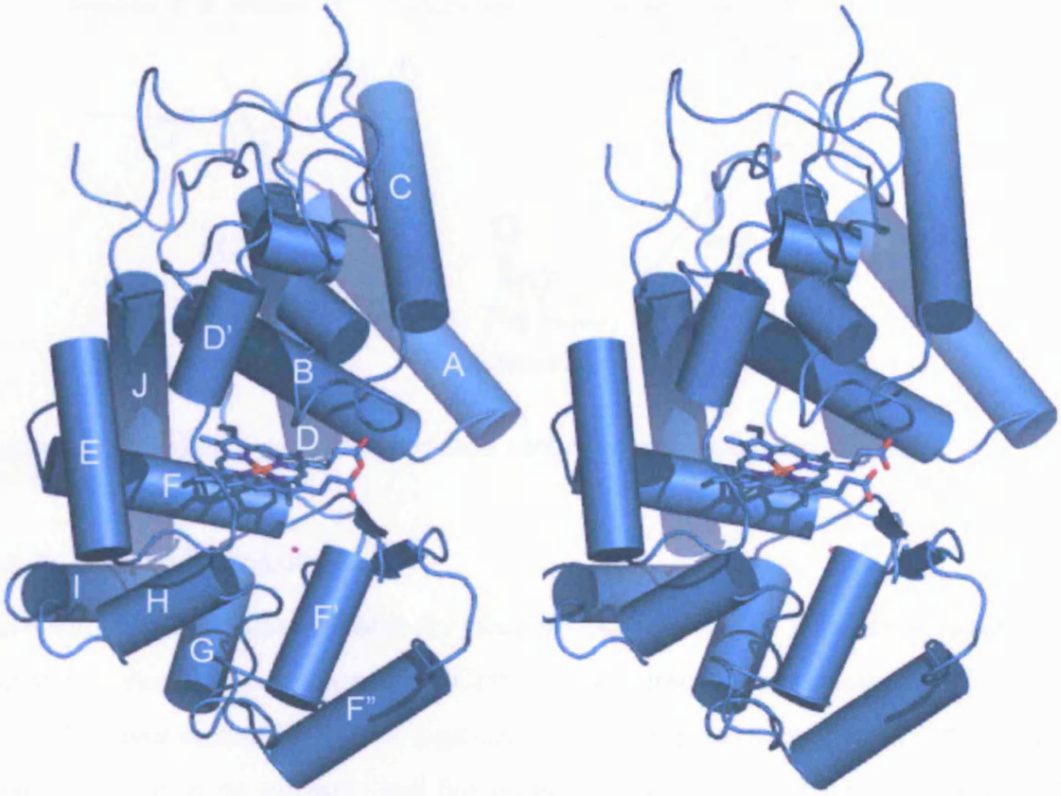

Figure 1.6: Stereo representation of HRP (*54*) with the 10 common peroxidase α-helices labelled A to J. D', F' and F" are only found in class III peroxidases. Calcium ions are represented by pink spheres.

This classification system provides a basis to order existing knowledge and predict unknown properties within the plant peroxidase superfamily.

1.4.2 The Catalytic Cycle

The catalytic cycle is common to all types of heme peroxidase (Figure 1.7). The transfer of two electrons to hydrogen peroxide from the ferric enzyme forms Compound I in the first step. The iron is in the ferryl state, and a radical is formed on the porphyrin ring or an amino acid in Compound I (*55*). This intermediate is reduced by a substrate in two single-electron transfers, the first of which produces Compound II, a ferryl-oxo complex. Compound II is then reduced by the second electron to return it to the ground state. The reduction of Compound II is usually the rate-limiting step in the cycle.

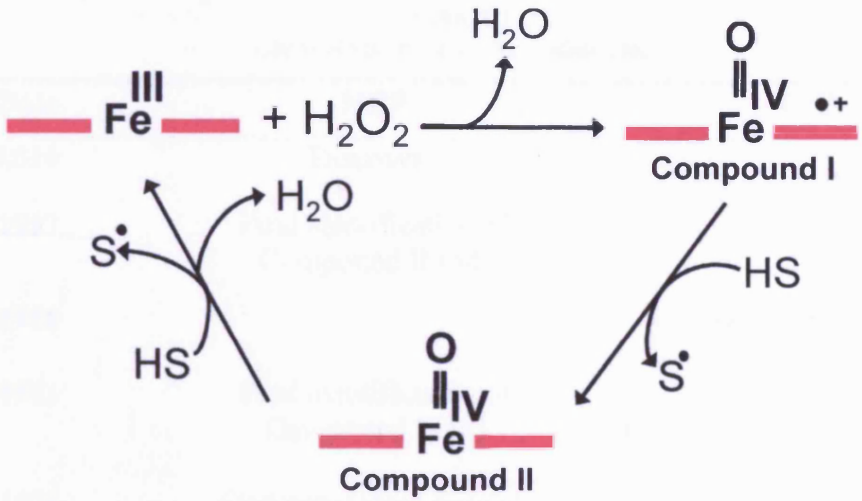

Figure 1.7: The catalytic cycle of a peroxidase. SH represents reduced substrate and $S^{\bullet}$ represents oxidised substrate.

1.4.3 Model Peroxidases

Most of the information available for plant peroxidases comes from the study of two enzymes, cytochrome *c* peroxidase (C*c*P) and horseradish peroxidase (HRP) (Table 1.1). However neither is ideal as a general model for peroxidases, since C*c*P utilizes a large protein as its substrate and has an atypical Compound I structure, and HRP contains disulfide bonds, calcium ions and has carbohydrate attachments. The biological role of HRP is also not known and neither is the biological substrate.

Table 1.1
Chronology of Early Peroxidase Data.

Date	HRP	CcP
1810	Discovery	
1937	First identification of Compound II (*56*)	
1940		Discovery (*57*)
1941	First identification of Compound I (*58*)	
1976	First peroxidase primary sequence (*59, 60*)	
1980		Primary sequence (*61*)
1980 and 1984		The first peroxidase X-ray crystal structure (*28*)
1986 and 1987		Recombinant enzyme expressed in yeast (*62*) and *Escherichia coli* (*63*)
1992		Structure used to classify the peroxidase family (*29*)

1.4.3.1 Evidence for the Structure of Compound I and II

Although Compound I for HRP was first discovered in 1941 the basic structure was not elucidated until some 30 years later. The UV-visible spectrum changes from the native protein to Compound I with a decrease in the Soret absorbance and new peaks appearing in the 500-700 nm region (Figure 1.8A). HRP Compound I was shown to contain a porphyrin π-cation radical: the evidence for this comes from electron paramagnetic resonance (EPR) (*64, 65*), ENDOR (*66*), NMR (*67*), and resonance Raman spectroscopy (*68*). Self-consistent-field theoretical calculations (*69*) used to calculate spin densities for the iron also indicate a porphyrin π-cation radical.

In C*c*P the EPR spectrum for Compound I indicated that the radical was not on the porphyrin (*70*). Site-directed mutagenesis (*71*) and ENDOR studies (*72, 73*) eventually led to the identification of Trp191 as the site of the radical. The Compound I spectra of C*c*P looks like the Compound II of other peroxidases with a

shift in the Soret peak to 420 nm and no decrease in intensity of the Soret peak (Figure 1.8B).

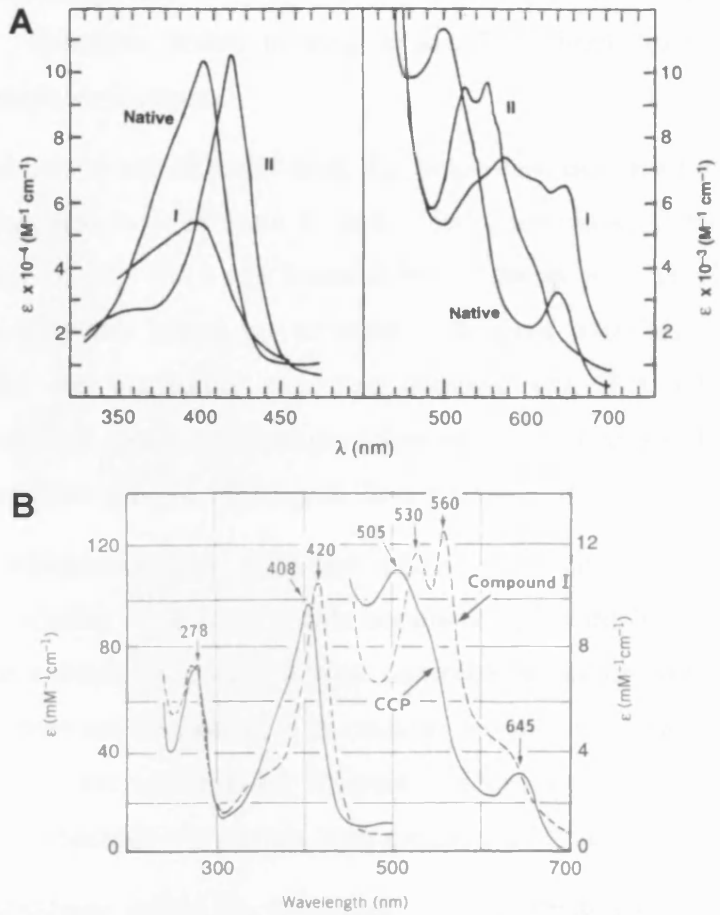

Figure 1.8: (A) Spectra of HRP: native, Compound I and Compound II (*74*). **(B)** Spectra of C*c*P: native (indicated by a solid line) and Compound I (indicated by a dashed line) (*75*).

1.4.3.2 Expression

In 1987 C*c*P was expressed and purified from *Escherichia coli* (*E. coli*) making mutagenesis possible and allowing preparation of larger quantities of enzyme. However, HRP was harder to express since it contains glycosylation sites and disulfide bridges which can not be processed in *E. coli*. It is possible to express HRP in *E. coli* but the protein has to be refolded and the heme added after extraction, and the resulting yields are low (*76, 77*). HRP has also been expressed using a baculovirus transfer vector in insect tissue culture, which produces a fully functional protein (*78*).

1.4.4 Bacterial Catalase-Peroxidases

The high sequence homology between C*c*P, ascorbate peroxidase (APX) and bacterial catalase-peroxidases led to the designation of class I (prokaryotic origin) peroxidases. Therefore, before moving on to APX a brief description of bacterial catalase-peroxidases is given.

Catalase-peroxidases are different from the heme catalases described earlier. They were first identified in 1979 from *E. coli*. Hydroperoxidase I (HP I) was isolated from bacteria (*79, 80*). HP I was found to be a tetramer with a molecular weight of 337,000 and only two hemes per tetramer. The gene encoding HP I, (*katG*) was identified and the nucleotide sequence obtained (*81, 82*). Catalase-peroxidase enzymes were also found in *Rhodopseudomonas capsulate* and the term catalase-peroxidase was first used in referring to these enzymes (*83*).

Normal peroxidases contain ~250-350 amino acids but the subunit of catalase-peroxidases contains ~730 amino acids because of gene duplication (*84*). The two halves of the subunit each have a high sequence homology with C*c*P but the C-terminal half does not bind heme. The catalase-peroxidases range in size from one to four subunits and are active under different conditions to catalases (*83*). This may account for why bacteria can contain both catalases and catalase-peroxidases (*85-90*).

Catalase-peroxidases may be important in the treatment of tuberculosis as *Mycobacterium tuberculosis* which have low catalase-peroxidase activity are resistant to isoniazid (an antibacterial drug used in tuberculosis treatment) (*91*). Catalase-peroxidases from *Mycobacterium tuberculosis* and a mutant from isoniazid resistant strains have been cloned in *E. coli* and characterized (*92, 93*). Both of these enzymes have high catalase activity and a broad peroxidase specificity (*92, 93*). Catalase-peroxidase is thought to activate isoniazid by either directly oxidizing it or by oxidizing Mn^{2+} which can react with isoniazid (*94*). *Mycobacterium tuberculosis* catalase-peroxidase has been crystallized (*44*) and isoniazid modelled into the δ-heme edge based on the NMR distances of isoniazid bound HRP (*94*) (Figure 1.9).

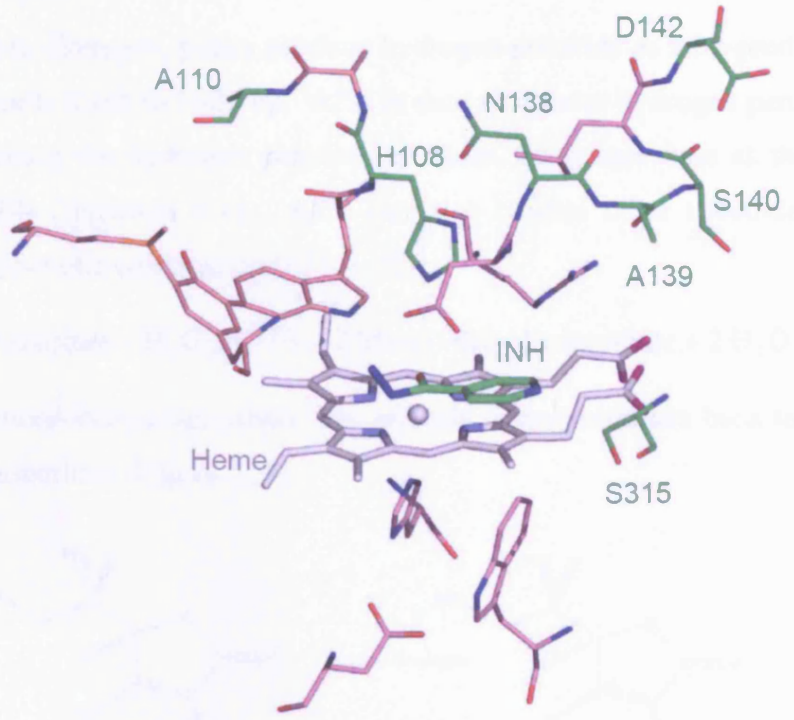

Figure 1.9: Model of isoniazid (green) bound to catalase-peroxidase showing the residues that are mutated in clinically isoniazid resistant mutants in green (*44*).

1.5 Ascorbate Peroxidase

Ascorbate peroxidase (APX) was discovered in 1979 but the enzyme was not isolated in a highly purified form until 1989. Because of this, there is not as much information available for APX as for C*c*P. APX is a class I enzyme found in plant chloroplasts, plant cytosol and nitrogen-fixing root nodules (*95*). Cytosolic APX enzymes have been isolated from pea (*23, 24, 96, 97*), Japanese radish (*98*), soybean (*99*), wheat (*100*), potato tubers (*101*), maize (*102*), komatsuna (*103*), tea (*95, 104, 105*), cucumber (*106*), spinach (*107, 108*), bean (*109*), and rice (*110*). Chloroplastic enzymes have been isolated from spinach (*107, 108, 111, 112*), pea (*113, 114*), wheat (*115*), tobacco (*46*) and tea (*95, 104, 116-118*). There are other APX enzymes including those from insects (*119*), bacteria (*120*), algae (*121-123*) and bovine eye (*22*).

APXs from tea leaves (*95, 116*), soybean root nodules (*99*), *E. gracilis* (*121*) and peas (*96, 124, 125*) have been purified and characterised. A few APX enzymes have been expressed in recombinant form, including pea APX (rpAPX) (*124, 125*) and soybean APX (rsAPX) (*126*).

1.5.1 Catalysis

When reducing dioxygen, plants produce hydrogen peroxide as a by-product, which can damage cells if left to build up. APX is used to remove hydrogen peroxide from cells by reducing the hydrogen peroxide to water, using ascorbate as the oxidised substrate (*112*) (Equation 1.4). APX can also oxidise other substrates such as sulfides and phenolic compounds (*127, 128*).

$$2\text{Ascorbate} + H_2O_2 \xrightarrow{APX} 2\ \text{Mono - dehydroascorbate} + 2\ H_2O \quad \textbf{...(1.4)}$$

Two of the mono-dehydroascorbate free radicals disproportionate back to ascorbate and dehydroascorbate (Figure 1.10).

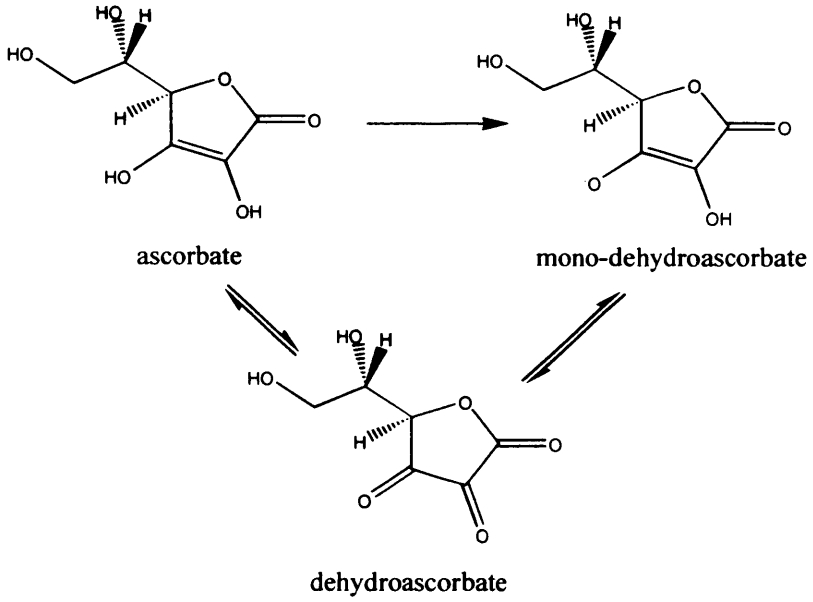

Figure 1.10: Structures of ascorbate, mono-dehydroascorbate and dehydroascorbate.

1.5.2 The X-Ray Crystal Structure of rpAPX

The X-ray crystal structure of rpAPX was solved in 1995 (Figure 1.11A) (*47*) and revealed a non-covalently bound dimer. In fact, there were two dimers in the unit cell which made interpreting the data more difficult. The interpretation of the original X-ray crystal structure data was based on the C*c*P structure and in actual fact, the crystal structure and sequence of rpAPX when compared to C*c*P shows remarkable similarity, confirming that APX is a class I peroxidase of prokaryotic origin (*29*) (Chapter 3, Figure 3.9). APX shares the same protein architecture as other types of peroxidase; *i.e.* it consists of two anti-parallel helices (Figure 1.5, B and F), which contain a heme in the crevice between them.

Figure 1.11: Overall structure of rpAPX (*47*).

Electrospray mass spectrometry of the rpAPX enzyme has revealed a molecular weight of 27,194 ± 3 Daltons which is very close to the predicted weight from the DNA sequence of 27,192.77 Daltons (*129*).

1.5.3 Compounds I and II

The crystal structure shows APX has a tryptophan residue on the proximal side of the heme (Trp179) (Figure 1.12A). The corresponding residue in C*c*P is the site of the Compound I radical but APX has a conventional porphyrin π-cation radical in its Compound I instead of Trp179. This has been shown for pea, soybean and tea APXs using EPR (*130, 131*) and UV-visible (*117, 132, 133*) spectra (Figure 1.12B and C). It has been suggested that the reason APX has a porphyrin π-cation radical is that a potassium binding site found in the pea crystal structure near Trp179 destabilises the tryptophan radical formation (*47*). This idea is discussed further in Chapter 3.

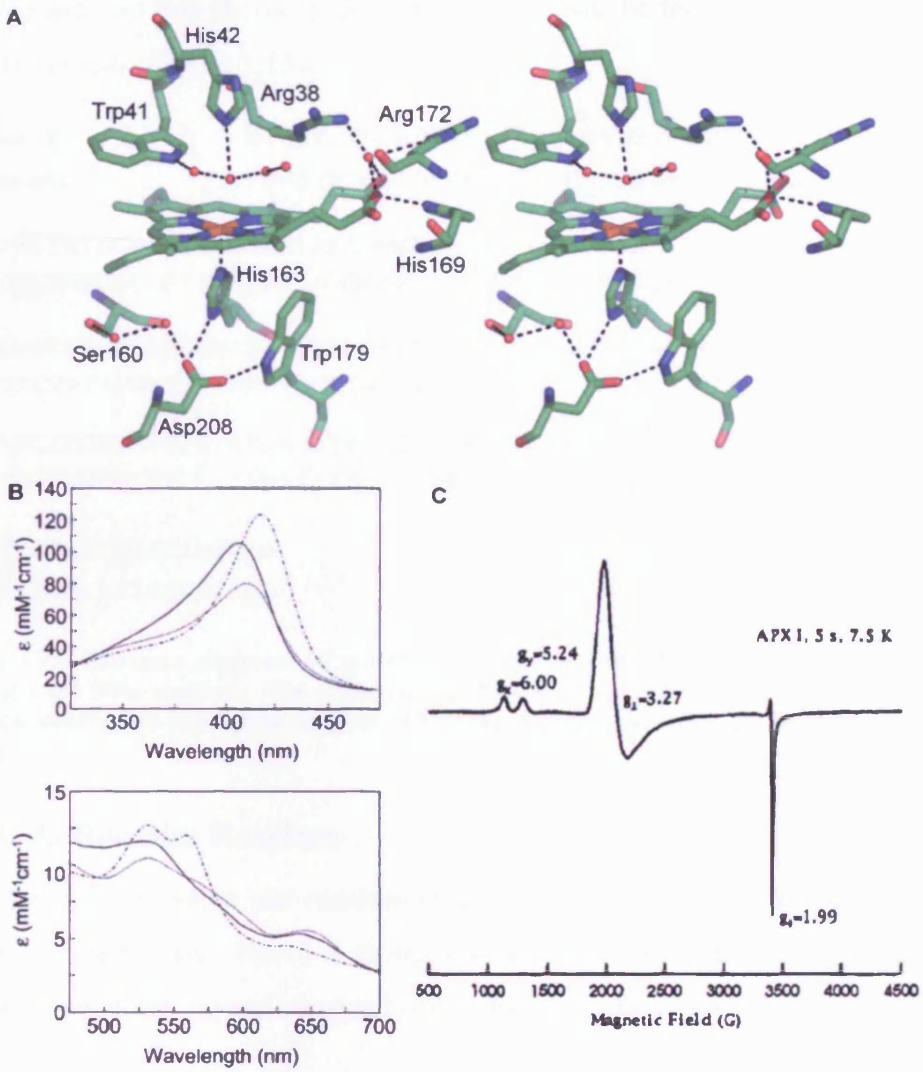

Figure 1.12: (A) Stereo representation of the area around the heme in rpAPX (*47*). Hydrogen and coordination bonds are indicated by black dashed lines, and water molecules by red spheres. **(B)** UV-visible spectra of native (solid line), Compound I (dotted line) and Compound II (dotted and dashed line) rsAPX (*133*). **(C)** EPR of rpAPX Compound I (*130*).

Compound I formation in APX is similar to that of HRP (*132-136*). Despite the similarities between C*c*P and APX, C*c*P reacts very slowly with ascorbate in steady state experiments (*137*). HRP Compound I, however, does react with ascorbate (*39, 138*) but the rate for APX Compound I and ascorbate is much faster (*133, 136*).

1.5.4 APX Sequences

Database analysis retrieved 52 sequences coding for APX (*139*). Sequence analysis of these resulted in seven types of APX. There are five cytosolic APXs (three of these are membrane bound) and two chloroplastic APXs. Key residues are conserved throughout the seven, and they all contain residues for a potassium

binding site. In this thesis rpAPX and rsAPX will be the two enzymes compared most frequently (Figure 1.13).

```
                                1                   20
Soybean APX                     MGKSYPTVSADYQKAVEKAKKKLRGFIAEKRCAPLMLRLAWHSA
Pea APX                         -GKSYPTVSPDYQKAIEKAKRKLRGFIAEKKCAPLILRLAWHSA

                                                   81
GTFDKGTKTGGPFATIKHPAELAHSANNGLDIAVRLLEPLKAEFPILSYADFYQLAGVVAVE
GTFDSKTKTGGPFATIKHQAELAHGANNGLDIAVRLLEPIKEQFPIVSYADFYQLAGVVAVE

                                                   14
VTGGPEVPFHPGREDKPEPPPEGRLPDATKGSDHLRDVFGKAMGLTDQDIVALSGGHTIGAA
ITGGPEVPFHPGREDKPEPPPEGRLPDATKGSDHLRDVFGKAMGLSDQDIVALSGGHTIGAA

                                                   20
HKERSGFEGPWTSNPLIFDNSYFTELLSGEKEGLLQLPSDKALLSDPVFRPLVDKYAADEDA
HKERSGFEGPWTSNPLIFDNSYFTELLTGEKDGLLQLPSDKALLTDSVFRPLVEKYAADEDV

FFADYAEAHQKLSELGFADA
FFADYAEAHLKLSELGFAEA
```

Figure 1.13: Sequence alignment of rpAPX and rsAPX with the differences underlined. The two sequences are 90% identical. The active site residues are highlighted in red. Residues involved in ascorbate binding are highlighted in green and residues involved in potassium binding are highlighted in blue.

1.5.5 Active Site Residues

The roles of key active site residues (Figure 1.12A) have been investigated by site directed mutagenesis. His42 is thought to act as an acid–base catalyst, facilitating the cleavage of the oxygen-oxygen bond in hydrogen peroxide (Figure 1.14) (*134*).

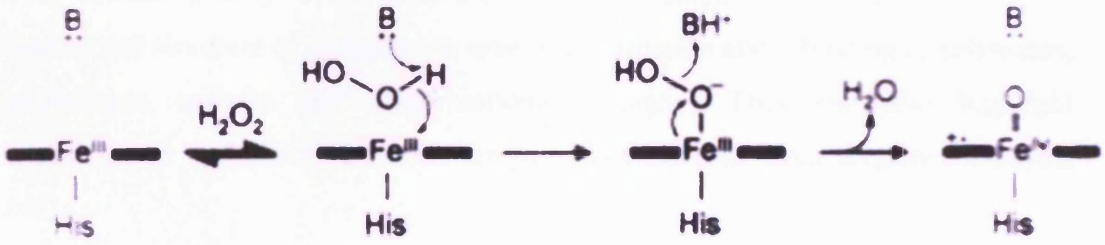

Figure 1.14: Role of the His42 residue in APX (*134*). B represents His42.

Site directed mutagenesis work on His42 by Lad *et al* showed that replacement with an alanine residue gave an inactive enzyme (*134*). However, replacing His42 with a glutamic acid residue created an enzyme with activity that was lower than that of wild type APX (*134*). These results indicated that the residue needs to be a base for enzyme activity.

1.5.6 Substrate Binding

Early work (*140*) showed that APX was capable of the oxidation of two types of substrate: ascorbate and aromatic substrates. Oxidation of aromatic substrates is analogous to that observed in the class III peroxidases. It was of key interest, therefore, to examine these substrate binding interactions in more detail. Two binding sites have been proposed for the substrate. Ascorbate and charged substrates are thought to bind near Cys32 and Arg172. This was concluded from work by Poulos *et al* on a Cys32Ser variant and an enzyme where Cys32 was chemically modified (*136*). The ascorbate binding site is discussed further in Chapter 3.

Aromatic and neutral substrates are thought to bind closer to the heme at a second site (*127, 136*). The second binding site is discussed further in Chapter 4.

1.5.7 Conclusions

APX is a relative newcomer to the peroxidase area and has substrate binding properties that are related to both class I (*e.g.* Cc*P*) and class III (*e.g.* HRP) peroxidases. In this thesis, substrate binding in APX is investigated using X-ray crystallography, kinetics and spectroscopy. Below, the principles of X-ray crystallography are discussed.

1.6 Protein X-Ray Crystallography

X-ray crystallography is the most direct way of imaging molecules. The three-dimensional structure of proteins can give us information about binding of substrates, mechanisms, activity and conformational change. They can also highlight similarities or differences between enzymes not obvious from sequence analysis (*141*).

Optical microscopes can only distinguish objects about 500 nm apart. This is because visible light has a wavelength of between 350 nm and 700 nm, and details can only be resolved if they are more than half a wavelength apart, even if the microscope is ideal. Atoms are between 1 and 2 Å (10 Å = 1 nm) apart if covalently bonded and hydrogen bonds are between 2.5 and 3.5 Å long, and therefore to create an image of atomic resolution an electromagnetic wave of less than a few Ångströms is needed. X-rays have a wavelength of approximately 0.2 to 2.0 Å (*142*).

1.6.1 X-Rays and X-Ray Diffraction

In electromagnetic waves, both electric and magnetic fields vary in a sinusoidal way (Figure 1.15A). The wavelength affects the properties of the waves and their absorption in air and water (Figure 1.15B). At wavelengths of less than 10 Å, air and then water become transparent and at wavelengths below 1 Å other materials become transparent. 'Soft' X-rays have a wavelength of 2 Å and are absorbed by water. In contrast, X-rays of wavelength 0.2 Å are more penetrating, only interacting weakly with matter, and are therefore commonly used for radiography of the human body. Wavelengths of between 0.5 and 1.6 Å are ideal for crystallography as they are penetrating enough to study samples of approximately 1 mm in size but are scattered strongly by matter (*141, 142*).

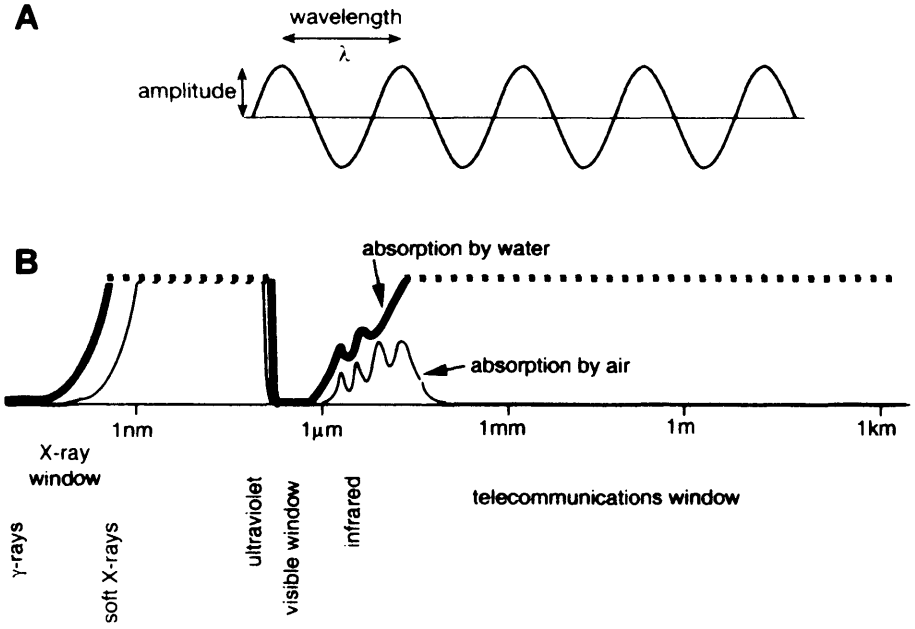

Figure 1.15: (A) Sinusoidal wave with wavelength and amplitude marked (*141*). **(B)** Electromagnetic spectrum with the air and water absorption marked (*141*).

X-ray microscopes are difficult to make for viewing images at a molecular size, since lenses for X-rays of smaller wavelengths have a refractive index close to that of a vacuum, and also because the molecule would be damaged by the X-rays focused upon it. Hence, instead of using a lens in X-ray crystallography a detector connected to a computer records the scattered rays. This means crystallographers have to use indirect methods to work out the phase (the time of arrival of the wave) (*141, 142*).

1.6.1.1 Scattering of X-Rays

Electromagnetic waves also have particle like properties and therefore are photons of a particular energy. If an X-ray photon encounters an electron it may be absorbed and set the electron vibrating at the X-ray frequency. The electron then emits an X-ray photon in a random direction, of the same energy and wavelength as the original X-ray. This is known as coherent scattering and is used in X-ray crystallography. Incoherent scattering is when the X-ray absorption causes transitions within the atom and therefore the photon released is of lower energy. This energy in the atom may leave it in an excited state and may lead to radiation damage. Photons will interact with nuclei but as they are a lot larger the vibration is small and the scattering negligible. Therefore the X-ray crystal structure represents the electron density of the molecule (*141, 142*).

1.6.1.2 Crystals

Crystals are used as they are highly ordered; every molecule is precisely positioned in relation to its neighbour. In X-ray crystallography, crystals are used to overcome the problem of X-rays damaging the molecule, since they contain many molecules and therefore damage to one or two is not as important. Incoherent scattering can totally disrupt molecules but since there are approximately 10^{15} molecules in every crystal many photons can be incoherently scattered before the crystal is destroyed (*141, 142*).

The X-rays used in crystallography are not very penetrating and will only go through a few millimetres of protein or water, therefore the ideal size for a crystal is 0.2-1.0 mm. If the source of X-rays is intense, crystals down to a few microns may be used. At a synchrotron, shorter wavelengths can be used (0.9 or 0.6 Å), making corrections for X-ray absorption in the crystal less important (*141, 142*).

One of the main problems with crystallography is the ability to produce crystals of a certain minimum size and with a high degree of order. Proteins are large molecules with complex irregular surfaces therefore it can be difficult to get a packing of them in a highly ordered lattice. The right environment for these interactions to occur can be found by varying a wide range of conditions in the crystal growth, including protein concentration, pH, temperature and precipitant concentration. The precipitant can be a salt or other chemical such as polyethylene glycol (*141, 142*).

Usually a large range of conditions needs to be applied to find suitable crystals, and for this the vapour diffusion method is used (Figure 1.16). A small drop of protein is placed above a well containing a solution of the precipitant at a certain pH and the system sealed (Figure 1.16A). This method allows small volumes of protein to be used (drops as small as ~0.1 µl with modern robotic techniques) and therefore many conditions can be tried with a small amount of protein. Two approaches are used to grow crystals. If no information is available on which conditions will give crystals, sparse matrix screening can be used. This is a set of solutions which have been used to grow protein crystals in the past. Several of these screens are now available commercially. This hopefully gives a starting point for the second approach, systematic variation of the conditions. If information is available on the crystallising conditions of the protein or a closely related protein, this approach can be carried out from the beginning. A starting point is quasi-crystals or small crystals in the well. The starting conditions can then be systematically varied to try and optimise crystal growth (Figure 1.16B) (*141, 142*).

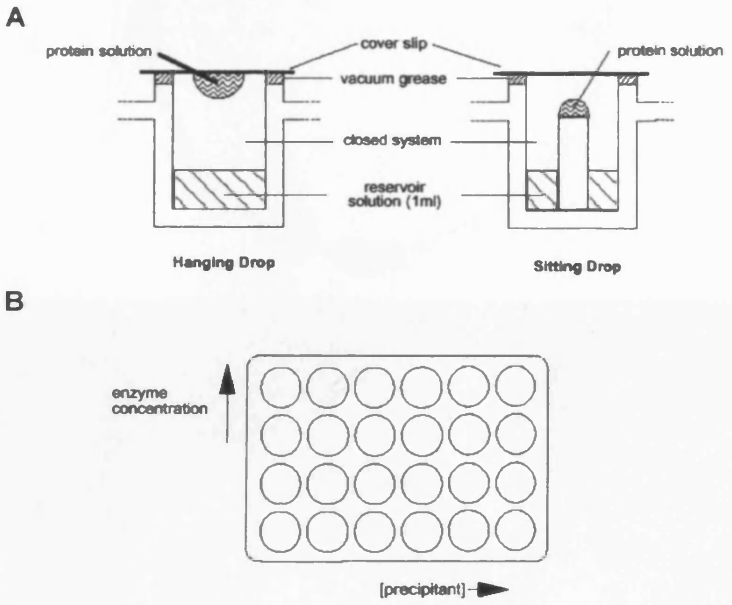

Figure 1.16: Vapour diffusion method. **(A)** Diagram of the wells and drops (*143*). **(B)** Plate of wells with a typical experiment, each row has a different enzyme concentration (e.g. 5, 10, 15 and 20 mg/ml) and each column has a different precipitant concentration (e.g. 0, 5, 10, 15 20, 25%) (*143*).

1.6.1.3 X-Ray Generators

X-rays can be generated in the laboratory by focusing a beam of electrons on a copper anode (X-ray wavelength ~1.54 Å) or molybdenum anode (X-ray wavelength ~0.71 Å) in a vacuum, but a synchrotron provides a more intense source of X-rays (Figure 1.17). Electrons travel on an approximately circular track in a vacuum and are kept at more than 99% of the speed of light by electric fields. When the electrons change direction they emit intense X-ray beams in the tangential direction. Synchrotron sources produce a continuous X-ray spectrum, consisting of all the wavelengths suitable for crystallography experiments (0.5-1.6 Å). In X-ray crystallography, monochromatic X-rays are usually used (*141, 142, 144*).

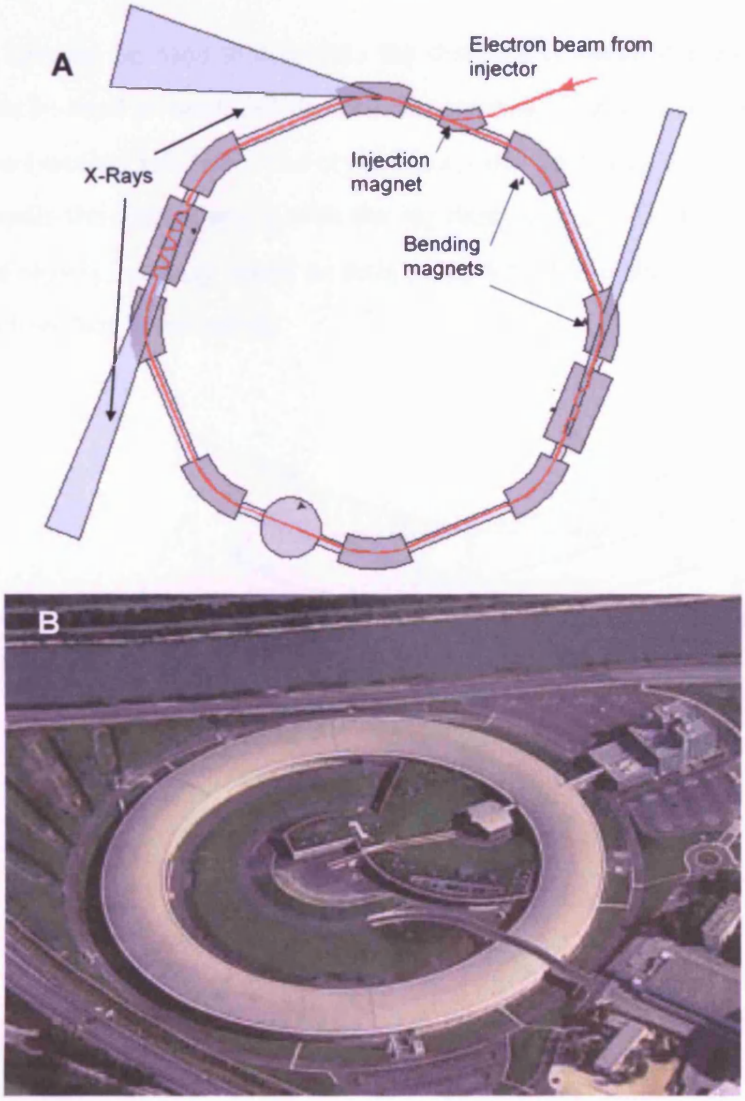

Figure 1.17: (A) Scheme of a synchrotron (*144*). **(B)** The European Synchrotron Research Facility in Grenoble, France (*144*).

1.6.1.4 Bragg's law

A diffraction pattern occurs when there are several identical objects an equal distance apart to diffract the beam, *i.e.* planes in the crystal lattice. When the X-rays are emitted by the electrons in all directions they tend to cancel each other out by having different phases. In one direction however the phase differs by exactly one wavelength and therefore they add up. For waves to interfere constructively, the path difference must be a whole number (n) of wavelengths (λ) (Equation 1.5, where, n is a whole number, λ is the wavelength, d is the distance between lattice planes, and θ is the angle of incidence, and Figure 1.19A) (*145*).

$$n\lambda = d\sin\theta \qquad \textbf{...(1.5)}$$

Bragg's law can be used to calculate the distance between planes (d, Figure 1.19A) which can be used to work out the cell dimensions. The unit cell is the repeat unit of the lattice (section 1.6.3.2). The crystal is rotated so Bragg's reflection can occur as it must make the correct angle with the incident beam (θ, Figure 1.19B). The crystal is rotated slowly, usually about an axis perpendicular to the beam at 1-2 ° intervals, as diffraction data is recorded.

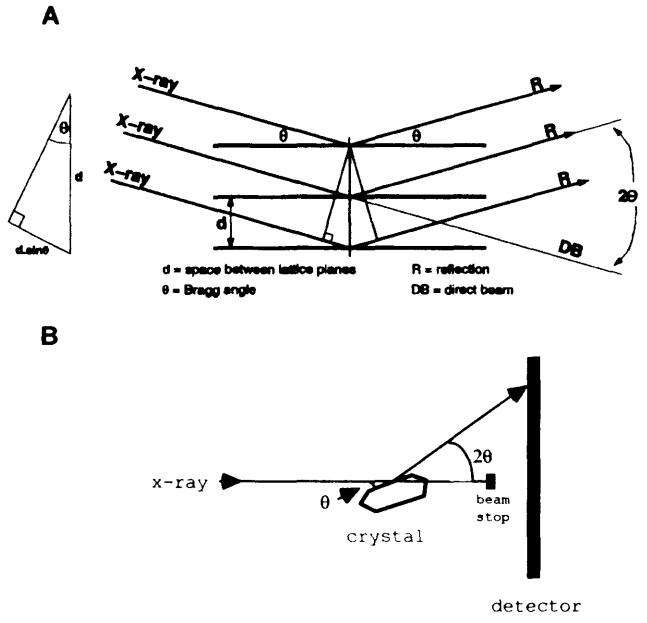

Figure 1.19: Simple diffraction. **(A)** Bragg's law, showing diffraction in phase from a crystal lattice (*143*). **(B)** Crystal diffracting (*143*).

To analysis the diffraction pattern, the crystal has to be a long way from the X-ray source compared to the crystal size, making the beam effectively parallel, and the distance to the detector large in comparison to the crystal size (*141*).

1.6.2 Symmetry of Protein Crystals

The point-symmetry of a protein crystal is defined by the point group – the list of the axes of symmetry in the unit cell. Note that since proteins are made up of chiral amino acids they can only have rotational and translational symmetry and only certain combinations are possible (Figure 1.20A). The lattice has symmetry too and this is called lattice symmetry, wherein the lattice is made up by repeats of the unit cell (Figure 1.20B). The symmetry possibilities of the lattice are restricted by the shape of the unit cell (Figure 1.20C). The rsAPX unit cell is tetragonal as it has one 4-fold axis with c parallel to it, and a and b perpendicular to it. α, β and α are 90° and a and b are of equal length. For other crystal systems see (*141*).

The whole symmetry of the crystal is represented by its space group, which combines the lattice symmetry and the point group. The space group is a list of the rotational axes prefaced by a letter referring to the type of unit cell. For the rsAPX crystals the space group is P 4_2 2_1 2. P refers to the primitive unit cell which is the unit cell with the smallest possible volume. A subscript indicates a screw axis. There are 65 possible space groups for proteins and they are listed in (*146*).

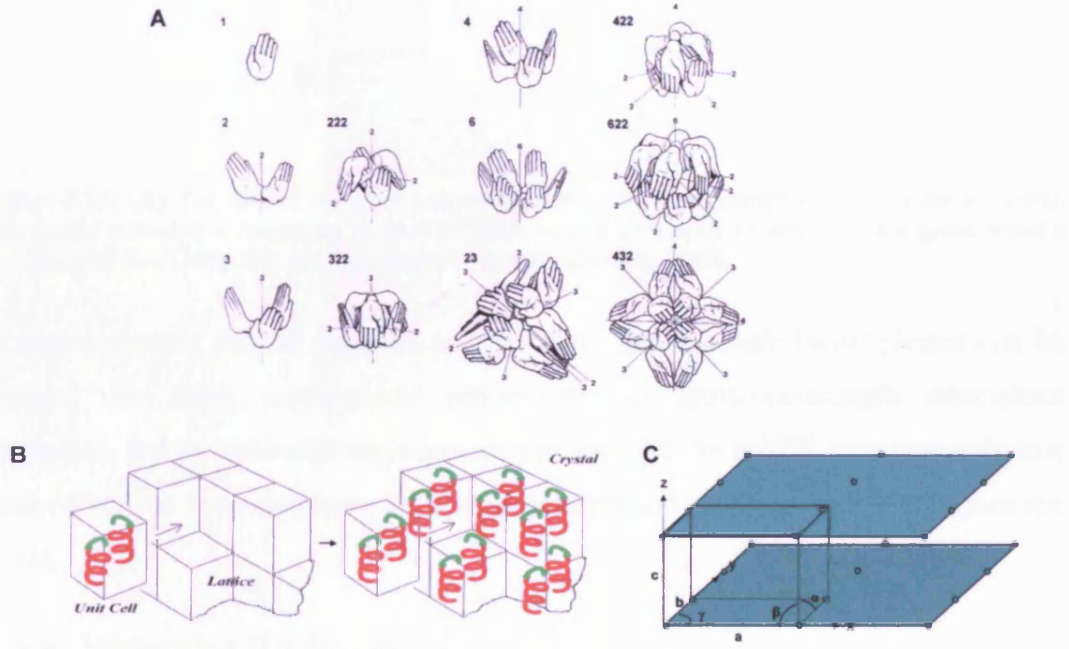

Figure 1.20: (A) Point groups possible in proteins represented by left hands (*141*). **(B)** Example of a unit cell and lattice the protein is red-green fluorescent protein (*147*). **(C)** Crystal lattice diagram showing a unit cell with the nomenclature used in this thesis.

1.6.3 Fourier Transforms

The amplitudes and phases of the different components of the X-rays detected can be used to calculate the density of the electrons in an inverse Fourier transformation. The Fourier method uses the fact that complex repetitive waves can be expressed as the sum of simpler waves whose frequencies are integral multiples of a fundamental frequency (Figure 1.21). The amplitudes and phases represent the Fourier transform of the scattered density (*141, 142*).

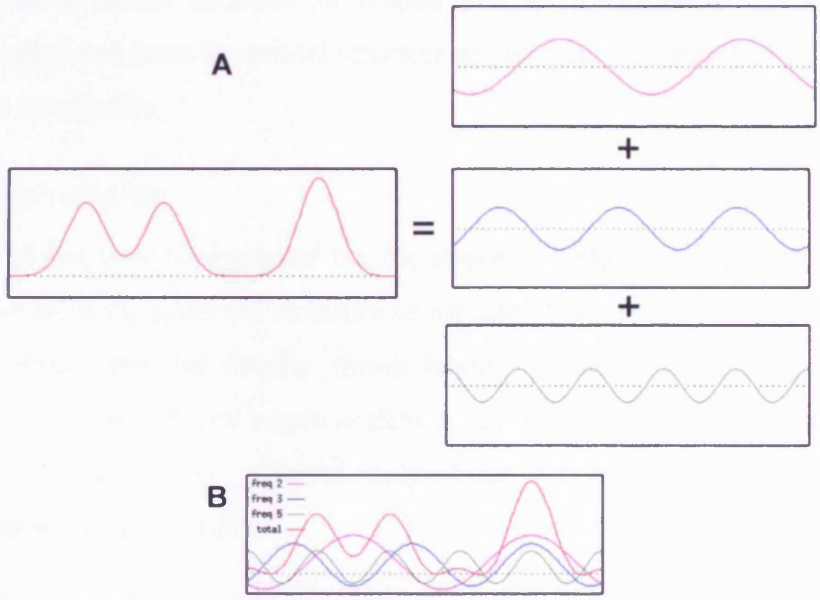

Figure 1.21: (A) The sum of the three sine waves makes the more complex wave on the left (red). The purple wave has a frequency of two, the blue wave a frequency of three and the green wave a frequency of five (*148*). **(B)** All four waves on top of each other (*148*).

In cases where a related structure is not known the structure factor phases can be worked out using isomorphous replacement or multi-wavelength anomalous dispersion, but as molecular replacement was used on the rsAPX structure only that method will be discussed here; for further information on these other techniques see (*141*).

1.6.4 Molecular Replacement

If a related structure is known when determining a structure, it can be used to help solve the new structure. To begin with, the space-group and cell dimensions of the new crystal need to be determined. Then the Matthews coefficient is checked to see how many molecules are likely to be in the asymmetric unit (*149*) (Equation 1.6).

$$\frac{\text{volume of the asymmetric unit}}{\text{no. of asymmetric units in the unit cell x molecular weight}} = \text{Matthews coefficient} \quad \textbf{...(1.6)}$$

If there is one molecule, the Matthew's coefficient should be between 1.9 and 4.2 $Å^3$ per Dalton of protein (*149*).

The next stage is rigid displacement, where the reference molecule is rotated and translated until it fits in the new data, using the Patterson function. The square of the amplitude of the diffracted X-ray is proportional to the intensity (which can be measured). The Patterson function is the Fourier transform of the intensities.

To generate a crystal structure the phases have to be estimated for each reflection. This is calculated from the model structure at this stage and attached to the observed structure amplitudes.

1.6.5 Rebuilding

The model has now been created but the structure factors from the calculated model will differ from the observed structure amplitude. This is seen in a difference density map, in which positive density shows features of the new structure that are not included in the model, and negative density shows features of the model that do not exist in the new structure. Careful study of this map allows the model to be refined to a better model (*141, 142*).

1.6.6 Refinement

The atomic positions and temperature factors are adjusted in the model to fit the observed data. As well as changing them to fit the observed data it is also important to refine them towards the ideal values of stereo-chemical features, *i.e.* bonding distances and angles. This is usually done by least squares refinement and simulated annealing. Least squares refinement uses a weighted function which is minimised to improve the agreement between F_{obs} and F_{calc}. It includes restraining to ideal values for stereo-chemical features such as bond distances and angles (Equation 1.7).

$$\phi = \sum_{r=1}^{m} W_r \left(\left| F_{obs_r} \right| + \left| F_{calc_r} \right| \right) \qquad \textbf{...(1.7)}$$

F_{obs} are the observed structure factors from the diffraction data and F_{calc} are the calculated structure factors from the model. m is the number of observations and W_r

is a weight, where $W_r = \frac{1}{\sigma^2}$ and σ is the variance of F_{obs}. In equation 1.7 ϕ represents the value for diffraction but the equation can be adapted for stereo-chemical features such as bonding distances (*141, 142*). The progress of the refinement can be checked manually and rebuilding done as above in between cycles.

Simulated annealing uses molecular dynamic techniques to describe the energy of the structure. The differences between the observed and calculated structure are minimised (*141, 142*).

1.6.7 Validation of the Model

1.6.7.1 Resolution

This is a method of assessing the quality of the diffraction data, as in practice the unit cells in the crystal are not totally identical. Due to thermal vibrations and variations in the crystal the observable diffraction pattern is Gaussian modified and fades off. This limits the best 'sharpness' or resolution possible for the image (*i.e.* the more of the diffraction pattern that can be seen the more detail that can be created from it (Figure 1.22)). The minimum distance between lattice planes (d_{min}) is calculated from the maximum value of θ observed and d_{min} is quoted as a measurement of resolution (*141, 142*).

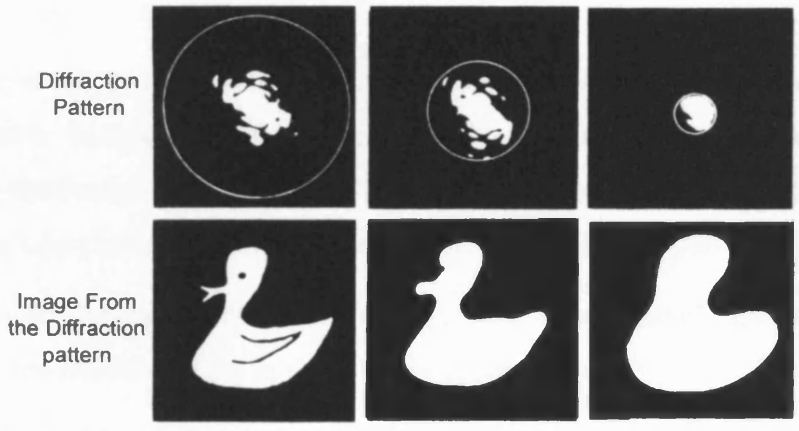

Figure 1.22: Two-dimensional duck diffraction patterns and detail visible in the images from various screening off points in the diffraction patterns (*141*).

1.6.7.2 R-Factor

The closeness of the model to the observed data is analysed by the crystallographic R-factor (Equation 1.8).

$$R = \sum \frac{\left\| F_{obs} \right| + \left| F_{calc} \right\|}{\sum \left| F_{obs} \right|} \qquad \text{...(1.8)}$$

F_{obs} are the observed structure factors from the diffraction data and F_{calc} are the calculated structure factors from the model. The refinement of the model is usually stopped when the R-factor stops changing. R_{free} is an R-factor calculated with 5-10% of the diffraction data which has not been used in the refinement process. This is useful as it helps prevent over-fitting and errors in refinement. If the R_{free} increases while the R-factor decreases in a refinement cycle, the cycle can be disregarded (*141, 142*).

1.7 Aims

In the context of the above discussion, an investigation into the substrate interactions in APX using X-ray crystallography, kinetics, spectroscopy and directed evolution is presented in this thesis. The objectives achieved through this research were:

- Crystallisation of rsAPX and the X-ray crystal structure of it (Chapter 2).
- The nitric oxide and cyanide bound X-ray crystal structures which provide information about Compound I formation in peroxidases (Chapter 2).
- The X-ray crystal structure of rsAPX in complex with the physiological substrate (Chapter 3).
- There are thought to be two sites where the substrate binds in APX (*136*). One is thought to be on the γ-edge of the heme (for ascorbate) and the other by the δ-edge of the heme (for aromatic compounds); this was confirmed by the salicylhydroxamic acid bound crystal structure (Chapter 4).
- All the crystal structures presented in this thesis provide insight into how proton transfer occurs in peroxidases (Chapter 4).
- A guaiacol screen is developed to screen APX mutants for enhanced activity towards aromatic substrates (Chapter 5). In the future this will be used to discover more about aromatic binding in peroxidases.

1.8 References

1. Lu, Y., Berry, S. M., and Pfister, T. D. (2001) *Chemical Reviews 101*, 3047.
2. Turano, P., and Lu, Y. (2001) in *Handbook on MetalloProteins* (Bertini, I., Sigel, H., and Sigel, A., Eds.) pp 269, Marcel Deckers, New York.
3. Scott, R. A., and Mauk, A. G. (1996) *Cytochrome c. A multidisciplinary Approach*, University Science Books, Sausilato, CA.
4. Valentine, J. S., Sheridan, R. P., Allen, L. C., and Kahn, P. C. (1979) *Proceedings of the National Academy of Science, USA 76*, 1009-1013.
5. Walker, F. A., Emrick, D., Rivera, J. E., Hanquet, B. J., and Buttlaire, D. H. (1988) *Journal of the American Chemistry Society 110*, 6234-6240.
6. Garau, G., Geremia, S., and Randaccio, L. (2002) *FEBS Letters 516*, 285-286.
7. Walker, F., Huynh, B. H., Scheidt, W. R., and Osvath, S. R. (1986) *Journal of the American Chemical Society 108*, 5288-5297.
8. Reid, L. S., Lim, A. R., and Mauk, A. G. (1986) *Journal of the American Chemical Society 108*, 8917-8201.
9. Springer, B. A., Sligar, S. G., Olson, J. S., and Phillips, G. N. (1994) *Chemical Reviews 94*, 699-714.
10. Quillin, M. L., Arduini, R. M., Olson, J. S., and Phillips, G. N. (1993) *Journal of Molecular Biology 234*, 140-155.
11. Brantley, R. E., Smerdon, S. J., Wilkinson, A. J., Singleton, E. W., and Olson, J. S. (1993) *Journal of Biolological Chemistry 268*, 6995-7010.
12. Rohlfs, R. J., Mathews, A. J., Carver, T. E., Olson, J. S., Springer, B. A., Egeberg, K. D., and Sligar, S. G. (1990) *Journal of Biological Chemistry 265*, 3168-3176.
13. Hargrove, M. S., Singleton, E. W., Quillin, M. L., Ortiz, L. A., Phillips, G. N., Olson, J. S., and Mathews, A. J. (1994) *Journal of Biological Chemistry 269*, 4207-4214.
14. Cameron, W. S., Smerdon, S. J., Wilkinson, A. J., Habash, J., Helliwell, J. R., Li, T., and Olson, J. S. (1993) *Biochemistry 32*, 13061-13070.
15. Kachalova, G. S., Popov, A. N., and Bartunik, H. D. (1999) *Science 284*, 473-476.

16. Lewis, D. F. S. (1996) *Cytochromes P450*, London.

17. Ortiz de Montellano, P. R. (1995) *Cytochrome P450: Structure, Mechanism and Biochemistry*, Prenum Press, London.

18. Sono, M., Roach, M. P., Coulter, E. D., and Dawson, J. H. (1996) *Chemical Reviews 96*, 2841-2887.

19. Li, H., and Poulos, T. L. (1997) *Nature Structural Biology 4*, 140-146.

20. Kirk, T. K., and Farrell, R. L. (1987) *Annual Review of Microbiology 41*, 465-501.

21. Wariishi, H., Marquez, L. A., Dunford, H. B., and Gold, M. H. (1990) *Journal of Biological Chemistry 265*, 11137-11142.

22. Wada, N., Kinoshita, S., Matsuo, M., Amako, K., Miyake, C., and Asada, K. (1998) *Biochemical and Biophysical Research Communications 242*, 256-261.

23. Groden, D., and Beck, E. (1979) *Biochimica et biophysica Acta 546*, 426-435.

24. Kelly, G. J., and Latzko, E. (1979) *Naturwissenschaften 66*, 617-618.

25. Sips, H. J., and Hamers, M. N. (1981) *Infection and Immunity 31*, 11–16.

26. Hogg, D. M., and Jago, G. R. (1970) *Biochemical Journal 117*, 779-790.

27. Hosoya, T., and Morrison, M. (1967) *Journal of Biological Chemistry 242*, 2828-2836.

28. Poulos, T. L., Freer, S. T., Alden, R. A., Edwards, S. L., Skogland, U., Takio, K., Eriksson, B., Xuong, N.-h., Yontani, T., and Kraut, J. (1980) *Journal of Biological Chemistry 255*, 575-580.

29. Welinder, K. G. (1992) *Current Opinion in Structural Biology 2*, 388-393.

30. Welinder, K. G., and Norskov-Lauritsen, L. (1986) in *Molecular and Physiological Aspects of Plant Peroxidases* (Greppin, H., Penel, C., and Gaspar, T., Eds.) pp 61-70, university of geneva, geneva.

31. Morita, Y., Mikami, B., Yamashita, H., Lee, J. Y., Aibara, S., Sato, M., Katsube, Y., and Tanaka, N. (1991) in *Biochemical, Molecular and Physiological Aspects of Plant Peroxidases* (Greppin, H., Penel, C., and Gaspar, T., Eds.) pp 81-88, university of Geneva Press, Geneva.

32. Morita, Y., Funatsu, J., and Mikami, B. (1993) in *Plant Peroxidases. Biochemistry and Physiology* (Welinder, K. G., Rasmussen, S. K., Penel, C., and Greppin, H., Eds.) pp 1-4, university of Geneva, Geneva.

33. Vainshtein, B. K., Melik-Adamyan, W. R., Barynin, V. V., Vagin, A. A., Grebenko, A. I., Borisov, V. V., Bartels, K. S., Fita, I., and Rossmann, M. G. (1986) *Journal of Molecular Biology 188*, 49-61.

34. Murthy, M. R. N., Reid III, T. J., Sicignano, A., Tanaka, N., and Rossmann, M. G. (1981) *Journal of Molecular Biology 152*, 465-499.

35. Kimura, S., and Ikeda-Saito, M. (1988) *Proteins 3*, 113-120.

36. Picot, D., Loll, P. J., and Garavito, R. M. (1994) *Nature 367*, 243-249.

37. Zeng, J., and Fenna, R. E. (1992) *Journal of Molecular Biology 226*, 185-207.

38. Poulos, T. L., and Fenna, R. E. (1994) *metal Ions in Biological Systems*, Vol. 30, H. Siegel, New York.

39. Dunford, H. B. (1999) *Haem peroxidases*, John Wiley, Chichester.

40. Pelletier, H., and Kraut, J. (1992) *Science 258*, 1748-1755.

41. Yamada, Y., Fujiwara, T., Sato, T., Igarashi, N., and Tanaka, N. (2002) *Nature Structural Biology 9*, 691-695.

42. Carpena, X., Loprasert, S., Mongkolsuk, S., Switala, J., Loewen, P. C., and Fita, I. (2003) *Journal of Molecular Biology 327*, 475-480.

43. Carpena, X., Melik-Adamyan, W., Loewen, P. C., and Fita, I. (2004) *Acta Crystallographica D 60*, 1824-1831.

44. Bertrand, T., Eady, N. A. J., Jones, J. N., Bodiguel, J., Jesmin, Nagy, J. M., Raven, E. L., Jamart-Gregoire, B., and Brown, K. H. (2004) *Journal of Biological Chemistry 279*, 38991-38999.

45. Wada, K., Tada, T., Nakamura, Y., Ishkawa, T., Yabuta, Y., Yoshimura, K., Shigoeka, S., and Nishimura, K. (2003) *Journal of Biochemistry 134*, 239-244.

46. Wada, K., Tada, T., Nakamura, Y., Yabuta, Y., Yoshimura, K., Takeda, T., Shigoeka, S., and Nishimura, K. (2002) *Acta Crystallographica D58*, 559-561.

47. Patterson, W. R., and Poulos, T. L. (1995) *Biochemistry 34*, 4331-4341.

48. Edwards, S. L., Raag, R., Warhshi, H., Gold, M. H., and Poulos, T. L. (1993) *Proceedings of the National Academy of Science, USA 90*, 750-754.

49. Sundaramoorthy, M., Kishi, K., Gold, M. H., and Poulos, T. L. (1994) *Journal of Biological Chemistry 269*, 32759-32767.

50. Petersen, J. F. W., Tams, J. W., Vind, J., Svensson, A., Dalboge, H., Welinder, K. G., and Larsen, S. (1993) *Journal of Biological Chemistry 232*, 989-991.

51. Prescott, L. M., Harley, J. P., and Klein, D. A. (1990) *Microbiology*, Wm. C. Brown, Dubuque (USA).

52. Gajhede, M., Schuller, D. J., Heriksen, A., Smith, A. T., and Poulos, T. L. (1997) *Nature Structural Biology 4*, 1032-1038.

53. Schuller, D. J., Ban, N., van Huystee, R. B., McPherson, A., and Poulos, T. L. (1996) *Structure 4*, 311-321.

54. Henriksen, A., Schuller, D. J., Meno, K., Welinder, K. G., Smith, A. T., and Gajhede, M. (1998) *Biochemistry 37*, 8054-8060.

55. Hiner, A. N. P., Raven, E. L., Thorneley, R. N. F., Garcia-Canovas, F., and Rodriguez-Lopez, J. N. (2002) *Journal of Inorganic Biochemistry 91*, 27-34.

56. Keilin, D., and Mann, T. (1937) *Proceedings of the Royal Society 122B*, 119-133.

57. Altschul, A. M., Abrams, R., and Hogness, T. R. (1940) *Journal of Biological Chemistry 136*, 777-794.

58. Theorell, H. (1941) *Enzymologia 10*, 250-252.

59. Welinder, K. G. (1979) *European Journal of Biochemistry 96*, 483-502.

60. Welinder, K. G. (1976) *FEBS letters 72*, 19-23.

61. Takio, K., Titani, K., Ericsson, L. H., and Yonetani, T. (1980) *Archives of Biochemistry and Biophysics 203*, 615-629.

62. Goodin, D. B., Mauk, A. G., and Smith, M. (1986) *Proceedings of the National Academy of Science, USA 83*, 1295-1299.

63. Fishel, L. A., Villafranca, J. E., Mauro, J. M., and Kraut, J. (1987) *Biochemistry 26*, 351-360.

64. Hanson, L. K., Chang, C. K., Davis, M. S., and Fajer, J. (1981) *Journal of the American Chemistry Society 103*, 663-670.

65. Dolphin, D., Forman, A., Borg, D. C., Fajer, J., and Felton, R. H. (1971) *Proceedings of the National Academy of Science, USA 68*, 614-618.

66. Roberts, J. E., Hoffman, B. M., Rutter, R., and Hager, L. P. (1981) *Journal of Biological Chemistry 256*, 2118-2121.

67. La Mar, G. N., de Ropp, J. S., Smith, K. M., and Langry, K. C. (1981) *Journal of Biological Chemistry 256*, 237-243.

68. Felton, R. H., Romans, A. Y., Yu, N.-T., and Schonbaum, G. R. (1976) *Biochimica et biophysica Acta 434*, 82-89.

69. Loew, G. H., and Herman, Z. S. (1980) *Journal of the American Chemistry Society 102*, 6173-6174.

70. Yonetani, T., Schleyer, H., and Ehrenberg, A. (1966) *Journal of Biological Chemistry 241*, 3240-3243.

71. Erman, J. E., Vitello, L. B., Mauro, J. M., and Kraut, J. (1989) *Biochemistry 28*, 7992-7995.

72. Huyett, J. E., Doan, P. E., Gurbiel, R., Houseman, A. L. P., Sivaraja, M., Goodin, D. B., and Hoffman, B. M. (1995) *Journal of the American Chemistry Society 117*, 9033-9041.

73. Houseman, A. L. P., Doan, P. E., Goodin, D. B., and Hoffman, B. M. (1993) *Biochemistry 32*, 4430-4443.

74. Dunford, H. B. (1982) *Advances in Inorganic Biochemistry 4*, 41-68.

75. Yonetani, T., and Anni, H. (1987) *Journal of Biological Chemistry 262*, 9547-9554.

76. Tams, J. W., and Welinder, K. G. (1995) *Analytical Biochemistry 228*, 48-55.

77. Smith, A. T., Santama, N., Dacey, S., Edwards, M., Bray, R. C., Thorneley, R. N. F., and Burke, J. F. (1990) *Journal of Biological Chemistry 265*, 13335-13343.

78. Hartmann, C., and Ortiz de Montellano, P. R. (1992) *Archives of Biochemistry and Biophysics 297*, 61-72.

79. Claiborne, A., Malinowski, D. P., and Fridovich, I. (1979) *Journal of Biological Chemistry 254*, 11664-11668.

80. Claiborne, A., and Fridovich, I. (1979) *Journal of Biological Chemistry 254*, 4245-4252.

81. Triggs-Raine, B. L., Doble, B. W., Mulvey, M. R., Sorby, P. A., and Loewen, P. C. (1988) *Journal of Bacteriology 170*, 4415-4419.

82. Loewen, P. C., Triggs, B. L., George, C. S., and Hrabarchuk, B. E. (1985) *Journal of Bacteriology 162*, 661-667.

83. Nadler, V., Goldberg, I., and Hochman, A. (1986) *Biochimica et biophysica Acta 882*, 234-241.

84. Welinder, K. G. (1991) *Biochimica et biophysica Acta 1080*, 215-220.

85. Loewen, P. C., and Switala, J. (1987) *Journal of Bacteriology 169*, 3601-3607.

86. Hochman, A., Figueredo, A., and Wall, J. D. (1992) *Journal of Bacteriology 174*, 3386-3391.

87. Hochman, A., and Goldberg, I. (1991) *Biochimica et Biophysica Acta 1077*, 299-307.

88. Goldberg, I., and Hochman, A. (1989) *Biochimica et Biophysica Acta 991*, 330-336.

89. Goldberg, I., and Hochman, A. (1989) *Archives of Biochemistry and Biophysics 268*, 124-128.

90. Abrams, J. J., and Webster, D. A. (1990) *Archives of Biochemistry and Biophysics 279*, 54-59.

91. Heym, B., Alzari, P. M., Honore, N., and Cole, S. T. (1995) *Molecular Microbiology 15*, 235-245.

92. Nagy, J. M., Cass, A. E. G., and Brown, K. A. (1997) *Journal of Biological Chemistry 272*, 31265-31271.

93. Johnsson, K., Froland, W. A., and Schultz, P. G. (1997) *Journal of Biological Chemistry 272*, 2834-2840.

94. Pierattelli, R., Banci, L., Eady, N. A. J., Moody, P. C. E., Bodiguel, J., Jamart-Gregoire, B., Raven, E. L., and Brown, K. A. (2004) *Journal of Biological Chemistry 279*, 39000-39009.

95. Chen, G. X., and Asada, K. (1989) *Plant and Cell Physiology 30*, 987-998.

96. Mittler, R., and Zilinskas, B. A. (1991) *Plant Physiology 97*, 962-968.

97. Gerbling, K.-P., kelly, G. J., Fischer, K.-H., and Latzko, E. (1984) *Journal of Plant Physiology 115*, 59-67.

98. Ohya, T., Morimura, Y., Saji, T., Mihara, T., and Ikawa, T. (1997) *Plant Science 125*, 137-145.

99. Dalton, D. A., Hanus, F. J., Russell, S. A., and Evans, H. J. (1987) *Plant Physiology 83*, 789-794.

100. De Gara, L., de Pinto, M. C., and Arrigoni, O. (1997) *Physiologia Plantarum 100*, 894-900.

101. Elia, M. R., Borracino, G., and Dipierro, S. (1992) *Plant Science 85*, 17-21.

102. Koshiba, T. (1993) *Plant and Cell Physiology 34*, 713-721.

103. Ishikawa, T., Takeda, T., and Shigeaka, S. (1996) *Plant Science 120*, 11-18.

104. Amako, K., Chen, G.-X., and Asada, K. (1994) *Plant and Cell Physiology 35*, 497-504.

105. Kvaratskhelia, M., Winkel, C., and Thorneley, R. N. F. (1997) *Plant Physiology 114*, 1237-1245.

106. Battistuzzi, G., D'Onofrio, M., Loschi, L., and Sola, M. (2001) *Archives of Biochemistry and Biophysics 388*, 100-112.

107. Tanaka, K., Takeuchi, E., Kubo, A., Sakaki, T., Haraguchi, K., and Kawamura, Y. (1991) *Archives of Biochemistry and Biophysics 286*, 371-375.

108. Yoshimura, K., Ishikawa, T., Nakumura, Y., Tamoi, M., Takeda, T., Tada, T., Nishimura, K., and Shigeaka, S. (1998) *Archives of Biochemistry and Biophysics 353*, 55-63.

109. Preger, V., Pesaresi, A., Pupillo, P., and Trost, P. (2001) *Protoplasma 217*, 137-145.

110. Ushimara, T., Maki, Y., Sano, S., Koshiba, K., Asada, K., and Tsuji, H. (1997) *Plant and Cell Physiology 38*, 541-549.

111. Miyake, C., Cao, W.-H., and Asada, K. (1993) *Plant and Cell Physiology 34*, 881-995.

112. Nakano, Y., and Asada, K. (1987) *Plant and Cell Physiology 28*, 131-140.

113. Gillham, D. J., and Dodge, A. D. (1986) *Planta 167*, 246-251.

114. Jablonski, P. P., and Anderson, J. W. (1982) *Plant Physiology 69*, 1407-1413.

115. Meneguzzo, S., Sgherri, C. L. M., Navari-Izzo, F., and Izzo, R. (1998) *Physiologia Plantarum 104*, 735-740.

116. Chen, G. X., Sano, S., and Asada, K. (1992) *Plant and Cell Physiology 33*, 109-116.

117. Kvaratskhelia, M., Winkel, C., Naldrett, M. T., and Thorneley, R. N. F. (1999) *Journal of Plant Physiology 154*, 273-282.

118. Heering, H. A., Jansen, M. A. K., Thorneley, R. N. F., and Smulevich, G. (2001) *Biochemistry 40*, 10360-10370.

119. Mathews, M. C., Summers, C. B., and Felton, G. W. (1997) *Archives of Insect Biochemistry and Physiology 34*, 57-68.

120. Tel-Or, E., Huflejt, M. E., and Packer, L. (1986) *Archives of Biochemistry and Biophysics 246*, 396-402.

121. Shigeoka, S., Nakano, Y., and Kitaoka, S. (1980) *Archives of Biochemistry and Biophysics 201*, 121-127.

122. Takeda, T., Yoshimura, K., Ishikawa, T., and Shigeaka, S. (1998) *Biochimie 80*, 295-301.

123. Takeda, T., Yoshimura, K., Yoshii, M., Kanahoshi, H., Miyasaka, H., and Shigeoka, S. (2000) *Archives of Biochemistry and Biophysics 376*, 82-90.

124. Mittler, R., and Zilinskas, B. A. (1992) *Journal of Biological Chemistry 267*, 21802-21807.

125. Mittler, R., and Zilinskas, B. A. (1991) *FEBS letters 289*, 257-259.

126. Dalton, D. A., del Castillo, L. D., Kahn, M. L., Joyner, S. L., and Chatfield, J. M. (1996) *Archives of Biochemistry and Biophysics 328*, 1-8.

127. Celik, A., Cullis, P. M., Sutcliffe, M. J., Sangar, R., and Raven, E. L. (2001) *European Journal of Biochemistry 268*, 78-85.

128. Celik, A., Cullis, P. M., and Raven, E. L. (2000) *Archives of Biochemistry and Biophysics 373*, 175-181.

129. Hill, A. P., Modi, S., Sutcliffe, M. J., Turner, D. D., Gilfoyle, D. J., Smith, A. T., Tam, B. M., and Lloyd, E. (1997) *European Journal of Biochemistry 248*, 347-354.

130. Patterson, W. R., Poulos, T. L., and Goodin, D. B. (1995) *Biochemistry 34*, 4342-4345.

131. Hiner, A. N. P., Martinez, J. I., Arnao, M. B., Acosta, M., Turner, D. D., Raven, E. L., and Rodriguez-Lopez, J. N. (2001) *European Journal of Biochemistry 268*, 3091-3098.

132. Marquez, L. A., Quitoriano, M., Zilinskas, B. A., and Dunford, H. B. (1996) *FEBS letters 389*, 153-156.

133. Lad, L., Mewies, M., and Raven, E. L. (2002) *Biochemistry 41*, 13774-13781.

134. Lad, L., Mewies, M., Basran, J., Scrutton, N. S., and Raven, E. L. (2002) *European Journal of Biochemistry 269*, 3182-3192.

135. Pappa, H., Patterson, W. R., and Poulos, T. L. (1996) *Journal of Biological Inorganic Chemistry 1*, 61-66.

136. Mandelman, D., Jamai, J., and Poulos, T. L. (1998) *Biochemistry 37*, 17610-17617.

137. Yonetani, T., and Ray, G. S. (1965) *Journal of Biological Chemistry 240*, 4503-4514.

138. Zhang, H. (1993), University of Alberta.

139. Jespersen, H. M., Kjaersgard, I. V. H., Ostergaard, L., and Welinder, K. G. (1997) *Journal of Biochemistry 326*, 305-310.

140. Dalton, D. A. (1991) in *Peroxidases in chemistry and biology* (Everse, J., Everse, K. E., and Grisham, M. B., Eds.) pp 140-150, CRC Press, Boca Raton.

141. Blow, D. (2002) *Outline of Crystallography for Biologists*, Oxford University Press, New York.

142. Glusker, J. P., and Trueblood, K. N. (1985) *Crystal Structure Analysis*, Oxford University Press.

143. Moody, P. C. E. (2002) in *Module BS336*, University of Leicester.

144. ESRF www.esrf.fr.

145. Bragg, W. L. (1913) *Proceedings of the Royal Society A 89*, 248-277.

146. Hahn, T. (1983) *International Tables for Crystallography*, Springer.

147. Rupp, B. *www-structure.llnl.gov/Xray/101index.html*.

148. Cowtan, K. www.ysbl.york.ac.uk/~cowtan/fourier/ftheory.html.

149. Matthews, B. W. (1968) *Journal of Molecular Biology 33*, 491-497.

Chapter 2

The X-Ray Crystal Structures of rsAPX and the rsAPX/NO and rsAPX/CN Complexes

2.1 INTRODUCTION

In heme redox enzymes, the binding of hydrogen peroxide in the sixth coordination site of the iron has been of great interest for many years, but the reaction is usually too fast to capture a bound form by X-ray crystallography. Substitutes are therefore used to model the binding of hydrogen peroxide and oxygen, thus providing insight into the structure of catalytic intermediates. Ligands such as azide (*1, 2*), fluoride (*3*), cyanide (*4*), hydroxide (*5*), carbon monoxide (*6*) and nitrogen oxide (*6, 7*) have been used in this context. In peroxidases, there are only a few known structures of ligand-bound forms and many of these are cytochrome *c* peroxidase (C*c*P) structures (*3, 4, 8, 9*); C*c*P has an unusual Compound I structure, since it contains a tryptophan radical instead of the more normal porphyrin π-cation radical. In this Chapter, the nitric oxide-bound and cyanide-bound forms of rsAPX have been examined. Analysis of the rsAPX/NO and rsAPX/CN complexes will provide insight into how hydrogen peroxide binds in APX and useful information on the mechanism of Compound I formation in C*c*P compared to other peroxidases.

2.1.1 Crystal Structures of Peroxidases

The first crystal structure of a peroxidase was obtained for C*c*P in 1980 (*10*), but it was several years before crystal structures of other peroxidases were solved. Several factors led to the solution of further crystal structures. In particular, crystal growth was greatly helped by the availability of recombinant enzymes from *E. coli*, which allowed greater quantities of purified enzyme to be obtained. Cryogenic techniques have limited the X-ray damage to crystals and therefore substantially extended the useful lifespan of a crystal (*11, 12*). Synchrotron radiation has reduced the time it takes to collect diffraction data and there are now numerous peroxidase crystal structures solved (Table 2.1).

The crystal structure of recombinant pea cytosolic APX (rpAPX) was solved in 1995 and provided the first insight into the structure of this unusual class I enzyme (*13*). (Classification of peroxidases is discussed in Chapter 1, section 1.3.) The active site was found to be similar to that of C*c*P, and APX was confirmed as a class I peroxidase (Chapter 1, section 1.5).

Table 2.1
Dates of publication of heme peroxidase (class I – III) crystal structures.

Date	Peroxidase
1980	Yeast cytochrome *c* peroxidase (*10*)
1991, 1993	Horseradish peroxidase E5 (preliminary data) (*14, 15*)
1993	Lignin peroxidase (*16*)
1993	*P. aeruginosa* cytochrome *c* peroxidase (*17*)
1994	*C. cinereus* peroxidase (*18, 19*)
1994	Manganese peroxidase (*20*)
1995	Ascorbate peroxidase (pea) (*13*)
1995	Chloroperoxidase (*21*)
1996	Peanut peroxidase (*22*)
1997	Horseradish peroxidase C (*23*)
1998	Barley peroxidase (*24*)
2001	Soybean seed coat peroxidase (*25*)
2002	*Haloarcula marismortui* catalase-peroxidase (*26*)
2002, 2003	Chloroplastic ascorbate peroxidase (tobacco) (*27, 28*)
2003	Ascorbate peroxidase (soybean) (*29*)
2003	*Mycobacterium tuberculosis* alkylhydroperoxidase (*30*)
2003	*Burkholderia Pseudomallei* catalase-peroxidase (*31*)
2004	*Mycobacterium tuberculosis* catalase-peroxidase (*32*)
2004	*E. coli* catalase-peroxidase (*33*)

2.1.2 Hydrogen Peroxide Binding and Compound I Formation

Compound I has been crystallised in C*c*P (Figure 2.1) (*34-36*). Data from the most recent paper (*36*), provided interesting information because the iron-oxygen bond was found to be longer than expected (1.87 Å). This agreed with the other two Compound I structures (*34, 35*) which were at lower resolution (1.8 ± 0.1 Å) but not with extended X-ray absorption fine structure (EXAFS) work on other peroxidases showing a shorter bond for Compound I (1.67 Å (*37*) and 1.6 Å (*38*)). These crystallographic and other spectroscopic data (Mössbauer (*39, 40*) and Raman (*41-44*)) suggest that Compound I of C*c*P contains a single bond between the iron and oxygen and that the oxygen is bound as hydroxide. This is in contrast to the conventional view of the iron-oxygen interaction as a double bond. The structure

also suggests a Compound I stabilising role for Arg48 (Figure 2.1) (equivalent to Arg38 in APX), which is consistent with the proposed role of this residue in proton transfer (*4*) (Chapter 4).

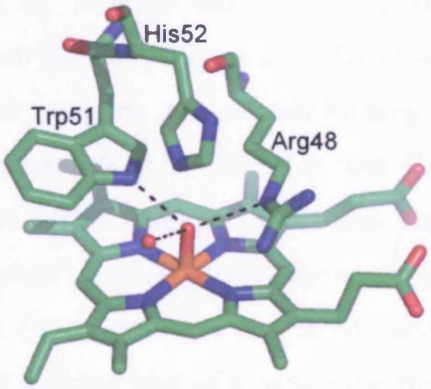

Figure 2.1: Active site structure of Compound I of C*c*P (*36*).

However, it is conceivable that other peroxidases may have a different Compound I structure since C*c*P contains an unusual protein-based radical in its Compound I rather than the more usual porphyrin-based radical. There are no Compound I peroxidase crystal structures except those for C*c*P, since the Compound I of C*c*P usually lasts for ~2 hours (*45*) whereas other peroxidases' Compound Is are stable for mere minutes (*46-48*) or seconds (*49, 50*).

In heme peroxidases, it is thought that a transient intermediate (Fe^{3+}-OOH^-, Figure 2.2) is formed prior to Compound I formation but this has been difficult to capture even in solution (*51-59*). It is unlikely to be observable crystallographically, and therefore diatomic ligands, such as cyanide, carbon monoxide and nitric oxide, are useful in trying to mimic it. Diatomic ligands form stable complexes with peroxidases, which last until the chemical conditions are changed (*4, 6, 7*), involving hydrogen-bond interactions that are relevant to hydrogen peroxide binding.

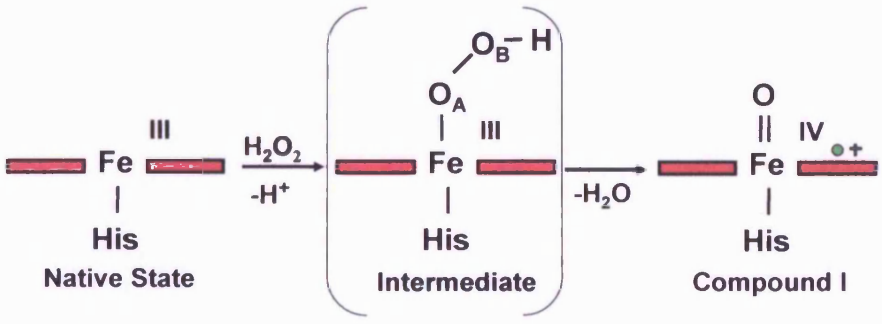

Figure 2.2: Proposed intermediate in the formation of Compound I in peroxidases, with the labelling of oxygen atoms used in this Chapter.

2.1.3 Aims

A crystal structure of APX with a diatomic molecule bound to the iron can provide useful insight into the structure of hydrogen peroxide binding and the reaction to form Compound I (*4, 8, 9*). Cyanide and nitric oxide structures were therefore used to model the intermediate shown in Figure 2.2. These ligands have previously been used to model hydrogen peroxide and oxygen binding in cytochrome *c* (*7*), heme oxygenase (*6*), myoglobin (*60, 61*), HRP (*4*) and C*c*P (*8*). Since rsAPX has properties of both class I (for example, C*c*P) and class III (for example, HRP) peroxidases, it may be possible to rationalise the existing data on the intermediate in Compound I formation (*4, 9*) from the rsAPX/NO and rsAPX/CN complex data. These data may also aid development of a proton transfer mechanism in peroxidases (Chapter 4).

2.2 RESULTS

2.2.1 Isolation and Purification of rsAPX

The purity of the rsAPX enzyme used to grow crystals was found to have an important influence on crystallisation. The purity of rsAPX was determined by measuring Reinheitzahl (R_z) values and by polyacrylamide gel electrophoresis (SDS-PAGE) (Figure 2.3). The protein was then further purified by Fast Protein Liquid Chromatography (FPLC) (Figure 2.3B). The ratio of the absorbance of the Soret peak at 407 nm and that of the protein peak at 280 nm is the Reinheitzahl (R_Z) number and relates to the purity of the peroxidase. The higher the R_Z number the higher the purity. The absorbance at 280 nm is due to aromatic residues with a contribution from the heme and the Soret peak is due to the heme.

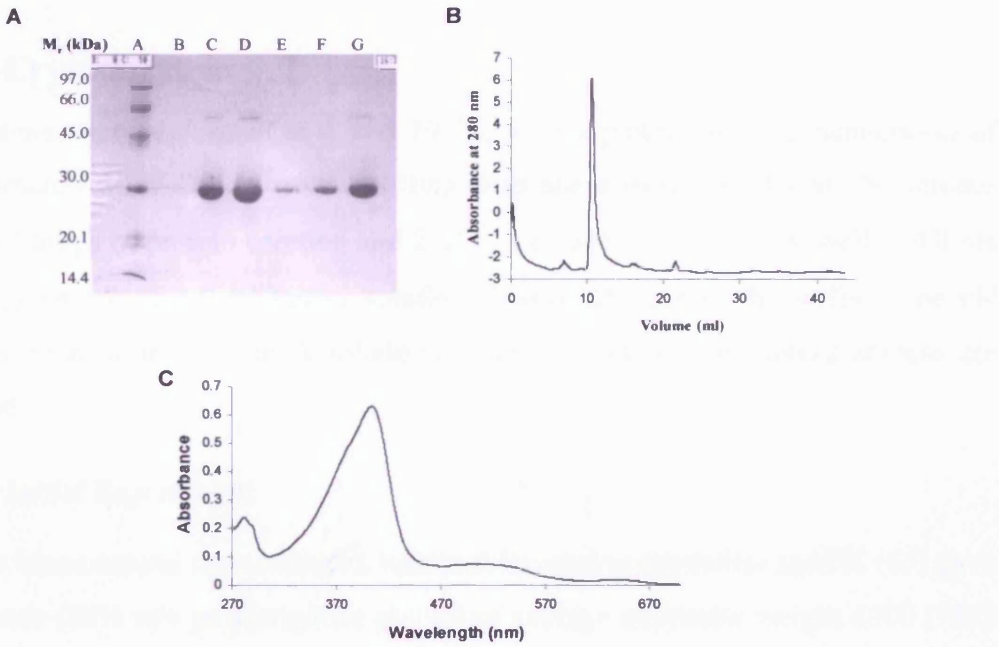

Figure 2.3: (A) SDS-PAGE gel of rsAPX. From the left: standard markers (lane A), rsAPX of increasing concentration (lanes B-D and again in lanes E-G). **(B)** FPLC trace of rsAPX. Conditions: Superdex 75 HR 10/30 gel filtration column, 0.15 M sodium phosphate buffer, pH 7.0, 200 µl injection of purified rsAPX, run time 45 minutes. **(C)** UV-visible absorption spectrum of rsAPX in the ferric state. Conditions: sodium phosphate buffer, pH 7.0, µ = 0.10 M, 25.0 °C.

Samples of rsAPX were prepared from *Escherichia coli* SG1300 cells (containing the pREP4 vector) incorporating a pQE30-derived expression vector and purified as described previously (*62*) using the incorporated His-tag (six histidine residues on the C-terminal end of the protein). The final elution from the Ni^{2+}-nitrilotriacetic acid agarose column (Qiagen) was using pH (4.2) rather than using imidazole and the

heme reconstitution step was left overnight rather than the 15 minutes described. Samples (≈ 20mg/ml) of rsAPX were stored in deionised water in 50 µl aliquots at -80 °C. Concentrations of enzyme were determined using the molar absorption coefficient for rsAPX (ε_{407} = 107 $mM^{-1}cm^{-1}$ (*63*)).

Prior to FPLC purification, the SDS-PAGE gel showed a second band on overloading with rsAPX which could be the dimer (Figure 2.3A). The size of this protein is ~30 kDa which agrees with the calculated value of 27 kDa (*64*). The protein was subsequently purified using FPLC (ÄKTA). The trace contained only one large peak (Figure 2.3B) because the protein was homogeneous. Homogeneity is crucial for crystals to form. The R_z value of the batch of rsAPX used for crystallisation was 2.7 (usually values of above ~2.0 are considered pure), indicating very pure protein (Figure 2.3C).

2.2.2 Crystallisation

All screens were performed at 4 and 19 °C, with a protein stock concentration of approximately 10 mg/ml in water. Sitting drop plates were used for all the screens with 2 µl drops of protein solution and 2 µl of well solution over 1 ml wells. All pH values given are of 1.0 M buffer solutions before addition to the wells. The pH values were measured for stock solutions, as this is how the commercial screens are prepared.

2.2.2.1 Initial Experiments

Screens based around the conditions successfully used to crystallise rpAPX (*65*) gave no crystals (30% w/v poly(ethylene glycol) of average molecular weight 4000 (PEG 4000), 0.2 M sodium acetate and 0.1 M tri[hydroxymethyl]aminomethene with hydrochloric acid (Tris-HCl) at pH 8.5). Commercial crystal screens were attempted and Molecular Dimensions Ltd (MDL) screen (I) gave quasi-crystals. Screens with sodium acetate and 2-propanol were performed around the conditions of the quasi-crystal growth. No crystals grew in these screens; an Emerald Wizard (I) screen was therefore tried. Quasi-crystals grew in a drop containing sodium citrate and 2-propanol. Therefore a further screen based around these conditions was tried but it did not yield crystals.

2.2.2.2 Screens with Homogeneous Protein

A new batch of purer protein (see section 2.2.1 for purity) was used to set up MDL screens (I) and (II). One month later crystals appeared in two wells of the MDL (I) screen at 19 °C. The first well contained 0.2 M ammonium acetate, 0.1 M tri-sodium citrate dihydrate pH 5.6 and 30% w/v PEG 4000. Screens were set up with ammonium acetate, tri-sodium citrate and PEG 4000 at 19 °C. The second well contained 0.1 M Hepes, pH 7.5 and 1.5 M lithium sulphate. A screen was set up with 0 to 2.0 M lithium sulphate and 0.1 M Hepes pH 6.0 to 8.5 at 19 °C. After two weeks crystals formed in the drop of the well containing 2.0 M lithium sulphate and Hepes pH 8.5.

More screens were set up with 1.50 to 2.25 M lithium sulphate and 0.1 M Hepes, pH 8.0 to 9.5 at a protein concentration of 10 mg/ml and 15 mg/ml. Several wells contained crystals of various sizes and shapes. The crystals in 0.1 M Hepes pH 8.3 and 2.25 M lithium sulphate at 10 mg/ml were the biggest ordered crystals of about 150 μm long and 75 μm in cross-section. The crystals appeared highly ordered (Figure 2.4).

Figure 2.4: Crystals of rsAPX (magnified). Conditions: 0.1 M Hepes pH 8.3, 2.25 M lithium sulphate and 10 mg/ml rsAPX.

2.2.3 Crystal Preparation and Data Collection

2.2.3.1 Crystal Preparation

The crystals were taken out of the well drops using a thin fibre loop (10 μm, rayon) of the type shown in Figure 2.6 and soaked in 20 μl drops of cyanide and hydrogen peroxide solutions for 5 minutes.

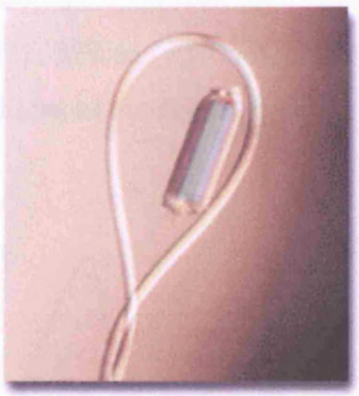

Figure 2.6: A crystal mounted in a thin fibre loop (*66*).

The cyanide and hydrogen peroxide solutions (~0.1 M) were prepared in Hepes (pH 8.3, 0.1 M) and lithium sulphate (2.25 M). The crystal placed in the cyanide solution went from a deep brown-red (Figure 2.4) to bright cherry red. The hydrogen peroxide soak was carried out to try and gain insight into the iron-oxygen bond in Compound I of rsAPX but the reaction occurred too quickly and no density relating to oxygen bound iron was found in the resulting crystal structure. Bubbles formed during the soak possibly due to APX having some catalase activity since the bubbles may be oxygen (Chapter 1, section 1.3).

The nitric oxide soak was carried out by soaking the crystals in a solution of sodium dithionite and then adding potassium nitrite to form nitric oxide *in situ* (*7*).

The soaked and un-soaked crystals were dipped in cryoprotectant oil (50% paratone-N and 50% paraffin oil) to remove the mother liquor (2.25 mM lithium sulphate and Hepes 0.1 M pH 8.3). They were then quickly plunged into liquid nitrogen, to stop ice crystals forming, and stored in liquid nitrogen until the diffraction data was collected at the synchrotron.

2.2.3.2 Confirmation of the Binding

To confirm the binding of cyanide to rsAPX in the crystal soak, the UV-visible absorption spectrum of the enzyme (0.05 μM enzyme, 0.1 M lithium sulphate and 0.1 M Hepes pH 8.3) was compared to a spectrum taken immediately after the addition of cyanide (~0.05 μM) (Figure 2.5). In the latter spectrum, the Soret peak has shifted to 421 nm and two new peaks have appeared at 529 and 570 nm. This is consistent with a 6-coordinate iron and the published wavelength maxima for cyanide bound rsAPX (431, 529 and 558 nm (*67*)), therefore the cyanide must bind to rsAPX under the conditions of the crystal soak.

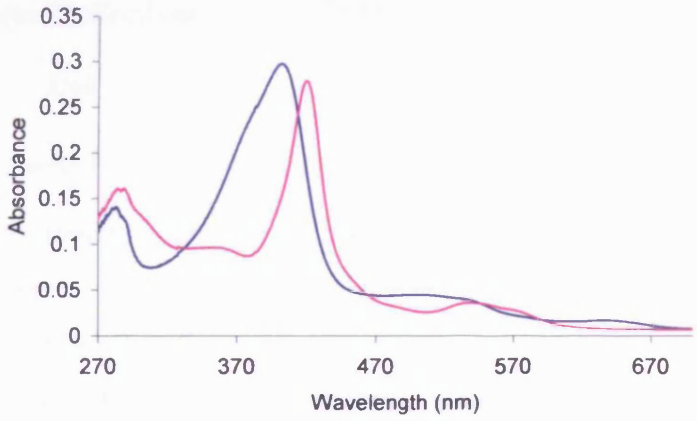

Figure 2.5: UV-visible absorption spectra of rsAPX (blue trace) and rsAPX with cyanide bound (~0.05 μM) (pink trace). Conditions: 0.05 μM enzyme, 0.1 M lithium sulphate and 0.1 M Hepes pH 8.3.

2.2.3.3 Data Collection

Diffraction data for the rsAPX, rsAPX/CN and rsAPX/NO structures were collected on beam-line X11 at the EMBL outstation at DESY Hamburg, using a marCCD detector (Marresearch) and 0.811 Å radiation at 100 K by Dr. D. Leys (Biochemistry Department). The rsAPX crystals diffracted to beyond 1.8 Å, and 108° data were collected using 1° oscillations. For the rsAPX/CN structure, the crystals diffracted to beyond 2 Å, and 64° data were collected using 0.5° oscillations. The rsAPX/NO crystals diffracted to beyond 2 Å, and 66° data were collected also using 0.5° oscillations. The first image for the rsAPX crystal was subject to the auto-indexing routines in DENZO (*68*) and gave a solution consistent with a primitive tetragonal cell. Measurement and reduction (using SCALEPACK (*68*)) allowed an examination of the distribution of intensities along the principal axes, allowing the space group to

be assigned as $P4_22_12$. The unit cell dimensions were a = 81.8 Å, b = 81.8 Å and c = 75.0 Å. In total, 5% of the data were flagged for the calculation of R_{free} and excluded from subsequent refinement. Data collection and reduction statistics are shown in Table 2.2.

Table 2.2
Data collection for rsAPX and the CN and NO Complexes.

	rsAPX	rsAPX/CN	rsAPX/NO
Resolution Ranges (Å)	1.75-57.74	2.00-56.80	2.01-58.72
Total Observations	92,501	58,820	59,132
Unique Reflections	26,092	15,798	16,455
I/σI	16.1	15.9	15.8
R_{merge} (%)	6.7	5.2	5.1
Completeness (%)	99.30	95.22	97.32

2.2.3.4 Data Interpretation

The data were interpreted with assistance from Dr. P. C. E. Moody (Biochemistry Department). The structure of rsAPX was solved by molecular replacement using the MOLREP program (*69*) in the CCP4 suite (*70*) using the rpAPX structure (PDB code 1APX) (*13*) as a search model. The rotational function peak was 3 times higher than any other peak (Rf/ = 12.46) and the translation correlation was 3 times higher than any other solution with an R-factor of 0.394. The initial resolution for the rsAPX structure was 3.0 Å. The rsAPX refined structure was then used as a start-point for interpreting the rsAPX/NO and rsAPX/CN data.

2.2.3.5 Refinement

Several cycles of refinement using CNS v1.1 (*71*) and rebuilding gave a model with a crystallographic R-factor for all data of 18.4% and an R_{free} of 21.7% for the rsAPX structure. Refinements of all three structures were completed with REFMAC5 (*70*) and the computer program XTALVIEW (*72*) was used throughout for manual readjustment and rebuilding. The refinement statistics are shown in Table 2.3. The rsAPX coordinates and structure factors have been deposited with the Protein Data Bank (PDB) (www.rcsb.org/pdb/ , accession code 1OAG).

Table 2.3
Refinement statistics for the rsAPX, rsAPX/NO and rsAPX/CN structures.

		rsAPX	rsAPX/NO complex	rsAPX/CN complex
R_{work} (R_{free})		0.178 (0.182)	0.169 (0.243)	0.168 (0.230)
r.m.s. deviation from ideal	Bonds (Å)	0.02	0.03	0.03
	Angles(°)	1.6	2.2	2.0

2.2.4 Structures

2.2.4.1 Overall Structure

Ferric enzyme was used in the crystallographic experiments to determine the rsAPX structure. However, reduction of the heme is possible during data collection (*73*). Therefore, the oxidation state of the heme during and after data collection was not known, but the oxidation state of the iron does not affect the overall structure of rsAPX or the conclusions derived from there. Although rsAPX is a homodimer in solution (*63*), only one monomer is found in the crystallographic asymmetric unit. The overall structure of the enzyme is not substantially affected by nitric oxide or cyanide binding. The overall rsAPX, rsAPX/NO and rsAPX/CN structures are shown in Figure 2.7.

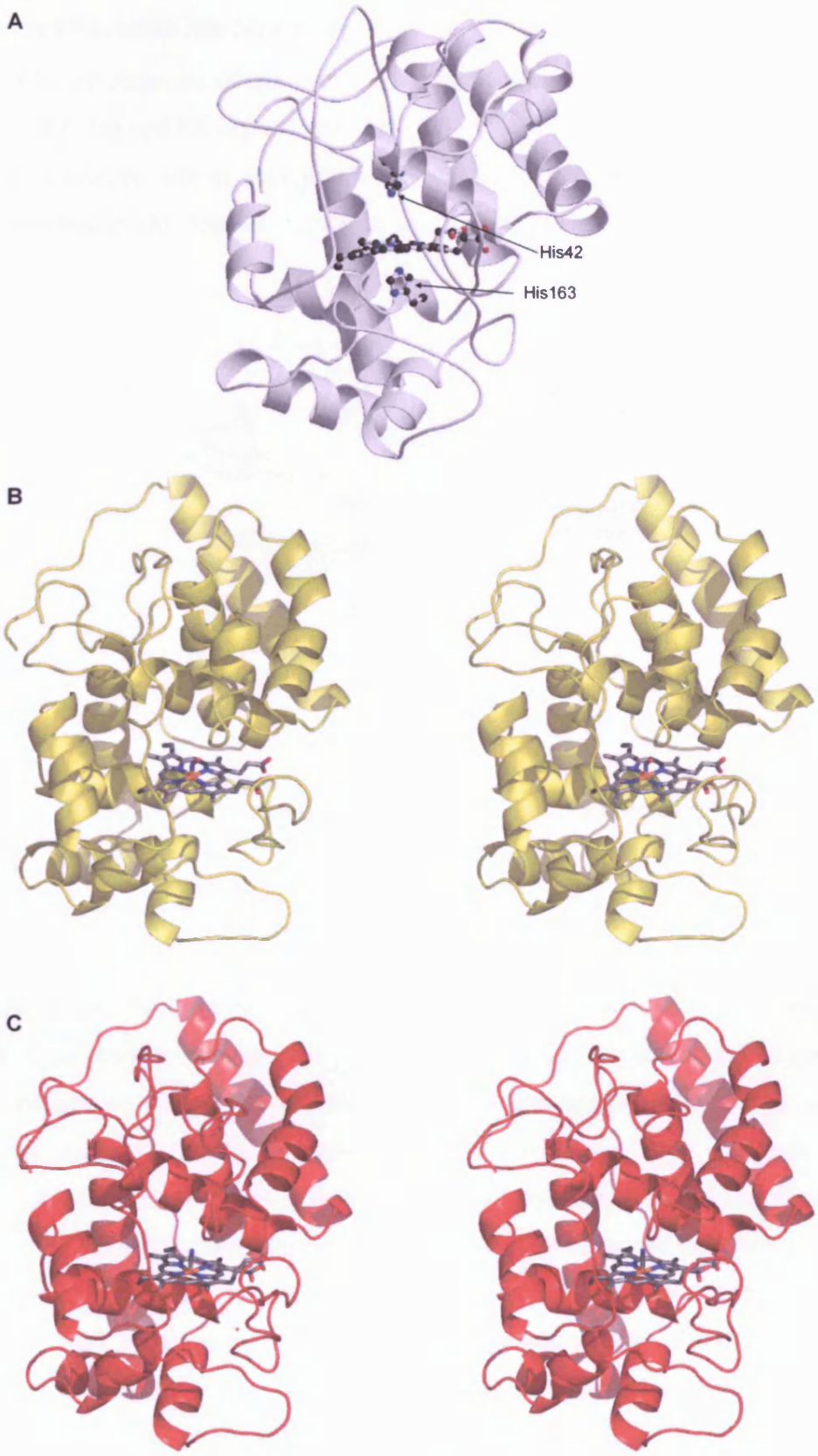

Figure 2.7: (A) The overall structure of rsAPX showing the heme, His42 and His163 (*29*). **(B)** Stereo representation of the overall structure of the rsAPX/NO complex showing the bound nitric oxide molecule. **(C)** Stereo representation of the overall structure of the rsAPX/CN complex showing the bound cyanide molecule. The heme orientation is the same in all three structures.

2.2.4.2 rsAPX Active Site Structure

In rsAPX, the structure of the active site around the heme is essentially unchanged compared to the rpAPX crystal structure. The iron is coordinated to His163 and the sixth coordination site is occupied by a well-ordered water molecule. His163 is hydrogen bonded to Asp208, which in turn is hydrogen bonded to Trp179 (Figure 2.8).

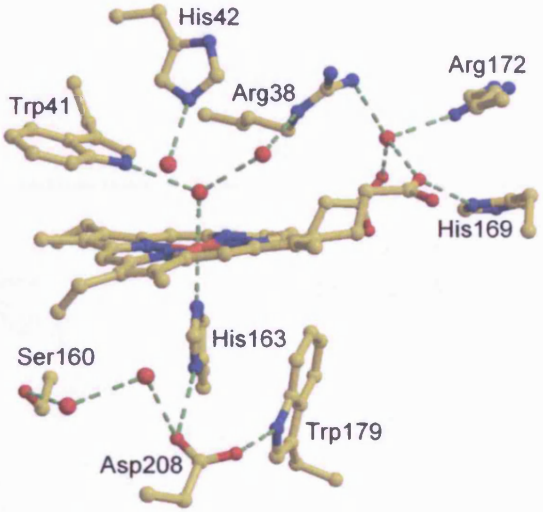

Figure 2.8: The active site structure of rsAPX. Water molecules are indicated by red spheres and hydrogen bonds by green dashed lines.

2.2.4.3 Ion Binding Site

A cation site near Trp179 has been identified in rpAPX which is thought to be occupied by a potassium ion (*13*). The rsAPX, rsAPX/NO and rsAPX/CN structures all show an electron density peak in a similar position, and the observed geometry and temperature factors are consistent with occupation of this site by a water molecule, sodium ion and potassium ion, respectively (Figure 2.9). The sodium and potassium ions were probably introduced from the crystal soaks since the nitric oxide soak contained sodium dithionite and the cyanide soak contained potassium cyanide. The observed distances are shown in Table 2.4. Although six hydrogen bonds around a water molecule are not simultaneously possible, the six distances shown are all within hydrogen-bonding distance, and therefore any four of these six residues could be bonded to the water molecule. The sodium and potassium ions are expected to be six coordinate (*74*), but in the rsAPX/NO and rsAPX/CN structures the number of coordinating atoms within bonding distance are four and five respectively.

Table 2.4
Distances between residues and the ion or water binding site. A dash (-) indicates that the ion is over 3.0 Å away.

Residue	Distances to H_2O, Na or K (Å)		
	rsAPX	rsAPX/ NO	rsAPX/ CN
Thr164	2.9	2.4	2.7
Thr164 (main chain oxygen)	3.0	-	-
Asn182	2.7	2.5	2.7
Ile185	3.0	2.5	2.6
Asp187	3.0	-	3.0
Thr180	3.0	2.7	3.0

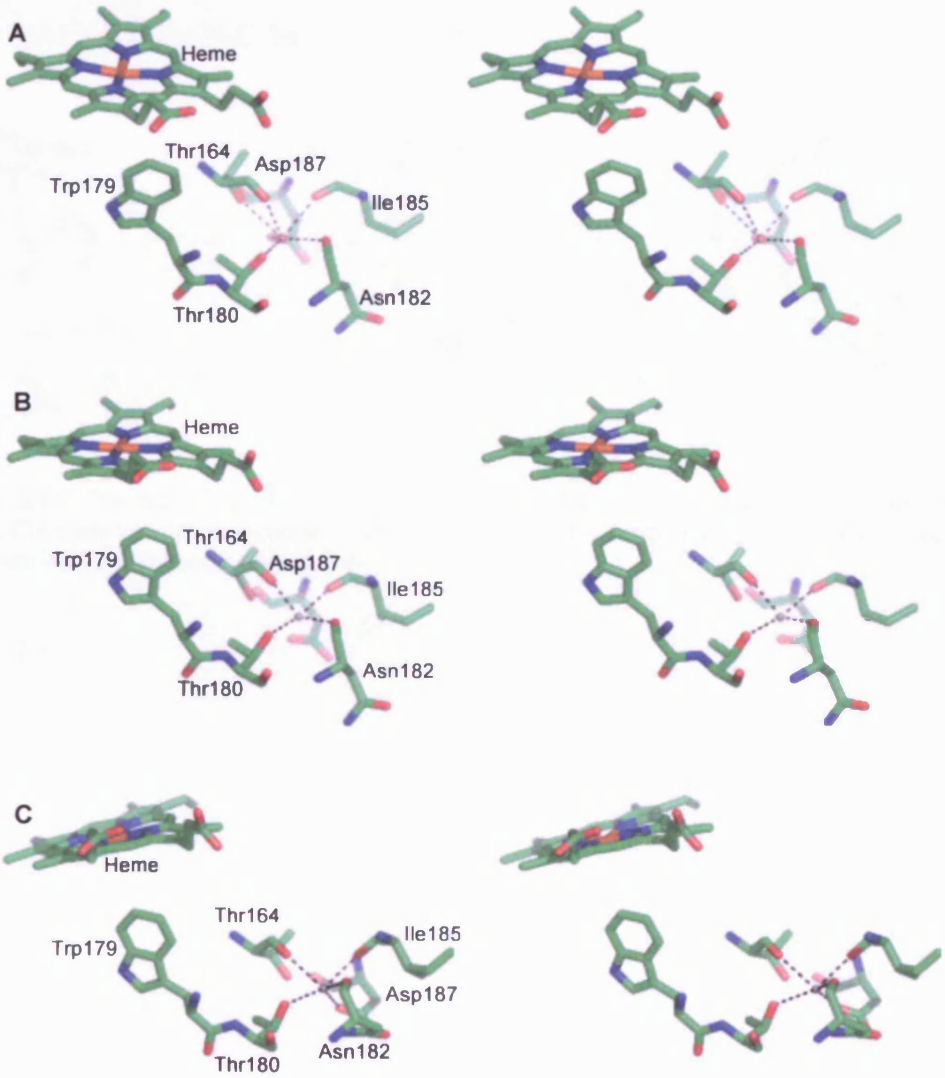

Figure 2.9: Stereo representation of the APX ion binding site in **(A)** rsAPX, **(B)** the rsAPX/NO complex and **(C)** the rsAPX/CN complex. In all cases red spheres indicate water molecules, grey spheres indicate metal ions and black dashed lines indicate possible hydrogen or coordination bonds.

2.2.4.4 Binding of Ligands

In both the rsAPX/NO and rsAPX/CN structures, the ligand fills the sixth coordination site of the iron (Figure 2.10), with the nitric oxide or cyanide molecule replacing two of the water molecules from the rsAPX structure. In the rsAPX/NO structure, the nitrogen atom of the nitric oxide molecule is hydrogen bonded to Trp41 (2.9 Å) and the oxygen atom to His42 (2.9 Å) and a water molecule (2.6 Å). This water molecule is in turn hydrogen bonded to Arg38 (2.9 Å). In the rsAPX/CN structure, the nitrogen atom of the cyanide molecule is hydrogen bonded to a water molecule (2.9 Å) which is in turn hydrogen bonded to Arg38 (3.1 Å). The iron-nitrogen bond in the rsAPX/NO complex is 1.7 Å and the iron-carbon bond in the rsAPX/CN bond is 1.5 Å. In the rsAPX/NO structure the O-N-Fe angle is 130° and in the rsAPX/CN the N-C-Fe angle is 170°.

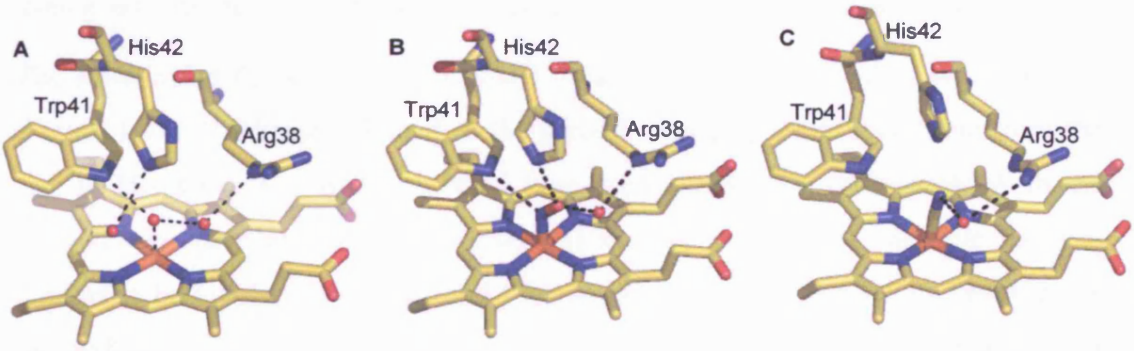

Figure 2.10: The active site structures of **(A)** rsAPX, **(B)** the rsAPX/NO complex, and **(C)** the rsAPX/CN complex. Water molecules are indicated by red spheres and hydrogen and coordination bonds are indicated by black dashed lines.

2.3 DISCUSSION

The occupation of the ion binding site and the coordination number of the ion varies in the three structures examined here. This is discussed further in Chapter 3, section 3.3.2.

2.3.1 The rsAPX Structure

2.3.1.1 Comparison with rpAPX

The overall structures of rsAPX and rpAPX are very similar; sequence alignments show that they have 91% sequence identity with each other. The r.m.s. deviation between Cα positions for the 249 residues in the A-chain of rpAPX and the refined rsAPX structure is 0.443 Å (*75*). Examination of the dimer contacts within the rsAPX crystal shows that the dimer interfaces observed in the rpAPX structure are conserved, despite rsAPX being a monomer in the crystallographic asymmetric unit.

The structure of the active site of rsAPX (Figure 2.8) is almost identical to rpAPX (Figure 1.9). The heme is bound to the protein through a coordinate bond from the iron to His163 and a hydrogen bond from the 7-propionate (propionate A in the Brookhaven nomenclature for heme atoms) to His169. The key catalytic residues thought to be involved in Compound I formation, His42 and Arg38, are observed as in rpAPX. There are three ordered water molecules in the distal pocket, one of which is within bonding distance (2.1 Å) of the heme iron as in rpAPX (2.7 Å).

2.3.2 The rsAPX/CN and rsAPX/NO Structures

A comparison of the rsAPX/CN and rsAPX/NO structures shows that the cyanide is not hydrogen bonded to any protein residues whereas nitric oxide is hydrogen bonded to His42 and Trp41. Hence rsAPX/NO may be a better model for the Fe^{3+}-OOH^- intermediate structure when comparing the geometry of the complexes. The geometry of complexes between transition metal ions and bound diatomic ligands depends on the interaction between the metal ion *d*-orbitals and the ligand π^*-orbitals (*76*). The lower the energies of the ligand's π^*-orbitals, the better π-accepter it is. The lower energy of the π^*-orbitals increases the amount of σ-π mixing with the metal *d*-orbitals, which causes the ligand to assume a bent geometry. Diatomic O-O systems have a low π^*-orbital energy and therefore have a bent geometry. Cyanide and carbon monoxide have higher π^*-orbital energies are not usually induced to bend

(*9*). Nitric oxide can be considered a good model for O-O bound species since nitric oxide has π^*-orbitals that are intermediate in energy and therefore assume a bent geometry like O-O species when bound to a transition metal ion (*9*).

2.3.2.1 Comparison of the rsAPX/NO and CcP/O_2 Complexes

The Fe^{3+}-OOH^- intermediate in Compound I formation (Figure 2.12) has a very short half life and is therefore very difficult to capture (*52*). This intermediate was modelled in C*c*P by binding oxygen to the Fe^{2+} form. The resulting complex was still too unstable to carry out crystallography with a half life of 200 ms at 23 °C (*77*). Internal electron transfer occurs from Trp191 to the bound dioxygen complex resulting in the cleavage of the oxygen-oxygen bond. Mutations at Trp191 that eliminate the electron transfer increase the half life of the complex. By mutating Trp191 to Phe the stability of the complex is improved to 2 hours at room temperature (*77*) making it possible to carry out crystallography (*9*). This C*c*P/O_2 complex structure (Figure 2.11B) provides a good model to study the structure of the Fe^{3+}-OOH^- intermediate and therefore a useful comparison for the rsAPX/NO structure. In the following discussion these two structures are compared and discussed in the context of the reaction mechanism and possible proton transfer pathway.

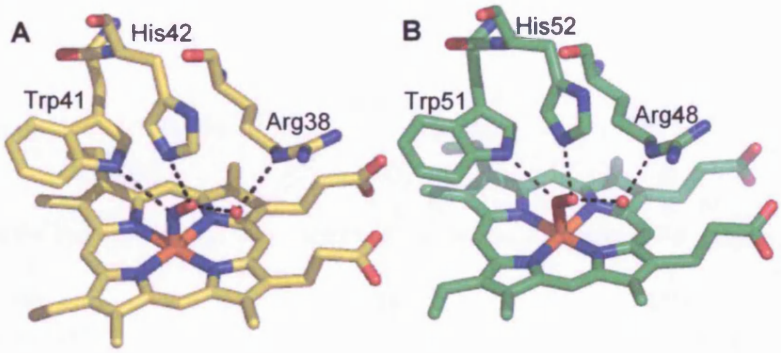

Figure 2.11: (A) The rsAPX/NO complex active site structure. **(B)** The C*c*P/O_2 complex active site structure. Hydrogen bonds are indicated by black dashed lines and red spheres indicate water molecules.

The nitric oxide ligand in the rsAPX/NO complex is bound in the same position as oxygen in the C*c*P/O_2 complex (*9*) (Figure 2.11). This leaves His52 of C*c*P (His42 in APX) in a favourable position to transfer a proton to O_B of the bound hydrogen peroxide (Figure 2.2) since it is less than 3.0 Å away from the O of the nitric oxide molecule (in the rsAPX/NO complex) or O_B of the oxygen molecule (in the C*c*P/O_2

complex). In C*c*P, replacement of His52 by leucine decreases the rate constant for Compound I formation by 10^5-fold (*78, 79*). In APX, His42 is also essential for Compound I formation (*80*). In both models, O_B does not bind to Arg38 or Arg48, which is consistent with the fact that mutations at Arg48 in C*c*P cause less disruption than those at His52 (Compound I formation in the R48K mutant is only two-fold slower than wild type C*c*P (*81*) and the R38A mutant of rpAPX also forms Compound I with a rate constant that is comparable to that of wild type (Mewies, M. and Raven, E. L. (2002), unpublished)). The rsAPX/NO structure therefore supports the mechanism proposed in the C*c*P/O_2 structure paper (*9*) which is as follows. The O_A atom of hydrogen peroxide transfers a proton to His42 or 52 while binding to the iron. Then His42 or 52 transfers the proton to O_B to form water. The water is ejected from its position within the site since it cannot hydrogen bond in the same position as the oxygen atom it was formed from (Figure 2.12).

In both structures the equivalent atom to O_A is hydrogen bonded to Trp51 (Trp41 in APX). Compound I in C*c*P has been found to be stabilised by Trp51 (*82*) and mutants replacing Trp51 with alanine and phenylalanine decreases the rate of reaction with hydrogen peroxide by 60% and 40% respectively (*83*). This indicates that Trp51 plays a role in Compound I formation by stabilising the intermediate and Compound I.

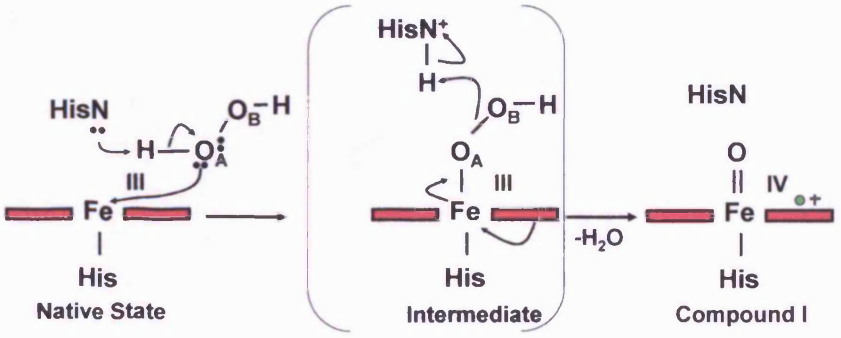

Figure 2.12: Mechanism of Compound I formation.

2.3.2.2 Comparison of the rsAPX/NO and HRP/CN Complexes

In the HRP/CN/ferulic acid complex, Arg38 is bound to the nitrogen of the cyanide molecule (*4*) (Figure 2.13B) and replacement of Arg38 by lysine in the R38K mutant, shows a 500-fold decrease in the rate of Compound I formation (*84*). This may be because HRP does not contain Trp41, and therefore it may use Arg38 instead to help cleave the O-O bond (Figure 2.13D).

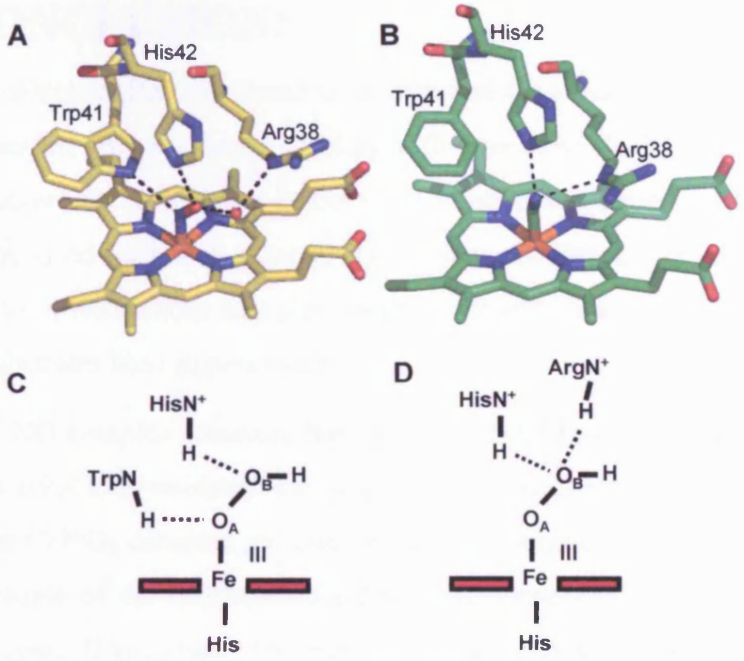

Figure 2.13: (A) The rsAPX/NO complex active site structure. **(B)** The HRP/CN/ferulic acid complex active site structure. **(C)** Intermediate in Compound I formation in class I peroxidases. **(D)** Intermediate in Compound I formation in class III peroxidases. Hydrogen bonds are indicated by black dashed lines and red spheres indicate water molecules.

Together the data suggest that the mechanism for Compound I formation may be slightly different for class I peroxidases compared to class II and III peroxidases, which do not contain a tryptophan at the active site (Figure 2.13C and D). Nevertheless, all three classes still use the active site histidine as a base in Compound I formation.

2.4 CONCLUSIONS

The purity of the rsAPX was found to be essential for successful crystallisation since the MDL screen only produced crystals with pure rsAPX. The rsAPX has a very similar structure to rpAPX but it does not contain the bound potassium ion near Trp179 (discussed further in Chapter 3). In later Chapters, this preliminary data is developed to provide more complex substrate-bound structures and provide insight into how substrates bind in peroxidases.

The rsAPX/NO complex structure has provided insight into the binding of hydrogen peroxide in APX and validated the proposed mechanism of Compound I formation based on the C*c*P/O_2 complex structure for class I peroxidases (*9*). It has also helped rationalise some of the mechanistic differences between Compound I formation in class I and class III enzymes. The rsAPX/NO complex structure along with those of the substrate bound forms of APX are used later to establish a more detailed mechanism for proton transfer (*4*) (discussed in Chapter 4).

2.5 REFERENCES

1. Maurus, R., Bogumil, R., Nguyen, N. T., Mauk, A. G., and Brayer, G. (1998) *Biochemical Journal 332*, 67-74.
2. Mattevi, A., Gatti, G., Coda, A., Rizzi, M., Ascenzi, P., Brunori, M., and Bolognesi, M. (1991) *Journal of Molecular Recognition 4*, 1-6.
3. Edwards, S. L., Poulos, T. L., and Kraut, J. (1984) *Journal of Biological Chemistry 259*, 12984-12988.
4. Henriksen, A., Smith, A. T., and Gajhede, M. (1999) *Journal of Biological Chemistry 274*, 35005-35011.
5. Hersleth, H.-P., Dalhus, B., Gorbitz, C. H., and Andersson, K. K. (2002) *Journal of Biological Inorganic Chemistry 7*, 299-304.
6. Friedman, J., Lad, L., Deshmukh, R., Li, H., Wilks, A., and Poulos, T. L. (2003) *Journal of Biological Chemistry 278*, 34654-34659.
7. Leys, D., Backers, K., Meyer, T. E., Hagen, W. R., Cusanovich, M. A., and Beeumen, J. J. V. (2000) *Journal of Biological Chemistry 275*, 16050-16056.
8. Edwards, S. L., and Poulos, T. L. (1990) *Journal of Biological Chemistry 265*, 2588-2595.
9. Miller, M. A., Shaw, A., and Kraut, J. (1994) *Nature Structural Biology 1*, 524-531.
10. Poulos, T. L., Freer, S. T., Alden, R. A., Edwards, S. L., Skogland, U., Takio, K., Eriksson, B., Xuong, N.-h., Yontani, T., and Kraut, J. (1980) *Journal of Biological Chemistry 255*, 575-580.
11. Rogers, D. W. (1994) *Structure 2*, 1135-1140.
12. Hope, H. (1990) *Annual Review of Biophysics and Biophysical Chemistry 19*, 107-126.
13. Patterson, W. R., and Poulos, T. L. (1995) *Biochemistry 34*, 4331-4341.
14. Morita, Y., Funatsu, J., and Mikami, B. (1993) in *Plant Peroxidases. Biochemistry and Physiology* (Welinder, K. G., Rasmussen, S. K., Penel, C., and Greppin, H., Eds.) pp 1-4, university of Geneva, Geneva.
15. Morita, Y., Mikami, B., Yamashita, H., Lee, J. Y., Aibara, S., Sato, M., Katsube, Y., and Tanaka, N. (1991) in *Biochemical, Molecular and Physiological Aspects of Plant Peroxidases* (Greppin, H., Penel, C., and Gaspar, T., Eds.) pp 81-88, university of Geneva Press, Geneva.

16. Edwards, S. L., Raag, R., Warhshi, H., Gold, M. H., and Poulos, T. L. (1993) *Proceedings of the National Academy of Science, USA 90*, 750-754.

17. Fulop, V., Ridout, C. J., Greenwood, C., and Hadju, J. (1995) *Structure 3*, 1225-1233.

18. Petersen, J. F. W., Kadziola, A., and Larsen, S. (1994) *FEBS Letters 339*, 291-296.

19. Petersen, J. F. W., Tams, J. W., Vind, J., Svensson, A., Dalboge, H., Welinder, K. G., and Larsen, S. (1993) *Journal of Biological Chemistry 232*, 989-991.

20. Sundaramoorthy, M., Kishi, K., Gold, M. H., and Poulos, T. L. (1994) *Journal of Biological Chemistry 269*, 32759-32767.

21. Sundaramoorthy, M., Terner, J., and Poulos, T. L. (1995) *Structure 3*, 1367-1377.

22. Schuller, D. J., Ban, N., van Huystee, R. B., McPherson, A., and Poulos, T. L. (1996) *Structure 4*, 311-321.

23. Gajhede, M., Schuller, D. J., Heriksen, A., Smith, A. T., and Poulos, T. L. (1997) *Nature Structural Biology 4*, 1032-1038.

24. Henriksen, A., Schuller, D. J., Meno, K., Welinder, K. G., Smith, A. T., and Gajhede, M. (1998) *Biochemistry 37*, 8054-8060.

25. Henriksen, A., Mirza, O., Indiani, C., KaareTeilum, Smulevich, G., Welinder, K. G., and Gajhede, M. (2001) *Protein Science 10*, 108-115.

26. Yamada, Y., Fujiwara, T., Sato, T., Igarashi, N., and Tanaka, N. (2002) *Nature Structural Biology 9*, 691-695.

27. Wada, K., Tada, T., Nakamura, Y., Ishkawa, T., Yabuta, Y., Yoshimura, K., Shigoeka, S., and Nishimura, K. (2003) *Journal of Biochemistry 134*, 239-244.

28. Wada, K., Tada, T., Nakamura, Y., Yabuta, Y., Yoshimura, K., Takeda, T., Shigoeka, S., and Nishimura, K. (2002) *Acta Crystallographica D58*, 559-561.

29. Sharp, K. H., Mewies, M., Moody, P. C. E., and Raven, E. L. (2003) *Nature Structural Biology 10*, 303-307.

30. Koshkin, A., Nunn, C. M., Djordjevic, S., and Oritz de Montellano, P. R. (2003) *Journal of Biological Chemistry 278*, 29502-29508.

31. Carpena, X., Loprasert, S., Mongkolsuk, S., Switala, J., Loewen, P. C., and Fita, I. (2003) *Journal of Molecular Biology 327*, 475-480.

32. Bertrand, T., Eady, N. A. J., Jones, J. N., Bodiguel, J., Jesmin, Nagy, J. M., Raven, E. L., Jamart-Gregoire, B., and Brown, K. H. (2004) *Journal of Biological Chemistry 279*, 38991-38999.

33. Carpena, X., Melik-Adamyan, W., Loewen, P. C., and Fita, I. (2004) *Acta Crystallographica D 60*, 1824-1831.

34. Fulop, V., Phizackerley, R. P., Soltis, S. M., Clifton, I. J., Wakatsuki, S., Erman, J. E., Hajdu, J., and Edwards, S. L. (1994) *Structure 2*, 201-208.

35. Edwards, S. L., huu Xuong, N., Hamlin, R. C., and Kraut, J. (1987) *Biochemistry 26*, 1503-1511.

36. Bonagura, C. A., Bhaskar, B., Shimizu, H., Li, H., Sundaramoorthy, M., McRee, D. E., Goodin, D. B., and Poulos, T. L. (2003) *Biochemistry 42*, 5600-5608.

37. Chance, B., Powers, L., Ching, Y., Poulos, T. L., Schonbaum, G. R., Yamazaki, I., and Paul, K. G. (1984) *Archives of Biochemistry and Biophysics 235*, 596-611.

38. Penner-Hahn, J., McMurry, T., Renner, M., Latos-Grazynsky, L., Eble, K. S., Davis, I. M., Balch, A. L., Groves, J. T., Dawson, J. H., and Hodgson, K. O. (1983) *Journal of Biological Chemistry 258*, 12761-12764.

39. Groves, J. T., Quinn, R., McMurray, T. J., Nakamura, M., Lang, G., and Boso, B. (1985) *Journal of the American Chemistry Society 107*, 354-360.

40. Lang, G., Spartalain, K., and Yonetani, T. (1967) *Biochimica et Biophysica Acta 451*, 250-258.

41. Makino, R., Uno, T., Nishimura, Y., Lizuka, T., Tsuboi, M., and Ishimura, Y. (1986) *Journal of Biological Chemistry 261*, 8376-8382.

42. Sitter, A. J., Reczek, C. M., and Terner, J. (1985) *Journal of Biological Chemistry 260*, 7515-7522.

43. Hashimoto, S., Teraoka, J., Inubushi, T., Yonetani, T., and Kitagawa, T. (1986) *Journal of Biological Chemistry 261*, 11110-11118.

44. Reczek, C. M., Sitter, A. J., and Terner, J. (1989) *Journal of Molecular Structure 214*, 27-41.

45. Erman, J. E., and Vitello, L. B. (2002) *Biochimica et Biophysica Acta 1597*, 193-220.

46. Dolphin, D., Forman, A., Borg, D. C., Fajer, J., and Felton, R. H. (1971) *Proceedings of the National Academy of Science, USA 68*, 614-618.

47. Dunford, H. B. (1982) *Advances in Inorganic Biochemistry 4*, 41-68.

48. Hiner, A. N. P., Martinez, J. I., Arnao, M. B., Acosta, M., Turner, D. D., Raven, E. L., and Rodriguez-Lopez, J. N. (2001) *European Journal of Biochemistry 268*, 3091-3098.

49. Regelsberger, G., Jakopitsch, C., Ruker, F., Krois, D., Peschek, G. A., and Obinger, C. (2000) *Journal Biolological Chemistry 275*, 22854-22861.

50. Jakopitsch, C., Ruker, F., Regelsberger, G., Dockal, M., Peschek, G. A., and Obinger, C. (1999) *Biological Chemistry 380*, 1087-1096.

51. Baek, H. K., and Van Wart, H. E. (1989) *Biochemistry 28*, 5714-5719.

52. Baek, H. K., and Van Wart, H. E. (1992) *Journal of the American Chemical Society 114*, 718-725.

53. Filizola, M., and Loew, G. H. (2000) *Journal of the American Chemistry Society 122*, 18-25.

54. Harris, D. L., and Loew, G. H. (1996) *Journal of the American Chemistry Society 118*, 10588-10594.

55. Loew, G. H., and Dupuis, M. (1996) *Journal of the American Chemistry Society 118*, 10584-10587.

56. Ozaki, S.-I., Inada, Y., and Watanabe, Y. (1998) *Journal of the American Chemistry Society 120*, 8020-8025.

57. Poulos, T. L., and Kraut, J. (1980) *Journal of Biolological Chemistry 255*, 8199-8205.

58. Rodriguez-Lopez, J. N., Smith, A. T., and Thorneley, R. N. F. (1996) *Journal of Biolological Chemistry 271*, 4023-4030.

59. Wirstam, M., Blomberg, M. R. A., and Siegbahn, P. E. M. (1999) *Journal of the American Chemistry Society 121*, 10178-10185.

60. Brucker, E. A., Olson, J. S., Ikeda-Saito, M., and Phillips, G. N. (1998) *Proteins-Structure Function and Genetics 30*, 352-361.

61. Conti, E., Moser, C., Rizzi, M., Mattevi, A., Lionetti, C., Coda, A., Ascenzi, P., Brunori, M., and Bolognesi, M. (1993) *Journal of Molecular Biology 233*, 498-510.

62. Dalton, D. A., del Castillo, L. D., Kahn, M. L., Joyner, S. L., and Chatfield, J. M. (1996) *Archives of Biochemistry and Biophysics 328*, 1-8.

63. Jones, D. K., Dalton, D. A., Rosell, F. I., and Lloyd Raven, E. (1998) *Archives of Biochemistry and Biophysics 360*, 173-178.

64. Chatfield, J. M., and Dalton, D. A. (1993) *Plant Physiology 103*, 661-662.

65. Patterson, W. R., and Poulos, T. L. (1994) *Journal of Biological Chemistry 269*, 17020-17024.

66. Hampton Research *www.hamptonresearch.com/hrproducts/4981.html*.

67. Dalton, D. A., Hanus, F. J., Russell, S. A., and Evans, H. J. (1987) *Plant Physiology 83*, 789-794.

68. Otwinoski, Z., and Minor, W. (1997) *Methods Enzymology 227*, 366-396.

69. Vagin, A., and Teplyakov, A. (1997) *Journal of Applied Crystallography 30*, 1022-1025.

70. Project, N. C. C. (1994) *Acta Crystallographica D50*, 760-763.

71. Brunger, A. T., Adams, P. D., Clore, G. M., DeLano, W. L., Gros, P., Grosse-Kunstleve, R. W., Jiang, J.-S., Kuszewski, J., Nilges, M., Pannu, N. S., Read, R. J., Rice, L. M., Simonson, T., and Warren, G. L. (1998) *Acta Crystallographica D54*, 905-921.

72. McRee, D. (1992) *Journal of Molecular Graphics 10*, 44-47.

73. Berglund, G. I., Carlsson, G. H., Smith, A. T., Szöke, H., Henriksen, A., and Hajdu, J. (2002) *Nature 417*, 463-468.

74. Harding, M. M. (2002) *Acta Crystallogaphica D 58*, 872-874.

75. Matching, S. S. *http://www.ebi.ac.uk/msd/ssm*.

76. Hoffman, R., Chen, M. M.-L., and Thorn, D. (1977) *Inorganic Chemistry 16*, 503-511.

77. Miller, M. A., Bandyopadhyay, D., Mauro, J. M., Traylor, T. G., and Kraut, J. (1992) *Biochemistry 31*, 2789-2797.

78. Erman, J. E., Vitello, L. B., Miller, M. A., Shaw, A., Brown, K. A., and Kraut, J. (1993) *Biochemistry 32*, 9798-9806.

79. Erman, J. E., Vitello, L. B., Miller, M. A., and Kraut, J. (1992) *Journal of the American Chemical Society 114*, 6592-6593.

80. Lad, L., Mewies, M., Basran, J., Scrutton, N. S., and Raven, E. L. (2002) *European Journal of Biochemistry 269*, 3182-3192.

81. Vitello, L. B., Erman, J. E., Miller, M. A., Wang, J., and Kraut, J. (1993) *Biochemistry 32*, 9807-9818.

82. Pfister, T. D., Gengenbach, A. J., Syn, S., and Lu, Y. (2001) *Biochemistry 40*, 14942-14951.

83. Goodin, D. B., Davidson, M. G., Roe, J. A., Mauk, A. G., and Smith, M. (1991) *Biochemistry 30*, 4953-4962.

84. Smith, A. T., Sanders, S. A., Greschik, H., Thorneley, R. N. F., Burke, J. F., and Bray, R. C. (1992) *Biochemistry Society Transactions 20*, 340-345.

Chapter 3

The X-Ray Crystal Structure of the rsAPX/Ascorbate Complex

3.1 INTRODUCTION

Until recently, the crystal structure of a peroxidase with a genuine physiological small organic substrate has proved elusive. There have been a few examples of peroxidase structures with physiological substrates, such as the CcP/cytochrome *c* complex (*1*) and the manganese peroxidase/Mn^{2+} complex (*2*), but these peroxidases utilise atypical substrates that are not representative of the family as a whole. In the literature there are also examples of crystal structures of peroxidases with non-physiological small organic substrates or inhibitors. Examples of these include: HRP in complex with benzhydroxamic acid (BHA) (*3*) and ferulic acid (FA) (*4*), and *Arthromyces ramosus* peroxidase (ARP) with BHA (*5*) and salicylhydroxamic acid (SHA) (*6*). When the structure of rpAPX was solved the importance of the ascorbate bound form was realised, but attempts to obtain a crystal structure of the rpAPX/ascorbate complex were unsuccessful (*7*). The X-ray crystal structure of rsAPX/ascorbate complex will provide insight into how peroxidases, from all three classes, bind physiological substrates. (Classification of peroxidases is discussed in Chapter 1, section 1.3.)

To date, substrate binding in APX has been investigated by NMR (*8*), site-directed mutagenesis (*9, 10*) and chemical modification (*8, 10*), but no definitive view of the binding location has emerged. Summarised below is the information that was available prior to the elucidation of the rsAPX/ascorbate structure.

NMR studies were carried out on the cyanide bound form of APX to discover the distance from the non-exchangeable protons on ascorbate (Figure 3.1A) to the heme iron (0.9-1.12 Å) (*8*). These NMR data, along with the crystal structure (*7*) were used to model possible ascorbate binding sites in APX (*8*). From this analysis, two ascorbate binding sites were identified at the δ- and γ-heme edges (Figure 3.1B and C) (*8*).

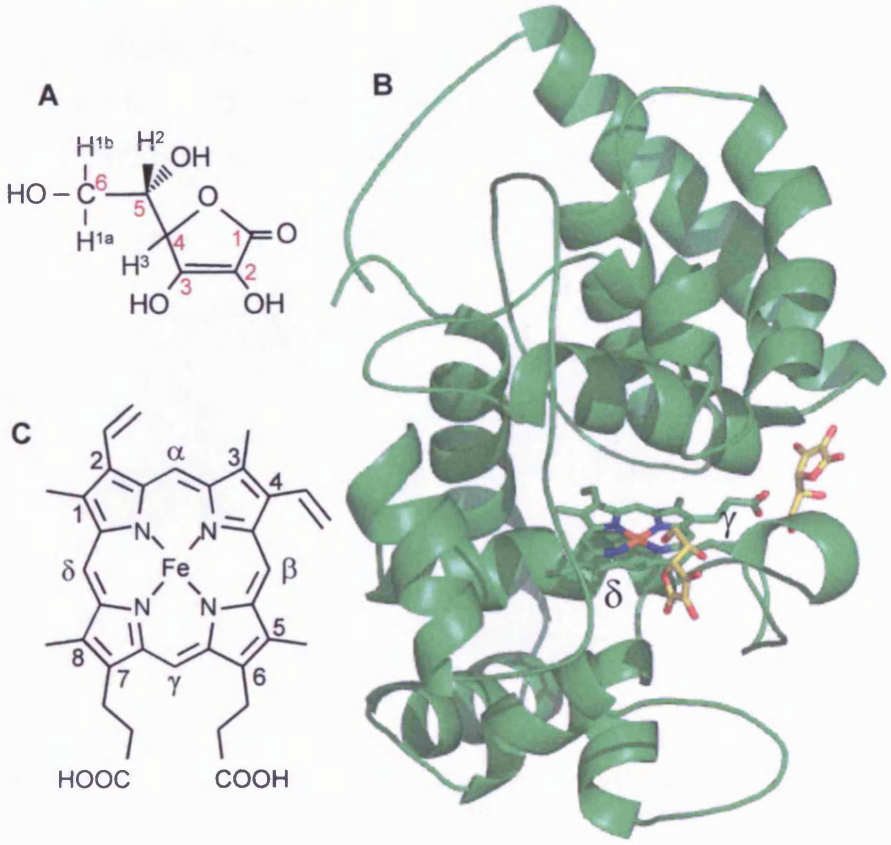

Figure 3.1: (A) The structure of ascorbate with the non-exchangeable protons (numbered according to Hill *et al.* (*8*) (1a, 1b, 2 and 3)) and the carbon numbering used in this Chapter (red). **(B)** Model of the structure of APX showing the two possible sites for binding of ascorbate (yellow) based on the NMR data and rpAPX crystal structure (*8*). The δ- and γ-edges of the heme are indicated. **(C)** The structure of protoporphyrin IX showing the nomenclature used in this Chapter.

In separate experiments, modification of the heme with phenylhydrazine showed that the majority of the heme (60%) was modified at the δ position (sometimes referred to as the C20 position) (Figure 3.1C) (*8*), indicating that the δ-heme edge is accessible to solvent. From these chemical modification experiments and previous studies of small molecule substrates in other peroxidases, particularly C*c*P (*11, 12*), the δ-heme edge was proposed to be the preferred binding site for small organic substrates in APX (*8*).

Later, chemical modification and mutagenesis of the Cys32 residue in rpAPX indicated that aromatic substrates and ascorbate bind at two different sites (*10*). Cys32 was modified with Ellman's reagent (DTNB, 5,5'–dithiobis(2-nitrobenzoic acid)), and the modified form was crystallised (Figure 3.2A) (*10*). The modified form retained full activity with aromatic substrates, such as guaiacol and pyrogallol, but had only 1.3% of wild type activity with ascorbate (*10*). Site-directed mutagenesis of the cysteine residue to a serine lost 70% of ascorbate activity while

retaining all guaiacol activity (*10*). Together, this indicated that ascorbate must bind in a different site to other aromatic compounds, and that this ascorbate site was located near Cys32, at the γ-edge of the heme (Figure 3.2B) (*10*).

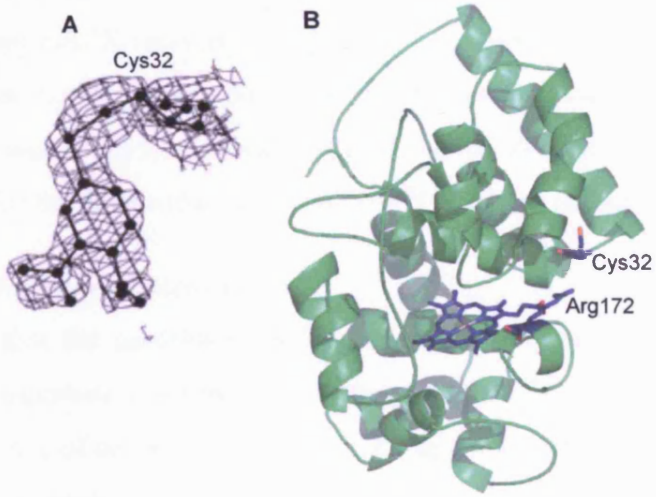

Figure 3.2: (A) Electron density of the chemically modified Cys32 in rpAPX (*10*). **(B)** Location of Cys32 (blue) and Arg172 (blue) in rpAPX (green) with the heme (blue) (*7*).

It was later shown that site-directed mutagenesis of Arg172 to lysine (R172K), glutamine (R172Q) or asparagine (R172N) resulted in significant loss of ascorbate activity, but the mutants retained the ability to oxidise guaiacol (*9*). This indicated that Arg172 was important for ascorbate oxidation but not for the oxidation of other aromatic substrates (*9*).

Prior to the publication of the rsAPX/ascorbate complex structure, the collective conclusions of all the data were as follows. NMR, chemical modification and site-directed mutagenesis data were all consistent with an ascorbate binding site close to the γ-heme edge, with the binding of aromatic substrates probably occurring at a separate site, possibly at the δ-heme edge.

3.2 RESULTS

3.2.1 Preparation of Crystals and Data Collection

3.2.1.1 Crystal Soak

Crystals of the rsAPX/ascorbate complex were obtained by soaking the best rsAPX crystals in the mother liquor containing sodium L-ascorbate (1.0 M) for ~5 minutes. The crystals were then frozen and prepared for the synchrotron in the same way as the crystals for the determination of the rsAPX structure (Chapter 2, section 2.2.3.1).

3.2.1.2 The Binding of Ascorbate

To confirm that the ascorbate did bind to rsAPX in the crystal soak, the rate of oxidation of ascorbate was measured in the presence of lithium sulphate and Hepes at pH 8.3. The rate of decrease in absorbance was measured at the ascorbate absorption maximum (290 nm) with an enzyme concentration of 5 μM. The rate was 0.175 au/min, which is similar to the maximum rate measured when rsAPX was assayed in phosphate buffer at pH 7.0 (0.179 au/min). Hence, the ascorbate must be oxidised by rsAPX under these conditions, and by implication ascorbate must bind to rsAPX under the conditions of the crystal soak.

3.2.1.3 Data Collection

Data were collected in two passes on beam-line ID14-4 at ESRF (Grenoble) using an ADSC Quantum-4 detector and 0.94 Å radiation. In the first pass, data to 1.4 Å were collected over 54°; this was followed by data collected to 1.8 Å over 90°. Data collection statistics are shown in Table 3.1.

Table 3.1
Data collection statistics for the rsAPX/ascorbate complex.

Resolution Ranges (Å)	1.40-57.74
Total Observations	339,792
Unique Reflections	49,370
I/sigI	23.2
R_{merge} (%)	8.3
Completeness (%)	96.2

3.2.1.4 Data Interpretation

The refined structure of rsAPX was used as the start-point for interpretation of data for the rsAPX/ascorbate complex. The model was stripped of solvent molecules and subjected to rigid-body refinement using 3.0 Å data. The structure was then broken into 24 segments corresponding to elements of secondary structure and each segment refined as a rigid body. The model was then further refined using all data. The computer program CNS v1.1 (*13*) was used in these steps.

3.2.1.5 Refinement and Rebuilding

From a difference density map the density for ascorbate was unambiguous. Therefore the structure was incorporated into the subsequent refinement. The refinement was concluded using REFMAC5 (*14*) with anisotropic atomic temperature factors (*15*). The computer program XTALVIEW (*16*) was used throughout for manual adjustment and rebuilding. The refinement statistics are shown in Table 3.2. Coordinates and structure factors have been deposited with the PDB (code 1OAF).

Table 3.2
Refinement statistics for rsAPX /ascorbate complex.

R_{work} (R_{free})		0.178 (0.182)
r.m.s. deviations from ideal	**Angles (°)**	0.016
	Bonds (Å)	1.593

3.2.2 The X-ray Crystal Structure

3.2.2.1 Overall Structure

The overall structure of the enzyme (Figure 3.3) is not significantly affected by ascorbate binding (r.m.s deviation in Cα positions of 0.174 Å from the rsAPX structure).

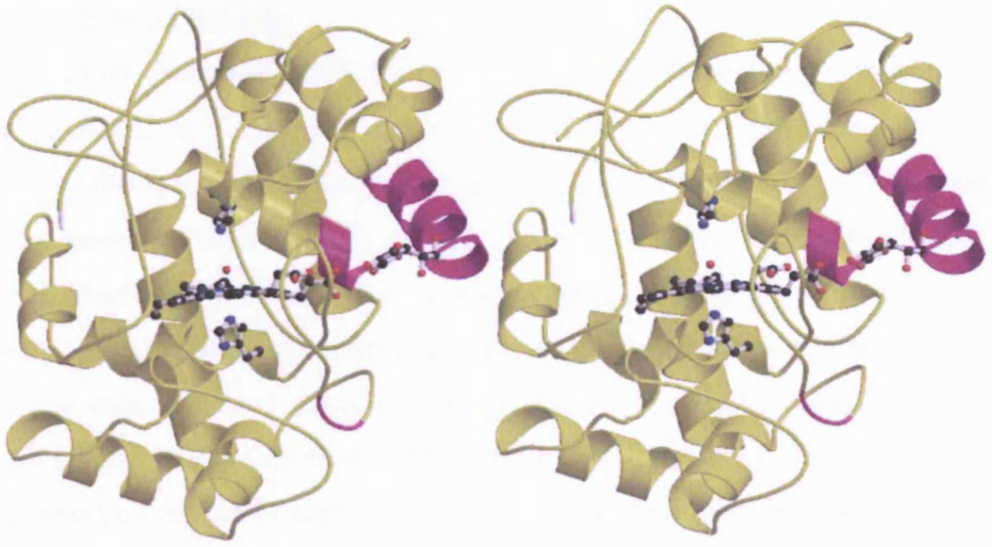

Figure 3.3: Stereo representation of the overall structure of the rsAPX/ascorbate complex. The regions shown in Figure 3.9C are highlighted in pink (*17*).

3.2.2.2 Ion Binding Site

A cation site near Trp179 has been identified in rpAPX (*7*) but in the rsAPX structure a water molecule occupies this site (Chapter 2, Figure 2.12). In the rsAPX/ascorbate structure, the electron density contains a peak that is characterized by short distances from the main-chain oxygens of Thr164 (2.2 Å), Asn182 (2.3 Å), Ile185 (2.3 Å), Thr180 (2.7 Å) and a solvent molecule (2.2 Å), which is in turn hydrogen-bonded to Asp187 (Figure 3.4).

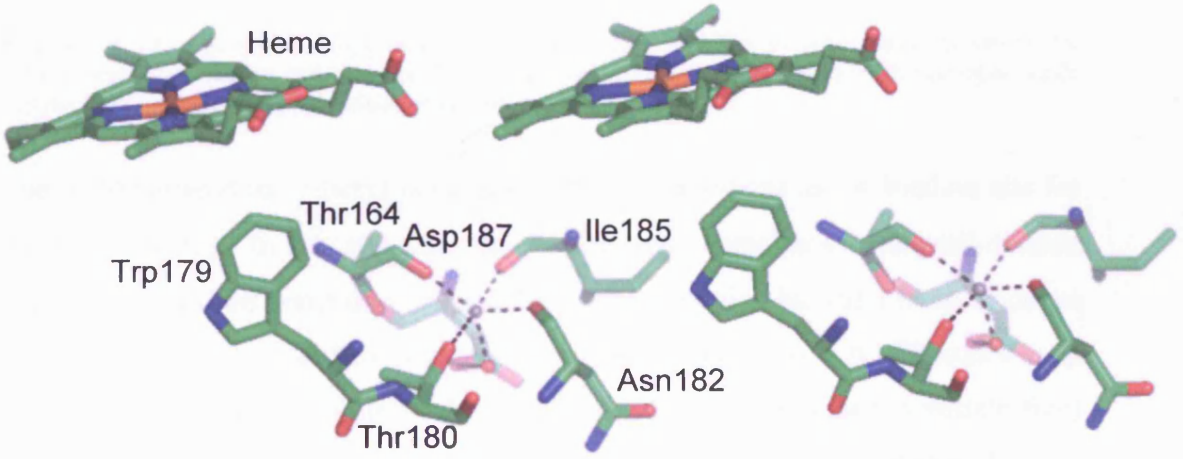

Figure 3.4: Stereo representation of the ion binding site in the rsAPX/ascorbate complex. The ion is indicated by a grey sphere and water molecules are indicated by red spheres. Coordination bonds are indicated by black dashed lines.

These observations are consistent with occupation of this site by a sodium ion (*18*), almost certainly introduced during the crystal soak (which contained 1 M sodium ascorbate). These data indicate a five coordinate ion.

3.2.2.3 Ascorbate Binding

As previously discussed, NMR (*8*) and chemical modification/mutagenesis (*9, 10*) have implicated the γ-meso position of the heme, in particular Cys32 and Arg172 (*9, 10*), in ascorbate binding. Examination of the electron density for rsAPX around the γ-meso position (Figure 3.5A) reveals 5 ordered water molecules directly or indirectly hydrogen-bonded to the side-chains of Arg172 and the heme 6-propionate (propionate D in the Brookhaven nomenclature). Electron density maps calculated from the data collected from the rsAPX/ascorbate complex clearly show that ascorbate binds in place of these water molecules (Figure 3.5B). There are hydrogen bonds between the 2-OH and 3-OH groups of ascorbate and the protein (Arg172), and between the 2-OH group of ascorbate and the (deprotonated) heme 6-propionate. Most notably, the side chain of Lys30 swings in from solvent to provide additional hydrogen bonding stabilization through the 6-OH group of the substrate.

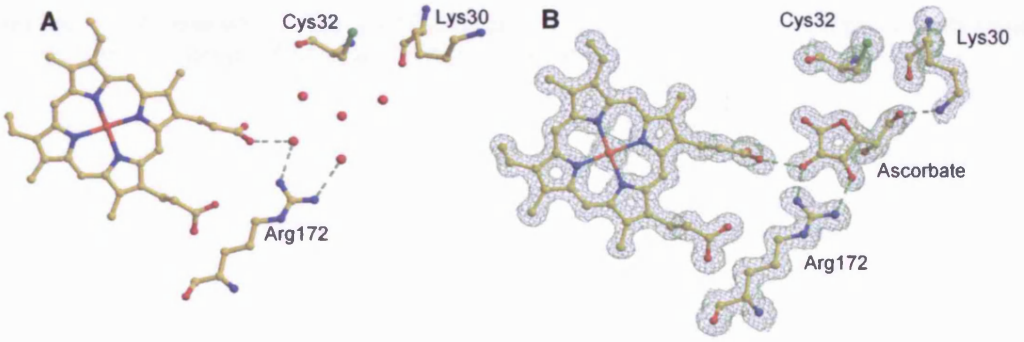

Figure 3.5: (A) The γ-heme edge in the rsAPX structure. **(B)** The ascorbate binding site in the rsAPX/ascorbate complex with electron density (green). Green dashed lines indicate hydrogen bonds and red spheres indicate water molecules in both A and B.

The region around the δ-heme edge has also been implicated as the binding site for ascorbate (*8, 19*). In this structure, the δ-heme edge contains several well-defined water molecules and some unaccounted for electron density, but there is no evidence for ascorbate binding at this position under these conditions. A difference map calculated between the data from the rsAPX/ascorbate complex and (substrate free) rsAPX shows strong positive density corresponding to the ascorbate, but no significant positive density around the δ–meso position (Figure 3.6). This site could possibly be used for ascorbate binding but if so it is either very weak or does not bind under the conditions used in these experiments.

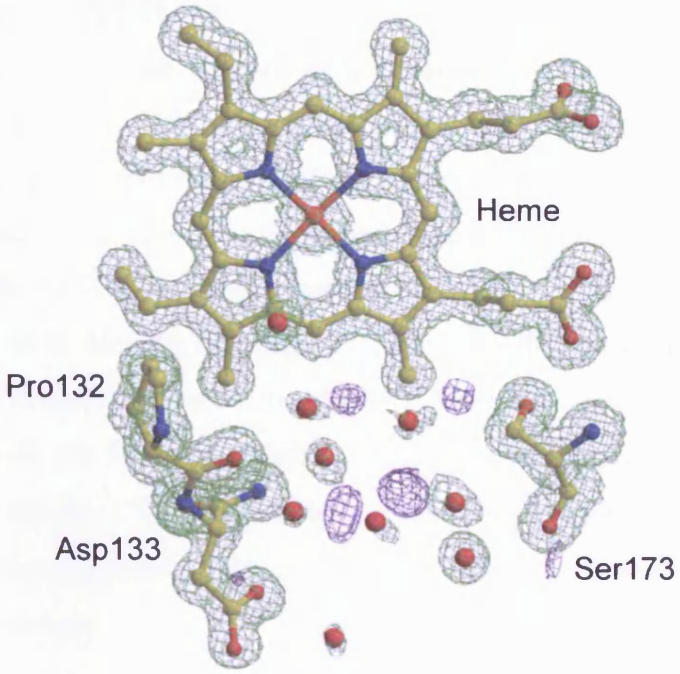

Figure 3.6: The δ-heme edge of the rsAPX/ascorbate complex with difference electron density (blue) and electron density (green). Red spheres indicate water molecules.

3.3 DISCUSSION

The best information that was previously available on the nature of the ascorbate-binding interaction in APX came from two sources. First, NMR-derived distances (*8*) indicated two possible binding sites, close to the 6-propionate (γ-meso) and δ-meso positions of the heme. In the crystal structure, the distance from the substrate (oxygen of the 2-OH group) to the heme iron is 11.2 Å, in reasonable agreement with the original NMR data (*8*) that suggested that the substrate protons bound between 9.0 and 11.2 Å from the heme iron. Second, mutagenesis and chemical modification experiments (*9, 10*) favoured ascorbate binding at the γ-heme edge, close to Cys32 (Figure 3.2) and Arg172 (which is close to the γ-meso position implicated by NMR (*8*)). The structure presented here is consistent with the γ-heme position as the site of ascorbate oxidation.

3.3.1 The Role of Individual Residues in Ascorbate Binding

The electrostatic role of Arg172 in substrate binding (*9*) is confirmed, but this residue has no direct role in electron transfer as previously suggested (*9*). The ascorbate is directly bound to the heme propionate (Figure 3.6) and presumably the electron is transferred directly to the heme through the heme propionate.

Cys32 has no direct interaction with the substrate, which is consistent with the modest (≈3-fold decrease) effect on ascorbate activity in the C32S variant (*10*). Modification of Cys32 with thiol-specific reagents (*e.g.* 5,5'-dithiobis(2-nitrobenzoic acid)) has a more dramatic (≈1000-fold) effect on ascorbate activity (*10*), but this is because the large DTNB group blocks the γ-site and not because of any direct role for Cys32 in substrate binding.

The role of Lys30 in ascorbate binding was not expected. In the substrate-free structure, this residue is oriented away from the heme and into solvent. A conformational change of this residue is induced when ascorbate binds to satisfy the hydrogen bonding requirements of the substrate.

3.3.2 Ion Binding Site

It has been proposed (*20*) that the potassium binding site present in APX, but not in *Cc*P, might destabilize radical formation at Trp179 on electrostatic grounds. This has not been demonstrated conclusively so comparison of all the known APX

structures at that site may provide insight into this theory. The distances between the metal ion and surrounding residues in all the rsAPX and rpAPX crystal structures are shown in Table 3.3.

Table 3.3
Distances between residues and the ion or water binding site (*7, 17, 21*). A dash (-) indicates that the ion is over 3.0 Å away.

Residue	Distance from K, Na or water/ Å					
	rpAPX	**rsAPX**	**rsAPX/ ascorbate**	**rsAPX/ SHA**	**rsAPX/ NO**	**rsAPX/ CN**
Thr164	2.5	2.9	2.2	2.2	2.4	2.7
Thr164 (main chain oxygen)	3.0	3.0	-	-	-	-
Asn182	2.8	2.7	2.3	2.4	2.5	2.7
Asn182 (main chain oxygen)	2.7	-	-	-	-	-
Ile185	2.5	3.0	2.3	2.3	2.5	2.6
Asp187	-	3.0	-	-	-	3.0
H_2O	-	-	2.2	2.2, 2.5	-	-
Thr180	2.9	3.0	2.7	2.7	2.7	3.0

The average metal-oxygen bond length for a potassium ion is 2.7-2.8 Å, whereas the average metal-oxygen bond length for a sodium ion is 2.4-2.6 Å (*18*). Hydrogen bonds to water are usually in the range 2.8-3.0 Å. Based on the distances above, APX can bind potassium, sodium and water depending on the preparation of the protein. In the rpAPX crystal structure, a potassium ion is proposed as occupying this site probably due to being stored in 50 mM potassium phosphate buffer pH 7.0 (*22*). The rsAPX/CN structure most likely has a potassium ion, as potassium cyanide was used in the crystal soak (Chapter 2). The rsAPX structure contains a water molecule (Chapter 2), as it was stored in water (although it was isolated and prepared using potassium phosphate buffers).

The distances at the metal binding site in the rsAPX/NO (Chapter 2), rsAPX/ascorbate (Figure 3.4) and rsAPX/SHA (Chapter 4) complexes are short and consistent with a bound sodium ion. This is probably because the ascorbate crystal soak contained 1 M sodium ascorbate, the SHA crystal soak contained sodium hydroxide (used to alter the pH) and the NO crystal soak contained sodium dithionite.

The X-ray crystal structure of tobacco plant stromal APX (*23*) has also been solved recently and this contains a sodium-binding site in a similar position (although the binding residues differ as it is a stromal APX and the sequence differences are greater) (Figure 3.7). The conditions in which it was crystallized contained ascorbate and Hepes, both of which were probably in the sodium salt form (*24*).

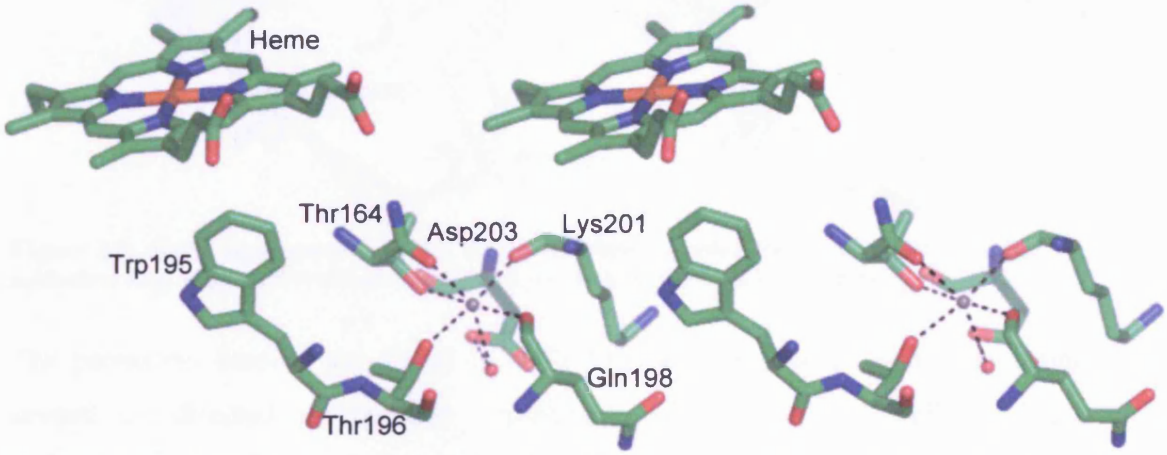

Figure 3.7: Stereo representation of the proximal ion binding site in tobacco stromal APX (*23*). A grey sphere indicates the ion and a red sphere indicates water.

This information indicates that the occupancy of the ion site would depend on the local ion concentrations. In plant cytosols, the concentration of potassium ions is ~100-200 mM (*25*) therefore APX should contain the potassium binding site when in the cytosol.

3.3.2.1 Comparison with CcP

The APX structure in this region contrasts with that found in C*c*P. C*c*P contains the loop where the ion is bound in APX but lacks the cationic ligands to bind an ion or water (Figure 3.8). The loop in APX contains coordinating residues - Asn182, Asp187, Thr180, Thr164 and Ile185 - whereas the equivalent residues in C*c*P are, respectively, Ala194, Thr199, Gly192, Ala176 and Glu201.

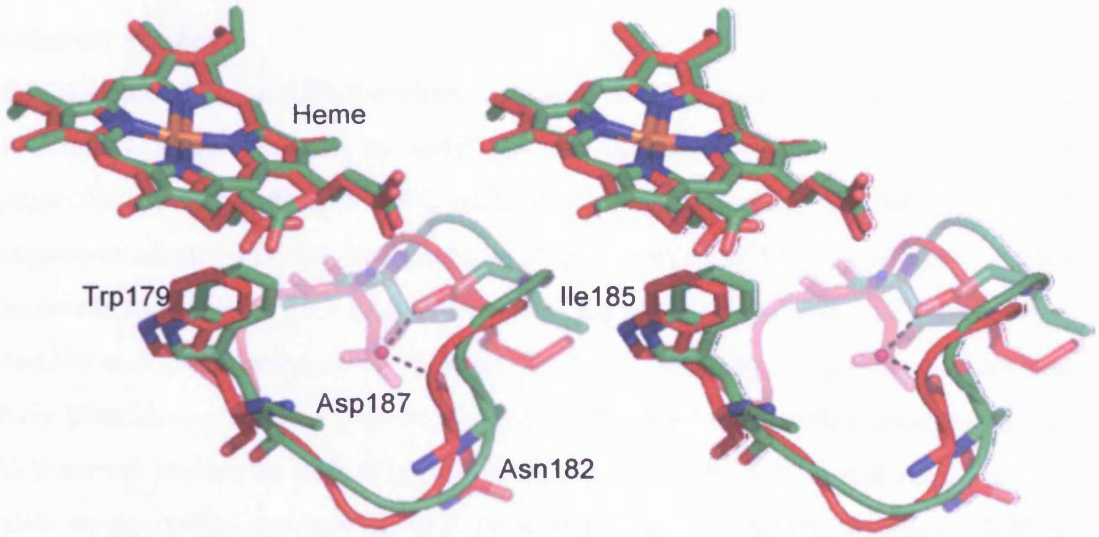

Figure 3.8: Stereo representation of the rsAPX/ascorbate complex (red) ion binding site and the equivalent loop in the C*c*P/cytochrome *c* (green) (*1*). Labels refer to APX residues.

The potassium binding site found in APX has been engineered into C*c*P during several site-directed mutagenesis experiments (*26-30*). The stability of the tryptophan radical in the C*c*P mutants dropped as the potassium ion concentration increased, and the enzyme activity decreased at the same time (*27*). In these mutants, the introduction of a potassium site appears to destabilize the tryptophan radical but in none of the mutants is formation of a porphyrin π-cation observed.

3.3.3 Comparison with Other Peroxidases

In this section, the data from this Chapter are compared to the crystal structures of the closely related C*c*P/cytochrome *c* complex (*1*) and of the MnP/Mn^{2+} complex (*2*), which also uses the γ-heme edge. Comparisons with the class III peroxidases are discussed in Chapter 4.

3.3.3.1 Comparison with Cytochrome c Peroxidase (Class I)

As mentioned in Chapter 1, C*c*P has become the paradigm for all other peroxidases. However, C*c*P has two anomalous features that are not reproduced in any other peroxidase, namely the unusual large protein substrate and the formation of a tryptophan radical in the catalytic cycle. The rsAPX/ascorbate structure will be used to rationalize aspects of these anomalies by comparison with the C*c*P/cytochrome *c* crystal structure (*1*).

Substrate Binding

Comparison of the rsAPX/ascorbate structure with that of the C*c*P/cytochrome *c* structure (*1*) can be used to fully account for the different substrate binding properties of the C*c*P and APX enzymes. Comparison of the APX and C*c*P sequences reveals that the key basic residues involved in binding of the (anionic) ascorbate molecule in APX (Arg172 and Lys30) are not present in C*c*P (replaced by Asn184 and Asp33 respectively) (Figure 3.9A). Conversely, the acidic residues that have been shown (*1, 31-37*) to be involved in binding of (cationic) cytochrome *c* to C*c*P are not present in APX (Figure 3.9A). Hence Asp34, Glu35 and Asp37 in C*c*P have no equivalent residues in APX because the loop containing residues 34-41 in C*c*P is missing in APX (Figure 3.9A, highlighted in red); Glu290 in C*c*P is also missing in rsAPX because of a C-terminal truncation (Figure 3.9B). Superimposition of the rsAPX/ascorbate and C*c*P/cytochrome *c* (*1*) complexes in this loop region (Figure 3.9C) clearly shows that the additional loop in C*c*P, and especially the side chain of Tyr36, would prevent the binding of ascorbate at the equivalent site.

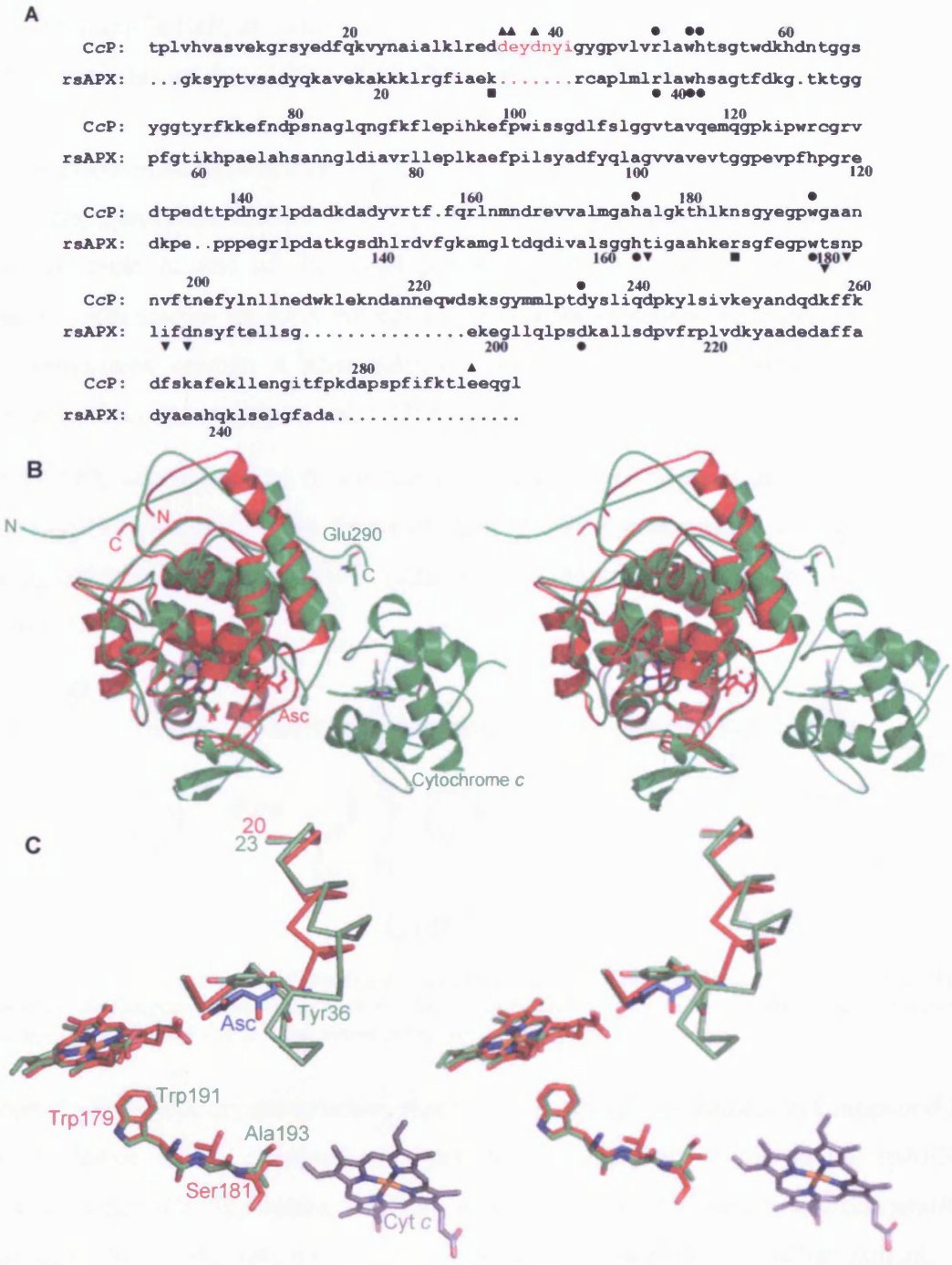

Figure 3.9: (A) Structural sequence alignment of rsAPX and C*c*P (*38*). ▼ indicates the residues used to bind potassium in rsAPX. ▲ indicates the residues involved in binding cytochrome *c* in C*c*P. The extra loop in C*c*P containing most of these residues is highlighted in red. ■ indicates the residues involved in ascorbate binding in rsAPX. ● indicates the residues from the active site. **(B)** Stereo representation of the overlay of the rsAPX/ascorbate (red) and the C*c*P/cytochrome *c* (green) complexes (*1*). C labels the C-terminus and N labels the N-terminus. **(C)** Stereo representation of C*c*P (green) and cytochrome *c* heme (grey) overlaid with rsAPX (red) and ascorbate (blue).

The comparison has shown that the structural architecture of the APX and C*c*P enzymes is subtly different: the key features required for substrate binding in APX

are not present in C*c*P, and *vice versa.* These differences account for the low activity of C*c*P towards ascorbate (*36*) and of APX towards cytochrome *c* (*39*).

The Tryptophan Radical in CcP

The other anomalous feature of C*c*P is that it uses a tryptophan radical during its catalytic cycle instead of the usual porphyrin π-cation radical. Before detailed spectroscopic studies on APX emerged, this was thought to be because class II and III peroxidases contain a phenylalanine at the position equivalent to Trp191. Phenylalanine cannot support radical formation (*20*).

When APX was sequenced it was found to have a tryptophan in the same place as C*c*P (Trp179) but all known forms of APX produce a porphyrin π-cation radical during catalysis, including rpAPX (*22*), rsAPX (*19*) and APX from tea leaves (*40*) (Figure 3.10).

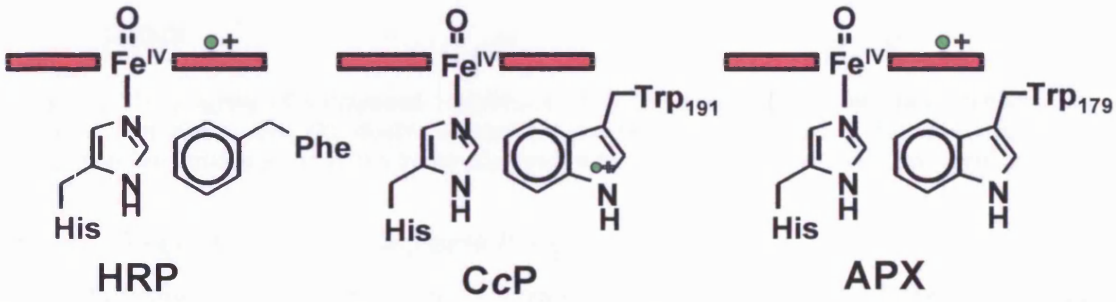

Figure 3.10: Diagram showing Compound I structure for HRP, C*c*P and APX. For clarity only the double bonded oxygen bound form is shown but in all cases the compound I structure may contain a hydroxide group with a single bond between the oxygen and iron.

When the first APX crystal structure was solved the porphyrin radical in Compound I was explained by the presence of a potassium-binding site found in the rpAPX structure near the tryptophan residue, which was put forward (on electrostatic grounds (*20*)) as a possible mechanism for destabilization of the tryptophan radical.

By the comparison of the rsAPX/ascorbate and C*c*P/cytochrome *c* structures, an alternative explanation can now be put forward. The ascorbate is directly bound to the heme and therefore the electron from ascorbate can transfer directly to the heme. This means the most efficient route for reduction of Compound I in APX occurs through a porphyrin π-cation intermediate, completely by-passing the need for involvement of Trp179 in ascorbate oxidation (*20*). (A direct link between the heme and the substrate also accounts for the increased stability of the chloroplastic APX

enzymes in the presence of ascorbate (*41*)). This implies APX does not need to use the tryptophan radical to transfer the electron to the heme iron during catalysis, which is indeed what is observed (*19, 22*) (Figure 3.11).

However, this contrasts with the substrate binding orientation in the C*c*P/cytochrome *c* complex, which indicates that cytochrome *c* binds in an orientation that involves delivery of an electron through Trp191 as part of an electron transfer pathway to the heme (Figure 3.9C). In this case, Trp191 would be expected to be essential for catalytic activity, which is consistent with data from mutagenesis work (*41*).

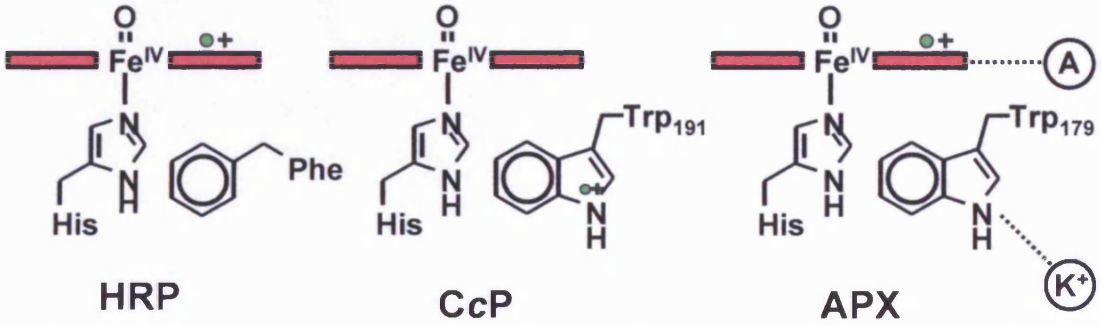

Figure 3.11: Diagram of Compound I formation with the potassium and ascorbate binding site marked. For clarity only the double bonded oxygen bound form is shown but in all cases the compound I structure may contain a hydroxide group with a single bond between the oxygen and iron.

3.3.3.2 Comparison with Manganese Peroxidase (Class II)

The manganese peroxidase (MnP) crystal structure has been solved with the physiological substrate bound (*2*). Although the substrate is very different (a manganese (II) ion); it is bound on the γ-side of the heme, through interactions with the heme propionate that are similar to those found in the rsAPX/ascorbate complex structure (Figure 3.12).

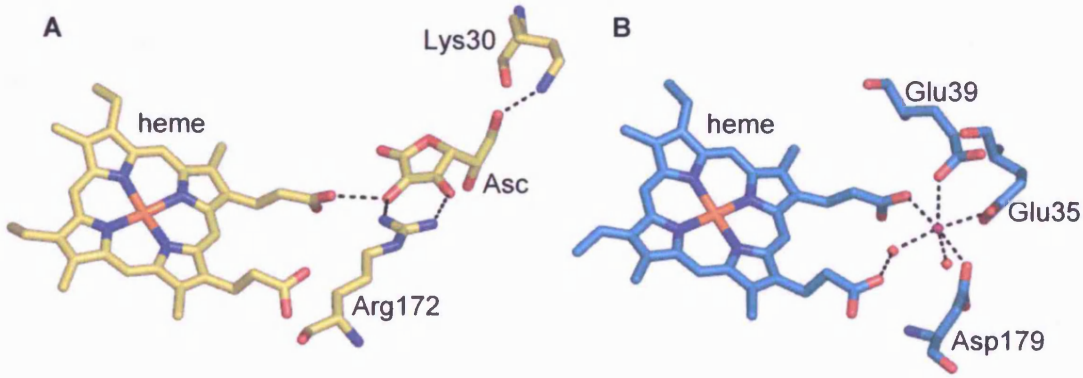

Figure 3.12: (A) Ascorbate binding in the rsAPX/ascorbate complex. **(B)** Manganese binding in the MnP/manganese complex (*2*). A pink sphere indicates a manganese ion, black lines indicate hydrogen bonds and water molecules are indicated by red spheres.

Comparison of the two structures shows that although MnP has an unusual substrate compared to APX, they both bind their substrates directly to the heme propionate, allowing in both cases direct electron transfer from the substrate to the heme, with no need for formation of a protein radical.

3.4 CONCLUSIONS

It is clear from the data presented above that despite their high sequence and structural similarities, the *modus operandi* of the APX and C*c*P enzymes are fundamentally different. C*c*P is truly anomalous, with properties that are not duplicated even within the class I peroxidase sub-group. In this context, it could be argued that APX is a better paradigm peroxidase than C*c*P. Direct, hydrogen-bonding contact between the substrate and the heme 6-propionate was not predicted in APX and widens the debate on our existing views on electron transfer in the heme peroxidases, in which substrate binding and oxidation at the δ-heme edge has been widely assumed (*42*). Since MnP (a class II enzyme) uses a similarly direct route for electron transfer – through the same heme 6-propionate – in its (physiological) complex with Mn(II) (*2*), this may represent a more widespread mechanism for electron delivery in other peroxidases.

3.5 REFERENCES

1. Pelletier, H., and Kraut, J. (1992) *Science 258*, 1748-1755.
2. Sundaramoorthy, M., Kishi, K., Gold, M. H., and Poulos, T. L. (1994) *Journal of Biological Chemistry 269*, 32759-32767.
3. Henriksen, A., Schuller, D. J., Meno, K., Welinder, K. G., Smith, A. T., and Gajhede, M. (1998) *Biochemistry 37*, 8054-8060.
4. Henriksen, A., Smith, A. T., and Gajhede, M. (1999) *Journal of Biological Chemistry 274*, 35005-35011.
5. Itakura, H., Oda, Y., and Fukuyama, K. (1997) *FEBS Letters 412*, 107-110.
6. Tsukamoto, K., Itakura, H., Sato, K., Fukuyama, K., Miura, S., Takahashi, S., Ikezawa, H., and Hosoya, T. (1999) *Biochemistry 38*, 12558-12568.
7. Patterson, W. R., and Poulos, T. L. (1995) *Biochemistry 34*, 4331-4341.
8. Hill, A. P., Modi, S., Sutcliffe, M. J., Turner, D. D., Gilfoyle, D. J., Smith, A. T., Tam, B. M., and Lloyd, E. (1997) *European Journal of Biochemistry 248*, 347-354.
9. Bursey, E. H., and Poulos, T. L. (2000) *Biochemistry 39*, 7374-7379.
10. Mandelman, D., Jamai, J., and Poulos, T. L. (1998) *Biochemistry 37*, 17610-17617.
11. Miller, V. P., Phillis, G. D. D., Ferrer, J. C., Mauk, A. G., and Montellano, P. R. O. d. (1992) *Journal of Biological Chemistry 267*, 8936-8942.
12. Wilcox, S. K., Jensen, G. M., Fitzgerald, M. M., McRee, D. E., and Goodin, D. B. (1996) *Biochemistry 35*, 4858-4866.
13. Brunger, A. T., Adams, P. D., Clore, G. M., DeLano, W. L., Gros, P., Grosse-Kunstleve, R. W., Jiang, J.-S., Kuszewski, J., Nilges, M., Pannu, N. S., Read, R. J., Rice, L. M., Simonson, T., and Warren, G. L. (1998) *Acta Crystallographica D54*, 905-921.
14. Project, N. C. C. (1994) *Acta Crystallographica D50*, 760-763.
15. Murshudov, G., Vagin, A., Lebedev, A., Wilson, K., and Dodson, E. (1999) *Acta Crystallogaphica D55*, 247-255.
16. McRee, D. (1992) *Journal of Molecular Graphics 10*, 44-47.
17. Sharp, K. H., Mewies, M., Moody, P. C. E., and Raven, E. L. (2003) *Nature Structural Biology 10*, 303-307.
18. Glusker, J. P. (1991) *Advances in Protein Chemistry 42*, 1-76.

19. Lad, L., Mewies, M., and Raven, E. L. (2002) *Biochemistry 41*, 13774-13781.

20. Pappa, H., Patterson, W. R., and Poulos, T. L. (1996) *Journal of Biological Inorganic Chemistry 1*, 61-66.

21. Sharp, K. H., Moody, P. C. E., Brown, K. A., and Raven, E. L. (2004) *Biochemistry 43*, 8644-8651.

22. Patterson, W. R., Poulos, T. L., and Goodin, D. B. (1995) *Biochemistry 34*, 4342-4345.

23. Wada, K., Tada, T., Nakamura, Y., Ishkawa, T., Yabuta, Y., Yoshimura, K., Shigoeka, S., and Nishimura, K. (2003) *Journal of Biochemistry 134*, 239-244.

24. Wada, K., Tada, T., Nakamura, Y., Yabuta, Y., Yoshimura, K., Takeda, T., Shigoeka, S., and Nishimura, K. (2002) *Acta Crystallographica D58*, 559-561.

25. Pardo, J. M., and Quintero, F. J. (2002) *Genome Biology 3*, 1017.1-1017.4.

26. Bhaskar, B., Bonagura, A. C., Jamal, J., and Poulos, T. L. (2000) *Tetrahedron 56*, 9471-9475.

27. Bhaskar, B., Bongura, C. A., Li, H., and Poulos, T. L. (2002) *Biochemistry 41*, 2684-2693.

28. Bonagura, C. A., Sundaramoorthy, M., Pappa, H. S., Patterson, W. R., and Poulos, T. L. (1996) *Biochemistry 35*, 6107-6115.

29. Bonagura, C. A., Bhaskar, B., Sundaramoorthy, M., and Poulos, T. L. (1999) *Journal of Biological Chemistry 274*, 37827-37833.

30. Bonagura, C. A., Sundaramoorthy, M., Bhaskar, B., and Poulos, T. L. (1999) *Biochemistry 38*, 5538-5545.

31. McLendon, G., Zhang, Q., Wallin, S. A., Miller, R. M., Billstone, V., Spears, K. G., and Hoffman, B. M. (1993) *Journal of the American Chemical Society 115*, 3665-3669.

32. Leesch, V. W., Bujons, J., Mauk, A. G., and Hoffman, B. M. (2000) *Biochemistry 39*, 10132-10139.

33. Guo, M., Bhaskar, B., Li, H., Barrows, T. P., and Poulos, T. L. (2004) *Proceedings of the National Academy of Science, USA 101*, 5940-5945.

34. Erman, J. E., and Vitello, L. B. (2002) *Biochimica et Biophysica Acta 1597*, 193-220.

35. Wei, Y., McLendon, G. L., Hamilton, A. D., Case, M. A., Purring, C. B., Lin, Q., Park, H. S., Lee, C.-S., and Yu, T. (2001) *Chemical Communications*, 1580-1581.

36. Yonetani, T., and Ray, G. S. (1965) *Journal of Biological Chemistry 240*, 4503-4514.

37. Zhou, J. S., Tran, S. T., McLendon, G., and Hoffman, B. H. (1997) *Journal of the American Chemistry Society 119*, 269-277.

38. Sharp, K. H., Moody, P. C. E., and Raven, E. L. (2003) *Dalton Transactions*, 4208-4215.

39. Dalton, D. A., del Castillo, L. D., Kahn, M. L., Joyner, S. L., and Chatfield, J. M. (1996) *Archives of Biochemistry and Biophysics 328*, 1-8.

40. Kvaratskhelia, M., Winkel, C., Naldrett, M. T., and Thorneley, R. N. F. (1999) *Journal of Plant Physiology 154*, 273-282.

41. Miyake, C., and Asada, K. (1996) *Plant and Cell Physiology 37*, 423-430.

42. Ator, M. A., and Ortiz de Montellano, P. R. (1987) *Journal of Biological Chemistry 262*, 1542-1551.

Chapter 4

X-Ray Crystal Structure of the rsAPX/Salicylhydroxamic Acid Complex

4.1 INTRODUCTION

In addition to ascorbate, APX is also able to catalyze the oxidation of aromatic substrates (e.g. guaiacol and pyrogallol (Figure 4.1)) that are typical of the class II and class III peroxidases (*1, 2*). In some cases, oxidation of these aromatic substrates is faster than oxidation of ascorbate itself (*3*) and it is not inconceivable that this has a physiological role, since there are high levels of phenolic compounds present *in planta*.

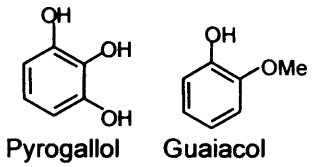

Figure 4.1: The structures of guaiacol and pyrogallol.

The hypothesis that has emerged for substrate binding in APX is as follows (*3-6*). There are two, separate substrate binding locations: the first, close to the γ-meso position of the heme (Figure 4.2), is utilised by ascorbate (Chapter 3. Figure 3.3); the second is used primarily by aromatic substrates (*4*). The aromatic binding site is known to be distinct from the ascorbate binding site because mutations at the γ-heme edge do not effect guaiacol or pyrogallol oxidation (*4, 6*).

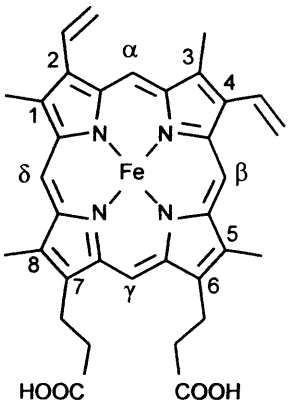

Figure 4.2: The structure of protoporphyrin IX showing the nomenclature used in this chapter.

The exact location of the aromatic binding site in APX is not known but there is evidence to suggest that it is close to the δ-edge of the heme, since this is solvent accessible in the rpAPX crystal structure (*7*). The only other clue as to where aromatic compounds bind comes from other peroxidases:

- The δ-edge of the heme is thought to be used by HRP (*8*, *9*) since modification with phenylhydrazine at the δ-heme edge affects aromatic substrate binding (*8*). HRP has also been crystallised in complex with aromatic compounds (benzhydroxamic acid (BHA) (*9*) and ferulic acid (*10*), Figure 4.3) which both bind at the δ-edge of the heme.
- There is some evidence that C*c*P also uses a different binding site for small aromatic substrates compared to cytochrome *c*. Reconstitution of C*c*P with different hemes modified at either the δ- or γ-heme edge showed that γ-modified hemes affected cytochrome *c* activity but not guaiacol activity, and δ- modified hemes affected guaiacol activity but not cytochrome *c* activity (*11*).
- The structure of *Arthromyces ramosus* peroxidase (ARP) has been solved in complex with BHA (*12*) and salicylhydroxamic acid (SHA) (Figure 4.3) (*13*) and both these structures contain the aromatic compound bound at the δ-heme edge.

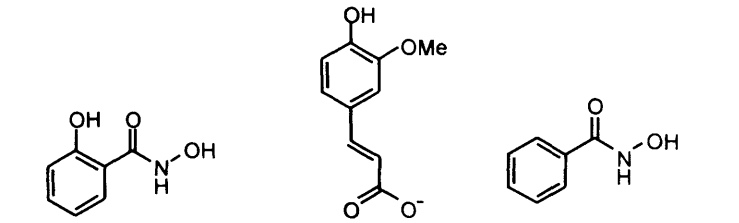

Salicylhydroxamic acid Ferulic acid Benzhydroxamic acid

Figure 4.3: Structures of BHA, SHA and ferulic acid.

4.1.1 Aims

The aim of this work is to identify the aromatic binding site in rsAPX. In this Chapter, therefore, the crystal structure of the rsAPX/SHA complex is presented. UV-visible absorbance data is also used to provide additional information on the location of the aromatic binding site in rsAPX. These structural and solution data have helped to define the aromatic binding site in APX for the first time. The results are relevant to our understanding of substrate binding across the entire heme peroxidase family since most peroxidases have an aromatic binding site at the δ-heme edge. Moreover, the structure of the rsAPX/SHA complex – together with substrate- and ligand-bound structures from Chapters 2 and 3 – will have important implications for the development of the mechanism of proton transfer in peroxidases.

4.2 RESULTS

4.2.1 UV-Visible Absorption Spectra

Addition of SHA to rsAPX leads to an increase in intensity and a red shift of the Soret band from 407 to 418 nm in the UV-visible absorption spectrum. New bands also appear at 540 and 580 nm (Figure 4.4). As shown previously (Chapter 2, section 2.2.2.2), cyanide binding leads to formation of a 6-coordinate iron with UV-visible maxima at 421, 529 and 570 nm. In addition, Compound II is also six coordinate with wavelength maxima of 417, 529 and 560 nm (*14*). Therefore the changes in the UV-visible spectrum on SHA binding – a Soret peak red shift and new peaks in the visible region (~530 and ~560 nm) – are consistent with the iron being six coordinate.

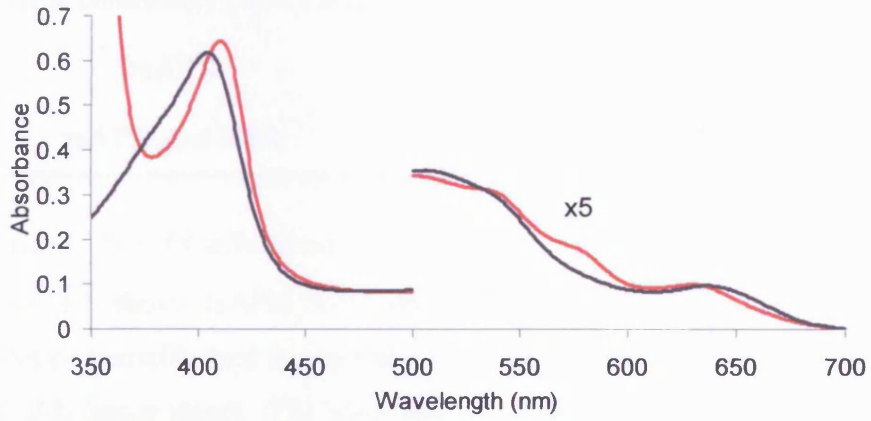

Figure 4.4: UV-visible absorption spectra of rsAPX (black trace) and the rsAPX/SHA complex (red trace). Conditions: 0.1 M potassium phosphate, pH 7.0.

4.2.1.1 Steady State Kinetics

Samples of rsAPX were assayed (100 mM phosphate, pH 7.0, 25.0 °C) against guaiacol using established protocols (*14*) by measuring the formation of tetraguaiacol at 470 nm (ε_{470} = 22.6 mM^{-1} cm^{-1} (*15*)). The resulting data were fitted to the Michaelis-Menten equation (*14*). At high concentrations of SHA ([SHA] = 315 μM), the k_{cat} value for oxidation of guaiacol by rsAPX is only ~50% of the value observed in the absence of SHA (Table 4.1). This decrease is thought to be due to inhibition of both guaiacol and hydrogen peroxide binding since the data do not fit simple inhibition (competitive or non-competitive) of one substrate *i.e.*, K_M and k_{cat} both change compared to the values without SHA present. If the inhibition is competitive, only K_M is predicted to change, since the maximum rate can still be achieved with the

addition of more substrate. Non-competitive inhibition is predicted to change k_{cat}: a certain percentage of the enzyme is rendered inactive by the inhibitor for the whole experiment and therefore the rates are altered but the amount of substrate added at half the maximum rate (K_M) stays the same. Binding of SHA to the heme will inhibit peroxidase activity by competing with hydrogen peroxide, analogous to the binding of other strong ligands (*e.g.* cyanide), but may also block the guaiacol binding site. It was not possible to assay rsAPX against ascorbate in the presence of SHA, since this reaction is usually monitored by the decrease in absorbance at 290 or 260 nm (ascorbate) and SHA absorbs light very strongly in the UV region.

Table 4.1
Steady-state parameters for oxidation of guaiacol by rsAPX and SHA inhibited rsAPX.

Enzyme	k_{cat} (s^{-1})	K_M (mM)	k_{cat}/K_M ($mM^{-1}s^{-1}$)
rsAPX (literature value (*14*))	68 ± 3	12.9 ± 1.3	5.3
rsAPX	66 ± 8	14 ± 5	4.7
rsAPX and SHA	29 ± 9	26 ± 4	1.1

4.2.1.2 Is SHA a Substrate?

Figure 4.5 shows rsAPX (0.05 μM) and SHA (0.1 mM) before the addition of hydrogen peroxide (red trace) and 1 minute after the addition of hydrogen peroxide (0.1 μM) (green trace). The Soret peak shifts from 416 to 419 nm on the addition of hydrogen peroxide, the peaks at 530 and 568 nm increase, and the peak at 645 nm decreases. This is consistent with the formation of a Compound II-like species which occurs when hydrogen peroxide is added to rsAPX without substrate (λ_{max} = 414, 527 and 558 nm (*16*)). If a substrate is present the enzyme would be returned to the native form before the second spectrum was taken. Therefore as the spectrum relating to rsAPX changes, SHA can not be a substrate for rsAPX.

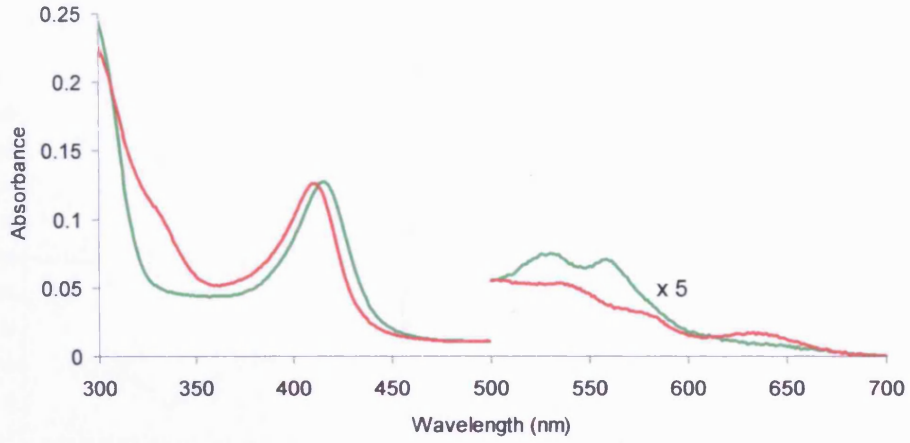

Figure 4.5: UV-visible spectra for rsAPX and SHA (red trace), and SHA, rsAPX and hydrogen peroxide (green trace). Conditions: 0.1 M potassium phosphate, pH 7.0.

4.2.1.3 Equilibrium Binding Constants

All equilibrium dissociation constants, K_d (100 mM potassium phosphate), for the binding of SHA to rsAPX were determined using UV-visible spectroscopy according to previously published procedures (*17*) by addition of known amounts of SHA to rsAPX ([rsAPX] ≈ 5 μM). Binding constants were determined from plots of fractional saturation against free ligand concentration (Chapter 6, Equation 6.3) (*17*).

On the basis of pH-dependent binding data for other peroxidases, which showed an increase in K_d with pH that corresponds with the pK_a of the SHA, it has been reported that only the neutral form of SHA binds (*18-20*). Equilibrium binding constants for SHA to rsAPX were measured over a range of pHs and binding of SHA to rsAPX was also found to be pH-dependent (Figure 4.6A). Binding data are therefore corrected for ionisation (pK_a = 7.4 (*21*)) of the hydroxamic acid group of SHA, as previously (*18, 19*). Reported values for K_d are an average of at least two independent measurements; a binding constant, K_d, of 8 ± 1 μM was determined for the rsAPX/SHA interaction at pH 8.3 (Figures 4.6B and C).

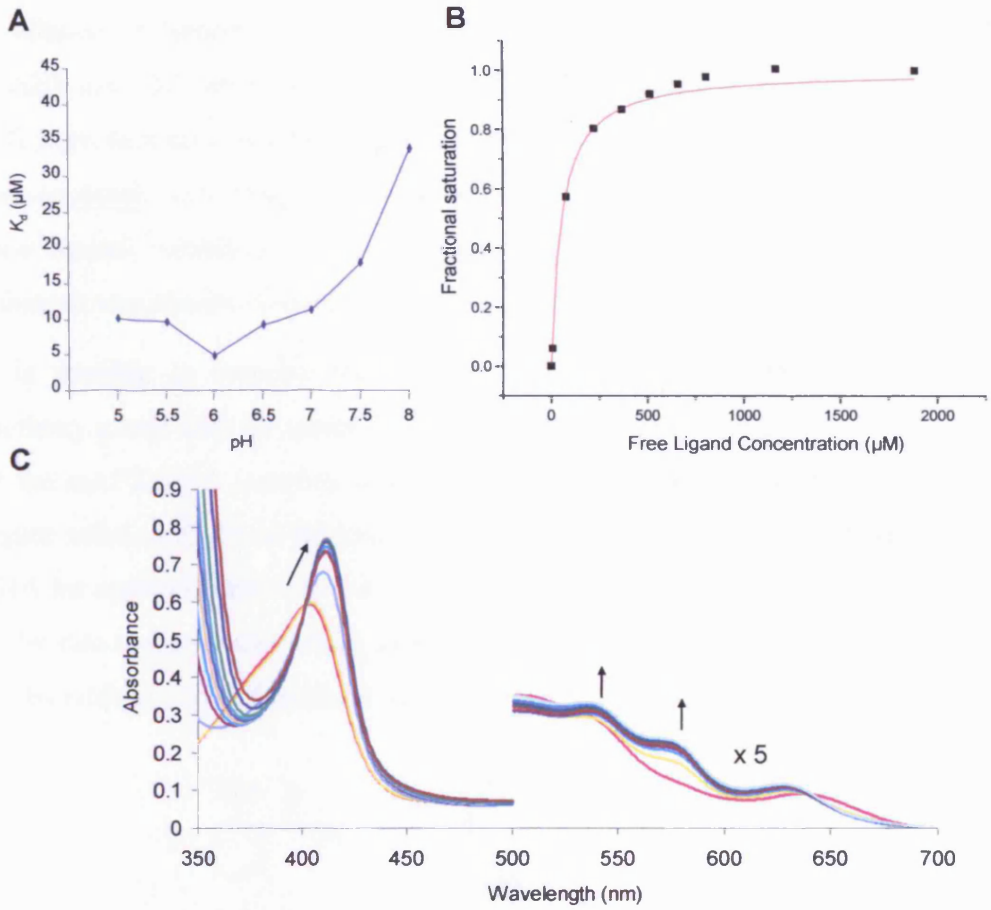

Figure 4.6: (A) Plot of binding constants for the rsAPX/SHA complex against pH. **(B)** Plot of fractional saturation against free ligand concentration for the rsAPX/SHA complex at pH 8.3. **(C)** UV-visible spectra collected during titration of rsAPX (5.6 μM) with SHA. Concentrations of SHA were (in the direction of the arrows): 0.00, 7.45, 81.9, 230, 378, 525, 672, 818, 1180 and 1900 μM. Conditions: potassium phosphate, pH 8.3, 25 °C, μ = 0.10 M.

To establish whether binding of SHA is affected by the presence of other substrates, the binding constant, K_d, for SHA was determined in the presence of both ascorbate (25 mM) and guaiacol (25 mM). Compared to the K_d value of SHA binding without a substrate present, the K_d value in the presence of guaiacol increases (K_d = 32 ± 2 μM) but the corresponding value in the presence of ascorbate does not change (K_d = 8 ± 1 μM). These data indicate that guaiacol and SHA compete for the same binding site but ascorbate does not compete with SHA and binds at a different site.

4.2.2 Data collection and Preparation of the Crystals

4.2.2.1 Crystal Soaks

Guaiacol is only sparingly soluble in water, but is soluble in ethanol or methanol; attempts to soak guaiacol (at various concentrations in ethanol or methanol) into

rsAPX crystals (Chapter 2) resulted in the cracking of the crystals under all conditions attempted. Salicylic acid, *p*-cresol, pyrogallol, 3,3'-diaminobenzalidine (DAB) and 2,2'-azino-di-(3-ethylbenzthiazoline-6-sulfonic acid) (ABTS) (Figure 4.7) were then used in crystal soaks as they are all APX substrates and more soluble than guaiacol. However, the concentrations of these substrates were still low due to their limited solubility in water (less than 0.1 M) and no density relating to the substrate was observed in the corresponding structures.

It is possible to increase the solubility of guaiacol by functionalisation of the methoxy group with the (more hydrophilic) hydroxamic acid group (SHA). Crystals of the rsAPX/SHA complex were obtained by soaking rsAPX crystals in a mother liquor solution (2.25 M lithium sulfate, 0.1 M Hepes pH 8.3) containing 100 mM SHA for approximately one minute. The SHA was dissolved by adding 1 M sodium hydroxide to the mother liquor to adjust the pH to ~10. The pH was then returned to 8.3 by adding 1 M hydrochloric acid.

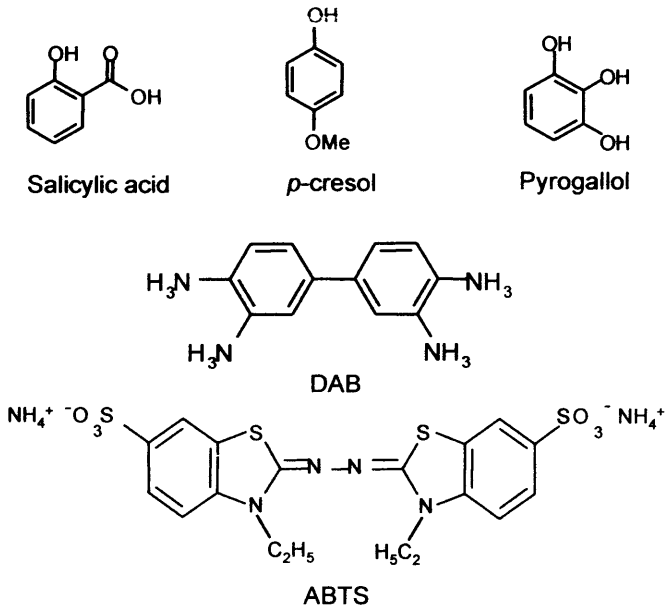

Figure 4.7: Structures of aromatic substrates of rsAPX.

4.2.2.2 Co-Crystallisation

Co-crystallisation was tried with salicylic acid, *p*-cresol, pyrogallol, DAB and ABTS by growing the rsAPX crystals in the presence of these substrates. After two weeks, crystals grew in the DAB screen but no density relating to DAB was observed in the corresponding structure.

4.2.2.3 Data Collection

Diffraction data were collected for the rsAPX/SHA complex on beam-line ID14-4 at ESRF (Grenoble) using an ADSC Quantum-4 detector. Data to 1.46 Å was collected over 90° rotation in 0.5° images. All data were collected at 100 K. Data collection statistics are shown in Table 4.2.

Table 4.2
Data collection statistics for the rsAPX/SHA complex.

Resolution Range (Å)	50.0-1.46
Total Observations	310,054
Unique Reflections	43,221
I/σI	32.2
R_{merge} (%)	7.6
Completeness (%)	99.2

4.2.2.4 Data Interpretation

A fraction of the data (5%) was flagged for the calculation of R_{free} and excluded from subsequent refinement. The structure was refined using a model derived from the 1.45 Å rsAPX/ascorbate complex (*22*) (Chapter 3) by the removal of bound ligand and water molecules.

4.2.2.5 Refinement and Rebuilding

Several cycles of refinement using REFMAC5 from the CCP4 suite (*23*) and incorporation of solvent molecules gave a model with a crystallographic R-factor for all data of 15.5% and an R_{free} of 18.5%. The electron density for SHA was clear and unambiguous; the structure was thus incorporated into the last cycles of refinement. The computer program XTALVIEW (*24*) was used throughout for manual adjustment, ligand fitting and interpretation of water structure. The refinement statistics are shown in Table 4.3. Coordinates and structure factors have been deposited with the PDB (code 1VOH).

Table 4.3
Refinement statistics for the rsAPX/SHA complex.

R_{work} (R_{free})		0.155 (0.185)
r.m.s. deviation from ideal	**Bonds (Å)**	0.011
	Angles (°)	1.344

4.2.3 The rsAPX/SHA Complex

4.2.3.1 Overall Structure

The overall structure of rsAPX in complex with SHA is shown in Figure 4.8A. Comparison with the structure of rsAPX (*22*) shows that binding of SHA leads to no major structural rearrangements of the enzyme (r.m.s deviation in Cα positions of 0.21 Å). However, there is a slight adjustment of the side chain dihedral angle α2 of His42 with respect to the rsAPX structure (Figure 4.8B).

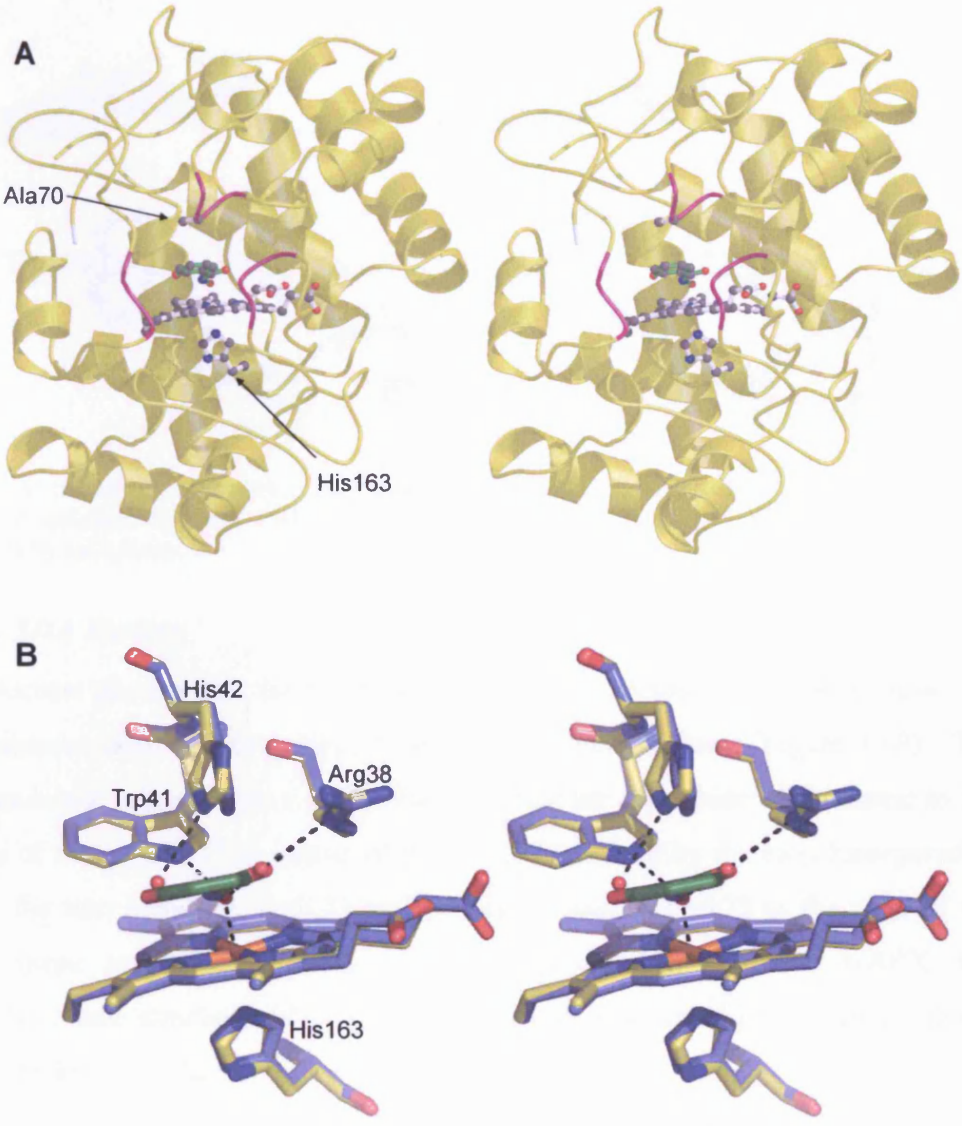

Figure 4.8: (A) Stereo representation of the overall structure of the rsAPX/SHA complex showing SHA (green), His163 and Ala70 (*25*). The areas around the δ-heme edge cavity are highlighted in pink. **(B)** Stereo representation of the active site overlay of rsAPX (yellow) and the rsAPX/SHA complex (blue with green SHA). Hydrogen bonds are indicated by black dashed lines. The water molecules are indicated by red spheres.

4.2.3.2 Cation Site

The cation site in the rsAPX/SHA complex contains an electron density peak that is characterized by short distances from the main chain oxygens of Thr164 (2.2 Å), Thr180 (2.7 Å), Ile185 (2.3 Å) and Asn182 (2.4 Å), and two water molecules (2.2 and 2.5 Å) (Figure 4.9). These observations are consistent with the occupation of the site by a sodium ion introduced during the soak which contained sodium hydroxide. The ion is six coordinate as in rpAPX. The ion binding site is similar to the site in rpAPX and is discussed further in Chapter 3, section 3.3.2.

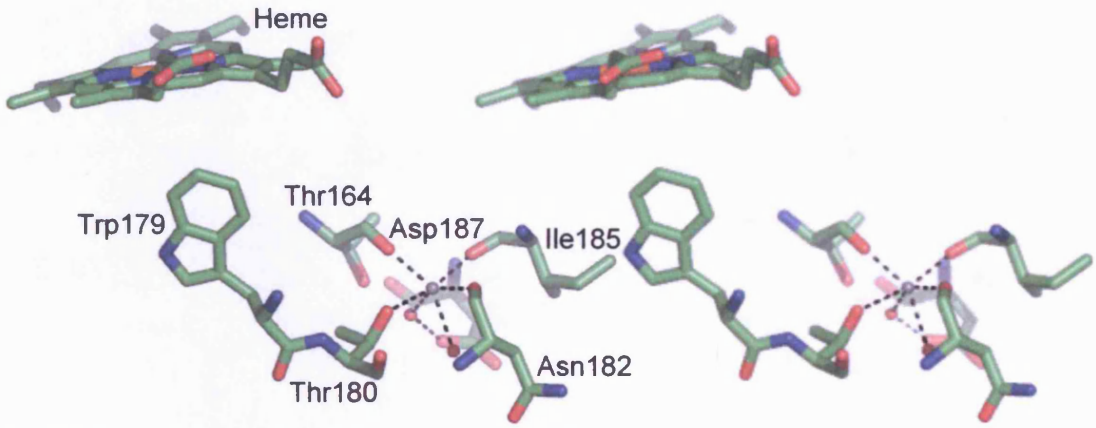

Figure 4.9: Stereo representation of the cation binding site in the rsAPX/SHA complex. Hydrogen bonds are indicated by black dashed lines, the cation is indicated by a grey sphere and water molecules by red spheres.

4.2.3.3 SHA Binding

The electron density for the SHA molecule in the region of the heme group is unambiguous, allowing its position to be defined with precision (Figure 4.10). The SHA molecule is located in a cavity that connects the distal side of the heme to the surface of the protein. The mouth of the cavity is defined by the loop incorporating Ala70, the turn including Asp133 and the region around Ser173 at the edge of the heme; these are highlighted in pink in Figure 4.8A. In the rsAPX and rsAPX/ascorbate structures (*22*), the equivalent site is occupied by five well-ordered solvent molecules (Chapter 3, Figure 3.7).

The phenolic group of the hydroxamic acid group (which is 89% deprotonated under the conditions used (pH 8.3), Chapter 6, Equation 6.6) is coordinated to the heme iron at a distance of 2.1 Å, which is consistent with the UV-visible spectra (Figure 4.4). The SHA molecule is also able to hydrogen bond to Trp41 (Figure 4.10). There are hydrogen bonds between the phenolic hydroxide (pK_a = 9.8 (*21*)) and

Pro132, and between the carbonyl oxygen of SHA and Arg38 (Figure 4.10). Although the N_ε of the distal histidine (His42) is 3.0 Å from the phenolic oxygen of SHA, the geometry is unsuitable for hydrogen-bond formation between His42 and SHA.

The aromatic ring of the SHA molecule is almost parallel (with separation 3.4 Å) to the heme; it makes a shallow angle of ~15° with the plane, and overlaps with the δ-heme edge (C20 position) and the 8-Me group of the heme. The Cα and Cβ of Ala70 are within van der Waals distance of the SHA (~ 3.5 Å, Figure 4.8A).

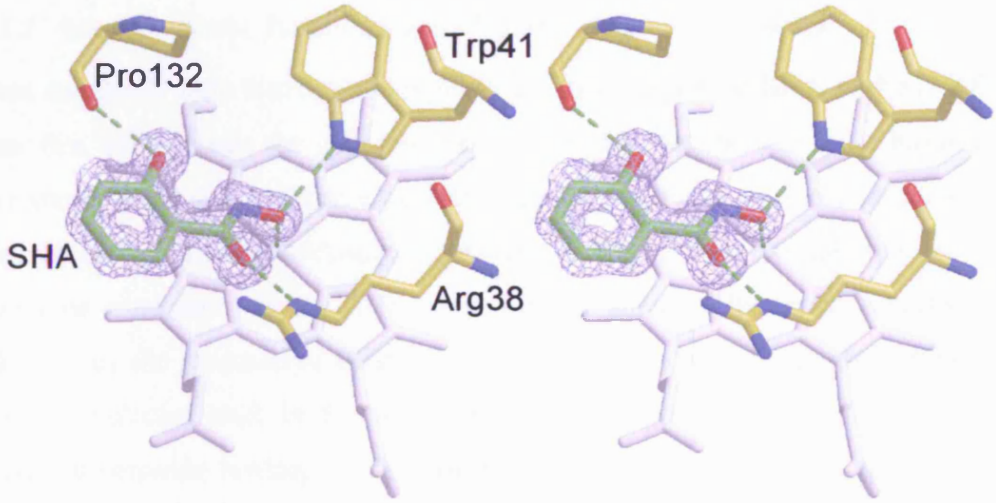

Figure 4.10: Stereo representation of SHA (green) binding in the rsAPX/SHA complex with difference electron density (blue). The heme is light grey and rsAPX is yellow. Hydrogen and coordination bonds are indicated by green dashed lines.

4.3 DISCUSSION

The solution data from this Chapter indicate that SHA binds at the aromatic binding site in rsAPX. The rsAPX/SHA structure helps define interactions at this site and shows that aromatic substrates bind at a separate site to ascorbate. This is the first time that both binding sites have been defined in APX. Since both binding sites are now known, it is possible to propose a proton transfer pathway that is common to both sites and could be used for all three classes of peroxidases; this is discussed at the end of this Chapter.

4.3.1 Steady State Kinetics and Dissociation Constants

From the steady state kinetics and equilibrium binding data of SHA with rsAPX, it is clear that SHA blocks the guaiacol binding site but not the ascorbate binding site. The steady state data suggest that SHA may be inhibiting guaiacol oxidation; if it were merely inhibiting hydrogen peroxide binding, simple competitive inhibition would be expected. In tea APX, oxidation of guaiacol has been reported to be inhibited by the presence of BHA (*2*), but in this enzyme BHA does not bind to the iron (no detected shift in the Soret band), and therefore it is unlikely to inhibit hydrogen peroxide binding. This indicates that in tea APX – as in rsAPX – BHA binds at the same site as guaiacol and SHA.

The experimentally obtained dissociation constants for SHA binding show that guaiacol and SHA compete for the same binding site and that ascorbate binds at a different site. The binding location of SHA in the crystal structure is in the same site as in the UV-visible spectroscopy data; the SHA is coordinated to the iron in the crystal structure and the UV-visible spectrum of rsAPX/SHA shows that the iron is six coordinate.

4.3.2 Comparison with Other Peroxidases

The results presented in this section are of relevance to our understanding of substrate binding across the heme peroxidase family. In this discussion, the rsAPX/SHA structure is compared with our current understanding of substrate binding in other class I, class II and class III peroxidase enzymes.

4.3.2.1 Comparisons with HRP (class III) and ARP (class II)

Binding Interactions

In Figure 4.11, the rsAPX/SHA structure is compared with the crystal structures of the ARP/SHA complex (*13*) (class II) (Figure 4.11A), the ARP/BHA complex (*12*) (Figure 4.11B), the HRP C/BHA complex (*9*) (class III) (Figure 4.11C), and the HRP C/CN/ferulic acid complex (*10*) (Figure 4.11D). It is clear from Figure 4.12 that the binding location of the substrate for all the structures is both similar and close to the δ-heme edge. In all cases, there are hydrogen-bonding interactions between the distal arginine residue and the substrate.

The backbone carbonyl of a proline is involved in hydrogen-bonding in all cases but for the HRP/CN/ferulic acid structure it is through a water molecule. There are other differences; the distal histidine hydrogen bonds to the substrate in the HRP/BHA structure and ARP structures, but not in rsAPX and the HRP/CN/ferulic acid structure. In the case of the HRP/CN/ferulic acid structure, this may be because of the cyanide pushing the substrate further out of the heme cavity. For the HRP and ARP structures, the interaction with the heme iron (or cyanide) is via a water molecule (compared to through the hydroxyl group of the SHA in rsAPX). Altogether, the bound ligand for the HRP and ARP structures is displaced by about a bond length out of the binding pocket relative to SHA in rsAPX. It is possible that the additional hydrogen-bonding interaction between SHA and Trp41 in rsAPX (Figure 4.9) is partly responsible for this difference (Trp41 is replaced by a Phe in both HRP and ARP). In fact, Trp41 is conserved in all but two APXs (*M. crystallinum* APX and a membrane-bound enzyme from spinach which contain Phe at this position).

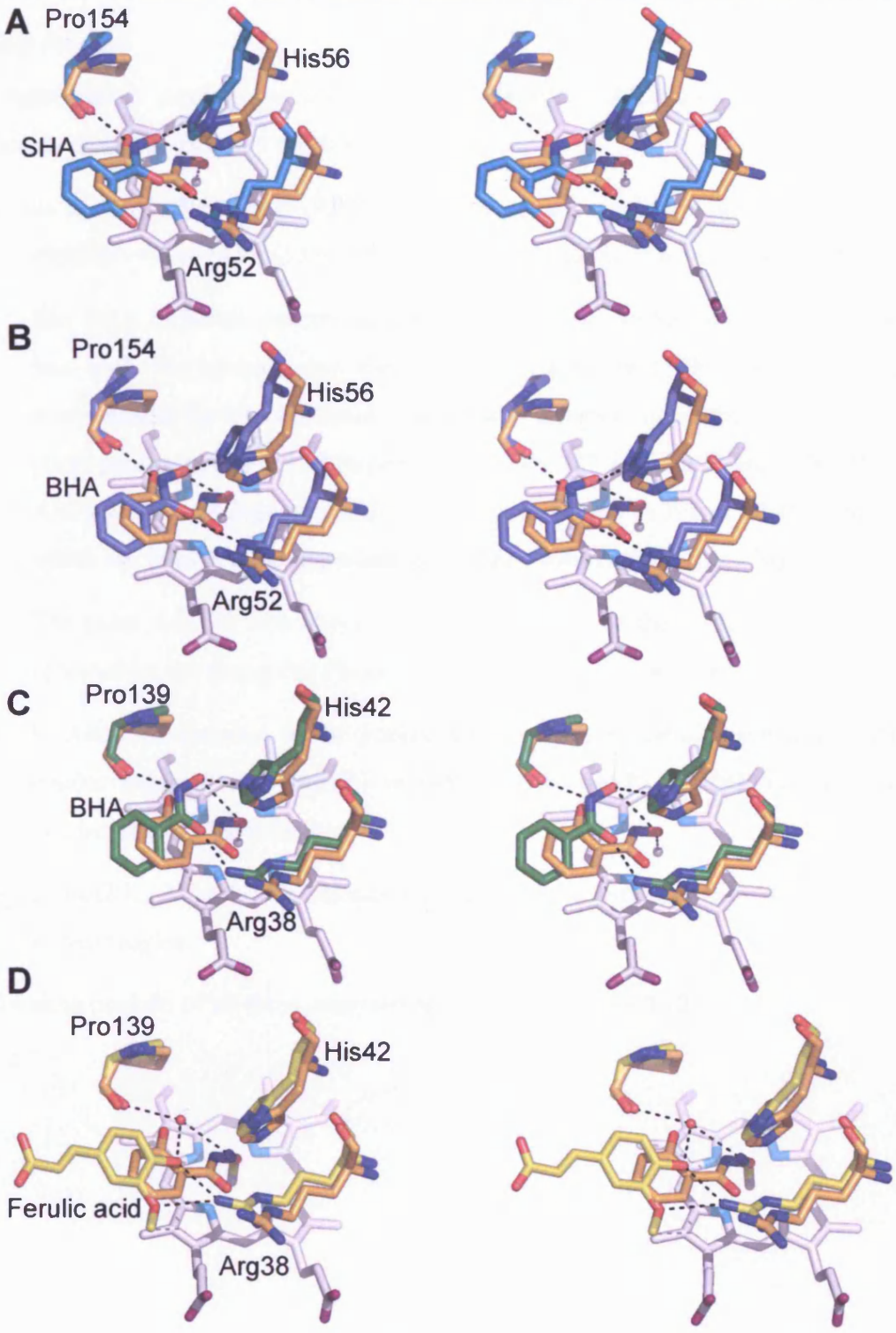

Figure 4.11: Stereo representation of structure–based alignments of the rsAPX/SHA complex (orange) and **(A)** the ARP/SHA complex (*13*) (light blue), **(B)** the ARP/BHA complex (*12*) (blue), **(C)** the HRP/BHA complex (*9*) (dark green) and **(D)** the HRP/CN/ferulic acid complex (*10*) (yellow). The heme is shown in grey. Hydrogen bonds for the ARP/SHA, ARP/BHA, HRP/BHA and HRP/CN/ferulic acid structures are indicated by black dashed lines; hydrogen bonds for the rsAPX/SHA are omitted for clarity, but are according to Figure 4.9.

Binding Pockets

The hydrophobic interactions are similar in the APX, ARP and HRP aromatic binding pockets but there are notable differences:

- In the HRP/BHA and ARP/SHA complexes the pocket is narrowed by the intrusion of Pro141 and Pro156 respectively, equivalent to Ala134 in APX.
- The BHA molecule penetrates less deeply into the pocket, and thus overlaps less with the hydrophobic δ-edge of the heme in HRP. This may be compensated for by additional hydrophobic interactions at the mouth of the HRP pocket with Phe179 (equivalent to Ser 173 in rsAPX and Gly191 in ARP) and Phe68 (equivalent to Ser69 in rsAPX and Pro91 in ARP), both of which are known to be important in aromatic substrate binding (*26*).
- The polar Asp133 side chain found at the mouth of the pocket in rsAPX is replaced by the non-polar Phe142 in HRP and Gly157 in ARP.
- In ARP, the entrance to the pocket is more open as the loop containing the residue equivalent to Ser173 in rsAPX and Phe179 in HRP (Gly191) is displaced away from the mouth.
- In rsAPX, the polar side-chains of Asp133 and Ser69 are extended into the solvent region.

The binding pockets of all three enzymes are shown in Figure 4.12.

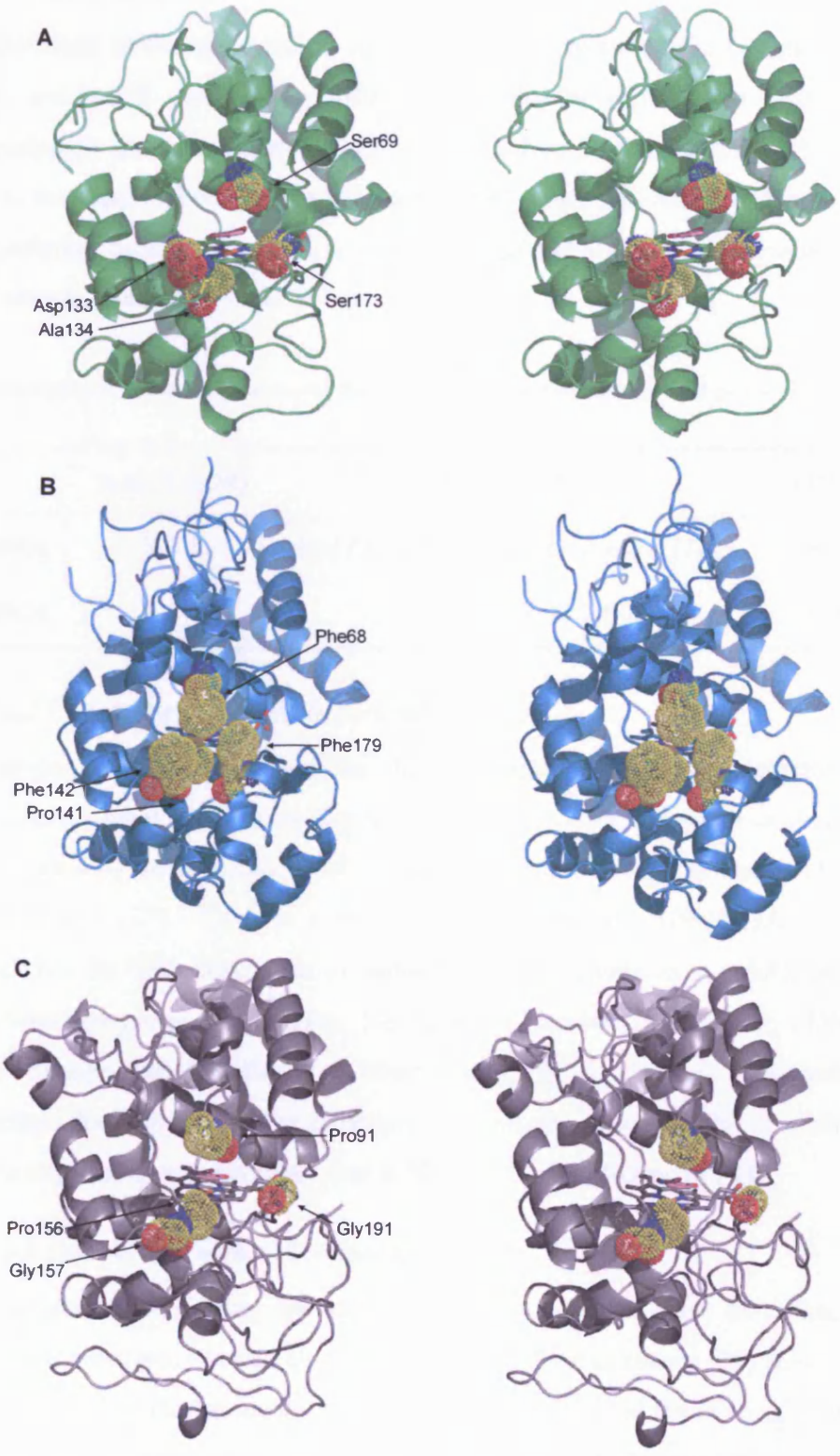

Figure 4.12: Stereo representation of the mouth of the aromatic binding pocket in: **(A)** the rsAPX/SHA complex, **(B)** the HRP/BHA complex and **(C)** the ARP/SHA complex. Ser69, Asp133, Ala134 and Ser173 from APX, Phe68, Pro141, Phe142 and Phe179 from HRP, and Pro91, Pro156, Gly157 and Gly191 from ARP are shown in yellow as space filling models.

Dissociation Constants

Comparison of the dissociation constants for hydroxamic acid complexes of HRP, ARP and rsAPX can provide further insight into the binding site (Table 4.4). The dissociation constant for rsAPX to SHA is tighter than for both HRP and ARP to SHA; this may be because the SHA also binds to the iron and Trp41 in rsAPX. The dissociation constant for SHA is weaker with ARP; this may be because the pocket entrance is more open in ARP.

Table 4.4
Dissociation constants (K_d) corrected for ionisation of the hydroxamic acid group of SHA and BHA (section 4.2.1.3).

	rsAPX (μM)	HRP (μM)	ARP (μM)
SHA	8 ± 1	85 (*13*), 11 ± 0.1 (*18*), 12 ± 0.4 (*18*)	1600 (*13*)
BHA	-	2.5 ± 0.05 (*18*), 2.3 (*13*)	1600 (*13*)

4.3.2.2 Comparison with Myeloperoxidase

Myeloperoxidase (MPO) is from the mammalian peroxidase superfamily but it oxidises guaiacol in the same way as the plant enzymes. Guaiacol oxidation in MPO is inhibited by the presence of SHA, and SHA binds strongly to the iron (K_d = 2 μM) as in rsAPX (*27*). There is a structure for the (human) MPO/SHA complex (*28*), which has the SHA binding in an almost identical location as in rsAPX (4.1 Å above the 8-methyl group of the heme, Figure 4.2). However, there is no PDB entry for this structure and therefore a detailed comparison is difficult. Nevertheless this structure does agree with the existence of a common aromatic binding site at the δ-heme edge in most peroxidases that is blocked by the binding of SHA.

4.3.2.3 Comparison with CcP (class I)

The δ-heme edge binding site may be used more generally for oxidation of related aromatic substrates in other class I peroxidases. *Cc*P is known (*29*) to bind aromatic substrates at a different location to cytochrome c (*11*), and the δ-heme edge has been implicated (*11, 30*). This is consistent with our data because the key hydrogen-bonding residues (Arg38, Trp41, Pro132) are conserved in CcP (Arg48, Trp51, Pro145) and because *Cc*P contains a similar binding pocket to that identified in APX. It is also likely that the same site is used for binding and oxidation of isoniazid in the catalase-peroxidase enzymes (*31, 32*) (Chapter 1, Figure 1.10).

4.3.3 Comparison with the rsAPX/ascorbate Structure

Figure 4.13 shows an overlay of the rsAPX/ascorbate (*22*) (Chapter 3) and rsAPX/SHA structures; this clearly highlights the different binding locations of the SHA and ascorbate close to the δ- and γ-heme edge, respectively. The identity of the aromatic substrate binding location was not known for APX prior to the solution of the rsAPX/SHA structure, but it was known to be different to the ascorbate binding site (*4*) and the region close to the δ-heme edge had been implicated (*5*) because heme modification experiments with phenylhydrazine showed substantial modification at the δ-meso position. The rsAPX/SHA and rsAPX/ascorbate structures are also consistent with steady state data that show that APX modified at the δ-heme edge using phenylhydrazine retains ~10% activity with ascorbate but is inactive against guaiacol (*5*).

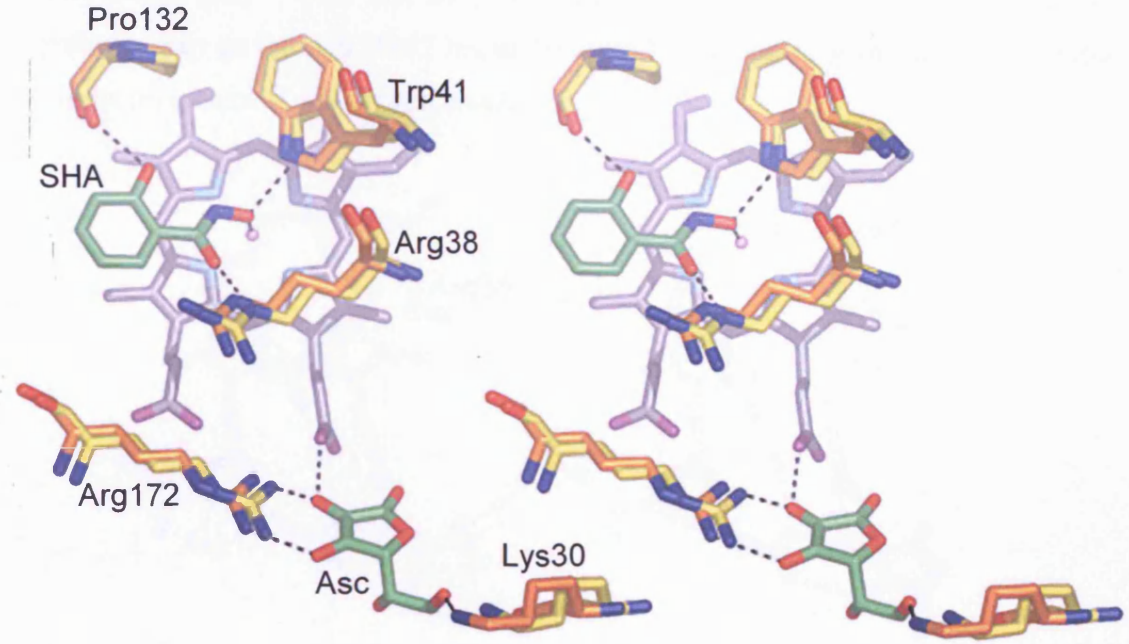

Figure 4.13: Stereo representation of an overlay of the rsAPX/ascorbate (yellow) and rsAPX/SHA (orange) complexes around the heme (grey). Ascorbate and SHA are shown in green. Hydrogen bonds are indicated by black dashed lines.

4.3.4 Mechanism of Proton Transfer

In the catalytic cycle (Chapter 1, section 1.4.2), proton transfer is needed in addition to electron transfer for the reduction of Compound I and Compound II for both aromatic substrates and ascorbate. The mechanism of proton transfer is not well defined for any peroxidase, however, but now that both substrate binding sites are known in rsAPX, it is possible to propose a mechanism in APX. Ascorbate is

hydrogen bonded directly to the heme and therefore it can be assumed that electron transfer occurs directly to the heme. In the case of SHA, there is direct van der Waals contact with the π-system of the heme and therefore the electron can transfer directly to the π-orbitals of the heme.

The theory of how proton transfer occurs is less well developed. Arg38 has been implicated in proton transfer (*10*) and could also be involved in proton transfer for oxidation of both aromatic substrates and ascorbate in APX. In the rsAPX/SHA structure, SHA is directly hydrogen bonded to Arg38 and in the rsAPX/ascorbate structure Arg38 is also linked to ascorbate through a hydrogen-bonding network (Figure 4.14). From the C^2 hydroxyl group in ascorbate there is a hydrogen bond network through Arg38 to the water bound to the iron (Figure 4.14). The C^2 hydroxyl group on protonated monodehydroascorbate (Chapter 1, Figure 1.10) is very acidic (pK_a = -0.45 (*33, 34*)) therefore readily deprotonates. In solution, this pathway may go through His42 but in the crystal structure the geometry is unsuitable for the formation of a hydrogen bond.

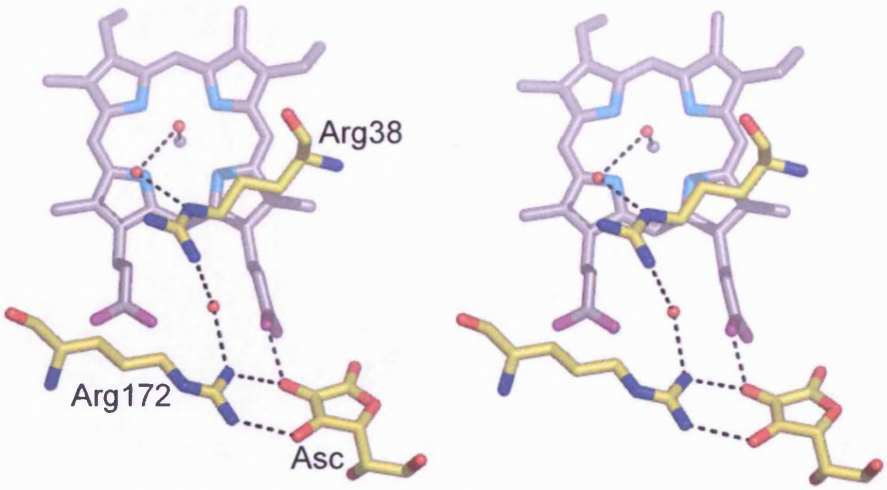

Figure 4.14: Stereo representation of the proposed proton transfer pathway in rsAPX using Arg38. Water molecules are indicated by red spheres and hydrogen bonds are indicated by black dashed lines.

A proton transfer scheme has been proposed for HRP that involves Arg38 and Pro139, both of which are conserved in most peroxidases (*35*). This proton transfer pathway for aromatic substrates agrees with the rsAPX/SHA structure and other available aromatic bound structures which all involve the equivalent proline and arginine in binding. It also ties in with the theory for Compound I formation discussed in Chapter 2 as the active site histidine (His42 in APX) is still involved. An oxidation mechanism proposed for isonazid by catalase-peroxidase enzymes (*31*)

also involves the active site histidine and proline in proton transfer and substrate binding.

4.4 CONCLUSIONS

The solution data in this Chapter show that SHA binds in the aromatic binding pocket of APX and the rsAPX/SHA complex structure has defined the aromatic binding site in APX. This has provided insight into the unusual fact that APX seems to lie between class I and III peroxidases in containing two substrate binding sites. The aromatic binding site is present in a diverse range of peroxidases and the conserved residues of arginine and proline (Arg38 and Pro132 in APX) are important for aromatic binding and oxidation in most plant peroxidases. Hydrophobic interactions in the binding pocket are also important in how strongly the substrates bind.

It has also been possible to use these data to propose a proton transfer pathway for peroxidases in classes I and III, involving the distal arginine residue (Arg38 in APX). This residue is conserved in all peroxidases (*35*) and has been implicated in proton transfer for HRP (*10*). In the rsAPX/SHA structure SHA is hydrogen bonded to Arg38, and in the rsAPX/ascorbate structure ascorbate has a hydrogen-bonding network to Arg38. Therefore the proton transfer pathway could involve this residue for both substrates at the δ-and γ-heme edge. This would be consistent with the idea that APX contains features of both class I and class III peroxidases using a common proton transfer mechanism.

4.5 REFERENCES

1. Raven, E. L. (2000) in *Subcellular Biochemistry: Enzyme Catalysed Electron and Radical Transfer* (Holzenberg, A., and Scrutton, N. S., Eds.) pp 318-350.
2. Heering, H. A., Jansen, M. A. K., Thorneley, R. N. F., and Smulevich, G. (2001) *Biochemistry 40*, 10360-10370.
3. Raven, E. L. (2003) *Natural Product Reports 20*, 367-381.
4. Mandelman, D., Jamai, J., and Poulos, T. L. (1998) *Biochemistry 37*, 17610-17617.
5. Hill, A. P., Modi, S., Sutcliffe, M. J., Turner, D. D., Gilfoyle, D. J., Smith, A. T., Tam, B. M., and Lloyd, E. (1997) *European Journal of Biochemistry 248*, 347-354.
6. Bursey, E. H., and Poulos, T. L. (2000) *Biochemistry 39*, 7374-7379.
7. Patterson, W. R., and Poulos, T. L. (1995) *Biochemistry 34*, 4331-4341.
8. Ator, M. A., and Ortiz de Montellano, P. R. (1987) *Journal of Biological Chemistry 262*, 1542-1551.
9. Henriksen, A., Schuller, D. J., Meno, K., Welinder, K. G., Smith, A. T., and Gajhede, M. (1998) *Biochemistry 37*, 8054-8060.
10. Henriksen, A., Smith, A. T., and Gajhede, M. (1999) *Journal of Biological Chemistry 274*, 35005-35011.
11. DePillis, G. D., Sishta, B. P., Mauk, A. G., and Ortiz de Montellano, P. R. (1991) *Journal of Biological Chemistry 266*, 19334-19341.
12. Itakura, H., Oda, Y., and Fukuyama, K. (1997) *FEBS Letters 412*, 107-110.
13. Tsukamoto, K., Itakura, H., Sato, K., Fukuyama, K., Miura, S., Takahashi, S., Ikezawa, H., and Hosoya, T. (1999) *Biochemistry 38*, 12558-12568.
14. Lad, L., Mewies, M., and Raven, E. L. (2002) *Biochemistry 41*, 13774-13781.
15. Santimone, M. (1975) *Canandian Journal of Biochemistry 53*, 649-657.
16. Hiner, A. N. P., Raven, E. L., Thorneley, R. N. F., Garcia-Canovas, F., and Rodriguez-Lopez, J. N. (2002) *Journal of Inorganic Biochemistry 91*, 27-34.
17. Bogumil, R., Hunter, C. L., Maurus, R., Tang, H.-L., Lee, H., Lloyd, E., Brayer, G. D., Smith, M., and Mauk, A. G. (1994) *Biochemistry 33*, 7600-7608.
18. Aitken, S. M., L.Turnbull, J., Percival, M. D., and English, A. M. (2001) *Biochemistry 40*, 13980-13989.

19. Indiani, C., Santoni, E., Becucci, M., Boffi, A., Fukuyama, K., and Smulevich, G. (2003) *Biochemistry 42*, 14066-14074.

20. Schonbaum, G. R. (1973) *Journal of Biological Chemistry 248*, 502-511.

21. O'Brien, E. C. O., Farkas, E., Gil, M. J., Fitzgerald, D., Castineras, A., and Nolan, K. B. (2000) *Journal of Inorganic Biochemistry 79*, 47-51.

22. Sharp, K. H., Mewies, M., Moody, P. C. E., and Raven, E. L. (2003) *Nature Structural Biology 10*, 303-307.

23. Project, N. C. C. (1994) *Acta Crystallographica D50*, 760-763.

24. McRee, D. (1992) *Journal of Molecular Graphics 10*, 44-47.

25. Sharp, K. H., Moody, P. C. E., Brown, K. A., and Raven, E. L. (2004) *Biochemistry 43*, 8644-8651.

26. Veitch, N. C., and Smith, A. T. (2000) *Advances in Inorganic Chemistry 51*, 107-162.

27. Ikeda-Saito, M., Shelley, D. A., Lu, L., Booth, K. S., Caughey, W. S., and Kimura, S. (1991) *Journal Biolological Chemistry 266*, 3611-3616.

28. Davey, C. A., and Fenna, R. E. (1996) *Biochemistry 35*, 10967-10973.

29. Yonetani, T., and Ray, G. S. (1965) *Journal of Biological Chemistry 240*, 4503-4514.

30. Wilcox, S. K., Jensen, G. M., Fitzgerald, M. M., McRee, D. E., and Goodin, D. B. (1996) *Biochemistry 35*, 4858-4866.

31. Pierattelli, R., Banci, L., Eady, N. A. J., Moody, P. C. E., Bodiguel, J., Jamart-Gregoire, B., Raven, E. L., and Brown, K. A. (2004) *Journal of Biological Chemistry 279*, 39000-39009.

32. Bertrand, T., Eady, N. A. J., Jones, J. N., Bodiguel, J., Jesmin, Nagy, J. M., Raven, E. L., Jamart-Gregoire, B., and Brown, K. H. (2004) *Journal of Biological Chemistry 279*, 38991-38999.

33. Creutz, C. (1981) *Inorganic Chemistry 20*, 4449-4452.

34. Bryan, D. M., Dell, S. D., Kumar, R., Clarke, M. J., Rodriguez, V., Sherban, M., and Charkoudian, J. (1988) *Journal of the American Chemical Society 110*, 1498-1506.

35. Welinder, K. G. (1992) *Current Opinion in Structural Biology 2*, 388-393.

Chapter 5

Towards Enhanced Aromatic Oxidation in rsAPX

5.1 INTRODUCTION

APX oxidises ascorbate and aromatic compounds at two different binding sites (Chapters 3 and 4). The aromatic binding site is near the δ-heme edge (Chapter 4) and is used by many other peroxidases. The aim of this Chapter is to enhance the oxidation of aromatic compounds by APX. This will be carried out by directed evolution, which firstly involves creating a screen to quickly assess the activity of mutants, and then creating a library of random mutants to screen. The development of a new screen is presented in this Chapter, along with preliminary results from the library creation.

5.1.1 Background

Enzyme function is altered routinely by rational design, which involves picking one or two amino acids at the active site and replacing them using site-directed mutagenesis, resulting in enhanced activity and/or selectivity. Although there have been many successful examples, there are numerous disadvantages to this method. One such disadvantage is that changing one or two amino acids in hundreds has little effect when planning total catalytic redesign. In addition, it is often very difficult to predict the effect of the change even if the structure and catalytic cycle are well known (*1-6*).

The other way to redesign enzymes is by irrational design. Usually, this is achieved by directed evolution, which involves creating a library of random mutants and screening them for the desired catalytic activity or selectivity (*1-6*). This technique is based on natural selection, which over a period of time creates a protein engineered for a specific task. The basic principles behind natural selection were discovered by Charles Darwin and published in 'The Origin of Species' (*7, 8*). Darwin compared how species adapted to their natural environment with the results when domestic species were bred for a specific purpose. In nature, the changes in the population occur when those individuals with beneficial characteristics survive to breed and create more offspring. Similar results can be artificially produced by animal and plant breeders by only mating specimens with the desired property. Darwin showed that if a particular characteristic had a benefit to the individual, then this individual was more likely to survive to pass on their characteristics. Hence the

species in general would over time acquire the characteristic, as those without it would not survive long enough to breed.

Shortly after Darwin's publication Gregor Mendel formulated the quantitative rules of genetics from observing cultivated plants (*7*). Mendel chose to breed peas since he could then know the exact parentage of the offspring, and for many generations he recorded details of the characteristics such as colour and shape. From these data he concluded that "alternative versions of genes account for variations in inherited character" and "for each character, an organism inherits two genes, one from each parent" (*9*). He also concluded that if the two genes differ the dominant one will be fully expressed in the organism's appearance and the other recessive gene has no noticeable affect on the organism (*9*). He found that the mathematical probability of a trait occurring was not affected by the emergence of another trait (*9*). These conclusions forms the basis of modern genetics, yet it was a considerable time before the consequences of both Darwin's and Mendel's work were combined to form population genetics (*7, 10*).

5.1.2 Population Genetics

The differential equations of population genetics are usually applied to sexually replicating species and therefore use recombination as the most common source of variation, but when using evolutionary design in the laboratory mutation is the more common source of variation. Mutation is rare in natural evolution of a sexually replicating species and therefore in the laboratory the equations for asexual evolution are required (*11, 12*). These equations express Darwin and Mendel's ideals mathematically. If a variant's fitness is above average this variant will increase in frequency. When the opposite is true, the variant will decrease and eventually approach zero (become extinct). Selection will therefore choose the variant with the highest fitness value and after time only that variant will exist, eventually making the population homogeneous.

This theory uses a low mutation rate since the introduction of a new variant is a rare event in nature. This means there is a slow initial phase in which the new species is in danger of dying out accidentally. Apart from that the outcome of the species is determined by the difference in fitness values. The difference in fitness values is determined by the number of generations required to select an advantageous mutant.

In nature the genetic advantage of a new variant is often very small and thus may take thousands of generations to dominate the population.

Motoo Kimura later suggested that adaptive mutations were very rare and that most mutations were neutral; the role of evolution therefore was to eliminate bad mutations (*13*). This view was supported by the comparison of protein and DNA sequences (*14*) and became the basis of modern molecular phylogeny (the term phylogeny refers to the evolutionary development of a species, used as a method of classifying species rather than classifying them according to similarities (*15*)). To date, most research data on evolution hints at neutral evolution but direct proof only came in the 1990s with experiments involving bacterial evolution under controlled conditions (*16, 17*) and computer models (*18, 19*). In Kimura's model, with a neutral variant the population migrates through sequence space in a random walk-like manner *i.e.* if the variants are neither good nor bad the sequence will continue to change randomly over time. Under high mutation frequencies there is a distribution of species called quasi-species, either of neutral mutants close to the original or of higher mutants with a better fitness (Figure 5.1). The concept of quasi-species is important in virus evolution (*20*).

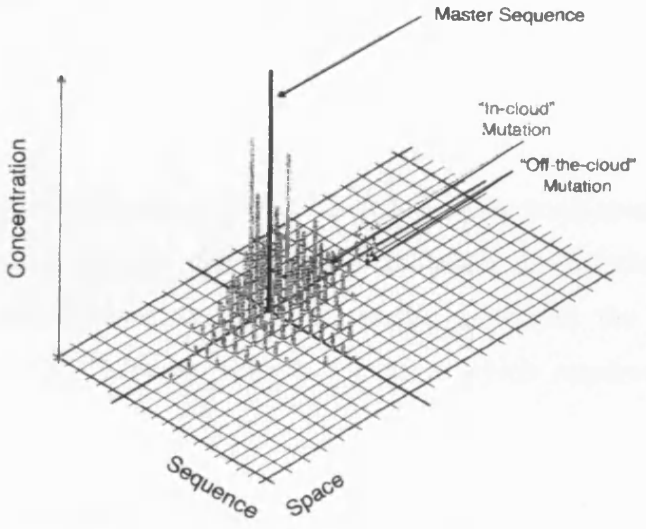

Figure 5.1: Quasi-species mutation distribution. The master sequence is surrounded by a "cloud" of closely related sequences (*11*).

The probability of a variant being produced can be assumed to be independent of the monomer to be changed in a simple model, and is therefore only reliant on the distance away in sequence space (*21, 22*) (Figure 5.1). There is a minimum level of replication accuracy, or a maximum level of mutation, at which the quasi-species

exists called the error threshold (*21, 22*). At mutation rates higher than this the distribution in sequence space would become uniform. However, this cannot happen with biopolymers; there are so many possible variants that no population on earth could be big enough and hence the population would drift randomly through sequence space. This error threshold limits the chain length that can be accurately copied. Therefore in nature chain length and mutation rate are related in a constant manner for most classes of organism (*23-25*).

5.1.3 Evolution in the Laboratory

The mimicking of natural evolution could not start until the 1960s when Spiegelman reproduced viral RNA in a test tube by placing it with an appropriate enzyme and active monomers (*26*). This was the first time RNA or DNA had been reproduced *in vitro* without being chemically synthesised.

Evolutionary techniques were first proposed to engineer biomolecules in 1965 and revised in 1984 (*26, 27*). The system was used practically for the first time in the late 1980s (*28-30*), and evolution of biomolecules to bind to specific targets was achieved artificially in 1990 (*28, 30*). It can be broken down into three steps:

1. Amplification
2. Diversification
3. Selection

Amplification and diversification can be achieved in many ways (see section 5.1.4). The diversity is introduced by enhancing the mutation rate of the amplification method in DNA and RNA synthesis. For smaller molecules the library can be chemically synthesised. It is the selection process which requires intuition and ingenuity (*11*).

5.1.4 Directed Evolution of Enzymes

Directed evolution aims to emulate natural evolution in the laboratory but to reduce the time scale from millions of years to months and even weeks. In nature there is no specific goal; the only aim is to survive and adapt to environmental change (*31-33*). This is carried out by remodelling existing protein scaffolds to evolve new properties and functions. Small point mutations can make a big difference, and changing one or two amino acids can dramatically alter the function of an enzyme. For example

substrate specificity can be changed by single amino acid changes in isocitrate dehydrogenase (*34*), lactate dehydrogenase (*35*) and T4 lysozyme (*36*).

By contrast, in the laboratory there is a definite goal and a good evolutionary strategy is needed. Purely random chains of amino acids present an almost infinite number of possibilities and therefore would be impossible to screen. The activity of the starting protein needs to be as close to the required function as possible. Directed evolution of enzymes basically follows these steps:

1. The DNA for the protein is prepared.
2. This DNA is mutated randomly.
3. Colonies of bacteria containing the mutated DNA are grown, producing a library of proteins.
4. The colonies are screened for the presence of the desired active protein.
5. The DNA is extracted from the colony containing the desired protein.
6. This DNA is mutated again as in step 2, repeating steps 2-6 until the desired activity level by the protein is reached.

Several starting points can be used in step 2 but the more residues that are mutated the more colonies that have to be screened (step 5). Therefore in order to have many starting points the screen must be quick and easy to perform. It is more productive to repeat steps 2-6 many times than have a high mutagenic rate in step 2. This is because it is better to know the effect of a single mutation on the protein before adding other mutations (*31-33*).

The most important part of the process is the screen for enhanced activity (point 5). It has to directly measure or at least couple strongly with the required effect, or the protein may end up without the desired activity. The screen limits the size of the protein library created because there are only so many mutants that can be prepared and processed in the time available. More mutants can be put through the screen if the screen is simplified so that the preparation and processing are quicker. This means a larger protein library can be screened.

5.1.4.1 The Screen

The ideal way to undertake selection of mutants is by survival as in nature (for example, for temperature resistance grow the library at high temperatures), but for some properties that is not possible and therefore a high throughput screen has to be developed. The screen needs to be simple and efficient, since there are usually between 10^3 and 10^6 mutants to be screened. The most popular way is by agar-plate format. Assays by this method are carried out on the whole cell; therefore care must be taken that the enzyme and substrate do indeed react. One way to ensure this is to make sure the enzyme is displayed on the surface of bacteriophage (*37*) or the whole bacteria (*38, 39*). Fluorescence activated cell sorting can then be used to screen for active mutants (*38*). In agar-plate based screening a library of micro-organisms expressing the enzyme of interest is spread on an agar plate. The enzyme activity is then monitored by a visible signal linked to enzyme function – the easiest way is by colour or fluorescence – so that the colonies containing an active mutant can be seen on the plate. This way many plates can be screened efficiently. An example of fluorescence is the protein whose functional variants fluoresce green under UV illumination (*40-43*).

Colorimetric assays are more widely used; for example β-galactosidase activity can be assayed as when it reacts with its substrate, 5-bromo-4-chloro-3-indolyl β-D-galoside (X-gal) a blue product is formed. Therefore in an assay the depth of blue colour is related to the activity of the β-galactosidase enzyme. This method has been extended to screening of glucosidases (*44*) and even catalytic RNA molecules (*45*). Colour assays have also been used successfully for phosphatases (*46*), dehydrogenases (*47*) and β-lactamases (*48*). They can be used to monitor complex metabolic functions as well as single enzymes; for example a carotenogenic gene cluster was discovered using a yellow pigment (*49*).

5.1.4.2 The Mutagenesis Step

The mutagenesis can be carried out over the whole gene or just a specific region of the gene. If the whole is mutated (Figure 5.2), residues away from the binding site may be found to affect the protein activity, but because a large number of mutants are created a simple screen is required. If a specific area is targeted, saturated point mutagenesis can be used to mutate only a few residues. This means all the different

combinations of amino acids are tried at one or two points in the protein and fewer mutants need to be screened.

Figure 5.2: Representation of a DNA library. For clarity only five mutants are shown but in reality there would be thousands.

Random Libraries

DNA libraries can be created in two ways: by PCR (the polymerase chain reaction) or by cloning the vector into a DNA repair deficient *Escherichia coli* (*E. coli*) strain. In the PCR method, the gene for the required protein or a vector containing the gene is replicated by a series of temperature cycles with primers and a polymerase. However, the polymerase used is of a low fidelity and therefore there are random mistakes made in the replication of the gene. These mutant genes are then cloned back into the vector and transformed into bacteria, or in the case of the mutant vector transformed straight into the bacteria. The bacteria can then be grown and screened for the desired property.

An alternative method is to transform the vector into *E. coli* which is deficient in some of the primary DNA repair pathways. The *E. coli* are grown in a culture (the length of time depends on the level of mutation required, and the more copies made the more mutations will occur). The mutant vectors are extracted from the deficient *E. coli* and transformed into an intact strain of *E. coli* to be screened.

Saturated Point Mutagenesis

This method is used to change between one and five amino acids in the protein. It is used to create every possible mutation at those sites. The PCR method is used again but with a high fidelity polymerase and instead of using two primers (as above in error-prone PCR) a mixture of primers which between them contain the codes for all 22 L-amino acids at the required point or points are used. The mutated vectors are transformed into *E. coli* for screening. Usually 1-5 amino acids are chosen to mutate, but for every amino acid approximately 200 mutants need to be screened to be sure

of testing all possible variations at that point. This means for n amino acids 200^n mutants need to be screened to ensure the screening of all possibilities. Therefore the number of residues mutated at once must depend on the speed of the screen and its level of automation.

5.1.4.3 DNA Shuffling

In 1994, Willem P. C. Stemmer invented DNA shuffling to introduce the advantages of sexual evolution to evolution in the laboratory. The method recombines pools of selected mutant genes by random fragmentation and PCR reassembly (*50*). The pool of mutant genes are advantageous mutants found using the techniques of directed evolution and/or site-directed mutagenesis. DNA shuffling is carried out with the un-mutated enzyme to delete any unnecessary mutations and to find new combinations of mutants which have a higher activity. The gene pool is randomly digested and then recombined to screen for the desired activity. It has been used successfully on a number of proteins to improve the desired property beyond what can be achieved with random mutagenesis alone (*40, 50-53*). This technique was improved using a staggered extension process (StEP) and PCR (*54*). The gene pool is used as a template in a PCR reaction, but the extension step is shortened, producing only a small section of the gene in each cycle. This step needs to be repeated more often to complete the gene, but because of the shortening of the cycle, template switching occurs and the resulting DNA has sections from each gene (Figure 5.3).

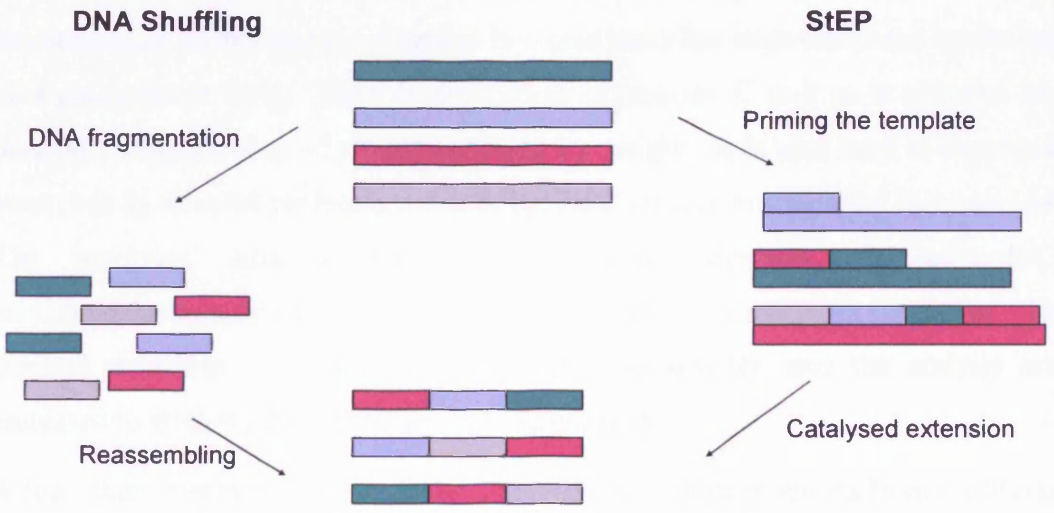

Figure 5.3: Comparison of DNA shuffling and StEP.

5.1.5 Direct Evolution of Heme Enzymes

Heme proteins are ideal for directed evolution as they already have a wide variety of functions, but not many of them have been subjected to directed evolution (*55*). Below are a few examples of heme proteins which have successfully been engineered by directed evolution.

For example, cytochrome P450s have been adapted by directed evolution, since they insert an oxygen atom into carbon hydrogen bonds which would be useful in industry. Several different screens have been used to find active mutants, mostly using colour (*56, 57*) or fluorescence (*58, 59*). Saturated point mutagenesis has also been used successfully on P450s (*60, 61*) since the active site structure is known (*62*).

5.1.5.1 Peroxidases

Since peroxidases oxidise a wide range of substrates they are ideally suited to directed evolution experiments. Commercially, ARP was successfully evolved to resist high temperatures, high pH and high concentrations of peroxide (*63*) for use as a dye-inhibitor in laundry detergents. This was achieved by combining several mutants – found by site-directed mutagenesis, random mutagenesis by error-prone PCR and saturated point mutagenesis – using DNA shuffling. The resulting enzyme had a 100-fold improvement in thermal stability and 2.8 times the oxidative stability compared to the un-mutated enzyme.

HRP was the first peroxidase to be discovered, but although a great deal of research has been done on this enzyme progress in recent years has been hampered by the lack of a recombinant form. HRP is difficult to express in *E. coli* as it contains four disulfide bridges and is ~21% glycosylated by weight. It is also hard to express in yeast, but by directed evolution a functional HRP mutant was secreted by yeast (*64*). The screening used a traditional peroxidase substrate, 2,2'-azino-di-(3-ethyl)benzthiazoline-6-sulfonic acid (ABTS), which turns red upon oxidation. The directed evolution was taken further to improve activity, and the activity was increased to 40 times that of the un-mutated enzyme.

A few other screens have been devised that use the colour produced from traditional aromatic peroxidase substrates to provide quick and easy screening (*65-69*).

5.1.6 Aims

Prior to the resolution of the rsAPX/SHA crystal structure (Chapter 4) little was known about aromatic substrate binding in APX, although from mutagenesis studies aromatic compounds were known to bind away from the ascorbate binding site (γ-heme edge) (*70, 71*). The rsAPX/SHA structure shows how aromatic compounds bind at the δ-heme edge, involving Arg38 and Pro132 in a solvent accessible pocket.

The overall aim of this work was to use random mutagenesis to elucidate how guaiacol binds in the aromatic site and to improve the oxidation rate of aromatic compounds by rsAPX. A quick and easy method to oxidise aromatic compounds could be very useful to both industry and academia as it is a common step in organic synthesis.

Initially, the major objective was to develop an efficient screen since this will allow a large number of mutants to be checked for the desired activity. Subsequently, DNA libraries can be created by random mutagenesis and saturated point mutagenesis. In this Chapter, the development of a rapid screen is described and preliminary work on preparation of a DNA library is presented.

5.2 RESULTS and DISCUSSION

5.2.1 Screen for Directed Evolution

This screen was developed in collaboration with Dr T. Fleming and Prof. N. Turner (Chemistry Department, The University of Edinburgh). It was based on a screen developed to detect the hydrogen peroxide produced when monoamine oxygenase (MAO) oxidises amines (*72*). The hydrogen peroxide detecting screen uses a kit from Sigma for detection of slight peroxidase activity in immunology assays (*SIGMAFAST™*, 3,3'diaminobenzidine tablets). The original screen used 3,3'diaminobenzidine (DAB) and HRP, since DAB forms a brown-black product when oxidised by HRP in the presence of hydrogen peroxide.

5.2.1.1 DAB Screen

The original screen was first tested on un-mutated rsAPX by adding DAB and urea-hydrogen peroxide to colonies of SG cells expressing rsAPX. *E. coli* containing the rsAPX gene were grown up overnight on a nitrocellulose membrane placed on agar plates. The membranes were then lifted off the plates and placed on agar plates containing isopropyl-β-D thiogalactopyanside (IPTG) for four hours, to induce expression of the protein. The membranes were then removed from the agar plates and frozen in a Petri dish at -80 °C to partially lyse the cells. Only partially lysing the cells caused the substrate and enzyme to react, but still allowed each colony to retain live *E. coli*. The membrane was taken out of the freezer at least half an hour before the screen.

The screen was then carried out. Aliquots of molten agar solution and potassium phosphate solution were kept at 50 °C in a water bath. The potassium phosphate solution contained DAB and urea-hydrogen peroxide. To carry out the screen, an aliquot of agar solution was added to an aliquot of potassium phosphate solution and quickly (to avoid the agar setting before it was on the membrane) poured over the membrane. The colonies rapidly turned brown and therefore several dilutions were tried until the brown colour took ~ 30 minutes to appear.

DAB is an un-typically large substrate therefore the screen was adapted to use guaiacol.

5.2.1.2 Guaiacol Screen

Guaiacol is rapidly oxidised by APX and is a more typically sized aromatic substrate, containing only one aromatic ring (Figure 5.4). Guaiacol when oxidised, forms tetraguaiacol which is red in colour and therefore offers an easy colorimetric assay.

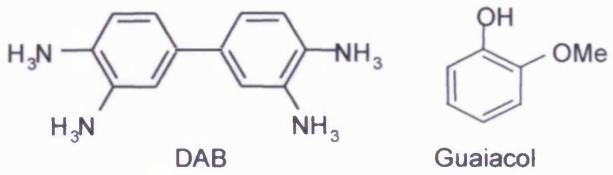

Figure 5.4: Structures of DAB and guaiacol.

The screen was therefore repeated replacing DAB with guaiacol. Guaiacol is not soluble in water and therefore ethanol had to be added to the screen to dissolve it. The concentration of guaiacol was systemically altered in repeat screens until a pale red colour appeared after approximately an hour. Therefore any colonies containing a mutant which oxidises guaiacol better than un-mutated rsAPX should go bright red in this time (Figure 5.5). To check the bacteria could survive the screening process, a colony was touched using a sterile pipette tip and the tip placed in LB media overnight. The SG cells reproduced and therefore the screening does not kill the bacteria. This meant any mutants found during screening could be grown up from the screen plate.

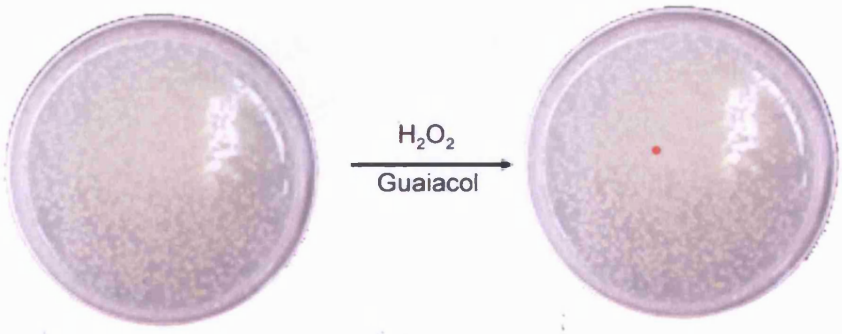

Figure 5.5: Representation of the guaiacol screen showing a mutant with increased activity towards guaiacol.

The screen presented above is fully developed and is very efficient so that many mutants can be screened quickly and easily. The colour producing reaction is directly coupled to the activity and therefore the screen will not give false positives. The screen development is usually the difficult part of random mutagenesis.

5.2.2 DNA Library Preparation

5.2.2.1 Random Mutagenesis by DNA Repair Pathway Deficient E. coli

The *E. coli* strain used to create these DNA libraries is commercially available (XL1-Red strain, Stratagene). This strain of *E. coli* was chosen since it had previously been used successfully in Prof. N. Turner's laboratory at Edinburgh University (*72*). The pQE30 vector containing the gene for rsAPX was extracted from SG cells (Chapter 2, section 2.2.1.1) and transformed into Top 10 cells (Invitrogen). This was carried out since SG cells contain a kanamycin resistant vector (pREP4, Qaigen). The Top 10 cells were grown up in media containing ampicillin only (since the gene for ampicillin resistance is contained within the pQE30 vector) overnight to encourage the rejection of the kanamycin resistant vector. The DNA was extracted and retransformed into Top 10 cells. This process was repeated until a gel of the digest of DNA only contained two bands. The vectors were digested with *Bam*HI and *Kpn*I enzymes (Stratagene) as the cutting sites for these were cloned into the pQE30 vector at only two places to extract the rsAPX gene (*73*). A DNA gel of the digested products only gave two bands, one at ~750 base pairs (bp) from the rsAPX gene and one at ~ 3000 bp for the pQE30 vector if the pQE30 vector was the only vector present (Figure 5.6).

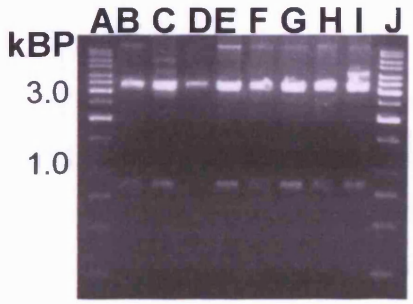

Figure 5.6: DNA gel of digested pQE30 vector containing the rsAPX gene. Lanes A and J are DNA ladders (Fermentas). Lanes B to I are samples from separate Top 10 colonies after transformation of the rsAPX vector. B, C and D show two bands corresponding to the pQE30 vector and rsAPX gene in size. E, F, G and H show three bands but as the third band has not run down the gel it is probably undigested circular vector containing the rsAPX gene. I contains a fourth band which may be the vector cut once.

The DNA vector from the Top 10 cells was transformed into XL1-red cells. These cells were grown up for ~72 hours, monitored by UV-visible spectroscopy and then the DNA extracted. This DNA was transformed into the deficient *E. coli* and the process repeated 4 times (Figure 5.7).

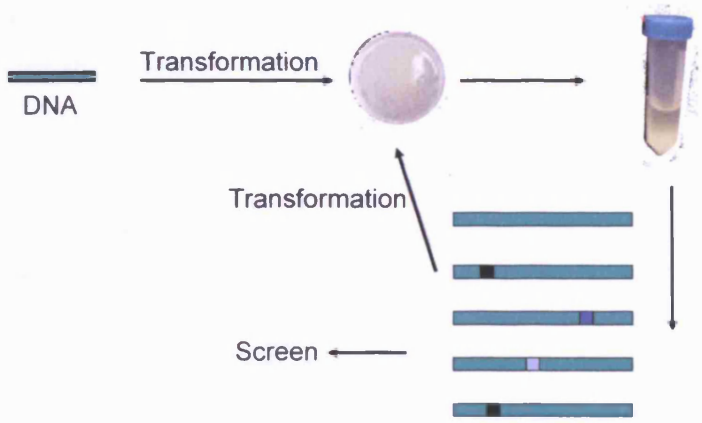

Figure 5.7: Representation of the creation of a DNA library by *E. coli* deficient in DNA repair pathways. The library is screened every four transformations.

The fourth DNA library was transformed into SG recombinant cells and the screen was carried out as described previously. The colour appeared in all the colonies at exactly the same rate as un-mutated rsAPX. Therefore the DNA was transformed into the XL1-red cells another 4 times as above. This whole process was carried out a total of 4 times to produce library 16, but the colonies still reacted in the same way as un-mutated rsAPX.

In order to determine the DNA sequence of mutants from the library five colonies were picked at random and grown up overnight before preparing their DNA and sending it to be sequenced (PNCL) with pQE30 standard forward and reverse primers (Qiagen). All five samples were found to be un-mutated rsAPX DNA. According to Stratagene (www.stratagene.co.uk) the mutation rate of XL1-red cells is 1 mutation per 2000 nucleotide bases after ~24 hours growing time. This meant that since the whole vector is ~4000 nucleotide bases long there should be two mutations after ~24 hours. The rsAPX gene is only ~750 bases and therefore should have ~0.4 mutations for every ~24 hours grown in XL1-red cells. As the cells were very slow growing ~24 hours was taken to be the time in which the cells reached an absorbance of greater than 1.5 at 260 nm. If the mutation was working each colony should have 11 point mutations by library 16. Therefore the mutagenesis was not working.

Blue and White Screening

Since no mutants had been found in the rsAPX libraries, a control reaction was carried out. The random mutation technique was carried out on the standard pUC18

control plasmid which contains the gene for β-galactosidase. The β-galactosidase enzyme catalyses the oxidation of X-gal, which forms a blue product. This gene is 634 base pairs in a vector of 2961 base pairs. This means for every ~24 hours grown in XL1-red cells, the whole vector should have 1.5 mutations and the gene should have 0.3 mutations. The protocol from the previous random mutagenesis work was followed and DNA library 4 was screened in SG cells.

The library was grown on nitrocellulose membranes on LB plates overnight. The membranes were transferred to LB plates containing X-gal and IPTG, and left overnight at 37 °C. In the morning most of the colonies had turned blue but a few were white, indicating that the β-galactosidase was inactive in the white colonies and therefore the gene must be mutated (Figure 5.8).

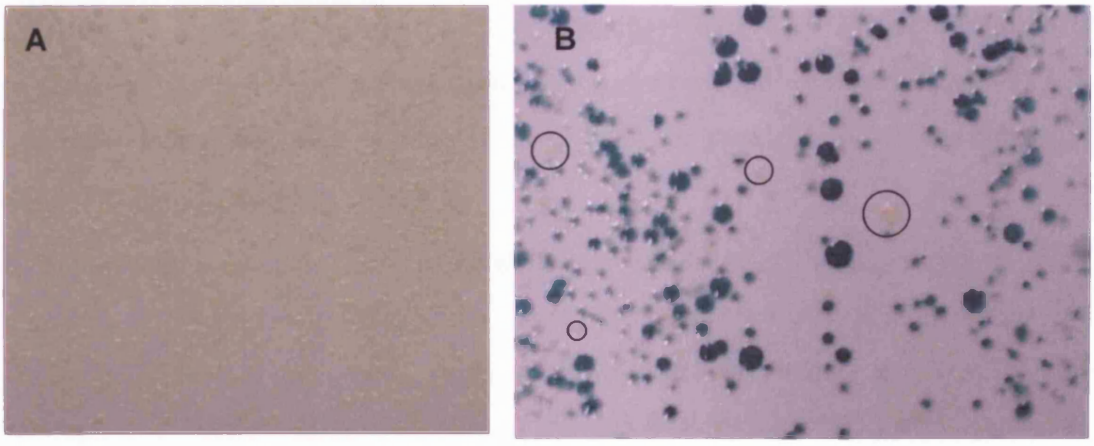

Figure 5.8: Random mutagenesis of β-galactosidase screening with X-gal. **(A)** Before addition of X-gal. **(B)** After the addition of X-gal. A few of the white colonies are circled.

The β-galactosidase gene should have 2.4 mutations per gene by library 4, but only a few of the possible mutations will result in no activity towards X-gal therefore only a few colonies do not turn blue. DNA sequencing was deemed unnecessary as the white colonies must be mutated to not react with X-gal. Hence, the technique used to create the library by DNA repair deficient *E. coli* functioned correctly on this standard vector, and therefore it must be concluded that the method of random mutagenesis used does indeed work.

5.2.2.2 Random Mutagenesis by PCR

This method was used as an alternative to the method described in section 5.2.2.1 and was carried out using a kit from Stratagene (GeneMorph random Mutagenesis Kit). The protocol was followed for medium level mutagenesis (3-7 mutations per

gene). The vector DNA (~40 ng) was added as this is equivalent to 10 ng of gene (750 bp/3000 bp = 0.25). The oligonucleotides used were pQE30 forward sequencing primer (Qiagen) and the reverse version of it. Unfortunately, a DNA gel of the PCR products revealed only the oligonucleotides.

5.2.2.3 Saturated Point Mutagenesis

To assess which residues to target for saturated point mutagenesis, guaiacol was modelled into the aromatic binding site based on the rsAPX/SHA complex structure (Figure 5.9). There were several residues which could affect binding of guaiacol: Ser69, Ala70, Leu131, Asp133 and Ser173 were all possibilities. Ser173 was thought to be close to the binding site and a hydrophobic residue would create a hydrophobic pocket for guaiacol, but since Ser173 is hydrogen bonded to the heme, changing it could destabilise the heme binding. Ala70 is already forming a hydrophobic pocket, therefore mutation could make the binding weaker. Leu131 is a hydrophobic residue, but it is oriented away from the guaiacol pocket and therefore any transformed residue may be too.

Ser69 is quite a distance from the modelled guaiacol (~6 Å) but if converted to an aromatic ring it may help provide a hydrophobic pocket for aromatic substrates. In HRP Phe68 is in the place of Ser69 in rsAPX and this makes the pocket more hydrophobic, binding BHA with a tighter dissociation constant (2.5 μM) than rsAPX binds SHA (Chapter 4, section 4.3.2.1). The SHA binding is worse in the HRP complex as it is more hydrophilic than BHA (k_d = 12 μM), but guaiacol is even more hydrophobic than BHA.

Asp133 is pointing towards the guaiacol and therefore if changed it may also help provide a hydrophobic pocket. In HRP this residue is also an aromatic ring (Phe142) making the pocket more hydrophobic (Chapter 4, section 4.3.2.1).

Thus, Ser69 and Asp133 were the first two residues to be subjected to saturated point mutagenesis, but two separate libraries were created since 200 colonies needed to be screened for each one.

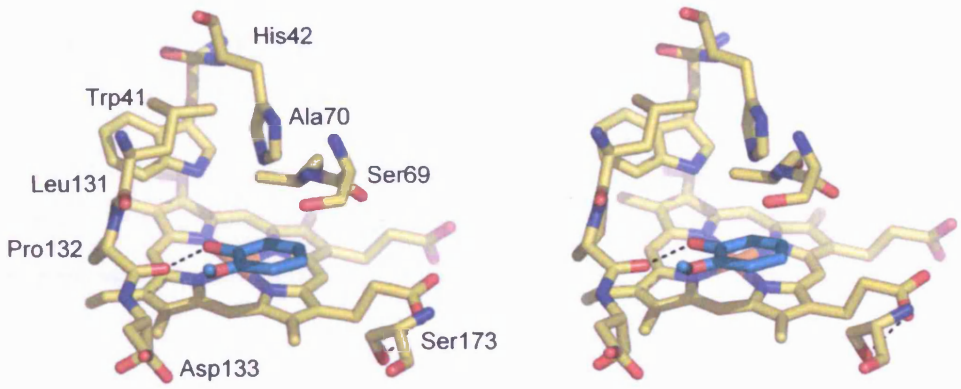

Figure 5.9: Model of guaiacol binding to rsAPX based on the rsAPX/SHA complex structure. Hydrogen bonds are indicated by black dashed lines and the guaiacol molecule is coloured pale blue.

The saturated point mutagenesis was carried out using a kit from Stratagene for site-directed mutagenesis (Quickchange). Oligonucleotides were designed with a degenerate codon (NNS) at the point of mutation. A mixture of oligonucleotides were then made with equal amounts of each base at position N, and half guanine (G) and half cytosine (C) at position S. The S is included since there are three codes for stop codons in bacterial systems and two of them end in thymine (T).

Mutagenesis was carried out according to the protocol of the kit, but only the oligonucleotides were visible on a DNA gel. The magnesium concentration was varied and the oligonucleotides concentration doubled, but the oligonucleotides were still the only bands visible on a DNA gel.

The PCR methods of random and saturated point mutagenesis were not successful but in future work the conditions under which the experiments were carried out could be varied. For example, the DNA libraries could be created by varying these conditions:

- The extension time could be increased to 2 minutes per 1000 bases
- The annealing temperature could be lowered
- Glycerol could be added (5-20%) to stop secondary structure
- Primer concentration could be increased
- Magnesium chloride concentration could be varied to change the ionic strength
- The amount of polymerase could be increased

All these parameters can be varied independently to achieve a product from error-prone and saturated-point-mutagenesis PCR.

5.3 CONCLUSIONS

The primary aim of this Chapter has been achieved with the creation of an efficient screen. Since the screen can be carried out on whole cells and relies on an easily detected colour change, it can be used to screen many mutants. This work can be continued once the DNA libraries have been created.

5.4 REFERENCES

1. Pluckthun, A., Schaffitzel, C., Hanes, J., and Jermutus, L. (1991) in *Methods in Enzymology* pp 367-429, Academic Press Inc.
2. Kuchner, O., and Arnold, F. H. (1997) *Trends in Biotechnology 15*, 523-530.
3. Giver, L., and Arnold, F. H. (1998) *Current Opinion in Chemical Biology 2*, 335-338.
4. Powell, K. A., Ramer, S. W., del Cardayre, S. B., Stemmer, W. P. C., Tobin, M. B., Longchamp, P. F., and Huisman, G. W. (2001) *Angewandte Chemie International Edition 40*, 3948-3959.
5. Saven, J. G. (2002) *Current Opinion in Strutural Biology 12*, 453-458.
6. Johnsson, K., and Brakmann, S. (2002) *Directed Evolution of Proteins*, Wiley-VCH.
7. de Beer, G. (1964) *Notes and Records of the Royal Society of London 19*, 192-226.
8. Darwin, C. (1859) *The Origin of the Species*, Penguin.
9. Califonia State University (Chico) *http://www.biopoint.com/engaging/MENDEL/*.
10. Fisher, R. A. (1930) *The genetic theory of natural selection*, Oxford University Press, Oxford.
11. Schuster, P. (2002) in *Directed Molecular Evolution of Proteins* (Brakmann, S., and Johnsson, K., Eds.) pp 5-28, Wiley-VCH.
12. Eigen, M. (1971) *Naturwissenschaften 58*, 465-523.
13. Kimura, M. (1983) *The Neutral Theory of Molecular Evolution*, Cambridge University Press, Cambridge.
14. King, J. L., and Jukes, T. H. (1969) *Science 164*, 788-798.
15. Prescott, L. M., Harley, J. P., and Klein, D. A. (1990) *Microbiology*, Wm. C. Brown, Dubuque (USA).
16. Papadopoulos, D., Schneider, D., Meier-Eiss, J. M., Arber, W., Lenski, R. E., and Blot, M. (1999) *Proceedings of the National Academy of Science, USA 96*, 3807-3812.
17. Elena, S. F., Cooper, V. S., and Lenski, R. E. (1996) *Science 272*, 1802-1804.
18. Huynen, M. A., Stadler, P. F., and Fontana, W. (1996) *Proceedings of the National Academy of Science, USA 93*, 397-401.

19. Derida, B., and Peliti, L. (1991) *Bullitin of Mathematical Biology 53*, 355-382.

20. Domingo, E., and Holland, J. J. (1997) *Annual Review of Microbiology 51*, 151-178.

21. Biebricher, C. K., and Gardiner, W. C. (1997) *Biophysical Chemistry 66*, 179-192.

22. Eigen, M., and Schuster, P. (1977) *Naturwissenschaften 64*, 541-565.

23. Drake, J. W., Charlesworth, B., Charlesworth, D., and Crow, J. F. (1998) *Genetics 148*, 1667-1686.

24. Drake, J. W. (1991) *Proceedings of the National Academy of Science, USA 88*, 7160-7164.

25. Drake, J. W. (1993) *Proceedings of the National Academy of Science, USA 90*, 4171-4175.

26. Spiegelman, S., Haruna, I., Holland, B., Beaudreau, G., and Mills, D. (1965) *Proceedings of the National Academy of Science, USA 54*, 919-927.

27. Eigen, M., and Gardiner, W. (1984) *Pure and Applied Chemistry 56*, 967-978.

28. Ellington, A. D., and Szostak, J. W. (1990) *Nature 346*, 818-822.

29. Smith, G. P. (1985) *Science 228*, 1315-1317.

30. Tureck, C., and Gold, L. (1990) *Science 249*, 505-510.

31. Arnold, F. H. (1998) *Accounts of Chemical Research 31*, 125-131.

32. Eness, J., Cardayre, S. B. D., Minshull, J., and Stemmer, W. P. (2001) *Advances in Protein Chemistry 55*, 261-292.

33. Avoigt, C., Kauffman, S., and Wang, Z. G. (2001) *Advances in Protein Chemistry 55*, 79-160.

34. Doyle, S. A., Fung, S. Y., and Koshland, D. E. (2000) *Biochemistry 39*, 14348-14355.

35. Wu, G., Fiser, A., ter Kuile, B., Sali, A., and Muller, M. (1999) *Proceedings of the National Academy of Science, USA 96*, 6285-6290.

36. Kuroki, R., Weaver, L. H., and Matthews, B. W. (1999) *Proceedings of the National Academy of Science, USA 96*, 8949-8954.

37. Legendre, D., Laraki, N., Graslund, T., Bjornvad, M. E., Bouchet, M., Nygren, P. A., Borchert, T. V., and Fastrez, J. (2000) *Journal of Molecular Biology 296*, 87-102.

38. Olsen, M. J., Stephens, D., Griffiths, D., Daugherty, P., Georgiou, G., and Iverson, B. L. (2000) *Nature Biotechnology 18*, 1071-1074.

39. Kim, Y. S., Jung, H.-C., and Pan, J.-G. (2000) *Applied and Environmental Microbiology 66*, 788-793.

40. Crameri, A., Whitehorn, E. A., Tate, E., and Stemmer, W. P. C. (1996) *Nature Biotechnology 14*, 315-319.

41. Heim, R., and Tsien, R. Y. (1996) *Journal of Current Biology 6*, 178-182.

42. Siemering, K. R., Golbik, R., Sever, R., and Haseloff, J. (1996) *Journal of Current Biology 6*, 1653-1663.

43. Youvan, D. C. (1995) *Science 268*, 264-264.

44. Gonzalez-Blasco, G., Sanz-Aparicia, J., Gonzalez, B., Hermoso, J. A., and Polaina, J. (2000) *Journal of Biological Chemistry 275*, 13708-13712.

45. Borrego, B., Wienecke, A., and Schwienhorst, A. (1995) *Nucleic Acids Research 23*, 1834-1835.

46. Messer, W., and Vielmetter, W. (1965) *Biochemistry and Biophysics Research Communications 21*, 182-186.

47. Henne, A., Daniel, R., Schmitz, R. A., and Gottschalk, G. (1999) *Applied and Environmental Microbiology 65*, 3901-3907.

48. Rondon, M. R., August, P. R., Bettermann, A. D., Brady, S. F., grossman, T. H., Liles, M. R., Loiacono, K. A., Lynch, B. A., MacNeil, I. A., Minor, C., Tiong, C. L., Gilman, M., Osburne, M. S., Clardy, J., Handelsman, J., and Goodman, R. M. (2000) *Applied and Environmental Microbiology 66*, 2541-2547.

49. Krubasik, P., and Sandmann, G. (2000) *Molecular Genomics and Genetics 263*, 423-432.

50. Stemmer, W. P. C. (1994) *Nature 370*, 389-391.

51. Harayama, S. (1998) *Trends in Biotechnology 16*, 76-82.

52. Crameri, A., Raillard, S. A., Bermudez, E., and Stemmer, W. P. C. (1998) *Nature 391*, 288.

53. Stemmer, W. P. C. (1994) *Proceedings of the National Academy of Science, USA 91*, 10747-10751.

54. Zhao, H., Giver, L., Shao, Z., Affholter, J. A., and Arnold, F. H. (1998) *Nature Biotechnology 16*.

55. Cirino, P. C., and Arnold, F. H. (2002) in *Directed Molecular Evolution of Proteins* (Brakmann, S., and Johnsson, K., Eds.), Wiley-VCH.

56. Joern, J. M., Sakamoto, T., Arisawa, A., and Arnold, F. H. (2001) *Journal of Biomolecular Screening 6*, 219-223.

57. Schwaneberg, U., Otey, C., Cirino, P., Farinas, E., and Arnold, F. H. (2001) *Journal of Biomolecular Screening 6*, 111-118.

58. Joo, H., Arisawa, A., Lin, Z., and Arnold, F. H. (1999) *Chemical Biology 6*, 699-706.

59. Joo, H., Lin, Z., and Arnold, F. H. (1999) *Nature 399*, 670-673.

60. Graham-Lorence, S., Trucan, G., Peterson, J. A., Falck, J. R., Wei, S., Helvig, C., and Capdevila, J. H. (1997) *Journal of Biological Chemistry 272*, 1127-1135.

61. Lentz, O., Li, Q.-S., Schwaneberg, U., Lutz-Wahl, S., Fischer, P., and Schmid, R. D. (2001) *Journal of Molecular Catalysis B: Enzymatic 15*, 123-133.

62. Li, Q. S., Schwaneberg, U., Fischer, M., Schmitt, J., Pleiss, J., lutz-Wahl, S., and Schmid, R. D. (2001) *Biochimica et biophysica Acta 1545*, 114-121.

63. Cherry, J. R., Lamsa, M. H., Schneider, P., Vind, J., Svendsen, A., Jones, A., and Pedersen, A. H. (1999) *Nature Biotechnology 17*, 379-384.

64. Morawski, B., Li, Z., Cirino, P., Joo, H., Bandara, G., and Arnold, F. H. (2000) *Protein Engineering 13*, 377-384.

65. Rai, G. P., Zong, Q., and Hager, L. P. (2000) *Israel Journal of Chemistry 40*, 63-70.

66. Matsuura, T., Yomo, T., Trakulnaleamsai, S., Ohashi, Y., Yamamoto, K., and Urabe, I. (1998) *Protein Engineering 11*, 789-795.

67. Trakulnaleamsai, S., Yomo, T., Yoshikawa, M., Aihara, S., and Urabe, I. (1995) *Journal of Fermintation and Bioengineering 79*, 107-118.

68. Wan, L., Twitchett, M. B., Eltis, L. D., Mauk, A. G., and Smith, M. (1998) *Proceedings of the National Academy of Science, USA 95*, 12825-12831.

69. Iffland, A., Tafelmeyer, P., Saudan, C., and Johnsson, K. (2000) *Biochemistry 39*, 10790-10798.

70. Bursey, E. H., and Poulos, T. L. (2000) *Biochemistry 39*, 7374-7379.

71. Mandelman, D., Jamai, J., and Poulos, T. L. (1998) *Biochemistry 37*, 17610-17617.

72. Alexeeva, M., Carr, R., and Turner, N. J. (2003) *Organic and Biomolecular Chemistry 1*, 4133-4137.

73. Dalton, D. A., del Castillo, L. D., Kahn, M. L., Joyner, S. L., and Chatfield, J. M. (1996) *Archives of Biochemistry and Biophysics 328*, 1-8.

Chapter 6

Experimental

6.1 General Experimental

6.1.1 Materials and Stock Solutions

All chemicals were obtained from commercial sources and used without further purification unless otherwise stated. All Glycerol was sterilised. All buffers and solutions were made using deionised water (PURELAB option DV 35) and are listed in the appendix.

6.1.2 UV-Visible Spectroscopy

Throughout the UV-visible absorption spectroscopy work, variable slit Perkin-Elmer Lambda 14, Lambda 35 or Lambda 40 (10 mm path length and a 1 mm slit width) UV-visible spectrometers were used with a water bath (NESLAB RTE-200) or Peltier device (Perkin Elmer, Peltier thermostatted reference holder, BS0510412) to control temperature.

6.1.3 Protein Expression

Recombinant soybean cytosolic APX (rsAPX) was prepared from *Escherichia coli* SG1300 cells (Qiagen, containing pREP4 vector) incorporating pQE30 expression plasmid (Qiagen) (*1*). All LB media used to grow the *E. coli* contained ampicillin (100 μg/ml) and kanamycin (30 μg/ml). SDS-PAGE analysis was used to monitor the reaction.

Agar plates containing ampicillin (100 μg/ml) and kanamycin (30 μg/ml) were streaked with *E. coli* cells from a –80 °C glycerol stock. The plates were incubated, inverted and grown at 37 °C overnight.

A single colony was used to inoculate LB media (5 ml). This was incubated overnight at 37 °C with shaking at between 225 to 250 rpm.

An aliquot of this overnight culture (930 μl) was added to glycerol (70 μl) to form the new glycerol stock, which was then frozen on dry ice. LB media (200 ml) was inoculated with the overnight culture (2 ml). This was incubated with shaking (between 225 and 250 rpm) at 37 °C until late log phase, taking approximately 2 to 3 hours and monitored spectroscopically (A_{600} = 0.6). This formed the starter culture for the next step.

Starter culture (25 ml per litre) was added to 1 x 8 litre of LB media. The flasks were shaken (225 - 250 rpm) at 37 °C until the absorbance of the culture of bacteria reached 1.0 A at 600 nm. This took approximately four hours. The incubator temperature was then adjusted to 27 °C. A sample of culture was removed (Figure 6.2, lane B) and IPTG (250 µl, 1 M) added to each flask to induce expression. The flasks were incubated at 27 °C overnight with shaking (225 - 250 rpm).

The cells were harvested by centrifugation (6,000 rpm for 10 minutes at 10 °C) and a sample was taken (Figure 6.2, lane C). The cell pellets were then frozen at -20 °C, until needed.

6.1.4 Protein Isolation and Purification

6.1.4.1 Cell Lysis

The cell pellets were thawed in sonication buffer (40 ml), and stirred with lysozyme (~5 mg) for 20 minutes at room temperature until the liquid became viscous. A sample was taken (Figure 6.2, lane D). DNase (~0.1 mg) was added and the suspension stirred until it became more fluid. The mixture was then sonicated on ice, at maximum power for 30 seconds, followed by a cooling period of approximately one minute. This process was repeated eight times and a sample was taken (Figure 6.2, lane E). Cell-free extract was obtained through pelleting the cell debris by centrifugation (20,000 rpm for 30 minutes, 10 °C). Samples of the cell pellet (Figure 6.2, lane F) and of the cell-free extract (Figure 6.2, lane G) were taken. The cell-free extract was kept at 4 °C. The cell debris pellet was resuspended in sonication buffer and the sonication and centrifugation steps repeated and the cell-free extract pooled and frozen. Samples of the cell pellet (Figure 6.2, lane H) and of the cell-free extract (Figure 6.2, lane I) were taken.

6.1.4.2 Nickel Resin Column

A Ni^{2+}-nitrilotriacetic acid (NTA) agarose column (Qiagen) was used to isolate the APX protein from the cell-free extract. The cell-free extract was thawed and made up to approximately 250 ml with sonication buffer. A column of 5 ml Ni-NTA super flow resin (Qiagen) was packed and flushed through with water (100 ml). The resin was equilibrated with sonication buffer (100 ml), and the cell-free extract loaded on

at a steady flow rate. A sample of the eluant was collected (Figure 6.2, lane J and K).

The column was flushed with sonication buffer until the eluant gave an absorbance of 0.01 at 280 nm. The column was then washed with wash buffer (100 ml).

The bound protein was eluted with elution buffer (100 ml). The eluant was fractionated over 24 fraction tubes each containing anti-denaturation buffer (3 ml). The tubes were mixed and assessed by UV-visible spectroscopy, and the fractions that contained high-spin enzyme were pooled (Figure 6.1).

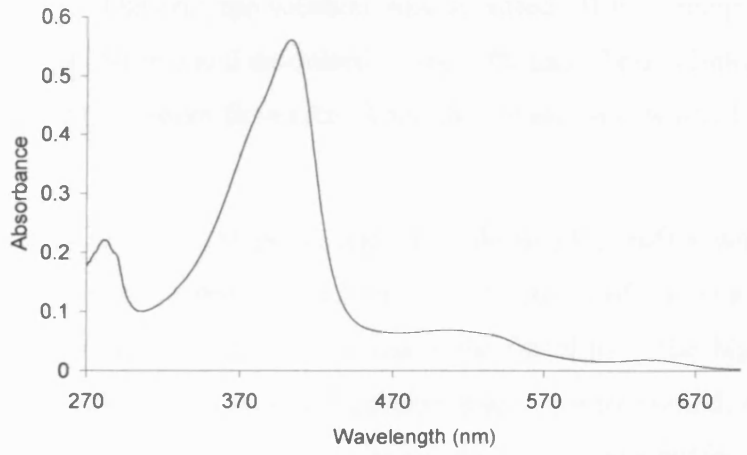

Figure 6.1: UV-visible absorption spectra of rsAPX in the ferric state when eluted from the nickel column.

The protein was concentrated using an Amicon device (Amicon, Bioseparations, Millipore) with nitrogen under pressure using an ultrafiltration regenerated cellulose membrane (MW cut off 10,000, Amicon) to a minimum volume of ~10 ml and then diluted to 50 ml with reconstitution buffer. This was concentrated to a minimum volume of ~10 ml using the same Amicon device.

6.1.4.3 Reconstitution

The protein solution was diluted to 20 ml with reconstitution buffer. Hemin solution (~10 mg/ml 0.1 M NaOH) was prepared. The concentration of the hemin solution was determined by the A_{380} of a dilution of 0.5 µl in 1.0 ml. The A_{280} of the protein was measured to assess how much hemin to add (Equation 6.1).

$$\frac{(A_{280}\ (\text{protein}) \times 6 \times 20)}{A_{380}\,(\text{hemin, } 0.5\,\mu\text{l in } 1.0\,\text{ml})} = x \qquad \ldots(6.1)$$

The x µl of hemin solution was titrated into the protein solution by six additions over 30 minutes. Hemin solution ($2x$ µl) was added before leaving the protein solution overnight at 4 °C wrapped in foil.

6.1.4.4 FFQ Column

The excess hemin was removed using a column (2.5 cm diameter and 20 cm long) packed with Q Sepharose fast flow (FFQ) resin. The enzyme and hemin solution was centrifuged (10 minutes, 9,000 rpm). FFQ resin (5 ml) was poured into a column and flushed with water (100 ml). The column was equilibrated with FFQ buffer (100 ml). The enzyme solution was decanted off the precipitate, and diluted with FFQ buffer (50 ml) and deionised water (100 ml). This solution was loaded on to the column at maximum flow rate. Then the column was washed with FFQ buffer (100 ml).

A gradient of 0 to 200 mM potassium chloride in FFQ buffer was applied to the column to elute the enzyme, collecting 5 ml fractions of the eluant. UV–visible absorption spectroscopy was used to assess the fractions. The high spin fractions (Soret peak at 402-404 nm) with an R_Z higher than 2.0 were pooled, and concentrated using an Amicon. The protein was exchanged into FFQ buffer and finally into deionised water using a centricon (Amicon, Bioseparations, Millipore). The spectrum was recorded and the protein frozen on dry ice and stored at -80 °C.

6.1.5 Polyacrylamide gel electrophoresis (SDS-PAGE)

To follow the progress of APX purification and to confirm the purity of the protein, SDS-PAGE was carried out for all proteins. Discontinuous polyacrylamide gels (15%) containing 0.1% SDS and 4% polyacrylamide stacking gel and a mini-Protean II gel system at 0.75 mm thickness were used. Samples were prepared by adding an equal volume of sample buffer and boiling for five minutes. The gels were run in SDS running buffer at 150 V until the dye front reached the end of the gel.

The gels were soaked in stain for thirty minutes, then destained by soaking in destain solution overnight. A typical SDS-PAGE gel of samples taken at various stages during the expression process is shown in Figure 6.2.

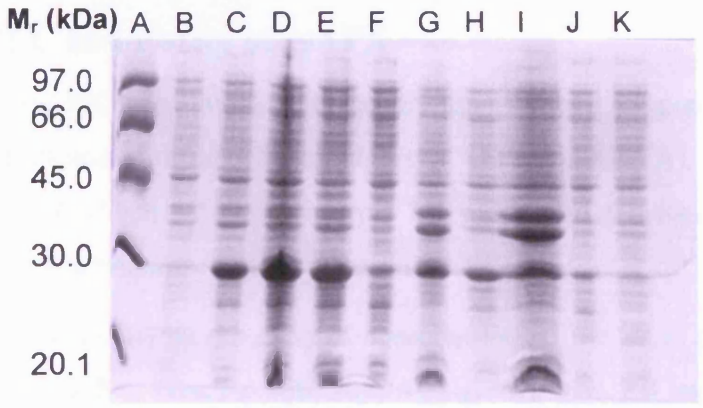

Figure 6.2: SDS-PAGE gel of samples taken during the purification of rsAPX. Lane **A** denotes the marker standards. Lanes **B** to **K** are samples taken at different stages of the purification process. The stages are: **B** = before induction; **C** = before harvesting; **D** = cell pellet with lysozyme; **E** = primary lysis (after sonication); **F** = cell free extract; **G** = cell pellet; **H** = second cell free extract; **I** = final cell pellet; **J** and **K** = the cell-free extract after the His-binding nickel column.

6.2 X-Ray Crystal Structures of rsAPX

6.2.1 FPLC and Purity of rsAPX

Samples of rsAPX were purified further by gel filtration (Superdex column 75 HR 10/30, Fast Protein Liquid Chromatography (FPLC), ÄKTA). The protein was eluted with 0.15 M sodium phosphate pH 7.0, monitored at a wavelength of 280 nm. The protein had a retention time of 45 minutes.

Purity was assessed using the ratio of absorbancies at the Soret (~407 nm) and 280 nm peaks: for rsAPX, samples with A_{407}/A_{280} greater than 2.0 were considered pure. Concentrations of enzyme were determined using the molar absorption coefficient for rsAPX (ε_{407} = 107 $mM^{-1}cm^{-1}$ (*2*)). Purity was also assessed by SDS-PAGE (Figure 6.3).

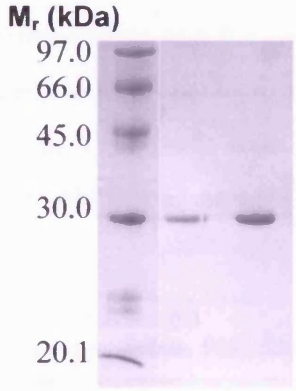

Figure 6.3: SDS-PAGE gel of rsAPX. From the left the first lane is a protein ladder and the other two lanes contain rsAPX purified by FPLC.

6.2.2 Crystallisation

All the screens for the crystallisation of rsAPX were carried out using the sitting drop method and using 24 well plates (4 x 6 Cryschem plates with 1 ml reservoirs, Hampton Research). Screening of crystallisation conditions used the sparse-matrix factorial search method (*3*) using commercially available kits (MDL screens (I) and (II) (Molecular Dimensions Ltd)). The screens were prepared in a temperature controlled room at 19 °C. The area was dusted before starting and lab coats were worn to prevent fibres contaminating the wells. The protein solution (10 mg/ml in deionised water) was kept on ice throughout. Each MDL screen solution (700 µl) was added to a separate well. Protein solution (2 µl) was added to the first eight of the small drop wells (4x2). Well solution (2 µl) was added to the drop of protein

solution, and the first eight wells sealed with clear postal tape making sure there were no air bubbles. The process was then repeated to complete the plate. This was done twice for all 100 of the solutions in the MDL kits, one set of plates kept at 4 °C and the other at 19 °C. The screens were left in temperature controlled rooms with no vibrations.

One month later small well-formed crystals (<10 μm) appeared in two wells of the MDL (I) screen at 19 °C, of which the first well contained 0.2 M ammonium acetate, 0.1 M tri-sodium citrate dihydrate pH 5.6 and 30% w/v PEG 4000, and the second contained 0.1 M sodium Hepes pH 7.5 and 1.5 M lithium sulfate.

Screens were then set up based around these initial conditions in an attempt to find the ideal crystallising conditions. Two screens were prepared with ammonium acetate, tri-sodium citrate and PEG 4000 at 19 °C (screen 6.1 and 6.2) and a screen was set up with 0 to 2.0 M lithium sulfate and 0.1 M Hepes pH 6.0 to 8.5 at 19 °C (screen 6.3). All the well solutions were prepared from the same stock solutions and all the buffer pHs were checked as 1 M stock solutions. The drops were 2 μl of protein solution and 2 μl of well solution as before. The wells contained 1 ml of reservoir solution.

Screen 6.1
All the wells contained 0.2 M ammonium acetate, PEG 4000 and 0.1 M tri-sodium citrate.

% PEG	pH of tri-sodium citrate					
	5.0	5.6	6.0	6.5	7.0	7.5
0						
20						
30						
35						

Screen 6.2
All the wells contained 30 % PEG 4000 and 0.1 M tri-sodium citrate.

Ammonium	pH of tri-sodium citrate					
acetate /M	5.0	5.6	6.0	6.5	7.0	7.5
0						
0.1						
0.2						
0.3						

Screen 6.3
All the wells contained 0.1 M Hepes.

Lithium	pH of Hepes					
sulfate /M	6.0	6.5	7.0	7.5	8.0	8.5
0						
1.0						
1.5						
2.0						

After two weeks, crystals formed in the drop of the well containing 2.0 M lithium sulfate and Hepes pH 8.5.

Further screens were set up with 1.50 to 2.25 M lithium sulfate and 0.1 M Hepes, pH 8.0 to 9.5 at a protein concentration of 10 mg/ml and 15 mg/ml at 19 °C (screen 6.4). All the well solutions were prepared from concentrated solutions. All the buffer pHs were checked as 1 M stock solutions. The drops were 2 µl of protein solution and 2 µl of well solution as before. The wells contained 1 ml of reservoir solution.

Screen 6.4
All the wells contained 0.1 M Hepes.

Lithium	pH of Hepes					
sulfate /M	8.0	8.3	8.5	8.8	9.0	9.5
1.5						
1.75						
2.0						
2.25						

Several wells contained crystals of various sizes and shapes. The crystals in 0.1 M Hepes pH 8.3 and 2.25 M lithium sulfate at 10 mg/ml were the largest ordered crystals. The crystals appeared to be highly ordered as they contained flat surfaces and sharp edges. The best crystals grew to about 150 μm long and 75 μm in cross-section. Several plates at the optimum conditions were then set up to grow crystals for soaking.

6.2.3 Crystal Soaks

Crystals were subsequently soaked to obtain the substrate or inhibitor bound forms of the protein. The soaks were done using a glass plate with small wells (~0.5 ml in size). A small drop (~20 μl) of the soaking solution was pipetted into one well and covered with a microscope slide. In another well a similar sized drop of oil (half paratone-N oil and half paraffin oil) was placed and covered with a slide. A drop containing crystals was selected and a scalpel blade used to cut through the tape. A mounting loop (Hampton Research, crystalcap copper™) on a magnetic holder was used to fish the crystal out of the drop underneath a microscope. The well was immediately covered with tape to prevent evaporation. The crystal was washed out of the loop by swirling it in a drop of soaking solution. The drop was then covered with a slide and left for ~5 minutes.

The mounting loop was then used to fish out the crystal and dip it in the oil drop. Some crystals were put directly in the oil drop from the screen wells to obtain the rsAPX structure. The crystal was carefully dabbed onto the plastic top to one of the screen plates until there was no liquid visible around the crystal under the microscope.

A plastic case for the mounting loop was held in callipers under liquid nitrogen with one hand until it filled with liquid nitrogen. In the other hand the mounting loop was plunged (very quickly to prevent ice crystals forming) into the liquid nitrogen using the magnetic holder. When both had cooled down (the liquid nitrogen having stopped boiling around them) the mounting loop was screwed into the case while still holding them under liquid nitrogen. A second person then quickly took a rack for the cases and the case was quickly removed from the nitrogen, clicked into the rack and the rack plunged back into the flask of liquid nitrogen. The rack was filled from the bottom and when it was full the plastic tube was placed over the top.

When the crystal soaks were completed the racks were placed in dewars full of liquid nitrogen to be taken to the synchrotron.

The cyanide soaking solution was obtained by dissolving a few crystals of potassium cyanide in 10 ml mother liquor (0.1 M Hepes pH 8.3 and 2.25 M lithium sulfate). The nitric oxide soaking solution was a strong sodium dithionite solution in the mother liquor. Potassium nitrite was added when the crystal was added, which reacts with excess dithionite to produce nitric oxide (*4*). The hydrogen peroxide solution was ~0.1 M, prepared in mother liquor.

6.2.4 The Binding of Cyanide (in mother liquor)

The UV-visible absorption spectrum of a solution of enzyme (0.05 μM enzyme in 0.1 M lithium sulfate and 0.1 M Hepes pH 8.3) was taken in a 1 ml cuvette at 27 °C. A crystal of potassium cyanide was added and a second spectrum taken immediately.

6.2.5 Data Collection and Interpretation

Dr. D. Leys collected the diffraction data for all the X-ray crystal structures in this thesis and Dr. P. C. E. Moody assisted in the interpretation of all the data.

6.3 rsAPX/Ascorbate Complex

6.3.1 Crystal soak

The ascorbate solution was obtained by dissolving 1 M sodium L-ascorbate (Sigma, >99.0%) in the mother liquor. The pH was readjusted to 8.3 with 1 M sodium hydroxide before soaking the crystals. The soaks were carried out as stated above (section 6.2.3).

6.3.2 Confirmation of Ascorbate Binding

A solution of enzyme and ascorbate (0.05 μM enzyme and 0.4 mM ascorbate in 1.0 M lithium sulfate and 0.1 M Hepes pH 8.3) was taken at 19 °C and hydrogen peroxide added to make a final concentration of 0.1 mM. The rate of decrease in absorbance was measured at 290 nm (absorbance due to ascorbate) using Kinlab software on a UV-visible spectrometer.

6.4 rsAPX/SHA Complex

6.4.1 Crystal Soak

All soaks were carried out as previously described (section 6.2.3). A solution of guaiacol (100 ml) was prepared in mother liquor (0.1 M Hepes pH 8.3 and 2.25 M lithium sulfate) with 10% ethanol for the guaiacol soak. This solution caused the crystal to crack; because of this ethanol was replaced with methanol (3%) in a 20 mM guaiacol solution. This time the crystals did not crack and were therefore frozen as previously described (section 6.2.3). Saturated solutions of salicylic acid, *p*-cresol, pyrogallol, DAB and ABTS were made in mother liquor and used as crystal soaks, the crystals then being frozen as previously described.

Crystals of the rsAPX/SHA complex were obtained by soaking the rsAPX crystals in a mother liquor solution containing 100 mM SHA (Aldrich, 99.0%) for ~1 minute. The SHA was dissolved by adding 1 M sodium hydroxide to the mother liquor to adjust the pH to ~10. The pH was then returned to ~8.3 by adding 1 M hydrochloric acid. The soaking was carried out as described above (section 6.2.3).

6.4.2 Co-Crystallisation

Screens were set up as in section 6.2.2 but instead of using mother liquor, solutions of saturated ABTS, salicylic acid, *p*-cresol, pryogallol and DAB in mother liquor were used in the wells.

6.4.3 Steady State Kinetics

Steady state kinetic assays were performed in 0.1 M sodium phosphate buffer at pH 7.0 using established protocols (*2*), and the concentrations of stock solutions were measured by UV-visible spectroscopy. Guaiacol (10 mM in 30% ethanol) and hydrogen peroxide (10 mM, $\varepsilon_{240\ nm}$ = 39.4 $M^{-1}cm^{-1}$) stock solutions were used. The enzyme stock solution was 5 μM. For each assay the concentration of enzyme varied but approximately 10 μl of stock solution was added. The guaiacol concentration was varied. The final volume was 1 ml of buffer using a 1 ml quartz cuvette. The hydrogen peroxide stock solution (10 μl) was added last and the temperature was maintained using a water bath at 27 °C. The formation of tetraguaiacol was measured at a wavelength of 470 nm ($\varepsilon_{470\ nm}$ = 26.6 $mM^{-1}cm^{-1}$ (*5*)) using the Kinlab program. Data were fitted to the Michaelis-Menten equation (*2*).

6.4.4 Equilibrium Dissociation Constants

Determination of equilibrium dissociation constants (K_d), for the binding of SHA to rsAPX was determined using electronic spectroscopy according to previously published procedures (*6*) by addition of known amounts of SHA to rsAPX ([rsAPX] ≈ 5 μM) (Equation 6.2).

$$\text{rsAPX /SHA} \underset{K_a}{\overset{K_d}{\rightleftharpoons}} \text{rsAPX} + \text{SHA} \qquad \text{...(6.2)}$$

Additions of SHA were determined gravimetrically. SHA was added in small amounts (1-10 μl) to minimise dilution from stock solutions (100, 10 and 1 mM). The rsAPX concentration was measured using the molar absorptivity. The increase in intensity of the Soret peak at 408 nm was measured. Binding constants were determined from plots of fractional saturation against free ligand concentration according to published procedures with at least 10 points (*6*) (Equation 6.3).

$$\bar{Y} = \frac{[\text{ligand}]_{\text{free}}}{(K_d + [\text{ligand}]_{\text{free}})} \qquad \text{...(6.3)}$$

$\bar{Y}$ is the fractional saturation, the difference in absorbance divided by the total difference in absorbance over all the points (Equation 6.4).

$$\bar{Y} = \frac{(A_i - A_t)}{(A_i - A_f)} = \frac{[\text{protein/ ligand}]}{[\text{protein}]} \qquad \text{...(6.4)}$$

In this equation, A_i is the initial absorbance, A_t is the absorbance at each point, A_f is the final absorbance, [protein] is the protein concentration, and [protein/ ligand] is the complex concentration. $[\text{ligand}]_{\text{free}}$ is the free ligand concentration and $[\text{ligand}]_{\text{tot}}$ is the total ligand concentration (Equation 6.5).

$$[\text{ligand}]_{\text{free}} = [\text{ligand}]_{\text{tot}} - [\text{protein/ ligand}] \qquad \text{...(6.5)}$$

All the titrations were carried out using potassium phosphate buffer (100 mM, 25 °C and of the pH stated for the experiment) and the SHA stock solutions were also made in potassium phosphate buffer (100 mM at 25 °C and of the pH stated for the experiment).

On the basis of pH-dependent binding data, which show an increase in K_d with pH that corresponds with the pK_a of the SHA, it has been reported that only the neutral form of SHA binds to peroxidases (*7-9*). Binding of SHA to rsAPX was also found

to be pH-dependent and we have therefore corrected binding data for ionisation (pK_a = 7.4 (*10*)) of the hydroxamic acid group of SHA, using the Henderson-Hasselbach equation (Equation 6.6) (*7, 8*). Reported values for K_d are an average of at least two independent measurements.

$$pH = pK_a + \log\frac{[base]}{[acid]} \qquad \textbf{...(6.6)}$$

6.5 Directed Evolution

6.5.1 DNA Preparation

The rsAPX DNA was extracted from cells using a QIAprep® Spin Miniprep kit (Qiagen, cat. no. 27104) from 10 ml overnight cultures using a microcentrifuge. The protocol from the kit (handbook p22) was followed, except the eluting step was performed with sterile water (not EB buffer). The cells were pelleted in a microcentrifuge tube, 1 ml of media at a time, at 13,000 rpm for 2 minutes discarding the supernatant each time. The pellet was then resuspended in buffer p1 (250 µl, with RNase added). Buffer p2 (250 µl) was added and the tube gently inverted 4-6 times, after which buffer N3 (350 µl) was added and the tube inverted 4-6 times. The tube was centrifuged (13,000 rpm) for 10 minutes. The supernatant was added to a QIAprep spin column and centrifuged for 60 seconds at 13,000 rpm discarding the flow through. The column was washed with buffer PB (0.5 ml) and centrifuged at 13,000 rpm for 60 seconds discarding the flow through. The column was then washed with buffer PE (0.75 ml) and centrifuged for 60 seconds at 13,000 rpm discarding the flow through. The column was centrifuged for 60 seconds at 13,000 rpm to remove residual ethanol. The column was placed in a clean 1.5 ml microcentrifuge tube with sterile water (50 µl) on the column and left for 4 minutes before centrifuging at 13,000 rpm for 60 seconds. The DNA sample obtained was stored at -20 °C.

6.5.2 Sequencing of DNA

The Protein and Nucleic Acid Chemistry Laboratory (PNCL) at the University of Leicester carried out all DNA sequencing. It was performed by automated fluorescent sequencing on an Applied Biosystems 373-Stretch machine and the data analysed using the program SeqED (Applied Biosystems).

6.5.3 Guaiacol Screen

The membranes containing the library (see section 6.5.4) were removed from the freezer ~1 hour before the screen was carried out. A 2% agar solution in water was melted and placed in a water bath at 50 °C in aliquots of 10 ml for every membrane to be screened. Aliquots of potassium phosphate (10 ml, pH 7.0, 0.1 M) containing 250 µM guaiacol (250 µl added from a stock solution in ethanol, 10 mM) and 125

μM hydrogen peroxide (10 μl of a 30% solution added to 1 ml of the phosphate buffer and the concentration assessed by UV-visible spectroscopy) were then heated to 50 °C in the water bath. The membranes were placed in the fumehood and the solutions of agar and guaiacol mixed quickly and poured over the membrane. The membranes were monitored for ~6 hours to note any colour change.

Red colonies were removed using a pipette and placed in 10 ml LB media with ampicillin (100 μg/ml) and kanamycin (30 μg/ml) and left shaking (between 225 and 250 rpm) overnight at 37 °C. A glycerol stock was made from the LB media left overnight by adding glycerol (70 μl) to the LB media (930 μl), snap freezing the solution on dry ice and storing at -80 °C. The DNA was extracted from the remaining LB media (section 6.5.1). This was then sequenced (pQE30 standard primers used, Qiagen) by PNACL (section 6.5.2).

If none of the colonies turned red the DNA library created at the end of section 6.5.3 was retransformed into XL1-red cells and the process repeated.

6.5.4 Transformation of the rsAPX Vector into Top 10 Cells

The rsAPX plasmid DNA was extracted from SG cells (section 6.5.1) (~50 ng) and added to Top 10 competent cells (Invitrogen) (100 μl) in a sterile 1.5 ml microcentrifuge tube on ice. The mixture was kept on ice for 20 minutes and then placed in a water bath at 42 °C for 90 seconds. Psi broth (500 μl) was added and the cells incubated at 37 °C with shaking (225-250 rpm) for 1 hour. Aliquots of the cells (100 μl) were then spread on LB-agar plates containing ampicillin (100 μg/ ml) and incubated at 37 °C overnight.

6.5.5 Random Library Generation using XL1-Red Competent Cells

SOC media was heated to 37-42 °C while the XL1-red competent cells (Stratagene, cat. no. #200129) were thawed on ice. The XL1-red cells were mixed very gently and 100 μl added (pipeting slowly and gently) to a pre-chilled 14 ml BD Falcon polypropylene round bottom tube (Fisher). β-mercaptoethanol (1.7 μl, 1.42 M) was added and mixed gently. The cells were left on ice for 10 minutes, gently swirling every 2 minutes.

The rsAPX plasmid DNA (~50 ng) (from Top 10 cells (Invitrogen) to avoid contamination with the 4REP plasmid) was added and swirled gently. The DNA concentration was calculated using Equation 6.7.

$$A_{260} \times 50 = \text{DNA concentration (ng/ µl)} \quad \text{...(6.7)}$$

The tube was left on ice for 30 minutes. A water bath was heated to 42 °C and the tube submerged for 45 seconds before putting back on ice (~2 minutes). SOC media (0.9 ml, pre-warmed to 42 °C) was added and the tube incubated at 37 °C with shaking at 225-250 rpm for 1 hour.

This solution (900 µl) was added to LB media (9 ml, containing 100 µg/ml ampicillin) and incubated at 37 °C with shaking (225-250 rpm) until late log phase (A_{600} > 1.5), ~48 hours. Fresh ampicillin (100 µg/ml) was added every 24 hours. The remaining solution from the transformation (100 µl) was spread on an LB plate containing ampicillin (100 µg/ml). The plate was left at 37 °C for 48 hours, sufficient time for colonies to become visible after a successful transformation.

The LB media solution from above (100 µl) was added to LB media (10 ml, containing 100 µg/ml ampicillin) and incubated at 37 °C with shaking (225-250 rpm) till late log phase (A_{600} > 1.5), ~48 hours. Fresh ampicillin (100 µg/ml) was added every 24 hours. The DNA was extracted from the cells (section 6.5.1) to create the DNA library.

This DNA library was used to retransform back into the XL1-red cells and the process repeated four times before screening.

6.5.6 Transformation of a DNA Library to a Protein Library

The DNA library was transformed into SG1300 cells (protocol based on p40 of The QIAexpressionist, available at www.Qiagen.com). DNA (~50 ng/µl) was chilled in a Falcon tube (as in previous transformation) on ice. An aliquot of the cells (100 µl) was thawed on ice and gently resuspended and added to the falcon tube. The tube was swirled gently and left on ice for 20 minutes.

The tube was placed in a water bath (42 °C) for 90 seconds and then on ice. Psi broth (500 µl) was added and incubated at 37 °C with shaking (225-250 rpm) for 60-90 minutes.

Nitrocellulose membranes (Hybond – C Extra from Amersham Biosciences, cat. no. RPN82E) were placed on 6 LB plates containing ampicillin (100 μg/ml) and kanamycin (30 μg/ml). Tweezers were used to remove any bubbles between the plate and membrane. Transformation solution (100 μl) was spread on each of the membranes and left at 37 °C overnight.

The membrane was transferred carefully with tweezers on to an LB plate (containing ampicillin (100 μg/ml) and kanamycin (30 μg/ml)) that had been spread with IPTG (20 μl of 1 M) and the plate was kept at 27 °C for ~4 hours. The membrane was placed in an empty petri dish using tweezers (taking care not to touch any of the colonies) with the colonies facing upwards. This was placed in the freezer (-20 °C or -80 °C) overnight.

6.5.7 Random Mutagenesis by PCR

6.5.7.1 Primer Design

pQE30 forward sequencing primer was used along with the complementary reverse primer (sequences shown in Table 6.1). The melting temperatures (T_m) of both primers was calculated (Equation 6.8), and needed to be above 68 °C for mutagenesis to be successful.

$$T_m = 81.5 + 0.41(\%GC) - \frac{675}{N} - \%\text{mismatch} \qquad \text{...(6.8)}$$

N is the primer length in bases, %GC is the percentage of GC content in the primer and %mismatch is the percentage of mismatching bases in the primer. All these numbers are rounded to whole numbers for the formula. The primers were prepared and desalted by PNACL. These primers were used to prepare the PCR random mutagenesis libraries for this thesis.

Table 6.1
The forward and reverse oligonucleotides used to prepare the PCR random mutagenesis libraries.

Primer	Sequence
Forward	5' CCC GAA AAG TGC CAC CTG 3'
Reverse	3' GGG CTT TTC CAG GTG GAC 5'

6.5.7.2 Mutagenesis

The random mutagenesis libraries were created using the GeneMorph® random mutagenesis kit (Stratagene) with the appropriate pair of primers. Reactions were prepared in thin walled PCR tubes. Each reaction was set up (Table 6.2) as in the protocol for media level mutation (3-7 per gene). All the chemicals were added in the order listed in Table 6.2 – with the exception of mutazyme, which was added later – to a PCR thin walled tube and kept on ice. Mutazyme is a DNA polymerase and was supplied with the kit along with 10x buffer (10x reaction buffer) and the dNTP mix. The template was pQE30 vector containing the rsAPX gene (12.5 ng/μl). The reaction contained 125 μg of each primer.

Table 6.2
Reaction volumes used in random mutagenesis PCR (μl).

Water	39
10x buffer	5
dNTP	1
Template	3.3
Primer F	0.4
Primer R	0.3
Mutazyme	1

The tubes were then centrifuged (13,000 rpm, ~10 seconds) and the PCR (polymerase chain reaction) block (Perkin Elmer, 480 DNA Thermocycler) turned on with the programs set as in Table 6.3. In the 30 cycles, the time at 72 °C (300 seconds) was calculated from the size of the template (60 seconds for every kbp) and the annealing temperature (63 °C) was calculated using Equation 6.9.

$$\text{Primer } T_m - 5 = \text{Primer annealing temperature} \qquad \textbf{...(6.9)}$$

When the block reached 94 °C, the mutazyme was added, a drop of nujol oil added to the surface of the reaction and the tube put in the cycler. When the reaction was complete agarose gel electrophoresis was run on 10 μl of the reaction. To the remainder, *Dpn* I (1.0 μl, standard solution in the kit) was added and then incubated at 37 °C for 1 hour. The reaction was then frozen. The agarose gel showed only one band equivalent to the primers.

Table 6.3
Temperature cycler program for random mutagenesis.

Number of Cycles	Temperature (°C)	Time (S)
1	94	30
30	94	30
	63	30
	72	300
1	72	600
	4	30

6.5.8 Saturated Point Mutagenesis

6.5.8.1 Primer Design

Complementary oligonucleotides (32-34 bases in length) were designed to have ~15 bases either side of the residue to be mutated and end in G or C. The melting temperatures (T_m) of both primers was calculated (Equation 6.8), and needed to be above 68 °C for mutagenesis to be successful. The mfold program (IDT SciTools, http://biotools.idtdna.com/mfold (*11*)) was used to predict any secondary structures. Primers were designed for saturated point mutagenesis at serine 69 and aspartic acid 133 in rsAPX (Table 6.4).

Table 6.4
Primer data for saturated point mutagenesis of rsAPX.

Primer	Serine 69	Aspartic acid 133
T_m	72 °C	76 °C
%GC	50	56
Number of folds	1	1
T_m of folds	35.7 °C	48.0 °C
%mismatch	9	9

The primers were prepared and desalted by PNACL. The sequences are shown in Table 6.5, where N is a mixture of all four bases and S is a G or C. These primers were used to prepare the saturated point mutagenesis libraries for this thesis.

Table 6.5
The forward and reverse oligonucleotides used to prepare the saturated point mutagenesis libraries.

Primer	Sequence
69: Forward	5' CGA ACT GGC TCA CNN SGC TAA CAA CGG TCT TG 3'
69: Reverse	3' GCT TGA CCG AGT GNN SCG ATT GTT GCC AGA AC 5'
133: Forward	5' GAG GGT CGC TTG CCC NNS GCC ACT AAG GGT TCT G 3'
133: Reverse	3' CTC CCA GCG AAC GGG NNS CGG TGA TTC CCA AGA C 5'

6.5.8.2 Mutagenesis

The saturated point mutagenesis libraries were created using the Quikchange™ mutagenesis kit (Stratagene) with the appropriate pair of primers. Reactions were prepared in thin walled PCR tubes. Four reactions were set up for each set of primers (Table 6.6) as in the protocol, but half the amounts were used. All the chemicals were added – with the exception of *pfuTurbo* which was added later – in the order listed in Table 6.6 to PCR thin walled tubes and kept on ice. *pfuTurbo* is a DNA polymerase and was supplied with the kit along with 10x buffer (10x reaction buffer). $MgCl_2$ (100 mM) was filter sterilized. The template used was pQE30 vector containing the rsAPX gene (12.5 ng/µl). The absorbancies (A_{260}) of the primers were S69XF (8.3), S69XR (7.7), D133XF (5.7) and D133XR (6.0).

Table 6.6
Reaction volumes used in saturated point mutagenesis PCR (µl).

	Ser69X				**Asp133X**			
	1	**2**	**3**	**4**	**1**	**2**	**3**	**4**
Water	13.7	12.7	11.7	10.7	13.3	12.3	11.3	10.3
Glycerol	2.5	2.5	2.5	2.5	2.5	2.5	2.5	2.5
10x buffer	2.5	2.5	2.5	2.5	2.5	2.5	2.5	2.5
$MgCl_2$	0	1	2	3	0	1	2	3
Template	4	4	4	4	4	4	4	4
Primer F	0.6	0.6	0.6	0.6	0.9	0.9	0.9	0.9
Primer R	0.7	0.7	0.7	0.7	0.8	0.8	0.8	0.8
pfuTurbo	0.5	0.5	0.5	0.5	0.5	0.5	0.5	0.5

The tubes were centrifuged (13,000 rpm, ~10 seconds) and the PCR (polymerase chain reaction) block (Perkin Elmer, 480 DNA Thermocycler) turned on with the programs set as in Table 6.7. In the 16 cycles, the time at 68 °C (300 seconds) was calculated from the size of the template (60 seconds for every kbp) and the annealing temperature (67 or 71 °C) was calculated using equation 6.9.

When the block reached 94 °C the *pfuTurbo* was added, a drop of nujol oil added to the surface of each reaction and the tubes put in the cycler. When the reaction was complete, an agarose gel was run on 10 µl of each reaction. To the remainder, *Dpn*I (1.0 µl, standard solution in the kit) was added and incubated at 37 °C for 1 hour. The reactions were then frozen. The agarose gel showed only one band equivalent to the primers for all the reactions.

Table 6.7
Temperature cycler program. Where two temperatures are shown the one in brackets is for the D133X reactions and the other temperature is for the S69X reactions.

Number of Cycles	Temperature (°C)	Time (S)
1	94	30
16	94	30
	67 (71)	60
	68	300
1	68	600
	4	30

6.5.9 Agarose Gel Electrophoresis

Agarose (2.0 g) was dissolved in TAE buffer (198 ml) in the microwave and ethidium bromide solution (20 µl of 10 mg/ml, stored at 4 °C) added. This gel was set on a horizontal bed with a well comb and covered in TAE buffer. The comb was removed and samples (10 µl DNA and 2 µl loading buffer (Fermentas)) loaded into the wells. A well was also loaded with 6 µl of a 1 kb DNA ladder (Fermentas, generuler™). The gel was run for an hour applying a 100 mA current, and DNA was visualised by placing under a UV light.

6.6 References

1. Dalton, D. A., del Castillo, L. D., Kahn, M. L., Joyner, S. L., and Chatfield, J. M. (1996) *Archives of Biochemistry and Biophysics 328*, 1-8.
2. Lad, L., Mewies, M., and Raven, E. L. (2002) *Biochemistry 41*, 13774-13781.
3. Jancarik, J., and Kim, S.-H. (1991) *Journal of Applied Crystollography 24*, 409-411.
4. Leys, D., Backers, K., Meyer, T. E., Hagen, W. R., Cusanovich, M. A., and Beeumen, J. J. V. (2000) *Journal of Biological Chemistry 275*, 16050-16056.
5. Santimone, M. (1975) *Canandian Journal of Biochemistry 53*, 649-657.
6. Bogumil, R., Hunter, C. L., Maurus, R., Tang, H.-L., Lee, H., Lloyd, E., Brayer, G. D., Smith, M., and Mauk, A. G. (1994) *Biochemistry 33*, 7600-7608.
7. Aitken, S. M., L.Turnbull, J., Percival, M. D., and English, A. M. (2001) *Biochemistry 40*, 13980-13989.
8. Indiani, C., Santoni, E., Becucci, M., Boffi, A., Fukuyama, K., and Smulevich, G. (2003) *Biochemistry 42*, 14066-14074.
9. Schonbaum, G. R. (1973) *Journal of Biological Chemistry 248*, 502-511.
10. O'Brien, E. C. O., Farkas, E., Gil, M. J., Fitzgerald, D., Castineras, A., and Nolan, K. B. (2000) *Journal of Inorganic Biochemistry* 79, 47-51.
11. Zucker, D. M. (2002), IDT, St. Louis.

SPECIAL NOTE

ITEM SCANNED AS SUPPLIED
PAGINATION IS AS SEEN

Appendix

Antidenaturation Buffer

50 mM potassium phosphate buffer pH 7.0

Destain (SDS-PAGE)

7.5% acetic acid

5% methanol

Elution Buffer

50 mM sodium phosphate buffer pH 4.2

0.3 M sodium chloride

10% glycerol

FFQ Buffer

10 mM potassium phosphate buffer pH 7.0

LB Media (Fisher or Sigma)

10 g NaCl

10 g tryptone

5 g yeast extract

Adjust to pH 7.0 with 5 N NaOH

Make up to 1.0 l with deionised water

Autoclave

Mother Liquor (rsAPX Crystallisation)

2.25 M lithium sulphate

0.1 M Hepes pH 8.3

Psi Broth

LB media autoclaved

Per 100 ml:

Add 1 ml of filter sterilised 1 M KCl

Add 0.4 ml of filter sterilised 1 M $MgSO_4$

Reconstitution Buffer

0.1 M potassium phosphate buffer pH 6.5

Sample Buffer (SDS-PAGE)

125 mM Tris-HCl, pH 6.8

4% SDS

20% w/v glycerol

0.002% bromophenol blue

SDS Running Buffer (SDS-PAGE)

25 mM Tris-HCl

192 mM glycerine

0.1% w/v SDS

SOC Media

2 g tryptone

0.5 g yeast extract

0.05 g NaCl

0.4 g glucose

Make up to 100 ml with deionised water

Autoclave

Add 1 ml of filter sterilised 1 M $MgCl_2$

Add 1 ml of filter sterilised 1 M $MgSO_4$

Sonication Buffer

50 mM sodium phosphate buffer pH 8.0

0.3 M sodium chloride

Stain (SDS-PAGE)

30% v/v methanol

12% w/v trichloroacetic acid

0.01% w/v Coomassie Blue R

10% w/v sulphosalicyclic acid

50x TAE Buffer (Agarose gel electrophoresis)

242 g Tris base

37.1 g glacial acetic acid

100 ml of 0.5 M EDTA

900 ml deionised water

Wash Buffer

50 mM sodium phosphate buffer pH 6.0

0.3 M sodium chloride

10% glycerol

Publications

SPECIAL NOTE

ITEM SCANNED AS SUPPLIED
PAGINATION IS AS SEEN

Crystal structure of the ascorbate peroxidase–ascorbate complex

Katherine H. Sharp[1], Martin Mewies[1], Peter C.E. Moody[2] and Emma Lloyd Raven[1]

Published online 17 March 2003; doi:10.1038/nsb913

Heme peroxidases catalyze the H_2O_2-dependent oxidation of a variety of substrates, most of which are organic. Mechanistically, these enzymes are well characterized: they share a common catalytic cycle that involves formation of a two-electron, oxidized Compound I intermediate followed by two single-electron reduction steps by substrate. The substrate specificity is more diverse — most peroxidases oxidize small organic substrates, but there are prominent exceptions — and there is a notable absence of structural information for a representative peroxidase–substrate complex. Thus, the features that control substrate specificity remain undefined. We present the structure of the complex of ascorbate peroxidase–ascorbate. The structure defines the ascorbate-binding interaction for the first time and provides new rationalization of the unusual functional features of the related cytochrome c peroxidase enzyme, which has been a benchmark for peroxidase catalysis for more than 20 years. A new mechanism for electron transfer is proposed that challenges existing views of substrate oxidation in other peroxidases.

Cytochrome *c* peroxidase (*Cc*P), a class I heme peroxidase[1], was the first of all of the peroxidases[2,3] to have its structure solved[4]. As such, *Cc*P became the paradigm for all other peroxidases. However, *Cc*P has two anomalous features that are not reproduced in any other peroxidase. First, it uses an atypical Compound I intermediate that contains a protein-based (Trp191), rather than the usual porphyrin-based, radical. Second, it uses an atypical protein substrate rather than a small organic molecule. Recently, work on another class I enzyme, ascorbate peroxidase (APX)[5,6], has provided a new opportunity to reassess the anomalous *Cc*P enzyme. APX, which catalyzes the H_2O_2-dependent oxidation of L-ascorbate ($2\text{ascorbate} + H_2O_2 \rightarrow 2\text{monodehydroascorbate} + 2H_2O$), has high (37%) sequence identity with *Cc*P but uses a more representative organic substrate (L-ascorbate). APX was expected to duplicate some of the properties of *Cc*P and revalidate *Cc*P as the model for other peroxidases. However, although Trp179 in APX corresponds to Trp191 in *Cc*P, a porphyrin π-cation radical is used instead during APX catalysis[7]. There has been no convincing rationalization for this observation. Furthermore, because of the absence of structural information for the APX–ascorbate complex, it has not been possible to fully account for the different substrate-binding properties of the *Cc*P and APX enzymes. Here we present answers to these questions based on the crystal structures of recombinant soybean cytosolic APX (rsAPX) and its complex with L-ascorbate.

Overall structure

The structures of rsAPX and the rsAPX–ascorbate complex have been determined (Table 1). These structures allow a detailed examination of ascorbate binding and a comparison with the structure of the recombinant pea cytosolic enzyme (rpAPX)[8] (rsAPX has 91% sequence identity with rpAPX). rsAPX is similar in its overall structure to rpAPX. Although rsAPX is a homodimer in solution[9,10], only one monomer is found in the crystallographic asymmetric unit. Examination of the contacts within the crystallographic dimer shows that the dimer interfaces observed in the rpAPX structure are conserved. The r.m.s. deviation between Cα positions for the 249 residues in the A-chain of the rpAPX homodimer and the refined rsAPX structure is 0.443 Å (*http://www.ebi.ac.uk/msd/ssm*).

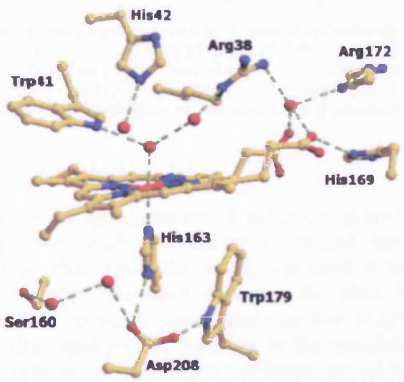

Fig. 1 The active site of rsAPX[32,33]. The key residues are labeled, and water molecules are shown as red spheres. Hydrogen bonds are indicated by green dotted lines.

The structure of the active site of rsAPX (Fig. 1) is similar to rpAPX. The heme is bound to the protein through a coordinate bond from the iron to His163 and a hydrogen bond from the 7-propionate (propionate A) to His169. The key catalytic residues involved in the formation of Compound I, His42 and Arg38, are observed as in rpAPX. There are three ordered water molecules in the distal pocket, one of which is within bonding distance (2.1 Å) of the heme iron.

A cation near Trp179 has been identified in rpAPX[8] and assigned as a potassium ion. The rsAPX structure shows an electron density peak in a similar position, although the observed geometry and temperature factors are consistent with occupa-

[1]Department of Chemistry and [2]Department of Biochemistry, University of Leicester, University Road, Leicester, LE1 7RH, England, UK.

Correspondence should be addressed to P.C.E.M. *e-mail: peter.moody@le.ac.uk*

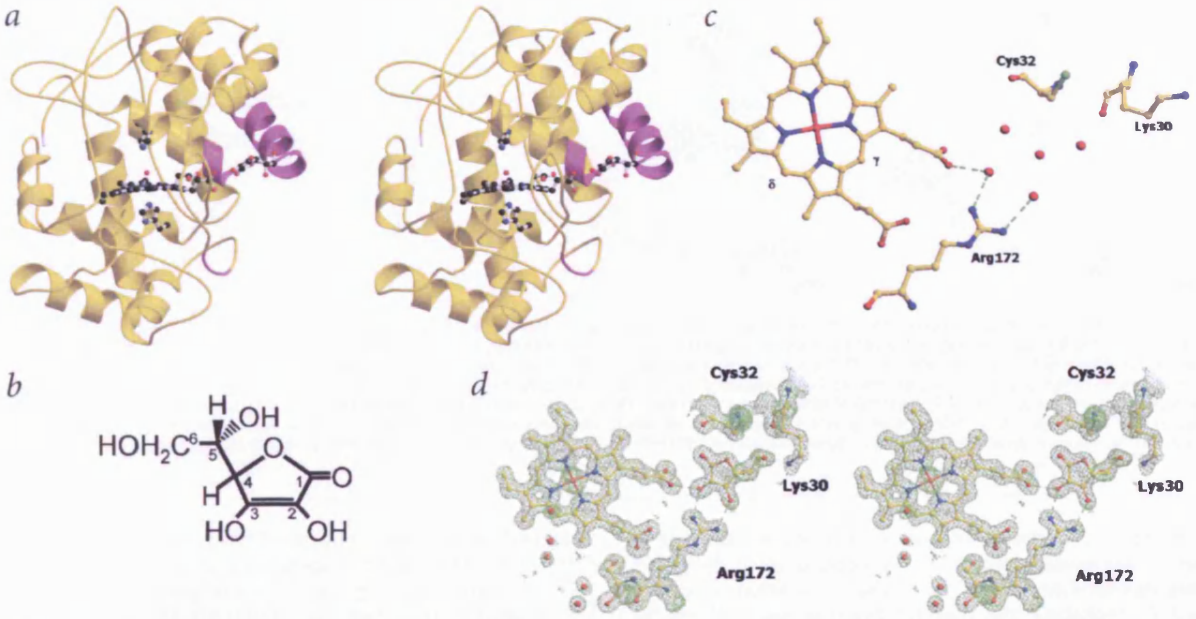

Fig. 2 The ascorbate-binding site. ***a***, Stereo representation of the overall structure of the rsAPX–ascorbate complex[34], showing the heme, the proximal and distal histidine residues, the coordinated water molecule and the bound ascorbate. The regions 20–35 and 179–181 (shown in Fig. 3) are highlighted in magenta. ***b***, The structure of L-ascorbic acid, showing the L configuration at C^5. The pK_as of the 2-OH and 3-OH groups are 11.3 and 4.0, respectively[35]. ***c***, The structure of rsAPX showing the γ-*meso* and δ-*meso* positions of the heme and bound solvent in the ascorbate-binding site. ***d***, Stereo view of the rsAPX–ascorbate complex, showing refined electron density (green) and the binding of the ascorbate. Hydrogen bonds are indicated (dotted lines)[32,33].

tion of this site by a water molecule. In contrast, the rsAPX–ascorbate structure has a peak that is characterized by short distances (2.2–2.4 Å) from the main chain oxygens of Thr164, Asn182, Ile185 and a solvent molecule that, in turn, is hydrogen bonded to Asp187. These observations are consistent with occupation of this site by a sodium ion[11], which is almost certainly introduced during soaking with (sodium) ascorbate.

Ascorbate binding

The overall structure of the enzyme (Fig. 2*a*,*b*) and the active site are unaffected by ascorbate binding (r.m.s deviation in Cα positions of 0.174 Å). Previous NMR[12] and chemical modification/mutagenesis[13,14] studies have implicated the γ-*meso* position of the heme, in particular Cys32 and Arg172 (refs. 13,14), in ascorbate binding. Examination of the electron density for rsAPX around the γ-*meso* position (Fig. 2*c*) reveals five ordered water molecules directly or indirectly hydrogen bonded to the side chains of Arg172 and the heme 6-propionate (propionate D). Difference electron density maps calculated from the data collected in the presence of substrate clearly show that ascorbate binds in place of these water molecules. The refined atomic positions (Fig. 2*d*) show hydrogen bonds between the 2-OH and 3-OH groups (Fig. 2*b*) of the substrate and the protein (Arg172), and between the 2-OH group of the substrate and the (deprotonated) heme 6-propionate. Most notably, the side chain of Lys30 swings in from solvent to provide additional hydrogen-bonding stabilization through the 6-OH of the substrate. Cys32, which has been (indirectly) implicated in substrate binding[13], plays no direct role in substrate binding (Fig. 2*d*). The region around the δ-heme edge has been implicated as the binding site for aromatic substrates[12,13], as well as for ascorbate[12,15]. In this model, the δ-heme edge contains several well-defined water molecules and some unaccounted-for electron density; however, there is no evidence for ascorbate binding at the δ-heme edge under the conditions used in this study. A difference map calculated between the data from the rsAPX–ascorbate complex and substrate-free rsAPX shows strong positive density corresponding to the ascorbate but no significant positive density around the δ-*meso* position (however, we note that if ascorbate binding occurs at this site, it is probably weak[15]).

Comparison with CcP

With the rsAPX–ascorbate interaction defined, it is possible to provide more detailed rationalization of the different substrate specificities observed in the APX and CcP enzymes. Comparison of the APX and CcP sequences reveals that the key basic residues involved in binding of the (anionic) ascorbate molecule in APX (Arg172 and Lys30) are not present in CcP (replaced by Asn184 and Asp33, respectively). Conversely, the acidic residues shown[16,17] to be involved in binding of (cationic) cytochrome *c* to CcP are not present in APX. Hence, Asp34, Glu35 and Asp37 in CcP have no equivalent residues in APX because the loop containing residues 34–41 in CcP is absent in APX (Fig. 3*a*); Glu290 in CcP is also absent in rsAPX because of a C-terminal truncation. Superposition of the rsAPX–ascorbate and CcP–cytochrome *c*[16] complexes in this loop region (Fig. 3*b*) clearly shows that the additional loop in CcP, especially the side chain of Tyr36, would prevent binding of ascorbate at the equivalent site.

Discussion and implications

Previous crystallographic information for peroxidase–substrate complexes[16,18–20] provides limited insight into the factors that

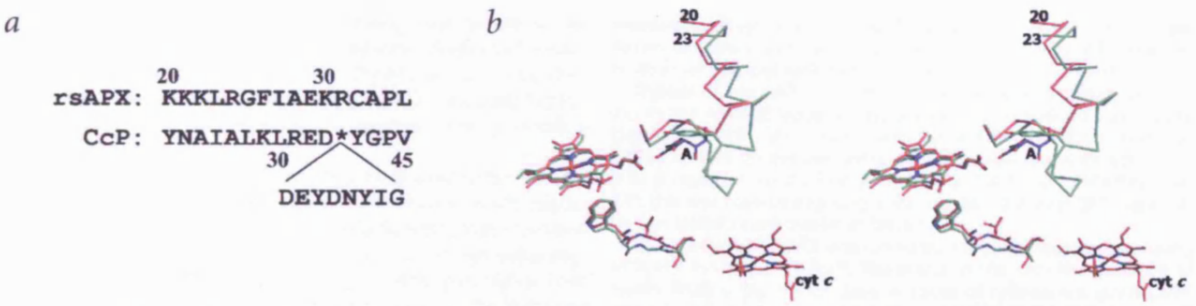

Fig. 3 Comparison of APX and CcP. ***a***, Structure-based alignment of rsAPX (residues 20–35) and yeast CcP (residues 23–45) in the region of the ascorbate-binding site. The sequence of rpAPX is identical to rsAPX in this region, except at positions 21 (Arg21 in rpAPX) and 31 (Lys31). In CcP, an eight-residue loop (indicated by an asterisk) replaces Arg31 in rsAPX. ***b***, Structural alignment of the CcP–cytochrome *c* (green) and APX–ascorbate (magenta) structures[32,33]. The rsAPX–ascorbate (residues 20–35) and CcP–cytochrome *c* (residues 23–45) structures are drawn as Cα plots, showing the additional loop in CcP (residues 34–41) that blocks the equivalent site in rsAPX. The side chain of Tyr36 in CcP is also shown close to the ascorbate site (labeled 'A'). The proposed pathway[16] for electron transfer from the heme in cytochrome *c* (cyt *c*, red) to CcP is shown below the heme (Trp191–Ala193, green) superimposed with the equivalent residues in rsAPX (Trp179–Ser181, magenta). The bound ascorbate is shown in blue and labeled A.

define substrate specificity because the substrates in these cases are either atypical or nonphysiological. The best information that was previously available on the nature of the ascorbate-binding interaction in APX came from two sources. First, NMR-derived distances[12] indicated two possible binding sites, close to the 6-propionate (γ-*meso*) and δ-*meso* positions of the heme. Second, mutagenesis/chemical modification experiments[13,14] favored ascorbate binding at the γ-heme edge, close to Cys32 and Arg172 (which is close to the γ-*meso* position implicated by NMR[12]). The structure presented in this paper is consistent with the γ-heme position as the site of ascorbate oxidation. The electrostatic role of Arg172 in substrate binding[14] is also confirmed, but this residue has no direct role in electron transfer, as was suggested[14]. Cys32 has no direct interaction with the substrate, which is consistent with the modest (~three-fold decrease) effect on ascorbate activity in the C32S variant[13]. Modification of Cys32 with thiol-specific reagents (for example, 5,5′-dithiobis(2-nitrobenzoic acid)) has a more dramatic (~1,000-fold) effect on ascorbate activity[13], but this is because the large DTNB group blocks the γ-site. The role of Lys30 in ascorbate binding was not expected: in the substrate-free structure, this residue is oriented away from the heme and into solvent, and binding of ascorbate induces a conformational change of this residue to satisfy the hydrogen bonding requirements of the substrate. The shortest distance from the substrate (oxygen of the 2-OH group) to the heme iron is 11.2 Å, in reasonable agreement with NMR data[12] that suggested that the substrate binds 9.0–11.2 Å from the iron.

With the determination of the structure of the rsAPX–ascorbate complex, the first for a truly representative peroxidase–small molecule complex, it is now possible not only to rationalize the different substrate binding specificities of the APX and CcP enzymes, but also to fully account for their different catalytic properties. Dealing first with substrate binding, we have shown that the structural architecture of the APX and CcP enzymes is subtly different. The key structural features required for substrate binding in APX are not present in CcP, and *vice versa*. These differences account for the low activity of CcP towards ascorbate[21] and of APX towards cytochrome *c*[6].

In terms of mechanistic differences, CcP uses a Trp radical (Trp191) in its Compound I derivative, and this residue is essential for cytochrome *c* oxidation[22]. The absence of an oxidizable amino acid in other peroxidases (replaced by a Phe or aliphatic residue) provided some rationalization of this observation, but this was undermined when it was conclusively established that APX, which contains the same Trp residue in almost exactly the same environment, uses a porphyrin π-cation intermediate and that Trp179 is not necessary for ascorbate oxidation[23]. It has been proposed[8] that the adjacent potassium site present in APX, but not in CcP, might destabilize radical formation at Trp179 on electrostatic grounds. This has not been demonstrated conclusively, however, and we note that our rsAPX structure was not consistent with the presence of a potassium ion. Our results provide a much more clear-cut explanation. Hence, the data presented here (Fig. 2*d*) clearly show direct coupling of the substrate to the heme group *via* the heme 6-propionate; therefore, reduction of Compound I in APX occurs through a porphyrin π-cation intermediate, completely bypassing the need for involvement of Trp179 in ascorbate oxidation[23]. This binding orientation, which clearly favors efficient reduction of Compound I by ascorbate, may also account for the slow conversion of Compound I of APX to a species containing a tryptophan radical when ascorbate is absent[24]. (A direct link between the heme and the substrate also accounts for the increased stability of the chloroplastic APX enzymes in the presence of ascorbate[25]).

Table 1 Data collection and refinement statistics

	rsAPX	rsAPX–ascorbate
Data collection		
Wavelength (Å)	0.811	0.94
Resolution (Å)[1]	57.74–1.75 (1.796–1.75)	57.74–1.40 (1.436–1.40)
Total observations	92,501	339,792
Unique reflections	26,092	49,370
$I/\sigma I$[1]	16.1 (2.4)	23.2 (2.9)
R_{merge} (%)[1]	6.7 (32.0)	8.3 (42.5)
Completeness (%)[1]	99.3 (99.3)	96.2 (96.2)
Refinement		
R_{work}	0.178	0.196
R_{free}	0.182	0.214
R.m.s. deviations from ideal		
Bonds (Å)	0.02	0.01
Angles (°)	1.6	1.5

[1]Numbers in parentheses are for the highest resolution shell.

This contrasts with the substrate binding orientation in the *Cc*P–cytochrome *c* complex[16], which indicates that cytochrome *c* binds in an orientation that involves Trp191 as part of an electron transfer pathway to the heme (Fig. 3*b*). In this case, Trp191 would be expected to be essential for catalytic activity, which is indeed observed[22].

Despite the high sequence and structural similarities of APX and *Cc*P, the *modus operandi* of these enzymes are clearly fundamentally different. *Cc*P is truly anomalous, with properties that are not duplicated even within the class I peroxidase subgroup. In this context, APX may be a better paradigm peroxidase than *Cc*P. Direct, hydrogen-bonding contact between the substrate and the heme 6-propionate was not predicted in APX and widens the debate on our existing views on electron transfer in the heme peroxidases, in which substrate binding and oxidation at the δ-heme edge has been widely assumed[26]. Because manganese peroxidase (a class II enzyme) uses the same heme 6-propionate in its (physiological) complex with Mn(II)[18], this may represent a more widespread mechanism for electron delivery in other peroxidases.

Methods

Protein purification and crystal growth. Recombinant soybean cytosolic APX (rsAPX) was prepared and purified as described[10]. Sitting drops made up of 2 μl protein solution (10 mg ml^{-1}) and 2 μl precipitant solution were allowed to equilibrate with 700 μl of precipitant (2.25 M lithium sulfate and 0.1 M HEPES, pH 8.3) to give crystals ~150 μm × 75 μm in cross-section. We have used ferric enzyme in all crystallographic experiments reported here. However, we recognize that reduction of the heme is possible during data collection[27].

Structure determination. Diffraction data for rsAPX were collected on beamline X11 at the EMBL outstation at DESY Hamburg, using a marCCD detector (marresearch) and 0.811 Å radiation. All data were collected at 100 K. Data from crystals diffracted to beyond 1.8 Å and 108° were collected using 1° oscillations. The first image was subject to the auto-indexing routines in DENZO[28] and gave a solution consistent with a primitive tetragonal cell. Examination of the distribution of intensities along the principal axes allowed the space group to be assigned as $P4_22_12$. Data were measured and reduced with DENZO and SCALEPACK[28]; statistics are shown in Table 1. In total, 5% of the data were flagged for the calculation of R_{free} and excluded from subsequent refinement.

Crystals of the rsAPX–ascorbate complex were obtained by soaking in the mother liquor incorporating 1.0 M sodium L-ascorbate (Sigma, >99.0%). Data were collected in two passes on beamline ID14-4 at ESRF (Grenoble) using an ADSC Quantum 4 detector and 0.94 Å radiation. In the first pass, data to 1.4 Å were collected over 54°; this was followed by data collected to 1.8 Å over 90°. Data collection statistics are shown in Table 1.

The structure of rsAPX was solved by molecular replacement using MOLREP in the CCP4 suite[29]. The search model was the structure of rpAPX (PDB entry 1APX)[8]. Several cycles of refinement using CNS[30] and rebuilding gave a model with a crystallographic *R*-factor for all data of 18.4% and an R_{free} of 21.7%. Refinement was completed with REFMAC5 (ref. 31). This refined structure was used as a starting point for interpretation of data for the rsAPX–ascorbate complex. The model was stripped of solvent molecules and subjected to rigid-body refinement using 3.0 Å data. The structure was then broken into 24 segments, corresponding to elements of secondary structure, and each segment was refined as a rigid body. The model was then further refined using all data; CNS was used in these steps. The density for ascorbate was unambiguous; the structure was incorporated into subsequent refinement. The refinement was concluded using REFMAC5 with anisotropic atomic temperature factors[31]. XtalView[32] was used throughout for manual adjustment and rebuilding. Figures were prepared using XtalView, Raster3D[33] or MolScript[34].

Coordinates. Coordinates and structure factors have been deposited in the Protein Data Bank (accession codes 1OAG (rsAPX) and 1OAF (rsAPX–ascorbate complex)).

Acknowledgments

We are grateful to D. Dalton for providing the expression vector for rsAPX. We thank K. Singh for technical assistance, D. Leys for data collection and C. Metcalfe for helpful discussions. We are grateful to the EMBL outstation at DESY Hamburg and ESRF Grenoble for the provision of synchrotron radiation. This work was supported by grants from the BBSRC, the Wellcome Trust, the EPSRC and the Royal Society.

Competing interests statement

The authors declare that they have no competing financial interests.

Received 6 November, 2002; 21 February, 2003.

1. Welinder, K.G. Superfamily of plant, fungal and bacterial peroxidases. *Curr. Opin. Struct. Biol.* **2**, 388–393 (1992).
2. Everse, J., Everse, K.E., & Grisham, M.B. *Peroxidases in Chemistry and Biology* Vol. I and II (CRC Press, Boca Raton; 1991).
3. Dunford, H.B. *Heme Peroxidases* (John Wiley, Chichester; 1999).
4. Poulos, T.L. *et al.* The crystal structure of cytochrome c peroxidase. *J. Biol. Chem.* **255**, 575–580 (1980).
5. Raven, E.L. Peroxidase-catalysed oxidation of ascorbate: structural, spectroscopic and mechanistic correlations in ascorbate peroxidase. in *Subcellular Biochemistry: Enzyme Catalysed Electron and Radical Transfer* (eds. Holzenberg, A. & Scrutton, N.S.) 318–350 (Kluwer Academic/Plenum, New York; 2000).
6. Dalton, D.A. Ascorbate peroxidase. in *Peroxidases in Chemistry and Biology* (eds. Everse, J., Everse, K.E. & Grisham, M.B.) 139–154 (CRC Press, Boca Raton, 1991).
7. Patterson, W.R., Poulos, T.L. & Goodin, D.B. Identification of a porphyrin π-cation radical in ascorbate peroxidase Compound I. *Biochemistry* **34**, 4342–4345 (1995).
8. Patterson, W.R. & Poulos, T.L. Crystal structure of recombinant pea cytosolic ascorbate peroxidase. *Biochemistry* **34**, 4331–4341 (1995).
9. Dalton, D.A., Hanus, F.J., Russell, S.A. & Evans, H.J. Purification, properties and distribution of ascorbate peroxidase in legume root nodules. *Plant Physiol.* **83**, 789–794 (1987).
10. Jones, D.K., Dalton, D.A., Rosell, F.I. & Lloyd Raven, E. Class I heme peroxidases: characterisation of soybean ascorbate peroxidase. *Arch. Biochem. Biophys.* **360**, 173–178 (1998).
11. Harding, M.M. Metal-ligand geometry relevant to proteins and in proteins: sodium and potassium. *Acta Crystallogr. D* **58**, 872–874 (2002).
12. Hill, A.P. *et al.* Chemical, spectroscopic and structural investigation of the substrate-binding site in ascorbate peroxidase. *Eur. J. Biochem.* **248**, 347–354 (1997).
13. Mandelman, D., Jamal, J. & Poulos, T.L. Identification of two-electron transfer sites in ascorbate peroxidase using chemical modification, enzyme kinetics, and crystallography. *Biochemistry* **37**, 17610–17617 (1998).
14. Bursey, E.H. & Poulos, T.L. Two substrate binding sites in ascorbate peroxidase: the role of arginine 172. *Biochemistry* **39**, 7374–7379 (2000).
15. Lad, L., Mewies, M. & Raven, E.L. Substrate binding and catalytic mechanism in ascorbate peroxidase: evidence for two ascorbate binding sites. *Biochemistry* **41**, 13774–13781 (2002).
16. Pelletier, H. & Kraut, J. Crystal structure of a complex between electron transfer partners, cytochrome c peroxidase and cytochrome c. *Science* **258**, 1748–1755 (1992).
17. Zhou, J.S., Tran, S.T., McLendon, G. & Hoffman, B.M. Photoinduced electron transfer between cytochrome c peroxidase (D37K) and Zn-substituted cytochrome c: probing the two-domain binding and reactivity of the peroxidase. *J. Am. Chem. Soc.* **119**, 269–277 (1997).
18. Sundaramoorthy, M., Kishi, K., Gold, M.H. & Poulos, T.L. The crystal structure of manganase peroxidase from *Phanerochaete crysosporium* at 2.06 Å resolution. *J. Biol. Chem.* **269**, 32759–32767 (1994).
19. Henriksen, A., Smith, A.T. & Gajhede, M. The structures of the horseradish peroxidase C-ferulic acid complex and the ternary complex with cyanide suggest how peroxidases oxidise small phenolic substrates. *J. Biol. Chem.* **274**, 35005–35011 (1999).
20. Henriksen, A. *et al.* Structural interactions between horseradish peroxidase C and the substrate benzhydroxamic acid determined by X-ray crystallography. *Biochemistry* **37**, 8054–8060 (1998).
21. Yonetani, T. & Ray, G.S. Studies on cytochrome c peroxidase. Purification and some properties. *J. Biol. Chem.* **240**, 4503–4514 (1965).
22. Mauro, J.M. *et al.* Tryptophan-191-phenylalanine, a proximal-side mutation in yeast cytochrome c peroxidase that strongly affects the kinetics of ferrocytochrome c oxidation. *Biochemistry* **27**, 6243–6256 (1988).
23. Pappa, H., Patterson, W.R. & Poulos, T.L. The homologous tryptophan critical for cytochrome c peroxidase function is not essential for ascorbate peroxidase activity. *J. Biol. Inorg. Chem.* **1**, 61–66 (1996).
24. Hiner, A.N.P. *et al.* Detection of a radical intermediate in the reaction of ascorbate peroxidase with hydrogen peroxide. *Eur. J. Biochem.* **268**, 3091–3098 (2001).
25. Miyake, C. & Asada, K. Inactivation mechanism of ascorbate peroxidase at low concentrations of ascorbate: hydrogen peroxide decomposes Compound I of ascorbate peroxidase. *Plant Cell Physiol.* **37**, 423–430 (1996).
26. Ator, M.A. & Ortiz de Montellano, P.R. Protein control of prosthetic heme reactivity. *J. Biol. Chem.* **262**, 1542–1551 (1987).
27. Berglund, G.I. *et al.* The catalytic pathway of horseradish peroxidase at high resolution. *Nature* **417**, 463–468 (2002).
28. Otwinoski, Z. & Minor, W. Processing of X-ray diffraction data collected in oscillation mode. *Methods Enzymol.* **227**, 366–396 (1997).
29. Collaborative Computational Project, Number 4. The CCP4 suite: programs for protein crystallography. *Acta Crystallogr. D* **50**, 760–763 (1994).
30. Brunger, A.T. *et al.* Crystallography & NMR system: a new software suite for macromolecular structure determination. *Acta Crystallogr. D* **54**, 905–921 (1998).
31. Murshudov, G., Vagin, A., Lebedev, A., Wilson, K. & Dodson, E. Efficient anisotropic refinement of macromolecular structures using FFT. *Acta Crystallogr. D* **55**, 247–255 (1999).
32. McRee, D. A visual protein crystallographic software system for X11/Xview. *J. Mol. Graph.* **10**, 44–47 (1992).
33. Merrit, E.A. & Murphy, M.E.P. Raster3D version 2.0 — a program for photorealistic molecular graphics. *Acta Crystallogr. D* **50**, 869–873 (1994).
34. Kraulis, P.J. MOLSCRIPT: a program to produce both detailed and schematic plots of protein structures. *J. Appl. Crystallogr.* **24**, 946–950 (1991).
35. Bryan, D.M. *et al.* Stable pentaammineruthenium(III) complexes of reductic acids: synthesis, linkage isomers and autoxidation kinetics. *J. Am. Chem. Soc.* **110**, 1498–1506 (1988).

SPECIAL NOTE

ITEM SCANNED AS SUPPLIED
PAGINATION IS AS SEEN

PERSPECTIVE

Dalton
www.rsc.org/dalton

A new framework for understanding substrate binding and functional diversity in haem peroxidases

Katherine H. Sharp,[a] Peter C. E. Moody[b] and Emma Lloyd Raven*[a]

[a] *Department of Chemistry and Department of Biochemistry, University of Leicester, University Road, Leicester, UK LE1 7RH. E-mail: emma.raven@le.ac.uk*

[b] *Department of Biochemistry, University of Leicester, University Road, Leicester, UK LE1 7RH*

Received 11th August 2003, Accepted 23rd September 2003
First published as an Advance Article on the web 13th October 2003

The haem-containing peroxidase enzymes catalyse the H_2O_2-dependent oxidation of a wide variety of substrates and have provided a focal point for our more general understanding of structure/function relationships in other, more complex haem enzymes. Mechanistically, the haem peroxidases are well characterised: they share a common catalytic cycle that involves formation of a high-oxidation-state (ferryl) intermediate. In contrast, our understanding of the structural features that control the diverse substrate specificity are less well defined. In this review, we discuss how recent spectroscopic and structural information for ascorbate peroxidase has provided new insight into the *modus operandi* of this enzyme and how this has helped to clarify certain aspects of the catalytic and, in particular, the substrate binding properties of the closely related cytochrome *c* peroxidase enzyme, which has been a benchmark for peroxidase catalysis over more than 20 years.

Introduction

There is an overwhelming body of evidence now available that establishes beyond doubt that the reactivity of a particular metal ion or metal complex can be altered when incorporated into a protein structure. The iron complex of protoporphrin IX, Fig. 1, is a good example. This simple macrocycle – or modifications of it – is an integral component of a very large group of proteins and enzymes and is capable of delivering an astonishing range of reactivity depending on the environment of the protein into which it is incorporated. Broadly, this includes electron transfer (the cytochromes), oxygen transport and storage (the globins) and redox catalysis (the haem enzymes). The availability of different oxidation states of the metal ion means that the haem group can be tuned into a particular reactivity according to the particular function required. Nature has been very efficient in her design and we are left to wonder precisely how this simple macrocycle, when incorporated into different protein structures, can deliver such a rich diversity of function. Or, in other words, how does the structure of the protein that surrounds the metal centre control its function?

This question has occupied the minds of many scientists over many years. We do not have a complete answer but there are several variables that are known to be influential. These include the identity of the axial ligands that occupy the fifth and sixth coordination positions of the haem, the solvent accessibility and the polarity of the haem environment. For the catalytic haem enzymes, the utilisation of different substrates, and

Katie Sharp was born in Oldham, Lancashire in 1979 and graduated with a Master of Chemistry with Drug Design and Toxicology from the University of Hull in 2001. She is currently studying for her PhD in chemistry at the University of Leicester. Her research work involves the molecular evolution of haem proteins for enhanced biocatalysis, and her PhD work is sponsored by the Institute of Applied Catalysis (iAc).

Peter Moody is a protein crystallographer with interests in enzyme structure and function. He has a BA in Biochemistry from the University of York and a PhD in Biophysics from Imperial College. Since then he has worked with William N. Lipscomb at Harvard, Andrew Leslie at Imperial College and Guy Dodson at York, before taking a post in the Biochemistry Department at the University of Leicester in 1995. He is currently a Senior Lecturer.

Emma Raven was born and brought up in Northamptonshire and obtained her BSc in Chemistry from the University of Leicester in 1988 and her PhD in Chemistry from the University of Newcastle Upon Tyne in 1991 (with Professor A. G. Sykes, FRS). She then moved to the west coast of Canada to work with Professor Grant Mauk at the University of British Columbia (Vancouver). In 1995, she returned to the UK to a Lectureship in Inorganic Chemistry at the University of Leicester and was promoted to Senior Lecturer in 2002. She currently holds a research fellowship from the Wellcome Trust.

Katie Sharp

Peter Moody

Emma Raven

DOI: 10.1039/b309648n

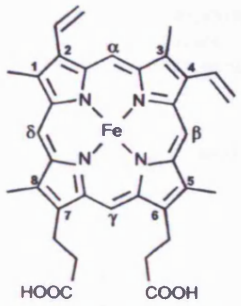

Fig. 1 The structure of iron protoporphyrin IX. The identity of the eight substituent groups bound to the porphyrin vary amongst different haem proteins,[25] but are not discussed here. Five- and six-coordinate haem proteins are known. For five-coordinate haem proteins, the axial ligand is provided by a protein residue capable of metal ligation (*e.g.* histidine, tyrosine, cysteine); six-coordinate haem proteins contain either two protein ligands, as above, or one protein ligand and an exogenous ligand (*e.g.* H_2O, O_2, CO *etc*). Haem nomenclature is non-systematic. The word haem is a general term that communicates no information about the structure of the porphyrin or the oxidation state; this nomenclature will be adopted in this Perspective.

variations in the accessibility of these substrates to the haem macrocycle, is also important.

There are various experimental routes through which one might address this question but, on the whole, isolation of any one of these variables, while keeping all others constant, is not a trivial exercise. By far the most powerful experimental approach is the application of site-directed mutagenesis methods[1,2] to the protein, or proteins, of interest. Using this technique, it is possible to alter one (or more than one) amino acid for any another of the remaining 19 amino acids at target positions in the protein architecture. This can provide unique information on the specific role(s) of individual amino acid residues in controlling function and can be used to build an overall picture of the *modus operandi*. This technique has been successfully applied to numerous haem-containing proteins and enzymes over the past 15–20 years (reviewed in refs. 3–21) and, collectively, the information that has emerged has allowed us to build a more integrated picture of haem structure/function relationships.

An absolute pre-requisite for site-directed mutagenesis work is that an expression system is available for production of the protein of interest in quantities that are sufficient for functional studies. If such a system is available, it is highly desirable (but not essential) that a high-resolution crystal structure for the protein also exists because it allows detailed rationalisation of functional data at the molecular level. A few haem proteins (cytochrome *c*, cytochrome b_5, myoglobin) met both of these criteria at an early stage and, inevitably, were therefore subjected to such intense experimental scrutiny that they provided an important benchmark against which all other haem proteins could be compared. One of these benchmark enzymes was cytochrome *c* peroxidase (C*c*P), which was first studied by mutagenesis in 1986.[22] In this Perspective, we describe how the study of the closely-related ascorbate peroxidase enzyme has provided an important new framework against which the established properties of C*c*P can be directly compared, and how very recent advances in our understanding of ascorbate peroxidase have helped to clarify our appreciation of some of the anomalous properties of C*c*P.

Haem peroxidases

We begin with a general introduction. The haem peroxidases (reviewed in refs. 6, 8, 10, 13, 14 and 23) are a very important family of enzymes that have provided a focal point for our more general understanding of haem enzymes and a workable experimental framework against which this can be measured. They are involved in a diverse range of biological processes,[24] from lignin degradation through to antibacterial and antifungal action. In general, they contain iron protoporphyrin IX, Fig. 1, as prosthetic group; although there are some exceptions to this (in the mammalian peroxidases),[25,26] these will not be considered here. They catalyse the H_2O_2-dependent oxidation of a very wide variety of substrates, usually (but not exclusively) organic substrates, and comprise two separate groups: the plant peroxidases and the mammalian peroxidases. The plant peroxidase family – which contains plant, fungal and bacterial enzymes – is by far the most well characterised, and has been classified[27] into three types. Class I peroxidases contain the prokaryotic enzymes (examples include cytochrome *c* peroxidase (C*c*P) and ascorbate peroxidase (APX)), class II peroxidases contain the fungal enzymes (*e.g.* lignin peroxidase and manganese peroxidase) and class III contain the classical secretory peroxidases (*e.g.* horseradish peroxidase (HRP)).

Structural and mechanistic aspects

From a structural and mechanistic standpoint, the haem peroxidases are very well characterised. For many years, C*c*P was the only peroxidase for which a crystal structure was available[28,29] but, after a lengthy gap, new structures emerged for other peroxidases. These included horseradish peroxidase,[30] manganese peroxidase,[31] myeloperoxidase (a mammalian enzyme),[32,33] barley peroxidase,[34] *A. ramosus* peroxidase,[35] *C. cinereus* peroxidase[36] (*A. ramosus* and *C. cinereus* peroxidases are identical), lignin peroxidase,[37–40] peanut peroxidase,[41] ascorbate peroxidase[42,43] and a (class I) catalase-peroxidase[44] enzyme. (A crystal structure for chloroperoxidase is also available,[45] but this enzyme is not part of the mammalian or plant superfamilies and has properties that liken it to cytochrome P450.) The active site structure of C*c*P is shown in Fig. 2(a). With the exception of Trp51 and Trp191, these active site residues are invariant across the plant peroxidase family and the active site topology is highly conserved.

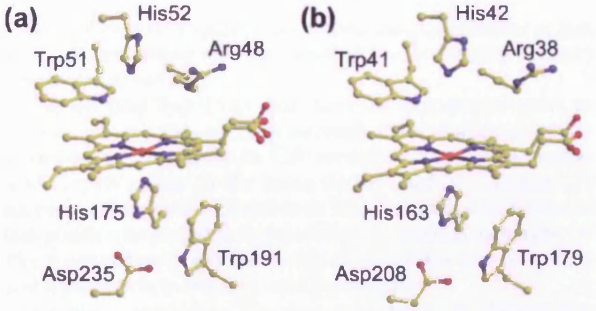

Fig. 2 The active site of (a) cytochrome *c* peroxidase[69] and (b) ascorbate peroxidase,[43] showing the haem and various active site residues.[104,105]

Their intimate mechanism has been studied in detail and site-directed mutagenesis work on C*c*P, and later HRP, has revealed an intricate picture of the roles of various active site amino acids. This work has been reviewed extensively (see, for example, refs. 10, 12–14, 21 and 46) and will not be rehearsed here. All peroxidases examined to date share a common catalytic cycle that involves reaction of the ferric haem with hydrogen peroxide in a rapid ($k \approx 10^7$ M^{-1} s^{-1}) reaction that leads to formation of a high-valent ferryl intermediate, known as Compound I, through heterolytic cleavage of the O–O peroxide bond and loss of a water molecule. Compound I is a two-electron oxidised intermediate that, for most peroxidases, contains a Fe^{IV}=O haem and a porphyrin π-cation radical. The distal histidine (His52 in C*c*P and His42 in HRP) is particularly important in Compound I formation.[10,12,14,21,46] Formation of Compound I is followed by one-electron reduction of

Compound I by substrate, first to Compound II and then back to ferric haem (although direct reduction of Compound I to ferric haem is also known, for example in the mammalian peroxidases), Scheme 1.

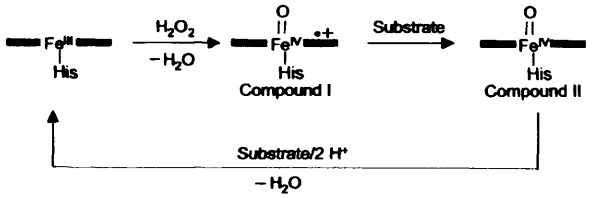

Scheme 1 The catalytic mechanism of haem peroxidases. The thick black line represents the haem ring. In the first step, the enzyme in the (ferric) resting state reacts with H_2O_2 in a very fast second-order reaction that leads to formation of the catalytic intermediate Compound I. Compound I is then reduced by the substrate in two sequential single electron transfer reactions, to regenerate the resting enzyme. A histidine residue (His) provides the fifth ligand to the haem iron.

A consistent picture has therefore emerged for Compound I formation in the haem peroxidases: they have broadly similar active site structures that have been designed to support a catalytic mechanism that, in all cases, favours formation of a common, high-oxidation state, haem intermediate. The precise structural features that favour stabilisation of ferryl haem, as opposed to ferrous haem (for example in the globins), have been examined extensively using mutagenesis but are not completely understood, although the presence of charged residues in the peroxidase active are thought to encourage separation of the O–O peroxide bond. This has been reviewed previously[17–19] and is not considered further here.

Substrate binding

In contrast to the structural and mechanistic aspects, the identity of the substrate that reduces Compound I, Scheme 1, varies enormously. It is this variety, and not the active site architecture (*vide supra*), that delivers such rich diversity of biological function across the family. For example, the substrate can be a metal ion (Mn^{2+} in manganese peroxidase), a halide (Cl^- in myeloperoxidase), an organic (L-ascorbate in ascorbate peroxidase) or phenolic (ferulic acid in horseradish peroxidase) substrate, or a protein molecule (cytochrome *c* in cytochrome *c* peroxidase). Quite often, the peroxidase will oxidise more than one substrate; in these cases it is difficult to establish which is the physiological substrate and to assign a biological role (horseradish peroxidase is an example).

Because the substrate identity is so varied, and because structural information for peroxidase/substrate complexes[47,31,33,48–53] has been slow to emerge compared to the mechanistic information, defining the structural features that control substrate binding and recognition – the substrate specificity – has been much more challenging. Indeed, this has been prohibitive in terms of our complete understanding of how functional diversity is achieved in this group of haem enzymes. Below, we discuss very recent advances in our understanding of substrate binding in ascorbate peroxidase, a class I haem peroxidase, and describe how this has shed new light on more general our understanding of the functional properties.

The class I haem peroxidases – cytochrome c peroxidase and ascorbate peroxidase. *Cytochrome c peroxidase.* Of all the peroxidases, cytochrome *c* peroxidase (*Cc*P) was the first to have its crystal structure solved[28,29] and the first to be over-expressed in *E. coli* for mutagenesis work.[54] These developments paved the way for extensive structure/function studies that defined many mechanistic aspects of peroxidase catalysis for the first time. Because of this, *Cc*P became *the* benchmark against which all other peroxidases were normally compared. However, although many of the key features of the *Cc*P enzyme are duplicated across the rest of the peroxidase family, it has two anomalous features that are not typical of other peroxidases:

(i) *Cc*P uses an atypical Compound I intermediate that contains a protein-based radical – localised on Trp191,[55–59] Fig. 3 – rather than the more usual porphyrin-based radical as observed in other peroxidases (*e.g.* HRP), Fig. 3;

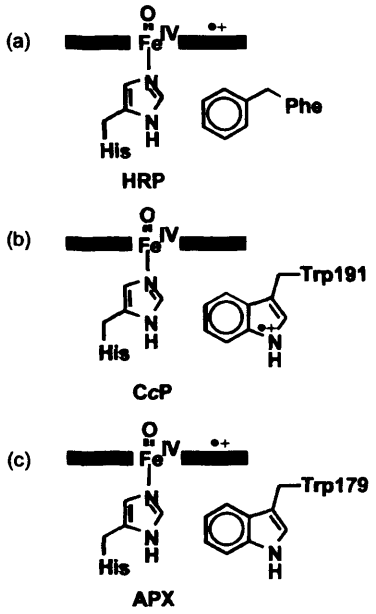

Fig. 3 The structures of the Compound I derivatives in (a) HRP, (b) *Cc*P and (c) APX. The thick black line represents the haem ring and the axial histidine ligand is shown. For HRP, the second oxidising equivalent resides on the porphyrin ring (porphyrin π-cation radical); for *Cc*P, an aromatic tryptophan residue, Trp191, adjacent to the haem is used ($Trp^{\bullet+}$ radical); for APX, a porphyrin π-cation radical is used despite APX containing the same Trp residue as is found in *Cc*P.

(ii) *Cc*P uses an atypical protein substrate, cytochrome *c*, that is not representative of other, small molecule (usually organic) peroxidase substrates.

The working hypothesis that emerged over several years to account for the first of these anomalies was based on amino acid sequence comparisons. *Cc*P contains an oxidisable amino acid (Trp191) close to the haem that is used in Compound I formation. Most other peroxidases lack an oxidisable residue at this position (replaced by a phenylalanine residue): oxidation of Phe is energetically less favourable (higher reduction potential) and a porphyrin π-cation is used instead, Fig. 3.

Ascorbate peroxidase. The first opportunity to directly test the above hypothesis was provided when it realised that another class I haem peroxidase, ascorbate peroxidase (APX), had high (>30%) sequence identity[60] to *Cc*P, including the residue equivalent to Trp191 in *Cc*P. Here we describe how functional studies on APX have helped to clarify our overall appreciation of the anomalous features of the *Cc*P enzyme.

Ascorbate-dependent peroxidase activity was first reported in 1979,[61,62] but early isolation procedures did not generate workable amounts of enzyme and very little detailed progress was made for another 15 years. All APXs (reviewed in refs. 63–65) identified to date contain iron protoporphyrin IX, Fig. 1. They catalyse the H_2O_2-dependent oxidation of ascorbate in plants, algae and certain cyanobacteria, eqn. (1).

$$2\,\text{ascorbate} + H_2O_2 \longrightarrow 2\,\text{monodehydroascorbate radical} + 2H_2O \quad (1)$$

APX enzymes show high specificity for L-ascorbate, Scheme 2, as electron donor, but will also oxidise non-physiological (usually organic) substrates that are characteristic of the class

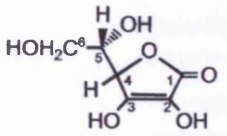

Scheme 2 The structure of L-ascorbic acid, showing the L configuration at C^5. The 2-OH and 3-OH groups have pK_a values of 11.3 and 4.0, respectively,[106] so that at neutral pH the 3-OH group is deprotonated and the molecule is anionic.

III peroxidases, in some cases at rates comparable to that of ascorbate itself.[63–65] Hence, and in direct contrast to the anomalous CcP molecule, the physiological substrate (ascorbate) in APX is much more typical of other peroxidases (this itself was a key driver for studies on APX). In fact, the substrate specificity of APX places it at the interface between the class I and class III peroxidases, a distinction that has been highlighted recently.[66] In principle, APX therefore provided a perfect opportunity to reassess the unusual properties of CcP and its status as the benchmark peroxidase, and at the same time provided a very convenient comparative framework that was important for our understanding of substrate binding and oxidation across the entire peroxidase family. The development of recombinant bacterial expression systems for pea cytosolic (rpAPX)[67] and soybean cytosolic[68] (rsAPX) APXs, together with new structural information,[42] provided the first major step towards this overall aim and made structure/function studies on APX feasible for the first time.

The first crystal structure to appear for an APX was that for the recombinant pea cytosolic enzyme (rpAPX), which was published by Patterson and Poulos in 1995.[42] Subsequently, a crystal structure for the closely related recombinant soybean cytosolic APX enzyme (rsAPX) appeared[43] (rsAPX has 91% sequence identity to rpAPX). The overall structure of the rsAPX enzyme is shown in Fig. 4 and was very similar to that rpAPX (r.m.s. deviation between Cα positions for the 249 residues in the A-chain of rpAPX and the refined rsAPX structure is 0.443 Å); both APX structures are similar to that of CcP.[69] The active site of rsAPX is shown in Fig. 2(b) and, as expected from the high sequence identity, is essentially identical to that of CcP. These structural similarities were discussed when the crystal structure of rpAPX first appeared[42] and are not repeated here.

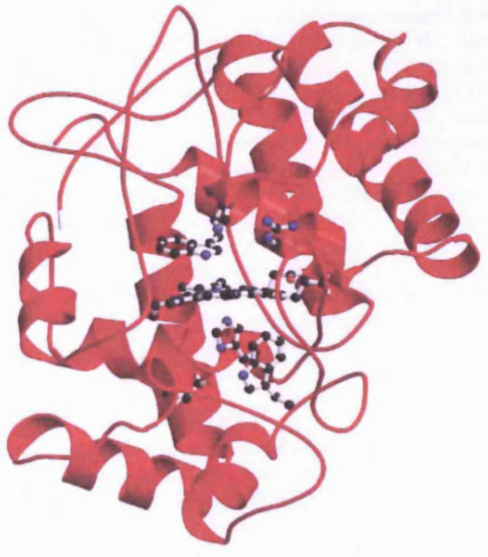

Fig. 4 The overall structure of rsAPX,[43] showing the haem and the active site residues.[105,107]

With its high sequence identity to CcP[60] and an almost identical three-dimensional structure,[42] APX was fully expected to duplicate the properties of the anomalous Compound I intermediate of CcP, to reconfirm the working hypothesis (above) and to revalidate CcP as the benchmark for other peroxidases. There was a very keen interest, therefore, in defining the nature of the Compound I intermediate in APX. This had not been attempted before the crystal structure was published, most probably due to low quantities of workable enzyme and the experimental difficulties associated with detection of the transient Compound I intermediate. Quite unexpectedly, however, APX was found not to duplicate the properties of CcP. Hence, despite containing exactly the same Trp residue (Trp179, Fig. 2(b)) that is used in CcP (Trp191, Fig. 2(a)) in almost exactly the same structural environment,[42] it was unambiguously demonstrated using EPR spectroscopy[70] that Compound I of rpAPX uses a porphyrin π-cation radical, Scheme 1. Spectroscopic work[71–75] from various laboratories has confirmed this original assignment for several other APXs, including rsAPX,[75] and there is complete agreement on this point.

A refinement to the original hypothesis was clearly necessary. It was proposed[70] that a potassium ion, located within 8 Å of Trp179 in rpAPX but not present in CcP (the residues ligating to the K^+ ion in APX – Thr164, Thr180, Asn182 and Asp187 – are replaced with Ala176, Gly192, Ala194 and Thr199, respectively in CcP,[65] Fig. 5), might destabilize radical cation formation at Trp179 on electrostatic grounds. Theoretical data were subsequently published in support of this hypothesis.[76] Although electrostatics may be influential, there are several reasons why we believe that this hypothesis is unlikely to provide a complete rationalisation of the results. First, we have shown[43] that the crystal structure of rsAPX contains no K^+ ion at the equivalent site and yet rsAPX also uses a porphyrin π-cation radical and not Trp179.[75] Second, we have evidence[77] that suggests that (slow) protein radical formation – most likely Trp radical formation – is possible in rpAPX if no substrate is present. Both observations argue against the K^+-destabilisation hypothesis. Finally, *ab initio* calculations[78,79] do not support a role for K^+ in defining Compound I structure. †

There was an additional complication. Site-specific removal of Trp179 in APX (Trp179Phe variant) has only a marginal effect on the ability of the enzyme to oxidise ascorbate,[85] in direct conflict with the CcP data which clearly indicate that Trp191 is absolutely essential for oxidation of cytochrome *c*.[86] No hypothesis had been advanced to explain this.

Development of a new hypothesis

We had suggested[64] that the key to defining these important functional differences might lie in understanding the conspicuously different substrate binding properties of the CcP and APX enzymes. In other words, that the properties of Compound I and the substrate binding specificity might be linked. To address this, we clearly needed information on the exact nature of the APX/ascorbate complex.

The first information on the substrate binding interaction came from NMR-derived distance restraints,[87] which indicated that the substrate was bound between 9.0 and 11.2 Å from the haem iron (NMR had been previously used in the study of substrate binding interactions in HRP, reviewed in ref. 46). These distances were consistent with two possible binding locations for the substrate: one close to close to the 6-propion-

† We note, however, that it has been possible to engineer a K^+-site, analogous to that found in APX, into CcP through a series of iterative mutations.[80–83] These experiments have shown that the new metal site destabilises protein radical formation at Trp191 but porphyrin π-cation formation was not observed instead. The corresponding experiment (removal of the K^+-site) has not been possible in APX because this leads to destabilisation of the active site structure.[84]

Fig. 5 Structural alignment of rsAPX and CcP (adapted from Veitch and Smith[46]). The numbering is as for the pea cytosolic APX enzyme.[60] The rpAPX sequence is identical to rsAPX except at positions 10 (Pro in rAPX), 16 (Ile), 21 (Arg), 31 (Lys), 36 (Ile), 49 (Ser), 50 (Lys), 63 (Gln), 69 (Gly), 84 (Ile), 86 (Glu), 87 (Gln), 91 (Val), 107 (Ile), 152 (Ser), 196 (Thr), 200 (Asp), 213 (Thr), 215 (Ser), 222 (Glu), 230 (Val), 240 (Leu) and 249 (Glu). Active site residues, Fig. 2, (●), the residues involved in binding of the potassium site in rpAPX (▼), the residues involved in binding of ascorbate in APX (■) and the residues involved in binding of cytochrome *c* in CcP (▲) are indicated. The additional loops in CcP and the C-terminal truncation in APX can be seen.

ate (γ-meso) and the other close to the δ-meso position of the haem, Fig. 1. (There is other (kinetic) evidence that APX may utilize a second binding site for ascorbate under certain conditions,[75] but the location of this second site is not known. CcP is also known to have more than one binding site for cytochrome *c*.[88–95]) Later, chemical modification and site-directed mutagenesis experiments[96,97] were used to show that Cys32 was close to the ascorbate site[96] and that the positively charged Arg172 residue (Arg172), located close to Cys32, was important in binding of the (anionic) ascorbate molecule.[97] These data implicated an ascorbate interaction close to Cys32 and the haem propionate groups, which was close to the γ-meso position originally implicated by NMR[87] but was not consistent with the substrate binding behaviour of most other peroxidases, which were known to use the δ-haem edge.[46,50–52,98]

In 2003, the crystal structure of the rsAPX enzyme in complex was ascorbate was published.[43] This structure confirmed the original predictions from NMR[87] and was consistent with the mutagenesis and chemical modification work.[96,97] In the absence of substrate, there are several ordered water molecules directly or indirectly hydrogen bonded to the side-chains of Arg172 and the haem 6-propionate group, Fig. 6(a), which are replaced by ascorbate in the rsAPX/ascorbate complex, Fig. 6(b). The ascorbate is bound to enzyme through hydrogen bonds between the 2-OH and 3-OH groups of the substrate, Scheme 2, and Arg172, and between the 2-OH group of the substrate and the (deprotonated) haem 6-propionate. The side chain of Lys30 swings in from solvent to provide additional hydrogen bonding stabilization (6-OH group of the substrate); this was not predicted from any functional work. Cys32 is close to the substrate binding site, but has no direct interaction with the substrate, which is consistent with the modest (≈3-fold) effect on ascorbate activity in the Cys32Ser variant.[96] The shortest distance from the substrate (oxygen of the 2-OH group) to the haem iron is 11.2 Å, in excellent agreement with the original NMR data[87] that predicted that the substrate binds between 9.0 and 11.2 Å from the iron.

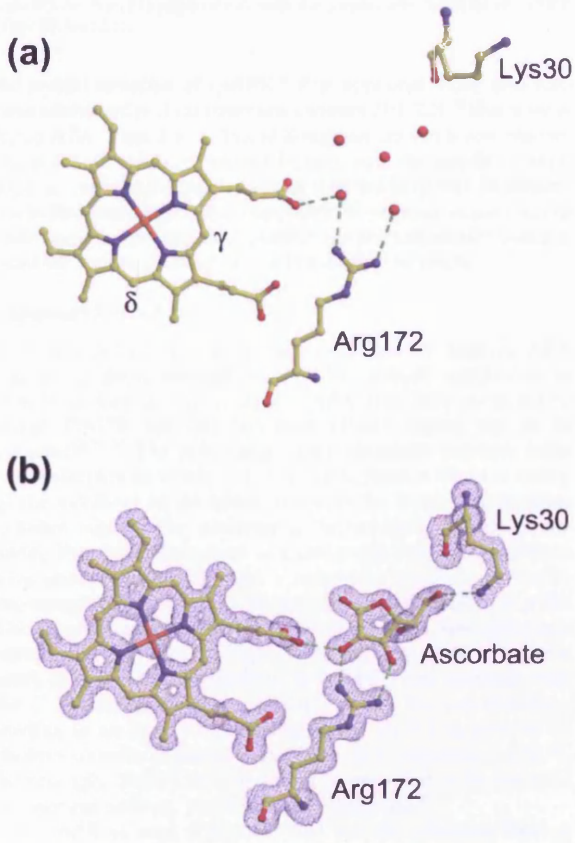

Fig. 6 (a) The structure of rsAPX showing the solvent water molecules bound in the ascorbate-binding site.[104,105] The γ-meso and δ-meso positions of the haem, Fig. 1, are indicated. (b) The rsAPX/ascorbate complex, showing refined electron density (blue) and the bound ascorbate. Hydrogen bonds are indicated (dotted lines).

Functional correlations

The rsAPX/ascorbate structure provides us with much more than just a glimpse of the ascorbate binding site. It has brought the more general question of substrate binding in other peroxidases – and how this is linked to functional diversity – into much sharper focus and has cast new light on the functional differences between the CcP and APX enzymes that is of relevance to our understanding of substrate binding and electron delivery in other haem enzymes. The main findings are most easily visualised with reference to Figs. 5–8.

Substrate binding

Despite high sequence identity, Fig. 5, and very similar three-dimensional structures,[29,42,43] the structural architecture of the APX and CcP enzymes is very subtly different and it is this that

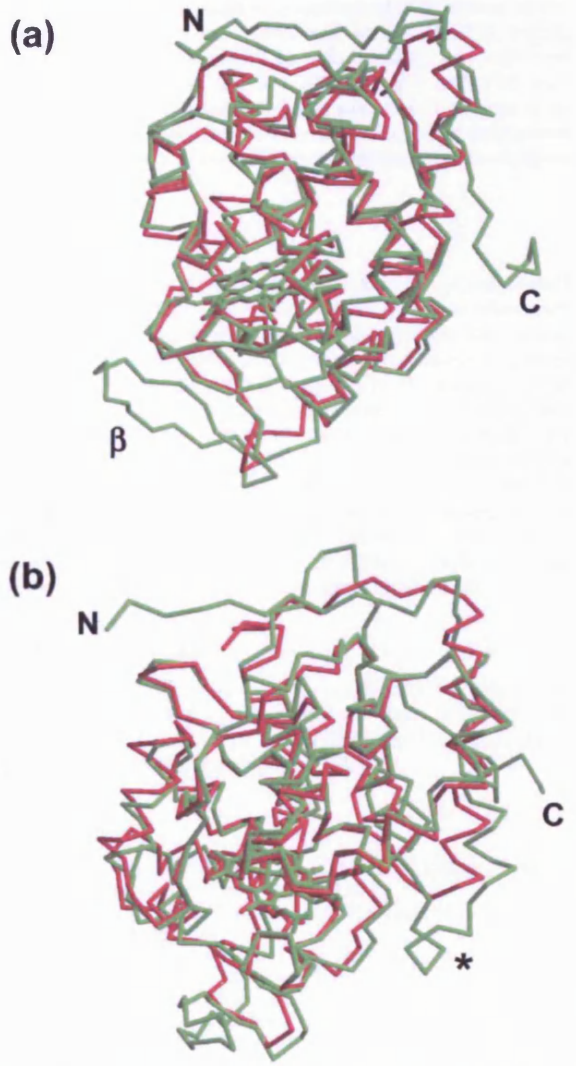

Fig. 7 Superposition of the CcP (green) and rsAPX (red) structures.[104,105] (a) Diagram showing the additional C-terminal tail (labelled C) and β-sheet structure (labelled β) in CcP; the N-terminus of CcP is also indicated (labelled N). (b) Diagram showing the additional loop (residues 34–41) in CcP (labelled *) that replaces Arg31 in rsAPX.

defines the substrate specificity. Hence, the key features required for substrate binding in APX (Arg172, Lys 30, Fig. 6) are not present in CcP (replaced by Asn184 and Asp33, Fig. 5). Similarly, the residues[47] required for substrate binding in CcP (Asp34, Glu35, Asp37, Glu290) are not present in APX because the loop containing residues 34–41 in CcP is completely missing in APX (replaced with Arg31) and because Glu290 in CcP is missing in APX because of a C-terminal truncation, Figs. 5 and 7. Superposition of the CcP and APX structures in this loop region is especially revealing and shows that the additional loop in CcP and the side chain of Tyr36 together prevent binding of ascorbate at the equivalent site, Fig. 8. We have proposed[43] that these differences account for the low activity of CcP towards ascorbate[99] and the low activity of APX towards cytochrome *c*.[63]

It is clear, therefore, that the additional loop in CcP (residues 34–41) and the residues in it (which were already known to be involved in binding of cytochrome *c*[47]), along with the C-terminal truncation in APX, are critical in defining substrate specificity. These differences are very easily visualised from a simple structural alignment, Fig. 5, and were even noted when

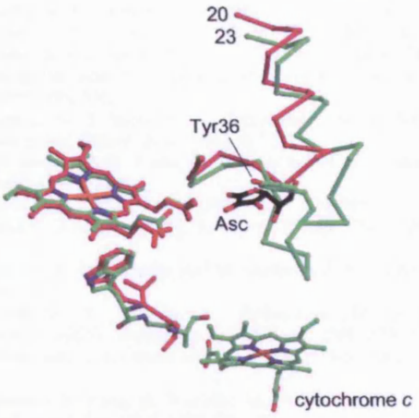

Fig. 8 Structural alignment of the CcP/cytochrome *c*[47] (residues 23–45, green) and APX/ascorbate[43] (residues 20–35, red) structures[104,105] showing the additional 8-residue loop in CcP (residues 34–41) that that replaces Arg31 in rsAPX and obscures the ascorbate binding site in rsAPX.[104,105] The side chain of Tyr36 in CcP is also shown (green) close to the bound ascorbate (Asc, black/red). The proposed pathway[47] for electron transfer from the haem in cytochrome *c* to CcP is shown (Ala193 to Trp191) superposed with the equivalent residues in rsAPX (Trp179-Ser181).

the crystal structure of rpAPX[42] first appeared. (CcP also contains additional β-sheet structure, residues 210–224,[42] that is missing in APX, Figs. 5 and 7(a), although we do not know whether this is functionally important.) Indeed, with the benefit of hindsight, is now much easier to predict that the loop may be important in fine-tuning substrate specificity. In practice, of course, our understanding of substrate specificity is not sufficiently sophisticated for accurate predictions of this kind to be made.

Compound I structure

As mentioned above, one of main incentives for studying APX was to establish whether it used the residue analogous to Trp191 in CcP during catalysis. APX was fully expected to utilize Trp179, but this has been clearly shown not to be the case.[42,71–75] The rsAPX/ascorbate structure provides some rationalization as to why not. For APX, there is direct coupling of the substrate to the haem, through the haem 6-propionate (γ-haem edge) – the substrate is 'hard-wired' directly to the haem, Fig. 6(b). Reduction of Compound I in APX therefore most sensibly occurs through a porphyrin π-cation intermediate, completely by-passing the need for involvement of Trp179. This would explain the unexpected observation that mutagenic replacement of Trp179 (Trp179Phe variant) does not affect catalytic oxidation of ascorbate by APX.[85] This contrasts with the CcP/cytochrome *c* interaction,[47] which has cytochrome *c* binding in an orientation that involves Trp191 as part of an electron transfer pathway to the haem in Compound I, Fig. 8. Accordingly, Trp191 of CcP would be expected to be essential for catalytic activity, which is indeed observed.[86]

For APX at least, it appears that it is the substrate binding orientation that defines the structure of the catalytic Compound I intermediate. If this is the case, a further question arises: is it the substrate, in the correct orientation, that precludes formation of a protein radical in Compound I of APX? There is no complete answer to this question, but this hypothesis would be consistent with experiments on rpAPX[77] in which protein radical formation has been observed in the absence of substrate (migration of the radical from the porphyrin to the the protein has also been observed in HRP[100,101]).

Electron delivery

The rsAPX/ascorbate structure also raises important questions in terms of our existing views on electron transfer in the haem

peroxidases, in which substrate binding and oxidation at the δ-haem edge, and not the γ-haem edge as seen in APX, Fig. 6, has been widely assumed.[98] In this context, we note that manganese peroxidase (a class II enzyme)[31] and NO synthase[102,103] both use the same γ-haem edge site. It remains to be seen whether that this represents a more widespread mechanism for electron delivery in other haem peroxidases or, indeed, haem enzymes more generally.

Summary

The role of the protein environment in controlling Compound I formation in the haem peroxidases has been studied extensively and a consistent mechanistic picture has emerged. Our understanding of the precise structural features that control substrate binding, and hence functional diversity, in the haem peroxidases is less well understood. In the case of APX, the sequence and structural similarity with that most famous of peroxidases, CcP, provides a particularly useful comparative framework that has raised questions that are relevant across the haem peroxidase family. A consensus view has not yet been reached, but the emergence of new crystallographic information for various peroxidase–substrate complexes is providing some answers and posing new questions that can subsequently be tested.

Acknowledgements

This work has been supported by the BBSRC (project grant 91/ B11469 to E. L. R.), the Wellcome Trust (grant 063688, fellowship to E. L. R.) and the EPSRC and The Institute of Applied Catalysis (studentship to K. H. S.).

References

1 C. A. I. Hutchison, S. Phillips, M. H. Edgell, S. Gillam, P. Jahnke and M. Smith, *J. Biol. Chem.*, 1978, **253**, 6551.
2 A. Razin, T. Hirose, K. Itakura and A. D. Riggs, *Proc. Natl. Acad. Sci. USA*, 1978, **75**, 4268.
3 P. R. Ortiz de Montellano, *Acc. Chem. Res.*, 1987, **20**, 289.
4 T. L. Poulos, *Adv. Inorg. Biochem.*, 1987, **7**, 1.
5 J. H. Dawson, *Science*, 1988, **240**, 433.
6 J. Everse, K. E. Everse and M. B. Grisham, *Peroxidases in Chemistry and Biology*, CRC Press, Boca Raton, FL, 1991, vol. I and II.
7 A. G. Mauk, *Struct. Bonding (Berlin)*, 1991, **75**, 131.
8 T. L. Poulos and R. E. Fenna, in *Metal Ions in Biological Systems: Metalloenzymes Involving Amino-Acid and Related Radicals*, ed. H. Sigel and A. Sigel, Marcel Dekker, New York, 1994, p. 25.
9 B. A. Springer, S. G. Sligar, J. S. Olson and G. N. Phillips, *Chem. Rev.*, 1994, **94**, 699.
10 A. M. English and G. Tsaprailis, *Adv. Inorg. Chem.*, 1995, **43**, 79.
11 D. B. Goodin, *J. Biol. Inorg. Chem.*, 1996, **1**, 360.
12 J. E. Erman, *J. Biochem. Mol. Biol.*, 1998, **31**, 307.
13 A. T. Smith and N. C. Veitch, *Curr. Opin. Chem. Biol.*, 1998, **2**, 269.
14 H. B. Dunford, *Heme Peroxidases*, John Wiley, Chichester, 1999.
15 S. G. Sligar, *Essays Biochem.*, 1999, **34**, 71.
16 G. H. Loew and D. L. Harris, *Chem. Rev.*, 2000, **100**, 407.
17 S.-I. Ozaki, T. Matsui, M. P. Roach and Y. Watanabe, *Coord. Chem. Rev.*, 2000, **198**, 39.
18 S.-I. Ozaki, M. P. Roach, T. Matsui and Y. Watanabe, *Acc. Chem. Res.*, 2001, **34**, 818.
19 E. L. Raven and A. G. Mauk, *Adv. Inorg. Chem.*, 2001, **51**, 1.
20 A. G. Sykes and A. G. Mauk *Heme-Fe proteins*, Academic Press, London, 2001, vol. 51.
21 J. E. Erman and L. B. Vitello, *Biochim. Biophys. Acta*, 2002, **1597**, 193.
22 D. B. Goodin, A. G. Mauk and S. M., *Proc. Natl. Acad. Sci. USA*, 1986, **83**, 1295.
23 I. S. Isaac and J. H. Dawson, *Essays Biochem.*, 1999, **34**, 51.
24 J. Everse, K. E. Everse and M. B. Grishham *Peroxidases in Chemistry and Biology*, CRC Press, Boca Raton, FL, 1991, vol. 1 and 2.
25 R. Timkovich and L. L. Bondoc, *Adv. Biophys. Chem.*, 1990, **1**, 203.
26 C. Colas and P. R. Ortiz de Montellano, *Chem. Rev.*, 2003, **103**, 2305.
27 K. G. Welinder, *Curr. Opin. Struct. Biol.*, 1992, **2**, 388.
28 T. L. Poulos, S. T. Freer, R. A. Alden, N. Xuong, S. L. Edwards, R. C. Hamlin and J. Kraut, *J. Biol. Chem.*, 1978, **253**, 3730.
29 T. L. Poulos, S. T. Freer, R. A. Alden, S. L. Edwards, U. Skogland, K. Takio, B. Eriksson, N. Xuong, T. Yonetani and J. Kraut, *J. Biol. Chem.*, 1980, **255**, 575.
30 M. Gajhede, D. J. Schuller, A. Henricksen, A. T. Smith and T. L. Poulos, *Nat. Struct. Biol.*, 1997, **4**, 1032.
31 M. Sundaramoorthy, K. Kishi, M. H. Gold and T. L. Poulos, *J. Biol. Chem.*, 1994, **269**, 32759.
32 J. Zeng and R. E. Fenna, *J. Mol. Biol.*, 1992, **226**, 185.
33 T. J. Fiedle, C. A. Davey and R. E. Fenna, *J. Biol. Chem.*, 2000, **275**, 11964.
34 A. Henricsen, K. G. Welinder and M. Gajhede, *J. Biol. Chem.*, 1998, **273**, 2241.
35 N. Kunishima, F. Amada, K. Fukuyama, M. Kawamoto, T. Matsunaga and H. Matsubara, *FEBS Lett.*, 1996, **378**, 291.
36 J. F. W. Petersen, A. Kadziola and S. Larsen, *FEBS Lett.*, 1994, **339**, 291.
37 S. L. Edwards, R. Raag, H. Wariishi, M. H. Gold and T. L. Poulos, *Proc. Natl. Acad. Sci. USA*, 1993, **90**, 750.
38 K. Piontek, T. Glumoff and K. H. Winterhalter, *FEBS Lett.*, 1993, **315**, 119.
39 T. L. Poulos, S. L. Edwards, H. Wariishi and M. H. Gold, *J. Biol. Chem.*, 1993, **268**, 4429.
40 T. Choinowski, W. Blodig, K. H. Winterhalter and K. Piontek, *J. Mol. Biol.*, 1999, **286**, 809.
41 D. J. Schuller, N. Ban, R. B. Van Huystee, A. McPherson and T. L. Poulos, *Structure*, 1996, **4**, 311.
42 W. R. Patterson and T. L. Poulos, *Biochemistry*, 1995, **34**, 4331.
43 K. H. Sharp, M. Mewies, P. C. E. Moody and E. L. Raven, *Nat. Struct. Biol.*, 2003, **10**, 303.
44 Y. Yamada, T. Fujiwara, T. Sato, N. Igarashi and N. Tanaka, *Nat. Struct. Biol.*, 2002, **9**, 691.
45 M. Sundaramoorthy, J. Terner and T. L. Poulos, *Structure*, 1995, **3**, 1367.
46 N. C. Veitch and A. T. Smith, *Adv. Inorg. Chem.*, 2001, **51**, 107.
47 H. Pelletier and J. Kraut, *Science*, 1992, **258**, 1748.
48 C. A. Davey and R. E. Fenna, *Biochemistry*, 1996, **35**, 10967.
49 K. Fukuyama, K. Sato, H. Itakura, S. Takahashi and T. Hosoya, *J. Biol. Chem.*, 1997, **272**, 5752.
50 H. Itakura, Y. Oda and K. Fukuyama, *FEBS Lett.*, 1997, **412**, 107.
51 A. Henriksen, D. J. Schuller, K. Meno, K. G. Welinder, A. T. Smith and M. Gajhede, *Biochemistry*, 1998, **37**, 8054.
52 A. Henriksen, A. T. Smith and M. Gajhede, *J. Biol. Chem.*, 1999, **274**, 35005.
53 K. Meno, S. Jennings, A. T. Smith, A. Henricksen and M. Gajhede, *Acta Crystallogr., Sect. D*, 2002, **58**, 1803.
54 L. A. Fishel, J. E. Villafranca, J. M. Mauro and J. Kraut, *Biochemistry*, 1987, **26**, 351.
55 J. E. Erman, L. B. Vitello, J. M. Mauro and J. Kraut, *Biochemistry*, 1989, **28**, 7992.
56 C. P. Scholes, Y. Liu, L. A. Fishel, M. F. Farnum, J. M. Mauro and J. Kraut, *Isr. J. Chem.*, 1989, **29**, 85.
57 M. Sivaraja, D. B. Goodin, M. Smith and B. M. Hoffman, *Science*, 1989, **245**, 738.
58 A. L. Houseman, P. E. Doan, D. B. Goodin and B. M. Hoffman, *Biochemistry*, 1993, **32**, 4430.
59 J. E. Huyett, P. E. Doan, R. Gurbiel, A. L. P. Houseman, M. Sivaraja, D. B. Goodin and B. M. Hoffman, *J. Am. Chem. Soc.*, 1995, **117**, 9033.
60 R. Mittler and B. A. Zilinskas, *FEBS Lett.*, 1991, **289**, 257.
61 D. Groden and E. Beck, *Biochim. Biophys. Acta*, 1979, **546**, 426.
62 G. J. Kelly and E. Latzko, *Naturewissenschaften*, 1979, **66**, 617.
63 D. A. Dalton, in *Peroxidases in Chemistry and Biology*, ed. J. Everse, K. E. Everse and M. B. Grisham, CRC Press, Boca Raton, FL, 1991, p. 139.
64 E. L. Raven, in *Subcellular Biochemistry: Enzyme Catalysed Electron and Radical Transfer*, ed. A. Holzenberg and N. S. Scrutton, Kluwer Academic/Plenum Publishers, New York, 2000, p. 318.
65 E. L. Raven, *Nat. Prod. Rep.*, 2003, **20**, 367.
66 H. A. Heering, M. A. K. Jansen, R. N. F. Thorneley and G. Smulevich, *Biochemistry*, 2001, **40**, 10360.
67 W. R. Patterson and T. L. Poulos, *J. Biol. Chem.*, 1994, **269**, 17020.
68 D. A. Dalton, L. Diaz del Castillo, M. L. Kahn, S. L. Joyner and J. M. Chatfield, *Arch. Biochem. Biophys.*, 1996, **328**, 1.
69 B. C. Finzel, T. L. Poulos and J. Kraut, *J. Biol. Chem.*, 1984, **259**, 13027.
70 W. R. Patterson, T. L. Poulos and D. B. Goodin, *Biochemistry*, 1995, **34**, 4342.
71 L. A. Marquez, M. Quitoriano, B. A. Zilinskas and H. B. Dunford, *FEBS Lett.*, 1996, **389**, 153.

72 M. Kvaratskhelia, C. Winkel and R. N. F. Thorneley, *Plant Physiol.*, 1997, **114**, 1237.
73 M. Kvaratskhelia, C. Winkel, M. T. Naldrett and R. N. F. Thorneley, *J. Plant Physiol.*, 1999, **154**, 273.
74 L. Lad, M. Mewies, J. Basran, N. S. Scrutton and E. L. Raven, *Eur. J. Biochem.*, 2002, **369**, 3182.
75 L. Lad, M. Mewies and E. L. Raven, *Biochemistry*, 2002, **41**, 13774.
76 G. M. Jensen, *J. Phys. Chem.*, 1998, **102**, 8221.
77 A. N. P. Hiner, J. I. Martínez, M. B. Arnao, M. Acosta, D. D. Turner, E. L. Raven and J. N. Rodriguez-López, *Eur. J. Biochem.*, 2001, **268**, 3091.
78 G. Naray-Szabo, *J. Biol. Inorg. Chem.*, 1997, **2**, 135.
79 D. K. Menyhard and G. Naray-Szabo, *J. Phys. Chem.*, 1999, **103**, 227.
80 C. A. Bonagura, M. Sundaramoorthy, H. S. Pappa, W. R. Patterson and T. L. Poulos, *Biochemistry*, 1996, **35**, 6107.
81 C. A. Bonagura, M. Sundaramoorthy, B. Bhaskar and P. T. L, *Biochemistry*, 1999, **38**, 5538.
82 B. Bhaskar, C. A. Bonagura, H. Li and T. L. Poulos, *Biochemistry*, 2002, **41**, 2684.
83 C. A. Bonagura, B. Bhaskar, M. Sundaramoorthy and T. L. Poulos, *J. Biol. Chem.*, 1999, **274**, 37827.
84 J. Cheek, D. Mandelman, T. L. Poulos and J. H. Dawson, *J. Biol. Inorg. Chem.*, 1999, **4**, 64.
85 H. Pappa, W. R. Patterson and T. L. Poulos, *J. Biol. Inorg. Chem.*, 1996, **1**, 61.
86 J. M. Mauro, L. A. Fishel, J. T. Hazzard, T. E. Meyer, G. Tollin, M. A. Cusanovich and J. Kraut, *Biochemistry*, 1988, **27**, 6243.
87 A. P. Hill, S. Modi, M. J. Sutcliffe, D. D. Turner, D. J. Gilfoyle, A. T. Smith, B. M. Tam and E. Lloyd, *Eur. J. Biochem.*, 1997, **248**, 347.
88 S. H. Northrup, J. O. Boles and J. C. L. Reynolds, *Science*, 1988, **241**, 67.
89 E. D. A. Stemp and B. M. Hoffman, *Biochemistry*, 1993, **32**, 10848.
90 M. R. Mauk, J. C. Ferrer and A. G. Mauk, *Biochemistry*, 1994, **33**, 12609.
91 J. S. Zhou, J. M. Nocek, M. L. DeVan and B. M. Hoffman, *Science*, 1995, **269**, 204.
92 H. Mei, K. Wang, S. McKee, X. Wang, J. L. Waldner, G. J. Pielak, B. Durham and F. Millett, *Biochemistry*, 1996, **35**, 15800.
93 J. S. Zhou, S. T. Tran, G. McLendon and B. M. Hoffman, *J. Am. Chem. Soc.*, 1997, **119**, 269.
94 V. W. Leesch, J. Bujons, A. G. Mauk and B. M. Hoffman, *Biochemistry*, 2000, **39**, 10132.
95 H. Mei, L. Geren, M. A. Miller, B. Durham and F. Millett, *Biochemistry*, 2002, **41**, 3968.
96 D. Mandelman, J. Jamal and T. L. Poulos, *Biochemistry*, 1998, **37**, 17610.
97 E. H. Bursey and T. L. Poulos, *Biochemistry*, 2000, **39**, 7374.
98 M. A. Ator and P. R. Ortiz de Montellano, *J. Biol. Chem.*, 1987, **262**, 1542.
99 T. Yonetani and G. S. Ray, *J. Biol. Chem.*, 1965, **240**, 4503.
100 V. P. Miller, D. B. Goodin, A. E. Friedman, C. Hartmann and P. R. Ortiz de Montellano, *J. Biol. Chem.*, 1995, **270**, 18413.
101 A. Morimoto, M. Tanaka, S. Takahashi, K. Ishimori, H. Hori and I Morishima, *J. Biol. Chem.*, 1998, **273**, 14753.
102 T. L. Poulos, H. Li, C. S. Raman and D. J. Schuller, *Adv. Inorg. Chem.*, 2001, **51**, 243.
103 C.-C. Wei, B. R. Crane and D. J. Stuehr, *Chem. Rev.*, 2003, **103**, 2365.
104 D. McRee, *J. Mol. Graph.*, 1992, **10**, 44.
105 E. A. Merrit and M. E. P. Murphy, *Acta Crystallogr., Sect. D*, 1994, **50**, 869.
106 D. M. Bryan, S. D. Dell, R. Kumar, M. J. Clarke, V. Rodriguez, M. Sherban and J. Charkoudian, *J. Am. Chem. Soc.*, 1988, **110**, 1498.
107 P. J. Kraulis, *J. Appl. Crystallogr.*, 1991, **24**, 946.

SPECIAL NOTE

ITEM SCANNED AS SUPPLIED
PAGINATION IS AS SEEN

Biochem. Soc. Symp. 71, 0–00
(Printed in Great Britain)

3

Defining substrate specificity and catalytic mechanism in ascorbate peroxidase

E.L. Raven*[1], L. Lad*, K.H. Sharp*, M. Mewies* and P.C.E. Moody†

*Department of Chemistry, University of Leicester, University Road, Leicester LE1 7RH, U.K., and †Department of Biochemistry, University of Leicester, University Road, Leicester LE1 7RH, U.K.

Abstract

Haem peroxidases catalyse the H_2O_2-dependent oxidation of a variety of, usually organic, substrates. Mechanistically, these enzymes are very well characterized: they share a common catalytic cycle that involves formation of a two-electron oxidized intermediate (Compound I) followed by reduction of Compound I by substrate. The substrate specificity is more diverse, however. Most peroxidases oxidize small organic substrates, but there are prominent exceptions to this and the structural features that control substrate specificity remain poorly defined. APX (ascorbate peroxidase) catalyses the H_2O_2-dependent oxidation of L-ascorbate and has properties that place it at the interface between the class I (e.g. cytochrome *c* peroxidase) and classical class III (e.g. horseradish peroxidase) peroxidase enzymes. We present a unified analysis of the catalytic and substrate-binding properties of APX, including the crystal structure of the APX–ascorbate complex. Our results provide new rationalization of the unusual functional features of the related cytochrome *c* peroxidase enzyme, which has been a benchmark for peroxidase catalysis for more than 20 years.

[1]To whom correspondence should be addressed (e-mail emma.raven@le.ac.uk).

Introduction

Haem peroxidases [1–8] catalyse the H_2O_2-dependent oxidation of a wide variety of substrates, usually organic substrates:

$$H_2O_2 + 2AH_2 \xrightarrow{\text{peroxidase}} 2H_2O + 2AH^{\cdot} \quad (1)$$

They have been classified [9] into three types: class I peroxidases contain the prokaryotic enzymes [e.g. C*c*P (cytochrome *c* peroxidase)], class II contain the fungal enzymes (e.g. manganese peroxidase, lignin peroxidase) and class III contain the classical secretory peroxidases [e.g. HRP (horseradish peroxidase)]. Of these, C*c*P and HRP have, historically, been the most extensively studied and almost every conceivable experimental technique has been adopted in the quest to understand these molecules.

Extensive kinetic work on site-directed variants of C*c*P and (later) HRP (reviewed in [10–14]) has provided a detailed molecular picture of the catalytic mechanism of the haem peroxidase enzymes. They share a common catalytic cycle that involves initial formation of a two-equivalent oxidized intermediate, known as Compound I, followed by reduction of Compound I by substrate. In contrast, definition of the structural features that control substrate specificity has developed much more slowly. This is in part because the substrate specificity is quite diverse–most peroxidases oxidize small organic substrates, although there are many prominent exceptions–but the absence of structural information for a truly representative peroxidase–substrate complex has also hampered progress. In this work, we address how the emergence of a new, previously uncharacterized member of this family of enzymes, APX (ascorbate peroxidase), has reinforced our understanding and has provided a more unified view of substrate-binding specificity in other, better-characterized, haem peroxidases.

APX

Ascorbate-dependent peroxidase activity was first reported in 1979 [15,16], more than 150 years after the first observation of peroxidase activity in horseradish plants [17] and almost 40 years after the discovery of C*c*P [18]. APXs [19,20] catalyse the H_2O_2-dependent oxidation of ascorbate in plants, algae and cyanobacteria:

$$2 \text{ Ascorbate} + H_2O_2 \longrightarrow 2 \text{ monodehydroascorbate radical} + 2\,H_2O \quad (2)$$

Detailed information for APX did not emerge until the mid-1990s when the development of a bacterial expression system [21] and new structural information [22] made structure–function studies on APX feasible for the first time. There were several reasons why APX, a class I peroxidase, was initially identified as a useful target. First, APX was known [23] to have high sequence identity

with perhaps the most well-characterized of all peroxidases, CcP (also a class I enzyme). CcP was the first peroxidase to have its crystal structure solved [24,25] and the first to be overexpressed in *Escherichia coli* [26], and has since been subjected to such intense experimental scrutiny that it has became *the* benchmark against which all other peroxidases are compared. CcP has two anomalous features that are not reproduced in any other haem peroxidase, however: (i) it utilizes an atypical Compound I intermediate that contains a protein-based (Trp-191) rather than the more usual porphyrin-based radical as observed in other peroxidases (e.g. HRP); (ii) it utilizes an atypical protein substrate instead of the more usual small organic substrate. The high sequence identity to CcP meant that APX provided a new opportunity to reassess the unusual properties of the CcP molecule. Second, and in contrast to CcP, the physiological substrate (ascorbate) used by APX is much more typical of other peroxidases, most notably the class III enzymes. In principle, therefore, there was an additional bonus on offer: it might be possible to account for the unusual substrate-binding specificity and functional properties of the closely related CcP molecule, the benchmark for peroxidase catalysis for more than 20 years.

Catalytic mechanism

Intermediates

The oxidation of ascorbate by APX is achieved by means of a Compound I intermediate, which is subsequently reduced by the substrate (HS) in two sequential single-electron-transfer steps:

where S$^{\cdot}$ is the one-electron oxidized form of the substrate. Despite the fact that APX contains the same active-site tryptophan residue (Trp-179; Figure 1),

$$\text{APX} + \text{H}_2\text{O}_2 \xrightarrow{k_1} \text{Compound I} + \text{H}_2\text{O} \quad (3)$$

$$\text{Compound I} + \text{HS} \xrightarrow{k_2} \text{Compound II} + \text{S}^{\cdot} \quad (4)$$

$$\text{Compound II} + \text{HS} \xrightarrow{k_3} \text{APX} + \text{S}^{\cdot} + \text{H}_2\text{O} \quad (5)$$

that in CcP (Trp-191) harbours a protein-based radical in its Compound I derivative (Trp-191), it has been clearly shown by EPR [27] that Compound I of rpAPX (recombinant pea cytosolic APX) contains a porphyrin π-cation radical instead. There is complete agreement on this point for all APXs in which the Compound I derivative has been subsequently observed (by electronic spectroscopy [28–31]). This early observation raised at least as many questions as it was originally intended to answer since APX had been expected to duplicate the anomalous

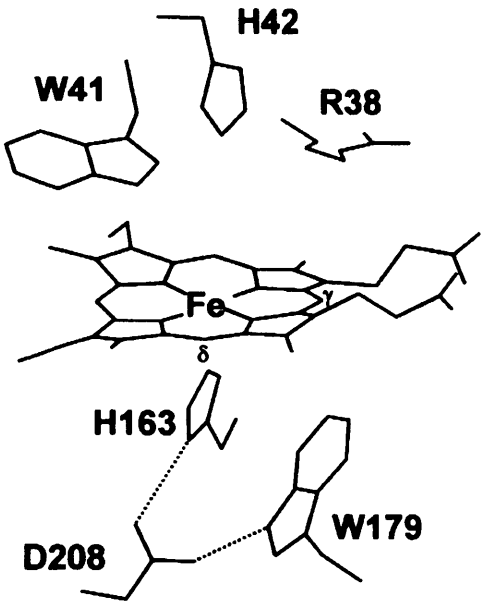

Figure 1 The active site of rpAPX [22]. The key active-site residues observed in the distal pocket of CcP (Arg-48, Trp-51, His-52) are also seen in APX (Arg-38, Trp-41, His-42). On the proximal side, the catalytic His-Asp-Trp triad (His-163–Asp-208–Trp-179) is also apparent and is analogous to that observed in CcP (His-175, Asp-235, Trp-191).

properties of CcP and revalidate CcP as the model for other peroxidase enzymes. It was proposed [27] that a potassium site in rpAPX, located only ≈8 Å from the α-carbon of Trp-179 but absent in CcP, may account for the failure of APX to form a protein radical on electrostatic grounds. Various theoretical arguments [32–34] were subsequently put forward in support of this proposal but this hypothesis seems unlikely since the corresponding recombinant cytosolic enzyme from soya bean (rsAPX) contains no metal site [35] and yet still uses a porphyrin π-cation radical [29]. An alternative explanation, based on differences in substrate binding between APX and CcP, has been put forward to account for the different behaviour of the two enzymes (see below).

Steady-state kinetics

It was noted early on that steady-state oxidation of L-ascorbate by the cytosolic enzymes from pea and soya bean [36,37] exhibits a non-hyperbolic (sigmoidal) dependence of rate on substrate concentration, instead of the more usual hyperbolic dependence as predicted by conventional Michaelis–Menten kinetics. This is not the case for all APXs, or indeed for other substrates (e.g. guaiacol) with the pea and soya bean enzymes, in which Michaelis (hyperbolic) kinetics are observed.

It was initially proposed that allosteric effects arising from the homodimeric structures of the pea and soya bean enzymes were responsible for the unusual (co-operative) behaviour, but site-directed mutagenesis experiments [38] do not support this. Sigmoidal kinetics are also consistent with a mechanism in which binding of substrate at one site induces conformational changes that affect binding of substrate at another and it has been shown [29] that the sigmoidal data for both rsAPX and rpAPX can be rationalized by implicating a model that incorporates co-operative binding involving a second binding site for ascorbate (Figure 2). Although this does not account for all of the published steady-state data for various APXs with either ascorbate or with other (aromatic) substrates, it provides the best rationalization of the data so far and is consistent with the published NMR [39] and kinetic [29] data for APX which have implicated more than one substrate-binding site (see below).

Pre-steady-state kinetics

The formation of Compound I (eqn 3), is very rapid. The reaction is pH-dependent [30], which has been shown [28] by mutagenesis to arise from titration of the distal His-42 residue (pK_a=4.9 for rpAPX; Figure 1), as observed previously for other peroxidases including *Cc*P [40,41] and HRP [14,42]. Replacement of His-42 by alanine (H42A variant) in rpAPX shows that this residue is critical for Compound I formation, and essentially eliminates catalytic activity towards ascorbate [28]. Kinetic data [28] for Compound I formation in the H42A variant provide evidence in support of a transient intermediate prior to Compound I formation. In this case, transient spectra (λ_{max}=401, 522 and 643 nm) are consis-

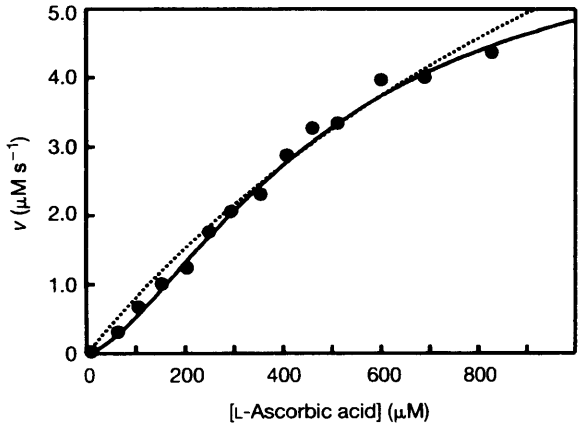

Figure 2 Steady-state oxidation of L-ascorbic acid by rpAPX. Data were fitted either to the Hill equation {solid line; $v/V_{max}=[S]^n/K^n+[S]^n$, where v is the initial rate, K is the substrate concentration at which the velocity is half-maximal, n is a qualitative indication of the level of co-operativity ($n=1.6\pm0.4$) and V_{max} is the maximum velocity} or to the Michaelis–Menten equation (dotted line; $n=1$ in Hill equation).

tent with a neutral ferric peroxide (Fe^{III}-HOOH) intermediate rather than a hyperporphyrin (Fe^{III}-OOH) structure [43–46] (Scheme 1).

Reduction of Compound I by ascorbate is competitive with Compound I formation ($k_2=2.7\times10^7$ $M^{-1}\cdot s^{-1}$ [29]; $k_2=3.4\times10^7$ $M^{-1}\cdot s^{-1}$ [47]). Reduction of Compound II is rate-limiting in the APX mechanism. Reduction of Compound II by ascorbate has been shown to be biphasic at high substrate concentrations [29]; the biphasic behaviour is eliminated when the enzyme is modified by Ellman's reagent [5,5′-dithiobis-(2-nitrobenzoic acid)], which has been shown [47] to selectively block binding of ascorbate close to Cys-32. This has been interpreted [29] as evidence for (distinct) high- and low-affinity binding sites for ascorbate in APX, which is consistent with NMR [39] and steady-state data [29] that have suggested a second binding site for ascorbate (possibly close the δ-meso position).

Substrate binding

As highlighted above, our understanding of the structural features that define substrate specificity in haem peroxidases has developed much more slowly than our appreciation of their mechanistic properties, and the absence of structural information for a truly representative peroxidase–substrate complex has significantly hampered progress. Where crystallographic information has been published (i.e. the *Cc*P–cytochrome *c* [48], manganese peroxidase–Mn^{2+} [49], HRP–benzhydroxamic acid [50,51], HRP–ferulic acid [51,52], myeloperoxidase–halide [53], *Arthromyces ramosus* peroxidase–benzhydroxamic acid [54] and *A. ramosus* peroxidase–iodide [55] complexes), these structures provided somewhat limited insight because the substrate is either not representative of peroxidases in general (e.g. cytochrome *c*, Mn^{2+} and halide), has no known physiological role or is not known to be the true biological substrate for the peroxidase in question. It was recognized early on that APX had substrate-binding properties that placed it at the interface between the class I and class III enzymes [19] – a distinction that has since been emphasized [56] – and there has been an on-going interest, therefore, in defining the substrate-binding site in APX in more detail. If this could be achieved, the high sequence identity of APX to *Cc*P means that it might be possible to account for the unusual sub-

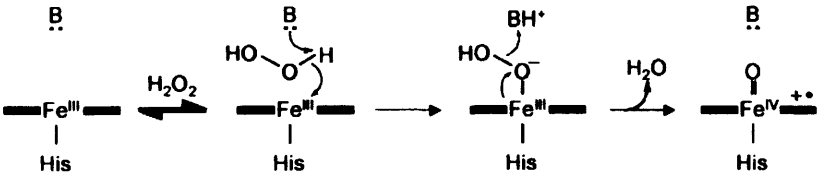

Scheme 1 Proposed mechanism for the formation of Compound I in APX, showing formation of the neutral peroxide-bound and anionic peroxide-bound intermediates. The distal histidine (His-42) residue that acts as the acid-base catalyst is indicated (B).

strate-binding specificity and functional properties of the CcP molecule, which has been *the* benchmark for peroxidase catalysis for more than 20 years.

The first evidence to emerge on the nature of the substrate-binding interaction came from NMR-derived distance restraints [39] in which individual distances between the non-exchangeable protons of ascorbate (Figure 3) and the haem iron were determined. Molecular modelling using the rpAPX structure [22] showed that the NMR-derived distances were consistent with two binding locations for the substrate: one close to close to the 6-propionate (γ-meso) and the other close to the δ-meso position of the haem (Figure 1). It was concluded [39] that the ascorbate-binding site was close to the δ-meso position on the basis of chemical-modification experiments with phenylhydrazine and by comparison with other peroxidases in which a precedent for substrate binding at the δ-meso position had been established previously [50,52,57].

More detailed information emerged when Poulos and co-workers [47] made the connection between the well-known inhibition of APX activity by thiol-specific reagents and the substrate-binding properties, and proposed that the single Cys-32 group in rpAPX might be close to the ascorbate-binding site. Hence it was shown [47] that removal or chemical modification of Cys-32 reduces the ascorbate activity and strongly implicated an ascorbate interaction close to Cys-32. This location was close to the γ-meso position originally implicated by NMR [39] as one of the two possible binding sites, but was not consistent with the behaviour of most other peroxidases, which were known to use the δ-haem edge. Site-directed mutagenesis experiments later implicated a positively charged arginine residue (Arg-172), located close to Cys-32, in binding of the (anionic) ascorbate molecule [58].

The question was finally resolved when the crystal structure of the rsAPX–ascorbate complex was published [35]. The structure validated the predictions from the mutagenesis/chemical-modification work [47,58] and from NMR [39], and confirmed the γ-meso position as the site of ascorbate oxidation. Electron density around the γ-meso position in the absence of ascorbate (Figure 4A), revealed five ordered water molecules directly or indirectly hydrogen bonded to the side chains of Arg-172 and the 6-propionate of the haem group. Ascorbate binds in place of these water molecules in the rsAPX–ascorbate complex (Figures 3 and 4B), through hydrogen-bonding

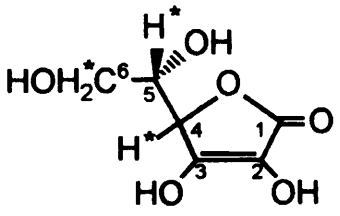

Figure 3 Structure of L-ascorbic acid, showing the L configuration at C-5. Non-exchangeable protons are indicated *. The pK_a values of the 2-OH and 3-OH groups are 11.3 and 4.0, respectively [64].

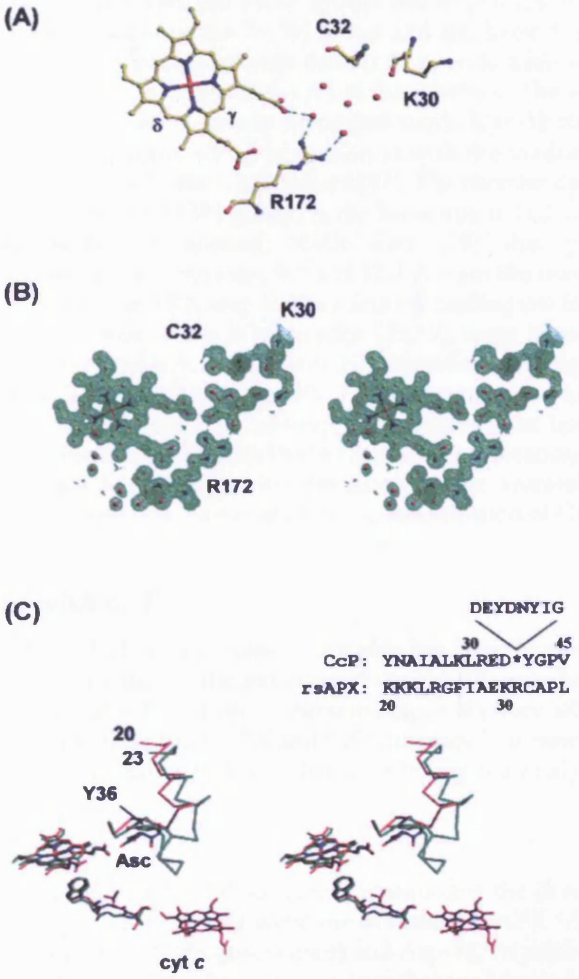

Figure 4 Title?. (**A**) The structure of rsAPX [35] showing the γ- and δ-meso positions of the haem and bound solvent in the ascorbate-binding site. (**B**) Stereo representation of the rsAPX–ascorbate complex [35], showing refined electron density (green) and the binding of ascorbate. Hydrogen bonds are indicated (dotted lines). (**C**) Structural alignment of the CcP–cytochrome *c* (green; residues 23–45) [48] and APX–ascorbate (magenta; residues 20–35) structures showing the additional loop in CcP (residues 34–41) that blocks the equivalent site in rsAPX. The side chain of Tyr-36 in CcP is also shown (green). The proposed pathway [48] for electron transfer from the haem in cytochrome *c* to CcP is shown (Ala-193–Trp-191) superimposed on the equivalent residues in rsAPX (Trp-179–Ser-181). The haem group of cytochrome *c* is in red and the bound ascorbate (Asc) in blue. Inset: structure-based alignment of rsAPX (residues 20–35) and yeast CcP (residues 23–45) in the region of the ascorbate-binding site. In CcP, an eight-residue loop (indicated *) replaces Arg-31 in rsAPX.

interactions between the 2-OH and 3-OH groups and Arg-172, as predicted by mutagenesis [58], and between the 2-OH group and the haem 6-propionate. The side chain of Lys-30 swings in from solvent to provide additional hydrogen-bonding stabilization through the 6-OH of the substrate. The involvement of Lys-30 was not predicted from any functional work. Cys-32 has no direct interaction with the substrate, which is consistent with the modest (≈3-fold) effect on ascorbate activity in the C32S variant [47]. The shortest distance from the substrate (oxygen of the 2-OH group) to the haem iron is 11.2 Å, in reasonable agreement with the original NMR data [39] that predicted a substrate-binding orientation between 9.0 and 11.2 Å from the iron. Although there is some evidence that APX may utilize a second binding site for ascorbate (see above), possibly close to the δ-haem edge [29,39], there is no direct evidence for this in the crystal structure; however, if ascorbate binding does occur at the δ-haem edge, it is probably weak [29]. This site remains the hot favourite for binding of aromatic substrates, however, and is consistent both with the phenylhydrazine experiments [39] and with chemical-modification/mutagenesis work [47], which have shown that oxidation of the aromatic substrate guiaicol is unaffected by mutagenesis or chemical modification of Cys-32.

Comparison with CcP

The structure of the CcP–cytochrome *c* complex has been known for some time [48] but the elucidation of the structure of the rsAPX–ascorbate complex has provided the missing link in our understanding of the very different substrate-binding specificities of the APX and CcP enzymes. It is now possible to present a unified comparative view of substrate binding and catalysis in these two enzymes.

Substrate specificity

Comparison of the APX and CcP sequences reveals that the (basic) residues involved in binding of the (anionic) ascorbate molecule in APX (Arg-172 and Lys-30) are replaced by Asn-184 (not shown) and Asp-33, respectively, in CcP (Figure 4C, inset). Conversely, the acidic residues that are known [48,59] to be involved in binding of (cationic) cytochrome *c* to CcP (Asp-34, Glu-35, Asp-37) are not present in APX because the loop containing residues 34–41 in CcP is missing (replaced with an arginine residue; Figure 4C, inset); Glu-290 in CcP [48] is also missing in APX because of a C-terminal truncation (Figure 5). When the rsAPX–ascorbate and CcP–cytochrome *c* [48] complexes are overlaid in this loop region (Figure 4C), it is clear that the additional loop in CcP and particularly the side chain of Tyr-36 prevent binding of ascorbate at the equivalent site. In short, the structural features required for substrate binding in APX are not present in CcP, and *vice versa*, which sensibly accounts for the low activity of CcP towards ascorbate [60] and of APX towards cytochrome *c* [19]. Although some of these structural differences were noted when the crystal structure of rpAPX appeared [22], it is only now that their functional implications are becoming clear.

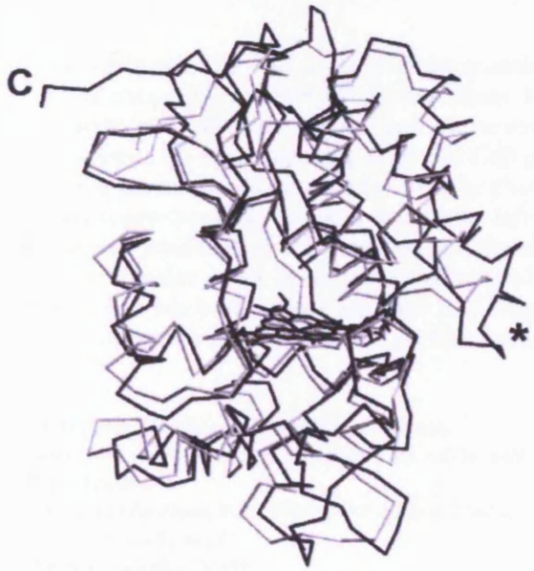

Figure 5 Superposition of the CcP (black) and rsAPX (grey) structures.
The Figure shows the additional loop (residues 34–41) (*) and the additional C-terminal tail (C) in CcP.

Function

CcP is unusual in that it uses a Trp radical (Trp-191) in its Compound I derivative; this residue is essential for cytochrome *c* oxidation [61]. The absence of an oxidizable amino acid in other peroxidases (replaced by a Phe or aliphatic residue) provided some rationalization of this observation, but this was undermined when it was conclusively established not only that rpAPX uses a porphyrin π–cation intermediate [27], but also that Trp-179 is not necessary for ascorbate oxidation [62]. As mentioned above, electrostatic arguments [32–34] do not account for the observed behaviour. Direct comparison of the APX–ascorbate and CcP–cytochrome *c* structures (Figure 4C), provides more convincing rationalization. Hence, for APX there is direct coupling of the substrate to the haem group through the haem 6-propionate, and reduction of Compound I therefore occurs through a porphyrin π–cation intermediate, completely bypassing the need for involvement of Trp-179. As expected, therefore, experiments on the W179F variant of rpAPX have shown that Trp-179 has no effect on ascorbate oxidation [62]. This is in contrast to the substrate-binding orientation in the CcP–cytochrome *c* complex [48], in which cytochrome *c* binds in an orientation that involves Trp-191 as part of an electron-transfer pathway to the haem. In this case, Trp-191 would be expected to be essential for enzyme activity, which is indeed observed [61].

Summary

The APX enzyme has confronted us with some difficult questions that have challenged our wider understanding of other haem peroxidases. It is now clear that despite their high sequence and structural similarities the *modus operandi* of the APX and *Cc*P enzymes are fundamentally different: *Cc*P is truly anomalous, with properties that are not duplicated even within the class I peroxidase sub-group. A direct, hydrogen-bonding contact between the substrate and the haem 6-propionate was not predicted in APX and widens the debate on our existing views of electron transfer in the haem peroxidases, in which substrate oxidation at the δ-haem edge has been widely assumed [63]. Might this represent a more general mechanism for electron delivery in other haem enzymes?

References

1. Dunford, H.B. (1999) Heme Peroxidases, John Wiley, Chichester
2. Isaac, I.S. and Dawson, J.H. (1999) in Essays in Biochemistry, vol. 34 (Ballou, D.P., ed.), pp. 51–69, Portland Press, London
3. Everse, J., Everse, K.E., and Grisham, M.B. (1991) Peroxidases in Chemistry and Biology, vols I and II, CRC Press, Boca Raton, FL
4. Dawson, J.H. (1988) Science **240**, 433–439
5. English, A.M. and Tsaprailis, G. (1995) Adv. Inorg. Chem. **43**, 79–125
6. Ortiz de Montellano, P.R. (1992) Ann. Rev. Pharmacol. Toxicol. **32**, 89–107
7. Ortiz de Montellano, P.R. (1987) Acc. Chem. Res. **20**, 289–294
8. Smith, A.T. and Veitch, N.C. (1998) Curr. Opin. Chem. Biol. **2**, 269–278
9. Welinder, K.G. (1992) Curr. Opin. Struct. Biol. **2**, 388–393
10. Veitch, N.C. and Smith, A.T. (2001) Adv. Inorg. Chem. **51**, 107–162
11. Erman, J.E. (1998) J. Biochem. Mol. Biol. **31**, 307–327
12. Erman, J.E. and Vitello, L.B. (2002) Biochim. Biophys. Acta **1597**, 193–220
13. Bosshard, H.R., Anni, H. and Yonetani, T. (1991) in Peroxidases in Chemistry and Biology, vol. 2 (Everse, J., Everse, K.E. and Grisham, M.B., eds), pp. 51–84, CRC Press, Boca Raton, FL
14. Dunford, H.B. (1991) in Peroxidases in Chemistry and Biology, vol. 2 (Everse, J., Everse, K.E. and Grisham, M.B., eds), pp. 1–24, CRC Press, Boca Raton, FL
15. Kelly, G.J. and Latzko, E. (1979) Naturewissenschaften **66**, 617–618
16. Groden, D. and Beck, E. (1979) Biochim. Biophys. Acta **546**, 426–435
17. Planche, L.A. (1810) Bulletin Pharmacie **2**, 578–580
18. Altschul, A.M., Abrams, R. and Hogness, T.R. (1940) J. Biol. Chem. **136**, 777–794
19. Dalton, D.A. (1991) in Peroxidases in Chemistry and Biology, vol. 2 (Everse, J., Everse, K.E. and Grisham, M.B., eds.), pp. 139–154, CRC Press, Boca Raton, FL
20. Raven, E.L. (2000) in Subcellular Biochemistry: Enzyme Catalysed Electron and Radical Transfer, vol. 35 (Holzenberg, A. and Scrutton, N.S., eds), pp. 318–350, Publisher?, Location?
21. Patterson, W.R. and Poulos, T.L. (1994) J. Biol. Chem. **269**, 17020–17024
22. Patterson, W.R. and Poulos, T.L. (1995) Biochemistry **34**, 4331–4341
23. Mittler, R. and Zilinskas, B.A. (1991) FEBS Lett. **289**, 257–259
24. Poulos, T.L., Freer, S.T., Alden, R.A., Xuong, N., Edwards, S.L., Hamlin, R.C. and Kraut, J. (1978) J. Biol. Chem. **253**, 3730–3735
25. Poulos, T.L., Freer, S.T., Alden, R.A., Edwards, S.L., Skogland, U., Takio, K., Eriksson, B., Xuong, N., Yonetani, T. and Kraut, J. (1980) J. Biol. Chem. **255**, 575–580
26. Fishel, L.A., Villafranca, J.E., Mauro, J.M. and Kraut, J. (1987) Biochemistry **26**, 351–360
27. Patterson, W.R., Poulos, T.L. and Goodin, D.B. (1995) Biochemistry **34**, 4342–4345

28. Lad, L., Mewies, M., Basran, J., Scrutton, N.S. and Raven, E.L. (2002) Eur. J. Biochem. **369**, 3182–3192
29. Lad, L., Mewies, M. and Raven, E.L. (2002) Biochemistry **41**, 13774–13781
30. Marquez, L.A., Quitoriano, M., Zilinskas, B.A. and Dunford, H.B. (1996) FEBS Lett. **389**, 153–156
31. Kvaratskhelia, M., Winkel, C. and Thorneley, R.N.F. (1997) Plant Physiol. **114**, 1237–1245
32. Menyhard, D.K. and Naray-Szabo, G. (1999) J. Phys. Chem. **103**, 227–233
33. Naray-Szabo, G. (1997) J. Biol. Inorg. Chem. **2**, 135–138
34. Jensen, G.M. (1998) J. Phys. Chem. **102**, 8221–8228
35. Sharp, K.H., Mewies, M., Moody, P.C.E. and Raven, E.L. (2003) Nat. Struct. Biol. **10**, 303–307
36. Dalton, D.A., Hanus, F.J., Russell, S.A. and Evans, H.J. (1987) Plant Physiol. **83**, 789–794
37. Mittler, R. and Zilinskas, B.A. (1991) Plant Physiol. **97**, 962–968
38. Mandelman, D., Schwarz, F.P., Li, H. and Poulos, T.L. (1998) Protein Sci. **7**, 2089–2098
39. Hill, A.P., Modi, S., Sutcliffe, M.J., Turner, D.D., Gilfoyle, D.J., Smith, A.T., Tam, B.M. and Lloyd, E. (1997) Eur. J. Biochem. **248**, 347–354
40. Vitello, L.B., Huang, M. and Erman, J.E. (1990) Biochemistry **29**, 4283–4288
41. Erman, J.E., Vitello, L.B., Miller, M.A., Shaw, A., Brown, K.A. and Kraut, J. (1993) Biochemistry **32**, 9798–9806
42. Rodriguez-Lopez, J.N., George, S.J. and Thorneley, R.N.F. (1998) J. Biol. Inorg. Chem. **3**, 44–52
43. Wirstam, M., Blomberg, M.R.A. and Siegbahn, P.E.M. (1999) J. Am. Chem. Soc. **121**, 10178–10185
44. Loew, G. and Dupuis, M. (1996) J. Am. Chem. Soc. **118**, 10584–10587
45. Harris, D.L. and Loew, G.H. (1996) J. Am. Chem. Soc. **118**, 10588–10594
46. Filizola, M. and Loew, G. (2000) J. Am. Chem. Soc. **122**, 18–25
47. Mandelman, D., Jamal, J. and Poulos, T.L. (1998) Biochemistry **37**, 17610–17617
48. Pelletier, H. and Kraut, J. (1992) Science **258**, 1748–1755
49. Sundaramoorthy, M., Kishi, K., Gold, M.H. and Poulos, T.L. (1994) J. Biol. Chem. **269**, 32759–32767
50. Henriksen, A., Schuller, D.J., Meno, K., Welinder, K.G., Smith, A.T. and Gajhede, M. (1998) Biochemistry **37**, 8054–8060
51. Meno, K., Jennings, S., Smith, A.T., Henricksen, A. and Gajhede, M. (2002) Acta Crystallogr. D **58**, 1803–1812
52. Henriksen, A., Smith, A.T. and Gajhede, M. (1999) J. Biol. Chem. **274**, 35005–35011
53. Fiedle, T.J., Davey, C.A. and Fenna, R.E. (2000) J. Biol. Chem. **275**, 11964–11971
54. Itakura, H., Oda, Y. and Fukuyama, K. (1997) FEBS Lett. **412**, 107–110
55. Fukuyama, K., Sato, K., Itakura, H., Takahashi, S. and Hosoya, T. (1997) J. Biol. Chem. **272**, 5752–5756
56. Heering, H.A., Jansen, M.A.K., Thorneley, R.N.F. and Smulevich, G. (2001) Biochemistry **40**, 10360–10370
57. Tsukamoto, K., Itakura, H., Sato, K., Fukuyama, K., Miura, S., Takahashi, S., Ikezawa, H. and Hosoya, T. (1999) Biochemistry **38**, 12558–12568
58. Bursey, E.H. and Poulos, T.L. (2000) Biochemistry **39**, 7374–7379
59. Zhou, J.S., Tran, S.T., McLendon, G. and Hoffman, B.M. (1997) J. Am. Chem. Soc. **119**, 269–277
60. Yonetani, T. and Ray, G.S. (1965) J. Biol. Chem. **240**, 4503–4514
61. Mauro, J.M., Fishel, L.A., Hazzard, J.T., Meyer, T.E., Tollin, G., Cusanovich, M.A. and Kraut, J. (1988) Biochemistry **27**, 6243–6256
62. Pappa, H., Patterson, W.R. and Poulos, T.L. (1996) J. Biol. Inorg. Chem. **1**, 61–66
63. Ator, M.A. and Ortiz de Montellano, P.R. (1987) J. Biol. Chem. **262**, 1542–1551
64. Bryan, D.M., Dell, S.D., Kumar, R., Clarke, M.J., Rodriguez, V., Sherban, M. and Charkoudian, J. (1988) J. Am. Chem. Soc. **110**, 1498–1506

SPECIAL NOTE

ITEM SCANNED AS SUPPLIED
PAGINATION IS AS SEEN

Crystal Structure of the Ascorbate Peroxidase−Salicylhydroxamic Acid Complex†

Katherine H. Sharp,‡ Peter C. E. Moody,§ Katherine A. Brown,|| and Emma Lloyd Raven*,‡

Department of Chemistry, University of Leicester, University Road, Leicester LE1 7RH, U.K., Department of Biochemistry, University of Leicester, University Road, Leicester LE1 7RH, U.K., and Department of Biological Sciences, Centre for Molecular Microbiology and Infection, Flowers Building, Imperial College London, London SW7 2AZ, U.K.

Received April 5, 2004; Revised Manuscript Received May 4, 2004

ABSTRACT: Ascorbate peroxidase is a bifunctional peroxidase that catalyzes the H_2O_2-dependent oxidation of both ascorbate and various aromatic substrates. The ascorbate binding site was recently identified as being close to the γ-heme edge [Sharp, K. H., Mewies, M., Moody, P. C. E., and Raven, E. L. (2003) *Nat. Struct. Biol. 10*, 303−307]. In this work, the X-ray crystal structure of recombinant soybean cytosolic ascorbate peroxidase (rsAPX) in complex with salicylhydroxamic acid (SHA) has been determined to 1.46 Å. The SHA molecule is bound close to the δ-heme edge in a cavity that connects the distal side of the heme to the surface of the protein. There are hydrogen bonds between the phenolic hydroxide of the SHA and the main chain carbonyl of Pro132, between the carbonyl oxygen of SHA and the side chain guanadinium group of Arg38, and between the hydroxamic acid group and the indole nitrogen of Trp41. The structure provides the first information about the location of the aromatic binding site in ascorbate peroxidase and, together with our previous data [Sharp, K. H., et al. (2003) *Nat. Struct. Biol. 10*, 303−307], completes the structural description of the binding properties of ascorbate peroxidase. The mechanistic implications of the results are discussed in terms of our current understanding of how APX catalyzes oxidation of different types of substrates bound at different locations.

The heme peroxidase enzymes (reviewed in refs *1*−*4*) catalyze the H_2O_2-dependent oxidation of a wide variety of substrates, in most cases small organic substrates. They have been classified on the basis of sequence homology (*5*) into three types. Class I heme peroxidases contain the prokaryotic enzymes, including cytochrome *c* peroxidase (CcP),[1] ascorbate peroxidase (APX), and the gene-duplicated bacterial catalase-peroxidases. Class II contains the fungal peroxidase enzymes, including manganese peroxidase and lignin peroxidase. Class III contains the classical secretory peroxidases, the most notable example being horseradish peroxidase (HRP). Mechanistically, these enzymes are very well characterized; they share a common catalytic cycle that involves formation of a two equivalent oxidized intermediate, known as Compound I, followed by reduction of Compound I by substrate (eqs 1−3, where P is peroxidase, HS is the substrate, and S$^\bullet$ is the one-electron oxidized form of the substrate).

$$P + H_2O_2 \rightarrow \text{Compound I} + H_2O \quad (1)$$

$$\text{Compound I} + HS \rightarrow \text{Compound II} + S^\bullet \quad (2)$$

$$\text{Compound II} + HS \rightarrow P + S^\bullet + H_2O \quad (3)$$

Much of the structure−function work (*1*−*4*, *6*−*8*) on the heme peroxidases has focused on Compound I formation (eq 1), and a consistent picture of this step has emerged: the peroxidases have very similar heme active site structures that, in all cases, have been designed to support formation of the high valent Compound I intermediate. In contrast, the identity of the substrate (eqs 2 and 3) varies enormously (it can be a metal ion, an organic/phenolic substrate, or a protein molecule), and it is this variety in substrate specificity, and not Compound I formation, that delivers the rich diversity of function across the peroxidase family. It follows that to understand biological function, we need an experimental framework that allows detailed rationalization of substrate binding.

On the whole, however, our understanding of the structural features that define substrate specificity in the heme peroxidase enzymes is poorly developed compared to our understanding of Compound I formation. This is in part because structural information for peroxidase−substrate complexes has been slower to emerge (*9*−*17*), but is also because, in

† This work was supported by The Wellcome Trust (Grant 063688/Z/01/Z to E.L.R.), the Engineering and Physical Sciences Research Council, and The Institute of Applied Catalysis (studentship to K.H.S.).

* To whom correspondence should be addressed. Telephone: +44 (0)116 252 2099. Fax: +44 (0)116 252 2789. E-mail: emma.raven@le.ac.uk.

‡ Department of Chemistry, University of Leicester.

§ Department of Biochemistry, University of Leicester.

|| Imperial College London.

[1] Abbreviations: APX, ascorbate peroxidase; rsAPX, recombinant soybean cytosolic ascorbate peroxidase; SHA, salicylhydroxamic acid (2-hydroxybenzhydroxamic acid); BHA, benzyhydroxamic acid; CcP, cytochrome *c* peroxidase; HRP, horseradish peroxidase; ARP, *A. ramosus* peroxidase.

10.1021/bi049343q CCC: $27.50
Published on Web 06/18/2004

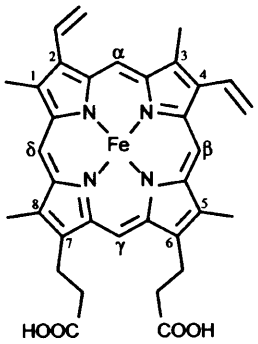

FIGURE 1: Structure of iron protoporphyrin IX, showing the nomenclature used in this work. This nomenclature is consistent with that used in our previous work (*26*).

some cases (*9*, *12*), the substrate is atypical and has not, therefore, provided the necessary generic insight. A lack of comparative substrate binding information, to allow connections to be made between different peroxidases, has also been prohibitive.

Within this wider framework, it was recently realized that ascorbate peroxidase (APX), which catalyzes the H_2O_2-dependent oxidation of ascorbate (*18*–*20*), has structural, functional, and substrate binding properties that places it at an important interface between peroxidases [a distinction that has been highlighted recently (*21*)]. Hence, the sequence of APX is highly identical with the most prominent and well-characterized class I peroxidase, CcP, as well as with the bacterial catalase-peroxidases. In addition to ascorbate, APX is also able to catalyze the oxidation of a variety of aromatic substrates [e.g., *p*-cresol, guaiacol, pyrogallol, *o*-dianisidine, and 2,2′-azinobis(3-ethylbenzothiazoline-6-sulfonic acid) (ABTS)] that are typical of the class II and class III peroxidases (*21*, *22*). In some cases, oxidation of these aromatic substrates is faster than oxidation of ascorbate itself (*18*), and it is likely that this is linked to a physiological role, since there are high levels of phenolic compounds present *in planta*. Altogether, the close sequence identity to CcP coupled with its bifunctional substrate specificity that mimics that of the class II and III peroxidases makes APX an exceptionally useful comparative model for our general understanding of substrate binding because it provides an overarching framework that encompasses many features that have, so far, only been found separately.

It is only recently that detailed information about substrate binding in APX has appeared. The hypothesis that has emerged is as follows (*23*–*25*). There are two, separate substrate binding locations. The first, close to the γ-meso (C15) position of the heme (Figure 1), is utilized by ascorbate; the second is used primarily by aromatic substrates (*23*), but its location is not known. We have recently determined the crystal structure of recombinant soybean cytosolic APX (rsAPX) in complex with ascorbate (*26*). The structure has confirmed the γ-heme edge as the primary site of oxidation of ascorbate and provides the first comparative rationalization of the different substrate specificities of APX and CcP. In this work, we have identified the second, aromatic binding site by determining the crystal structure of rsAPX in complex with salicylhydroxamic acid (SHA, Figure 2). Together with our previous data (*26*), this now provides a complete description of substrate binding in APX.

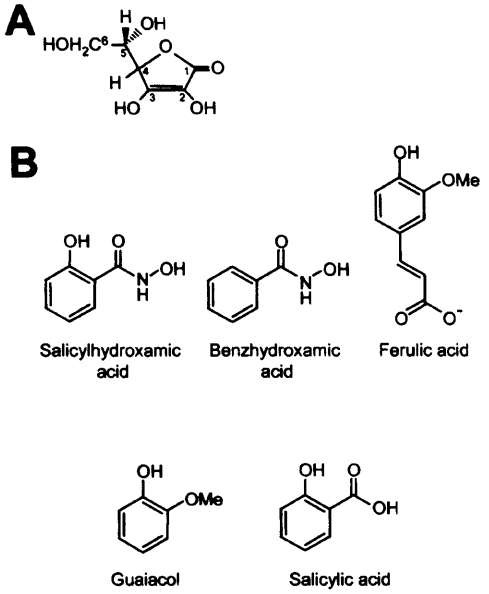

FIGURE 2: (A) Structure of ascorbic acid. The pK_a values of the 2-OH and 3-OH groups are 11.3 and 4.0, respectively (*42*). (B) Structures of the various aromatic compounds discussed in this paper. Salicylhydroxamic acid contains two acidic protons on the phenolic [pK_a = 9.8 (*33*)] and hydroxamic acid [pK_a = 7.4 (*33*)] groups.

EXPERIMENTAL PROCEDURES

Protein Purification and Preparation of Crystals. Recombinant soybean cytosolic APX (rsAPX) was prepared from *Escherichia coli* SG1300 (pREP4) by incorporation of a pQE30-derived expression vector and purified as described previously (*27*). The final elution from the Ni^{2+}–nitrilotriacetic acid agarose column (Qiagen) was carried out using pH (4.2) rather than using imidazole, and the heme reconstitution step was carried out and then left overnight rather than over 15 min as described. Samples prepared in this way eluted as a single band by SDS–PAGE and by FPLC using a Superdex 75 HR 10/30 column. Purity was also assessed using the ratio of absorbancies at the Soret and 280 nm peaks. For rsAPX, samples with an A_{407}/A_{280} of greater than 2.0 were considered pure. Samples (≈20 mg/mL) were stored in deionized water in 50 μL aliquots. Enzyme concentrations were determined using the molar absorption coefficient for rsAPX [ϵ_{407} = 107 mM^{-1} cm^{-1} (*27*)]. Samples of rsAPX were assayed (100 mM phosphate at pH 7.0 and 25.0 °C) against guaiacol using established protocols (*27*) and using an ϵ_{470} of 22.6 mM^{-1} cm^{-1} (*28*). Data were fitted to the Michaelis–Menten equation.

Crystals of rsAPX were prepared as described previously (*26*). The best crystals grew to ~150 μm in length and 75 μm in cross section. Guaiacol is too insoluble in water for sufficiently high concentrations to be obtained in solution for soaking into rsAPX crystals. Guaiacol is soluble in EtOH or MeOH, but attempts to soak it (at various concentrations in EtOH or MeOH) into the crystals resulted in cracking of the crystals under all conditions that were attempted. Solubility can be improved by functionalization of the methoxy group with the (more hydrophilic) hydroxamic acid group. In this case, it was possible to obtain crystals of the rsAPX–SHA complex by soaking the crystals in a mother

Table 1: Data Collection and Refinement Statistics for the rsAPX−SHA Complex[a]

data collection	
resolution range (outer bin) (Å)	50−1.46 (1.51−1.46)
total no. of observations	310054
no. of unique reflections	43221
$I/\sigma I$	32.2 (3.4)
R_{merge} (%)	7.6
completeness (%)	99.2
refined structure	
R_{work} (R_{free})	0.155 (0.185)
rms deviations from ideal	
bonds (Å)	0.011
angles (deg)	1.344

[a] The crystal cell dimensions are as follows: $a = b = 82.77$ Å, $c = 74.99$ Å. The space group is $P4_12_12$. Refined coordinates and structure factors have been deposited with the Protein Data Bank (*51*) as entry 1VOH.

liquor solution containing 100 mM SHA (Aldrich, 99.0%) for approximately 1 min. The SHA was dissolved by adding 1 M sodium hydroxide to the mother liquor to adjust the pH to ~10. The pH was then returned to 8.3 by adding hydrochloric acid.

Equilibrium Binding Constants. Equilibrium dissociation constants, K_d (100 mM potassium phosphate at pH 8.3), for the binding of SHA to rsAPX were determined using electronic spectroscopy according to previously published procedures (*29*) by addition of known amounts of SHA to rsAPX (≈5 μM rsAPX). Additions of SHA were determined gravimetrically. Binding constants were determined from plots of fractional saturation versus free ligand concentration according to published procedures (*29*). On the basis of pH-dependent binding data, which show an increase in K_d with pH that corresponds with the pK_a of the SHA, it has been reported that only the neutral form of SHA binds (*30*−*32*). Binding of SHA to rsAPX was also found to be pH-dependent (not shown), and we have therefore corrected binding data for ionization [pK_a = 7.4 (*33*)] of the hydroxamic acid group of SHA, as previously described (*30*, *31*). Reported values for K_d are an average of at least two independent measurements.

Data Collection and Refinement. Diffraction data were collected for the rsAPX−SHA complex on beam-line ID14-4 at ESRF (Grenoble, France) using an ADSC Quantum-4 detector. Data to 1.46 Å were collected over a 90° rotation in 0.5° images. All data were collected at 100 K. Data collection statistics are shown in Table 1, and 5% of the data were flagged for the calculation of R_{free} and excluded from subsequent refinement. The structure was refined from a model derived from the 1.45 Å rsAPX−ascorbate complex (*26*) (Protein Data Bank entry 1OAF) by the removal of bound ligand and water molecules. Several cycles of refinement using REFMAC5 from the CCP4 suite (*34*) and incorporation of solvent molecules gave a model with a crystallographic R-factor for all data of 15.5% and an R_{free} of 18.5%. The electron density for SHA was clear and unambiguous; the structure was incorporated into the last cycles of refinement. XTALVIEW (*35*) was used throughout for manual adjustment, ligand fitting, and interpretation of water structure.

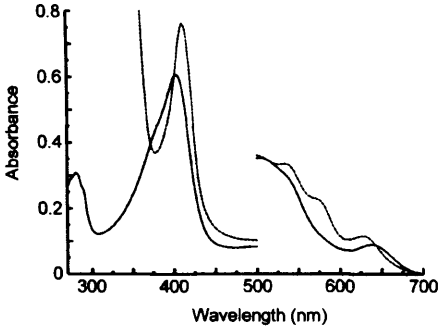

FIGURE 3: Electronic absorption spectra of rsAPX (—) and the rsAPX−SHA complex (- - -) (100 mM phosphate at pH 8.0). SHA absorbs strongly below 350 nm, and this spectrum has been truncated.

RESULTS

The UV−visible spectrum of rsAPX (λ_{max} = 407, 505, and 637 nm) and the rsAPX−SHA complex are shown in Figure 3. Addition of SHA leads to an increase in intensity and a red shift of the Soret band from 407 to 418 nm. New bands at 540, 580, and 630 nm appear. These changes are consistent with the formation of a predominantly six-coordinate heme derivative in the presence of SHA. A binding constant, K_d, of 8 ± 1 μM was determined for the rsAPX−SHA interaction (100 mM phosphate at pH 8.3) (data not shown). Binding of SHA to the heme will inhibit peroxidase activity by competing with H_2O_2, which is analogous to the binding of other strong ligands (e.g., cyanide). At high concentrations of SHA, the k_{cat} value for oxidation of guaiacol by rsAPX is only ≈50% of the value observed in the absence of SHA.[2] To establish whether binding of SHA is affected by the presence of other substrates, the binding constant, K_d, for SHA was determined in the presence of both ascorbate (25 mM) and guaiacol (25 mM). In this case, the K_d for SHA binding in the presence of guaiacol increases (K_d = 32 ± 2 μM), but the corresponding value in the presence of ascorbate does not change (K_d = 8 ± 1 μM) (data not shown), indicating that guaiacol and SHA compete for the same site but that ascorbate and SHA do not. When H_2O_2 is added to a solution of rsAPX and SHA, there is no decrease in the SHA peak at 300 nm, indicating that no oxidation occurs.

The overall structure of rsAPX in complex with SHA is shown in Figure 4. Comparison with the structure of the SHA-free enzyme (*26*) shows that binding of SHA leads to no major structural rearrangements of the enzyme (rms deviation in Cα positions of 0.21 Å). However, there is a slight adjustment of the side chain dihedral angle χ_2 of His42 with respect to that of the rsAPX structure (not shown). The electron density for the SHA molecule in the region of the heme group is unambiguous, allowing its position to be defined with precision (Figure 4). The SHA molecule is located in a cavity that connects the distal side of the heme to the surface of the protein. The mouth of the cavity is

[2] Competitive inhibition experiments with rsAPX and ascorbate−H_2O_2 in the presence of SHA were not carried out because SHA absorbs intensely at the wavelengths used for ascorbate assays (290 or 260 nm). The corresponding experiment with guaiacol showed a change in both K_M and k_{cat}. This may be due to the fact that both H_2O_2 and guaiacol are inhibited by SHA; these experiments were not pursued further, therefore.

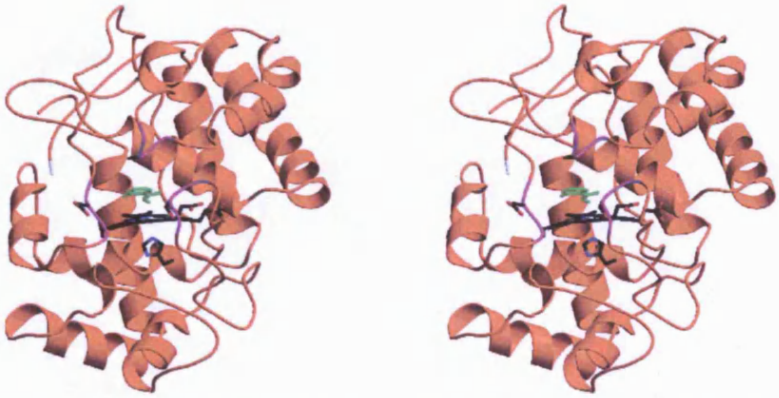

FIGURE 4: Stereo representation of the overall structure of the rsAPX−SHA complex, showing the heme with the proximal histidine residue in black and the bound SHA in green. The loops defining the mouth of the binding pocket are highlighted in magenta. The loop including Ala70 is shown directly above the SHA molecule; the loop including Asp133 is to the left of the SHA molecule, and the loop including Ser173 is to the right. The atoms of the side chains of Ala70, Asp133, and Ser173 are also shown. This figure was prepared using MOLSCRIPT (*48*) and RASTER3D (*49*).

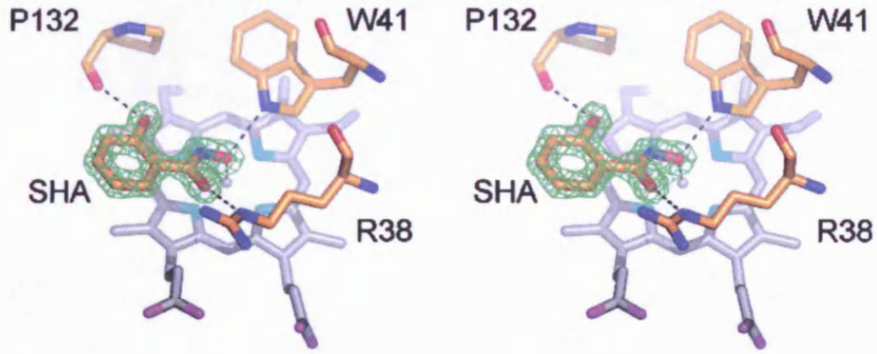

FIGURE 5: Stereoview of the rsAPX−SHA complex, showing the heme (gray) and the difference electron density (green) for the SHA. Hydrogen bonds are indicated by dashed lines (black). This figure was prepared using PyMOL (*50*).

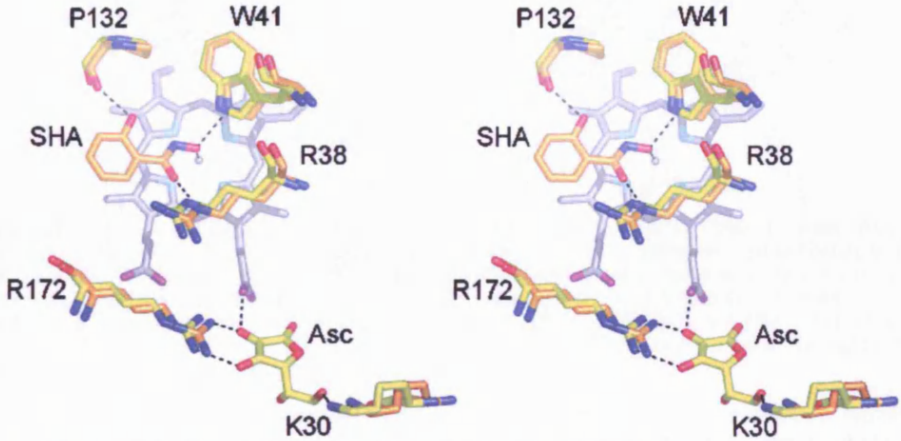

FIGURE 6: Structure-based alignment of the rsAPX−ascorbate complex [yellow (*26*)] and the rsAPX−SHA complex (orange). The residues involved in binding of ascorbate (Arg172 and Lys30) and SHA (Pro132, Arg38, and Trp41) are shown in both cases. The heme is shown in gray in both cases. The two hemes directly superimpose (for clarity, only one heme is indicated). Hydrogen bonds are indicated by dashed lines (black). This figure was prepared using PyMOL (*50*).

defined by the loop incorporating Ala70, the turn including Asp133 and the region of Ser173, and the edge of the heme; these are highlighted in Figure 4. The polar side chains of Asp133 and Ser69 extend into the solvent region. In the rsAPX and rsAPX−ascorbate stuctures (*26*), the equivalent site is occupied by five well-ordered solvent atoms.

The detailed structure of the rsAPX−SHA complex in the region of the heme is shown in Figure 5. The phenolic group [pK_a = 7.4 (*33*); Figure 2] of the hydroxamic acid group is coordinated to the heme iron at a distance of 2.1 Å, which is consistent with the electronic absorption spectra above. The SHA molecule is also able to hydrogen bond to the indole nitrogen of Trp41 (Figure 5). There are hydrogen bonds between the phenolic hydroxide [pK_a = 9.8 (*33*)] and the main chain carbonyl of Pro132, and between the carbonyl oxygen of SHA and the side chain guanadinium group of

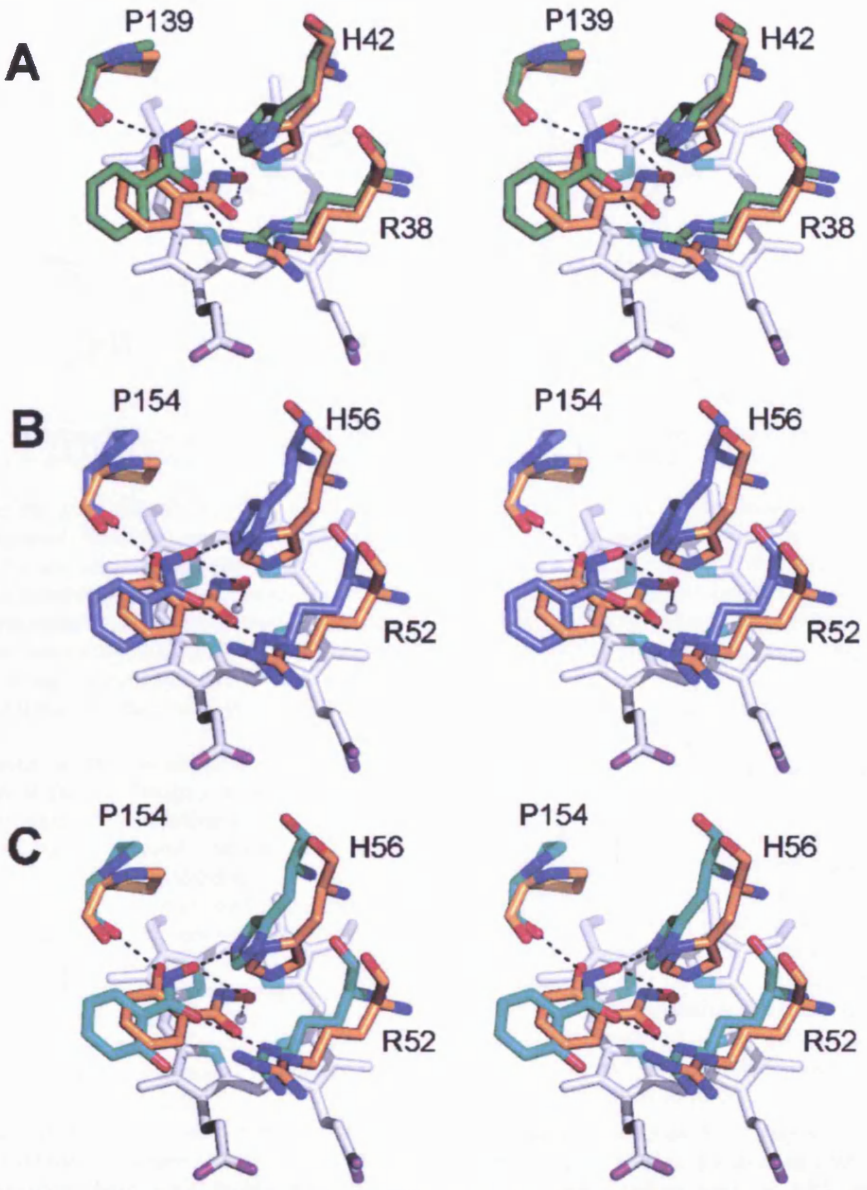

FIGURE 7: Structure-based alignments of the rsAPX−SHA complex (orange) and (A) the HRP−BHA complex (dark green; *13*), (B) the ARP−BHA complex (blue; *15*), and (C) the ARP−SHA complex (light blue; *38*). The residues involved in binding of the substrate for the HRP (Pro139, His42, and Arg38) and ARP (Pro154, His56, and Arg52) structures are overlaid with the corresponding residues in the rsAPX−SHA structure (Pro132, His42, and Arg38, respectively). The heme is shown in gray, and the two hemes directly superimpose in all cases; for clarity, only one heme is indicated. Hydrogen bonds for the HRP−BHA, ARP−BHA, and ARP−SHA structures are represented by dashed lines (black); hydrogen bonds for the rsAPX−SHA complex are omitted for clarity, but are according to Figure 6. This figure was prepared using PyMOL (*50*).

Arg38 (Figure 5). Pro132 and Arg38 are conserved in all APXs examined so far (*36*) as well as in other peroxidases (*5*). Trp41 is conserved in all but two APXs (*Mesembryanthemum crystallinum* APX and a membrane-bound enzyme from spinach which contain Phe at this position[3]). Although Nϵ of the distal histidine (His42) is 3.0 Å from the phenolic oxygen of SHA, the geometry is poor for formation of a hydrogen bond between His42 and SHA. The aromatic ring of the SHA molecule is almost parallel to the heme (separation of 3.4 Å) and makes a shallow angle of ~15° with the plane of the heme, and it overlaps with the δ-heme edge (C20 position) and the 8-Me group of the heme. The Cα and Cβ atoms of Ala70 are within van der Waals distance of the SHA (≈3.5 Å, Figure 4). Figure 6 shows an overlay of the rsAPX−ascorbate (*26*) and rsAPX−SHA structures; this clearly highlights the different binding locations of the SHA and ascorbate close to the δ- and γ-heme edge, respectively.

[3] In addition, these are also the only APXs examined so far that do not contain Trp at position 179 (replaced with Phe); they also lack one of the residues required for ascorbate binding (R172 → Ile for *M. crystallinum* and K30 → D for the spinach enzyme).

DISCUSSION

The identification of an ascorbate binding site close to the γ-heme edge (*26*) was counter to established thinking in

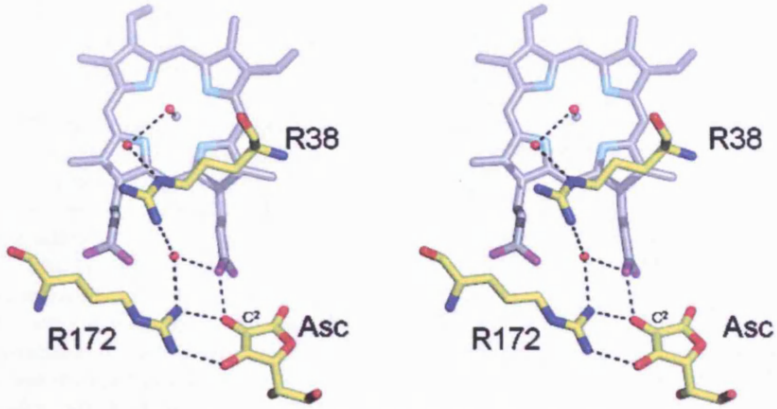

FIGURE 8: Proposed proton transfer pathway using Arg38. Water molecules are shown as red spheres, and hydrogen bonds are represented by dashed lines. The OH group on C^2 of ascorbate (Figure 2) is indicated. This figure was prepared using PyMOL (*50*).

which substrate binding and oxidation at the δ-heme edge had been widely assumed. However, most APXs that have been identified so far are also functionally competent for oxidation of aromatic substrates, and in some cases, oxidation of aromatic substrates occurs at a rate comparable to the rate of oxidation of ascorbate itself (*18*, *22*). The identity of this second substrate binding location was not known, but the region close to the δ-heme edge has been directly implicated (*23*, *24*).

The data presented in this work now complete the structural definition of the two binding sites in APX and confirm the δ-heme edge as the binding site for aromatic molecules. The structure is consistent with our steady-state data that show that APX modified at the δ-heme edge using phenylhydrazine retains ≈10% activity with ascorbate but is inactive against guaiacol (data not shown). The structure also provides rationalization of the empirical observation (*37*) that salicylic acid (2-hydroxybenzoic acid, Figure 2) is a (slow) substrate for APX with a possible role *in planta*. For salicylic acid, coordination to the iron is not observed (*37*) but the main hydrogen bonding interactions between Pro132 and Arg38 (Figure 5) are still possible.

Comparison with Other Peroxidases. In the following discussion, we correlate these structural data with our current understanding of substrate binding and oxidation in other class I, class II, and class III peroxidase enzymes. In Figure 7, we compare the rsAPX−SHA structure with the structures of the HRP−BHA complex (*13*) (Figure 7A), the ARP−BHA complex (*15*) (Figure 7B), and the ARP−SHA complex (*38*) (Figure 7C). It is clear from Figure 7 that the binding location of the substrate for all the structures is similar and close to the δ-heme edge. (We note also that oxidation of guaiacol has been reported to be inhibited by the presence of BHA (*21*), indicating that BHA also binds at the same δ-heme site in APX.) In all cases, there are hydrogen bonding interactions between the backbone carbonyl of a proline and between the distal arginine residue and the carbonyl of the BHA or SHA molecule; the distal histidine hydrogen bonds to the substrate in the HRP and ARP structures, but not in rsAPX.[4] There are other differences. For the HRP and ARP structures, the interaction with the heme iron is via a water molecule (compared to through the hydroxyl group of the SHA in rsAPX) and the proline carbonyl interacts with the NH group of the hydroxamic group (compared to the phenolic group of SHA in rsAPX). Altogether, the bound ligand for the HRP and ARP structures is displaced by approximately a bond length from the binding pocket relative to SHA in rsAPX. It is possible that the additional hydrogen bonding interaction between SHA and Trp41 in rsAPX (Figure 5) is partly responsible for this difference (Trp41 is replaced with a Phe in both HRP and ARP).

Might this binding site be used more generally for oxidation of related aromatic substrates in other class I peroxidases? Cytochrome *c* peroxidase is known (*39*) to bind aromatic substrates at a different location compared to cytochrome *c* (*40*), and the δ-meso heme edge has been implicated (*40*, *41*). This is consistent with our data because the key hydrogen-bonding residues (Arg38, Trp41, and Pro132) are conserved in CcP (Arg48, Trp51, and Pro145, respectively) and because CcP contains a similar binding pocket as identified in APX.

Mechanistic and Functional Implications. In light of these new data, and with the location of both the ascorbate (*26*) and aromatic binding sites in APX now defined, it is appropriate to correlate the new structural information with functional data and to consider the broader mechanistic question of how APX might most effectively deal with oxidation of different types of substrates bound at different locations. For ascorbate oxidation, our data (*26*) show direct coupling of the heme to the substrate through the 6-propionate and electron transfer to the heme is presumed to be facile. The data presented in this work show SHA to be in van der Waals contact with the porphyrin π-system, and for aromatic substrates, we therefore assume that electron transfer is directly through the π-orbitals of the porphyrin. Reduction of both Compound I and Compound II by both ascorbate (at the γ-heme edge) and aromatic substrates (at the δ-heme edge) also requires proton transfer (eqs 1−3); however, the mechanism of proton transfer is not well-developed for any heme peroxidase, and there is no information at all for APX. For ascorbate, oxidation of the (anionic, Figure 2) substrate gives the protonated monodehydroascorbate radical which is very acidic [$pK_a = -0.45$ for C^2-OH

[4] The distal histidine and arginine groups, and the main chain carbonyl of proline, are also involved in binding of ferulic acid to HRP (*14*).

(*42*, *43*); Figure 2] and will rapidly deprotonate. A proton transfer pathway from the ascorbate to a water molecule bound to the heme iron is identified that involves Arg38 (Figure 8). (Proton transfer to His42 may subsequently occur in solution, but the crystallographic data do not show a good hydrogen bonding interaction between this water and His42.) This distal arginine residue, which is known to be mobile in CcP (*44*−*47*) and which is conserved across all peroxidases (*5*), is also involved in binding of SHA in rsAPX (Figure 7), so might this residue also provide a conduit for proton delivery for aromatic substrates bound at the δ-heme edge, thereby providing APX with a common mechanism for proton shuttling during oxidation of both types of substrates? Clearly, this has yet to tested experimentally, but it would be consistent with the idea that APX is a hybrid enzyme that combines features that are characteristic of both class I and class III peroxidases (*21*) and with the suggestion that Arg38 in HRP is involved in proton transfer during oxidation of ferulic acid (*14*).

ACKNOWLEDGMENT

We thank Dr. David Leys for collection of crystallographic data. Mr. K. Singh is gratefully acknowledged for technical assistance.

REFERENCES

1. Everse, J., Everse, K. E., and Grisham, M. B. (1991) *Peroxidases in Chemistry and Biology*, Vols. I and II, CRC Press, Boca Raton, FL.
2. English, A. M., and Tsaprailis, G. (1995) Catalytic structure−function relationships in heme peroxidases, *Adv. Inorg. Chem. 43*, 79−125.
3. Veitch, N. C., and Smith, A. T. (2001) Horseradish peroxidase, *Adv. Inorg. Chem. 51*, 107−162.
4. Dunford, H. B. (1999) *Heme Peroxidases*, John Wiley, Chichester, U.K.
5. Welinder, K. G. (1992) Superfamily of plant, fungal and bacterial peroxidases, *Curr. Opin. Chem. Biol. 2*, 388−393.
6. Erman, J. E., and Vitello, L. B. (2002) Yeast cytochrome *c* peroxidase: mechanistic studies via protein engineering, *Biochim. Biophys. Acta 1597*, 193−220.
7. Smith, A. T., and Veitch, N. C. (1998) Substrate binding and catalysis in heme peroxidases, *Curr. Opin. Chem. Biol. 2*, 269−278.
8. Erman, J. E. (1998) Cytochrome *c* peroxidase: a model heme protein, *J. Biochem. Mol. Biol. 31*, 307−327.
9. Pelletier, H., and Kraut, J. (1992) Crystal structure of a complex between electron transfer partners, cytochrome *c* peroxidase and cytochrome *c*, *Science 258*, 1748−1755.
10. Davey, C. A., and Fenna, R. E. (1996) 2.3 Å resolution X-ray crystal structure of the bisubstrate analague inhibitor salicylhydroxamic acid bound to human myeloperoxidase, *Biochemistry 35*, 10967−10973.
11. Meno, K., Jennings, S., Smith, A. T., Henricksen, A., and Gajhede, M. (2002) Structural analysis of the two horseradish peroxidase catalytic residue variants H42E and R38S/H42E: implications for the catalytic cycle, *Acta Crystallogr. D58*, 1803−1812.
12. Sundaramoorthy, M., Kishi, K., Gold, M. H., and Poulos, T. L. (1994) The crystal structure of manganase peroxidase from *Phanerochaete crysosporium* at 2.06 Å resolution, *J. Biol. Chem. 269*, 32759−32767.
13. Henriksen, A., Schuller, D. J., Meno, K., Welinder, K. G., Smith, A. T., and Gajhede, M. (1998) Structural interactions between horseradish peroxidase C and the substrate benzhydroxamic acid determined by X-ray crystallography, *Biochemistry 37*, 8054−8060.
14. Henriksen, A., Smith, A. T., and Gajhede, M. (1999) The structures of the horseradish peroxidase C-ferulic acid complex and the ternary complex with cyanide suggest how peroxidases oxidise small phenolic substrates, *J. Biol. Chem. 274*, 35005−35011.
15. Itakura, H., Oda, Y., and Fukuyama, K. (1997) Binding mode of benzhydroxamic to *Arthromyces ramosus* peroxidase shown by X-ray crystallographic analysis of the complex at 1.6 Å resolution, *FEBS Lett. 412*, 107−110.
16. Fiedler, T. J., Davey, C. A., and Fenna, R. E. (2000) X-ray crystal structure and characterisation of halide-binding sites of human myeloperoxidase at 1.8 Å resolution, *J. Biol. Chem. 275*, 11964−11971.
17. Fukuyama, K., Sato, K., Itakura, H., Takahashi, S., and Hosoya, T. (1997) Binding of iodide to *Arthromyces ramosus* peroxidase investigated with X-ray crystallographic analysis, ^{1}H and ^{127}I NMR spectroscopy and steady state kinetics, *J. Biol. Chem. 272*, 5752−5756.
18. Raven, E. L. (2003) Understanding functional diversity and substrate specificity in haem peroxidases: what can we learn from ascorbate peroxidase? *Nat. Prod. Rep. 20*, 367−381.
19. Sharp, K. H., Moody, P. C. E., and Raven, E. L. (2003) Defining substrate specificity in haem peroxidases, *Dalton Trans.*, 4208−4215.
20. Dalton, D. A. (1991) Ascorbate peroxidase, in *Peroxidases in Chemistry and Biology* (Everse, J., Everse, K. E., and Grisham, M. B., Eds.) pp 139−154, CRC Press, Boca Raton, FL.
21. Heering, H. A., Jansen, M. A. K., Thorneley, R. N. F., and Smulevich, G. (2001) Cationic asorbate peroxidase isozyme II from tea: structural insights into the heme pocket of a unique hybrid peroxidase, *Biochemistry 40*, 10360−10370.
22. Raven, E. L. (2000) Peroxidase-catalysed oxidation of ascorbate: structural, spectroscopic and mechanistic correlations in ascorbate peroxidase, in *Subcellular Biochemistry: Enzyme Catalysed Electron and Radical Transfer* (Holzenberg, A., and Scrutton, N. S., Eds.) Kluwer Academic/Plenum Publishers: New York pp 318−350.
23. Mandelman, D., Jamal, J., and Poulos, T. L. (1998) Identification of two-electron-transfer sites in ascorbate peroxidase using chemical modification, enzyme kinetics, and crystallography, *Biochemistry 37*, 17610−17617.
24. Hill, A. P., Modi, S., Sutcliffe, M. J., Turner, D. D., Gilfoyle, D. J., Smith, A. T., Tam, B. M., and Lloyd, E. (1997) Chemical, spectroscopic and structural investigation of the substrate-binding site in ascorbate peroxidase, *Eur. J. Biochem. 248*, 347−354.
25. Bursey, E. H., and Poulos, T. L. (2000) Two substrate binding sites in ascorbate peroxidase: the role of arginine 172, *Biochemistry 39*, 7374−7379.
26. Sharp, K. H., Mewies, M., Moody, P. C. E., and Raven, E. L. (2003) The crystal structure of the ascorbate peroxidase/ascorbate complex, *Nat. Struct. Biol. 10*, 303−307.
27. Lad, L., Mewies, M., and Raven, E. L. (2002) Substrate binding and catalytic mechanism in ascorbate peroxidase: evidence for two ascorbate binding sites, *Biochemistry 41*, 13774−13781.
28. Santimone, M. (1975) Titration study of guaiacol oxidation by horseradish peroxidase, *Can. J. Biochem. 53*, 649−657.
29. Bogumil, R., Hunter, C. L., Maurus, R., Tang, H.-L., Lee, H., Lloyd, E., Brayer, G. D., Smith, M., and Mauk, A. G. (1994) FTIR analysis of the interaction of azide with horse heart myoglobin mutants, *Biochemistry 33*, 7600.
30. Aitken, S. M., Turnbull, J. L., Percival, M. D., and English, A. M. (2001) Thermodynamic analysis of the binding of aromatic hydroxamic acid analogues to ferric horseradish peroxidase, *Biochemistry 40*, 13980−13989.
31. Indiana, C., Santoni, E., Becucci, M., Boffi, A., Fukuyama, K., and Smulevich, G. (2003) New insight into the peroxidase-hydroxamic acid interactions revealed by the combination of spectroscopic and crystallographic studies, *Biochemistry 42*, 14066−14074.
32. Schonbaum, G. R. (1973) New complxes of peroxidases with hydroxamic acids, hydrzides and amides, *J. Biol. Chem. 248*, 502−511.
33. O'Brien, E. C. O., Farkas, E., Gil, M. J., Fitzgerald, D., Castineras, A., and Nolan, K. B. (2000) Metal complexes of salicylhydroxamic acid (H_2SHA), anthranilic hydroxamic acid and benzohydroxamic acid. Crystal and molecular structure of $[Cu(phen)_2Cl]Cl$. H_2SHA, a model for a peroxidase-inhibitor complex, *J. Inorg. Biochem. 79*, 47−51.
34. Collaborative Computational Project No. 4 (1994) The *CCP*4 suite: programs for protein crystallography, *Acta Crystallogr. D50*, 760−763.
35. McRee, D. (1992) A Visual Protein Crystallographic Software System for X11/Xview, *J. Mol. Graphics 10*, 44−47.

36. Jespersen, H. M., Kjaersgard, I. V. H., Ostergaard, L., and Welinder, K. G. (1997) From sequence analysis of three novel ascorbate peroxidases from *Arabidopsis thaliana* to structure, function and evolution of seven types of ascorbate peroxidase, *Eur. J. Biochem. 326*, 305−310.
37. Kvaratskhelia, M., George, S. J., and Thorneley, R. N. F. (1997) Salicylic acid is a reducing substrate and not an effective inhibitor of ascorbate peroxidase, *J. Biol. Chem. 272*, 20998−21001.
38. Tsukamoto, K., Itakura, H., Sato, K., Fukuyama, K., Miura, S., Takahashi, S., Ikezawa, H., and Hosoya, T. (1999) Binding of salicylahydroxamic acid and several aromatic donor molecules to *Arthromyces ramosus* peroxidase, investigated by X-ray crystallography, optical difference spectroscopy and NMR relaxation, molecular dynamics and kinetics, *Biochemistry 38*, 12558−12568.
39. Yonetani, T., and Ray, G. S. (1965) Studies on cytochrome *c* peroxidase. Purification and some properties, *J. Biol. Chem. 240*, 4503−4514.
40. DePillis, G. D., Sishta, B. P., Mauk, A. G., and Ortiz de Montellano, P. R. (1991) Small substrates and cytochrome *c* are oxidized at different sites of cytochrome *c* peroxidase, *J. Biol. Chem. 266*, 19334−19341.
41. Wilcox, S. K., Jensen, G. M., Fitzgerald, M. M., McRee, D. E., and Goodin, D. B. (1996) Altering substrate specificity at the heme edge of cytochrome *c* peroxidase, *Biochemistry 35*, 4858−4866.
42. Bryan, D. M., Dell, S. D., Kumar, R., Clarke, M. J., Rodriguez, V., Sherban, M., and Charkoudian, J. (1988) Stable pentaammineruthenium(III) complexes of reductic acids: synthesis, linkage isomers and autoxidation kinetics, *J. Am. Chem. Soc. 110*, 1498−1506.
43. Creutz, C. (1981) The complexities of ascorbate as a reducing agent, *Inorg. Chem. 20*, 4452−4453.
44. Bonagura, C. A., Bhaskar, B., Shimizu, H., Li, H., Sundaramoorthy, M., McRee, D. E., Goodin, D. B., and Poulos, T. L. (2003) High-resolution crystal structures and spectroscopy of native and Compound I cytochrome *c* peroxidase, *Biochemistry 42*, 5600−5608.
45. Edwards, S. L., Poulos, T. L., and Kraut, J. (1984) The crystal structure of fluoride-inhibited cytochrome *c* peroxidase, *J. Biol. Chem. 259*, 12984−12988.
46. Edwards, S. L., Xuong, N., Hamlin, R. C., and Kraut, J. (1987) Crystal structure of cytochrome *c* peroxidase Compound I, *Biochemistry 26*, 1503−1511.
47. Fulop, V., Phizackerley, R. P., Soltis, S. M., Clifton, I. J., Wakatsuki, S., Erman, J., Hajdu, J., and Edwards, S. L. (1994) Laue diffraction study on the structure of cytochrome *c* peroxidase compound I, *Structure 2*, 201−208.
48. Kraulis, P. J. (1991) MOLSCRIPT: A program to produce both detailed and schematic plots of protein structures, *J. Appl. Crystallogr. 24*, 946−950.
49. Merrit, E. A., and Murphy, M. E. P. (1994) Raster3D Version 2.0: A program for photorealistic molecular graphics, *Acta Crystallogr. D50*, 869−873.
50. DeLano, W. L. (2002) The PyMOL Molecular Graphics System, DeLano Scientific, San Carlos, CA.
51. Berman, H. M., Westbrook, J., Feng, Z., Gilliland, G., Bhat, T. N., Weissig, H., Shindyalov, I. N., and Bourne, P. E. (2000) The Protein Data Bank. *Nucleic Acids Res. 28*, 235−242.

BI049343Q